TRITIUM ANALYSIS OF SEAWATER

THESIS

submitted for the degree of

DOCTOR OF PHILOSOPHY

of the

UNIVERSITY OF GLASGOW

by

H. MARK BLAUER

Chemistry Department

May, 1977

ProQuest LLC.
789 East Eisenhower Parkway
P.O. Box 1346
Ann Arbor, MI 48106 – 1346

ACKNOWLEDGEMENTS.

The author is indebted to the Natural Environmental Research Council for financial support throughout this research project and to the University of Glasgow for laboratory and support facilities.

Thanks are extended to A. Anderson and his staff for design and construction of the Constant Current Density Units and maintenance of all electronic equipment; to A. Hislop and his staff for construction of the reaction vessels and other equipment; and to J. Connelly and his staff for glassblowing.

Appreciation is extended to the crew of the U.S.N.S. Bartlett, Drs. W.S. Moore, M.S. Baxter and A.E. Fallick for collection of eastern tropical Pacific Ocean samples and supplementary hydrographic data. The same is extended to the crew of the U.S.N.S. Eltanin (Cruise 47) and Dr. J.M. Edmond for the Antarctic samples. The International Atomic Energy Agency and Dr. C.B. Taylor supplied tritium standards and intercalibration facilities. The expertise of A. Ritchie for mass-spectrometric measurements of D/H ratios and the extended collection of tritium results by K. McKay are acknowledged.

Thanks are also due to Drs. A.E. Fallick and A.B. MacKenzie and Messrs. D. Swan and J. Campbell for providing the opportunity for many frank and illuminating discussions in the best of Scottish tradition.

Appreciation for final preparation of this manuscript is extended to Messrs. C. Stuart, C. Cook and M. Gray, and most especially to Miss T. Collins.

The author is especially grateful to Dr. M.S. Baxter for his diligent supervision, guidance and constructive criticism throughout the period of research. Without his assistance this thesis would never have been possible.

TABLE OF CONTENTS.

TABLE OF CONTENTS (continued).

LIST OF FIGURES.

LIST OF FIGURES (continued.)

LIST OF FIGURES (continued.)

LIST OF TABLES.

LIST OF TABLES (continued.)

ABSTRACT.

In applying chemical knowledge to the solution of natural terrestrial problems it is necessary to know the abundances of the chemical and isotopic components of the systems being studied. Broader studies in geochemistry require knowledge of such abundances in various major reservoirs (lithosphere, hydrosphere, atmosphere) and of the mutual exchanges which occur. Concomitant problems are the origins of particular isotopic species, their fates within each reservoir and variations in their budgets with time. While these topics warrant study in their own right, a desirable outcome is the application of such knowledge to related disciplines.

This study is firstly an attempt to establish a routine laboratory for the extraction and measurement of geochemical tritium, ^{3}H or T, an isotope of hydrogen. Experimental techniques for the determination of tritium levels in natural waters are described. These include one stage conversion of water to methane and significant improvements in electrolytic procedures for isotopic enrichment.

Secondly, water samples from areas of the Pacific and Antarctic Oceans have been collected and analysed for tritium. Conventional hydrographic data have been used in conjunction with the tritium results to determine the physical oceanography of these areas with emphasis on water mass structure and mixing characteristics.

CHAPTER I.

INTRODUCTION.

I.1 PROLEGOMENA.

In their treatise on geochemistry, Rankama and Sahama (1950) devoted one paragraph to deuterium and mentioned tritium only in passing while discussing carbon-14. In 1950 the major developments in tritium geochemistry were thus still to come. It is necessary, however, to go back to the nineteen thirties to find the origins of this work.

Following the discovery by Urey (1933) that natural hydrogen is composed of two isotopes, protium and deuterium, the next logical step was the search for still heavier hydrogen isotopes. Initially, the search for tritium (or triterium as it was then called) was based on the assumption that tritium would be stable. The Norsk Hydro-Electrisk Kvoelstofakteislab of Oslo, Norway electrolysed 13,000 tons of ordinary water to 11 cc (Rutherford, 1937) and the sample was analysed on the then newly developed mass spectrograph by Aston. This showed that the tritium:deuterium atomic ratio is less that 50,000. The radioactivity of tritium was established by Alvarez and Cornog (1939) who found that the radiation is of very short range and that the half-life is long. Their further studies (Alvarez and Cornog, 1940) implied a half-life in excess of 10 years. Subsequent work by Eichelberger et al (1963) has established the half-life of tritium as 12.36 ± 0.03 years although the half-life value

of 12.262 ± 0.004 years as determined by Jones (1955) is more commonly referred to in the literature. Tritium decays by the emission of a soft beta particle, with a maximum energy of 18 keV and an average energy of 5.7 keV, to form ^{3}He. Early assays of the tritium content of natural surface waters indicated that there was about one tritium atom per 10^{18} atoms of hydrogen (Grosse et al, 1951).

It became quite convenient to express tritium assays in relation to the number of hydrogen atoms in the sample. The term "tritium unit" (T.U.) is commonly used to denote the number of tritium atoms per 10^{18} atoms of hydrogen. Recently the International Commission on Radiological Units and Measurements (1963) raised an objection to the use of this term and suggested that it be replaced by the term "tritium ratio" (TR). The tritium unit (T.U.), however, remains the most commonly used in tritium measurements of natural water samples and will be employed throughout this thesis.

Surveys of the tritium content of natural waters have been performed by Kaufman and Libby (1954), by Buttlar and Libby (1955) and are continuing with Ostlund et al (1974) in co-operation with the Geosecs programme, the latter being the most recent and complete set of oceanographic data for the North Atlantic Ocean. Continuous monitoring of the tritium content of precipitation, on a world-wide basis, has been maintained by various laboratories under the auspices of the International Atomic Energy Agency since 1957 (I.A.E.A., 1969, 1970, 1971, 1973, 1975).

I.2 PROPERTIES OF TRITIUM AND TRITIUM OXIDE.

The atomic weight of tritium is 3.016997 ± 0.000011 g, compared with the atomic weights for ^{1}H and ^{2}H of 1.00814 ± 0.000003 g and 2.014735 ± 0.000006 g, respectively (Lange and Forker, 1961). At room temperature the combination of H_2 and T_2 to form HT is favoured. Furthermore, the mass action equilibrium coefficient for the reaction (I.1) $HT + H_2O \rightleftarrows HTO + H_2$ is approximately 6 at 25°C (Jacobs, 1968) so that formation of tritiated water is also favoured. Because of the predominance of reaction (I.1), any discussion of the properties of tritium must necessarily include a discussion of tritiated water since this is the probable major tritiated species in man's environment. Bond (1962) indicates that tritium produced by a nuclear explosion will be practically 100% converted to tritiated water and mixed with environmental water.

I.3 SOURCES OF TRITIUM.

The natural origins of tritium involve cosmic-ray interaction with atmospheric constituents. Hence a tracer experiment on a world-wide scale is occurring continuously. Cornog and Libby (1941) found that neutron irradiation of nitrogen compounds forms tritium according to the reactions:

$$^{14}N + {}^{1}n \rightarrow {}^{12}C + {}^{3}H + 4.3 \text{ MeV} \qquad (I.2)$$

and

$$^{14}N + {}^{1}n \rightarrow 3\ {}^{4}He + {}^{3}H + 11.5 \text{ MeV} \qquad (I.3)$$

These reactions require a source of energetic neutrons.

Proton bombardment and helium bombardment also produce tritum (e.g. Gonzalez-Vidal and Wade, 1960). Libby (1946) had first suggested that tritium was produced from atmospheric nitrogen by bombardment with cosmic-ray neutrons and that most atmospheric helium results from decay of tritium (Grosse et al, 1951). Later studies of tritium production via high-energy protons led Currie et al (1956) to the conclusion that most of the naturally occurring tritium is produced by primary cosmic-ray reactions. The rate of production was estimated to be 0.082 tritons/cm^2/sec compared with 0.05 for intermediate energy neutron reactions and 0.01 for low energy neutron reactions. Some controversy arises whether some of the tritium is accreted from extra-terrestrial sources or whether it is all produced in the earth's atmosphere and in incoming meteors.

Various estimates of the natural tritium distribution have been made (see among others, Bishop et al, 1962; Harteck, 1954). Kaufman and Libby (1954) estimated a terrestrial inventory of about 1800 g of tritium, with 11 g occurring in the atmosphere, 13 g in ground water, and the remainder in the sea. Begemann (1963) later estimated the tritium distribution shown in Table I.1.

The introduction of the thermonuclear and nuclear fission detonations, nuclear reactors, and fuel reprocessing plants has greatly altered the environmental tritium inventory. In a deuterium-tritium bomb, 10 single deuterium-tritium

NATURAL DISTRIBUTION OF TRITIUM

	Tritium Distribution %	Tritium Concentration (T.U.)
Hydrosphere	~ 90	< 10
Troposphere		
Water vapour	0.1	< 80
Molecular hydrogen	0.02 - 0.2	$4 \times 10^3 - 3.5 \times 10^4$
Methane	< 0.04	$< 10^3$
Stratosphere		
Water	~ 10	6×10^5
Molecular hydrogen	0.004 - 0.007	$3 \times 10^3 - 6 \times 10^4$

TABLE I.1

THERMONUCLEAR ENERGY YIELDS OF ATMOSPHERIC TESTS IN MEGATONS.

Inclusive Years	U.S. & U.K. Tests	Soviet Tests	Chinese Tests	French Tests	Total Fusion Yield
1945 - 1951	-	-	-	-	0
1952 - 1954	21.5-22	0.5			22
1955 - 1956	11	4			15
1957 - 1958	24	21			45
1959 - 1960					0
1961		95			95
1962 - 1966	10	113			123
1967			3		3
1968			3	3½	6½
1969			3		3
1970			3	1	4
1971 -1973				1	1
1974				1	1

*Underground tests not included; Foreign tests impossible to determine accurately.

TABLE I.2

reactions release 180 MeV of energy (which is equivalent to the energy released by a single fission event) plus 10 neutrons, in contrast to 2.5 neutrons in a fission device of the same energy (Leipunsky, 1957). In a pure thermonuclear detonation, Leipunsky (1957) estimated that there is a residual of about 0.7 kg of tritium per megaton-equivalent explosion. In addition to this yield of tritium from the fusion reaction, the neutron irradiation of nitrogen may yield an additional 0.15 kg of tritium. Miskel (1964) suggests that the residual may be as high as 5.0 kg of tritium per megaton-equivalent.

The concentration levels of tritium in rain rose sharply after the Castle series of tests in the spring of 1954 (Begemann and Libby, 1957) and briefly reached concentrations two orders of magnitude above natural. The quantity of tritium deposited during these tests suggests a minimum production of 1.16 kg of tritium per megaton explosion (Martell, 1963). The production history of artificial tritium from thermonuclear explosions is considerable and can be approximately reconstructed from unclassified weapons yield information (Atmospheric Radioactivity Research Project, 1963; Cambray, personal communication). These data, summarised in Table I.2, and based on Leipunsky's 1957 estimate of 0.7 kg of residual tritium per megaton of fusion energy were used in constructing the cumulative bomb-produced tritium inventory curve (Figure I.1). It can be seen that over 200 kg of tritium has been added to the natural system. It is not clear how reliable or generally applicable Leipunsky's estimate of 0.7 kg residual per megaton of

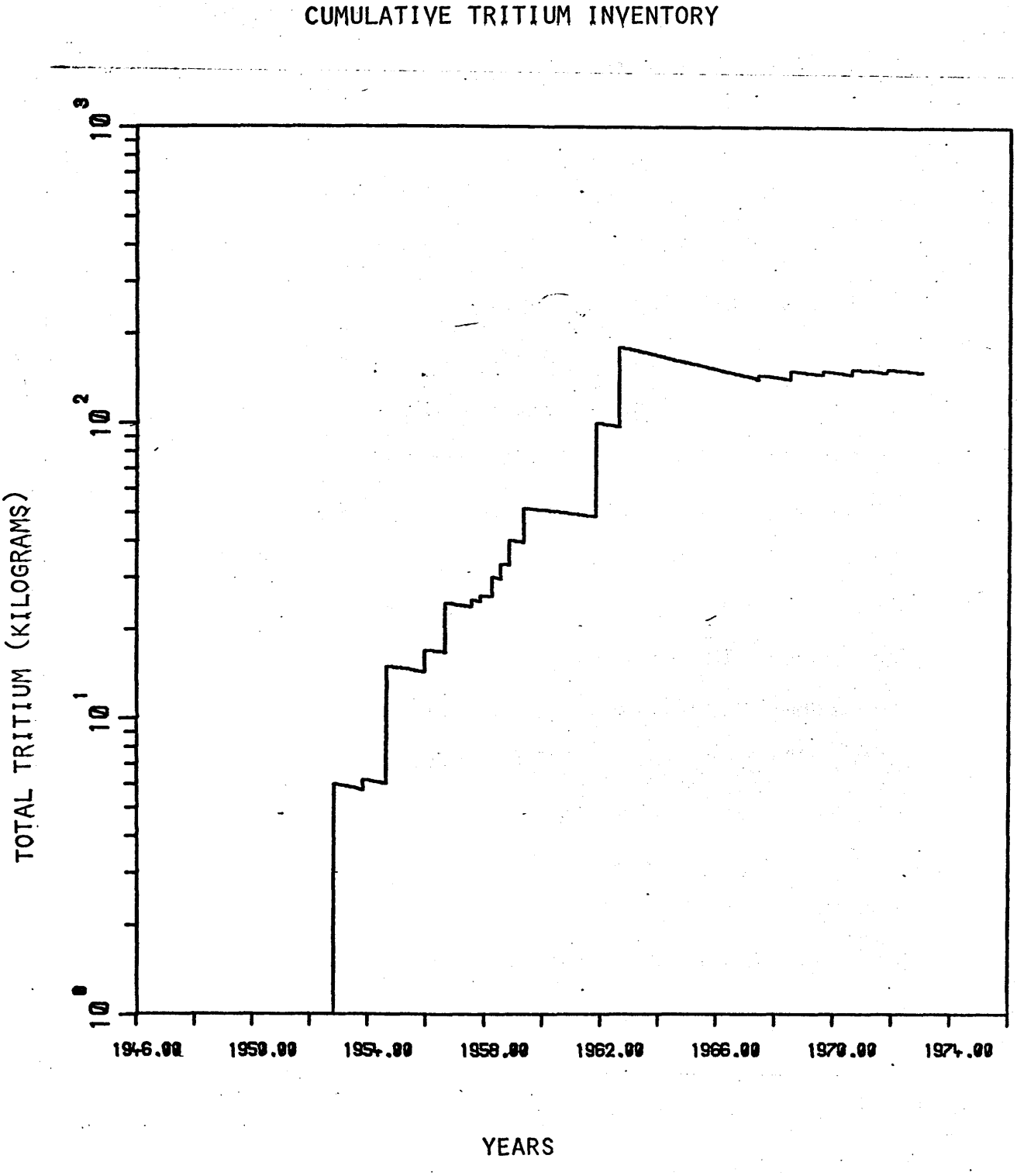

Figure I.1 Cumulative bomb produced tritium inventory based on 0.7 kg/megaton fusion energy released.

fusion energy may be since the 1954 Castle tests involved less than 22 megatons of fusion energy release (Table I.2) corresponding to a minimum production of 1.16 kg of tritium per megaton of fusion for the Castle tests. Since the uncertainty in this estimate for Castle tritium deposition is large, the difference in the values of 0.7 and 1.16 kg is no indication of the uncertainty in bomb-produced tritium (Martell, 1963).

Recently, Ostlund and Mason (1974) have re-examined atmospheric HT and HTO and have re-established that the main reservoir of atmospheric HTO is the stratosphere and that its source is primarily the testing of fusion devices in the atmosphere. For HT, their data suggest, however, that the source is at ground level and that in the troposphere there is now more tritium as gas (HT or T_2) than HTO (water vapour). It is probably that these sources for HT are as follows:

(1) reprocessing of nuclear fuel elements, releasing hydrogen containing HT,

(2) the handling of tritium gas in the nuclear industry and in research, and

(3) underground explosions of fusion devices resulting in seepage of tritium gas into the atmosphere.

Tritium then is produced by artificial and natural processes, is deposited in the atmosphere and can be followed through precipitation to ground waters and the oceans. Measurement of tritium levels within these reservoirs enables investigation of the geophysical processes occuring therein.

I.4 TRITIUM IN THE OCEAN.

In contrast to rivers, the oceans and seas represent vast reservoirs for storing water. Tritium deposited into the oceans and seas, therefore, is greatly diluted by mixing processes. Buttlar and Libby (1955) analysed four 1953 Atlantic surface seawater samples, obtained values ranging over a factor of 8 (from 0.19 - 1.16 T.U.) and concluded that the mean concentration was 0.58 T.U. in 1953. Meanwhile Giletti and Kulp (1956) reported a mean range of 1 - 3 T.U. for 1953 and Giletti and Bazan (1956) showed that for seven samples the mean was 1.0 T.U. A progress report by Begemann and Libby (1957) concluded on the basis of further work that the mean ocean value in 1953 was 1.0 T.U. and not 0.5 - 0.6 T.U. as originally suggested. Thermonuclear weapons testing in 1954 subsequently modified this natural concentration and these 1953 surface water data therefore provide virtually the only record of natural levels. The importance of these early values cannot be overemphasised since, in addition, they form the basis of the natural tritium production rate estimates which underlie most ocean circulation studies. This fundamental parameter is used repeatedly in all calculations relating to oceanographic problems.

Current trends in oceanographic tritium research have involved measurements of tritium inventories in surface and subsurface waters of the oceans to determine rates of exchange between water masses and mixing times (or turnover rates) of tritium in surface waters. For radioisotopes

other than tritium a major limiting consideration is their possible transfer into deeper water masses by particulate settling. For tritium, this possibility can definitely be excluded, as tritiated water is indistinguishable in its chemical properties from ordinary water and therefore is the ideal tracer of water transport.

Concomitant with tritium measurement is the collection of hydrographic data for each water sample. Prior to embarking on detailed discussion of tritium, its distribution and analysis, it is essential therefore to review here the main features of the definitions and applications of conventional hydrographic data. These normally consist of temperature, salinity and depth with additional parameters such as dissolved oxygen, nutrients (e.g. dissolved phosphates and nitrates) often being included. Density of the sample is calculated from salinity, temperature and depth values and is expressed in grams per cubic centimetre. As a matter of convenience it is usual in oceanography to quote only the last four figures in the form of a quantity called $\sigma_{s,t,p}$ defined as:

$$\sigma_{s,t,p} = (\text{density} - 1) \times 10^3 \qquad \text{(I.4)}$$

This is referred to as the *in situ* value. For many applications in synoptic oceanography the pressure effect on density can be ignored and a quantity $\sigma_{s,t,0}$ is used, commonly abbreviated to σ_t. This is the density difference of the water sample when the total pressure on it has been reduced to atmospheric (i.e. the water pressure equals zero) but salinity and temperature are as *in situ*. The relationship between σ_t, salinity and temperature is a complicated

non-linear expression which has been derived by several investigators (see amongst other, Knudsen, 1901; Bein et al, 1935; Li, 1967; Wang and Millero, 1973) with the latter accepted as being most accurate. A computer programme has been written for Wang and Millero's equation of state of seawater (Appendix 1) and is used in the calculation of σ_t. Alternative methods include the use of tables which are entered with the appropriate values of salinity and temperature. Values for σ_t are quoted without units because specific gravity is actually used in the definition rather than density. The reason the pressure terms of $\sigma_{s,t,p}$ can be omitted is that water masses at the same depth (i.e. the same pressure) or over the same range of depths, are usually being compared. (According to classical definition (e.g. Sverdrup et al, 1942) a *water type* is identified by single temperature (T) and salinity (S) values, whereas a *water mass* is normally characterised by a portion of a T-S curve.) Associated with the change of density with pressure is a change of temperature if the water does not exchange heat with its surroundings (adiabatic change). The temperature a water sample would attain if raised adiabatically to the sea surface is called the *potential temperature* and has been designated θ . The density of a water sample appropriate to its salinity and potential temperature is called *potential density*.

The *specific volume* is the reciprocal of density and for some purposes is more useful in the calculation of currents from the distribution of mass. The specific volume *in situ* is written as $\alpha_{s,t,p}$; for convenience a

specific volume anomaly (also called steric anomaly by Montgomery and Wooster (1954)) δ is defined as:

$$\delta = \delta_{s,t,p} - \delta_{35;0,p} \qquad (I.5)$$

The last quantity is the specific volume of an arbitrary standard seawater of salinity $35^{o}/_{oo}$ and temperature $0^{o}C$ at pressure p. This standard was chosen so that δ is usually positive. Again the connection between α or δ and salinity, temperature and pressure is complicated. Bjerknes and Sandstrom (1910) showed that δ could be broken down into components as:

$$\delta = \delta_{s} + \delta_{t} + \delta_{s,t} + \delta_{s,p} + \delta_{t,p} + \delta_{s,t,p} \qquad (I.6)$$

where δ_{s} represents the main effect of salinity, $\delta_{s,t}$ represents the interacting effect of salinity and temperature, etc. In the strict sense of isanosteric analysis (i.e. equal entropy surfaces), potential steric anomaly must be used. However, Montgomery and Wooster (1954) pointed out that in the actual oceans the sum of the first three terms, $\delta_{s} + \delta_{t} + \delta_{s,t} = \delta_{T}$, is adequate in most practical cases to describe the specific volume of water masses and called this term, δ_{T}, the *thermosteric anomaly*. In recent years this parameter has come to be used frequently instead of σ_{t} to describe the physical properties of ocean water. The fundamental units for α, the δ's and δ_{T} are cm^{3}/g with numerical values for δ_{T} between 50-600 x 10^{-5} cm^{3}/g. To avoid having to write the 10^{-5} in numerical values, it is practice to express these quantities in centilitres per metric ton (i.e. cl/t), the small difference between the litre and

1000 cm^3 being disregarded. As with σ_t, tables exist for the computation of these variables, but, in this thesis, the equation of state of seawater (Wang and Millero, 1973) is used throughout (Appendix 1).

There are two kinds of physical process which influence the distribution of hydrographic properties and of dissolved or suspended substances in seawater. In *advective processes* large scale movements of water occur carrying dissolved or suspended matter with them, while in *diffusive processes* an exchange of these properties takes place without any overall transport of water. The first class of processes includes ocean currents at all depths and vertical movements of upwelling or sinking water masses. Diffusive effects are produced by turbulent mixing both in vertical and horizontal directions on a very wide range of scales. Molecular diffusion usually occurs so slowly relative to turbulent mixing that its direct influence may be neglected, except in a few specialised circumstances, such as gas exchange across the sea surface.

Oceanic turbulence, which includes all processes contributing to mixing and dispersion in ocean-waters, may be classified in general terms as mean flow, turbulence and molecular motion. In the molecular case, motion takes place on an extremely small scale (i.e. the movements of individual molecules). The effect of molecular movements on the dynamics of the mean flow is parameterised by introducing a coefficient of viscosity. The mixing effect is represented by a coefficient of diffusion and both

coefficients can be related to statistical properties of molecular motion. For diffusion of a given substance, the coefficient of diffusion is a physical property of the fluid, dependent on temperature, salinity and pressure, but not on position in the fluid or on flow pattern.

The separation of a field of flow into mean and turbulent components involves averaging over certain intervals of time or space. The mean velocities and concentrations determined are then treated explicitly as functions of time and position. Fluctuations from the mean are treated statistically and their influences on mean flow or mean concentration of a dissolved substance, for example, are parameterised by introducing eddy coefficients of viscosity and diffusion. The analogy between the eddy coefficients and molecular coefficients is only partial, in that eddy coefficients depend on the scale of motion, the position in the field of flow and the overall flow pattern.

The closer the network of measurements in space and time, the more detailed are the observed patterns of water movements or of the concentration of a particular substance. Fairly coarse horizontal station spacing permitted detection of large eddies associated with the Gulf Stream, just as large vertical separations of sample bottles in a typical hydrographic cast allow the main water masses of the oceans to be distinguished. There are usually differences of several orders of magnitude between vertical and horizontal scales of turbulent movement and in the effects which they produce. This is due partly to the ratio of width to

depth of the ocean and also to the influence of the stable density gradient, which greatly inhibits turbulent movements in the vertical without appreciably affecting the horizontal components. Because of this difference, it is often convenient to treat vertical and horizontal mixing separately.

The turbulance responsible for vertical mixing is generated in two main ways: (i) by the stress of the wind on the sea surface, acting through wave motion and surface drift and (ii) by vertical shear in currents, arising in various ways in the interior of the sea and from the action of bottom friction. A very broad spectrum of horizontal motions occurs in the ocean. The largest scale are the wind-driven circulations of ocean-wide dimensions. Developing from these are eddies of about 100 km in diameter breaking down into smaller ones (ca. 10 km in diameter) and so on through a cascade of decreasing sizes.

The quantitative treatment of mixing problems has therefore led to the development of the advection-diffusion equation. Using the nomenclature of Bowden (1975), u, v and w are the components of velocity of water parallel to the rectangular axes OX, OY and OZ respectively, with OX and OY in a horizontal plane and OZ vertically downwards. Considering the distribution of some property which has a concentration c per unit mass and assuming that the turbulent transport analogy of molecular diffusion can be regarded as a process of eddy diffusion, then across a plane perpendicular to OZ the rate of transport per unit area may be

represented by:

$$T_z = -\rho K_z \frac{\partial c}{\partial z} \qquad (I.7)$$

where ρ is the density of water, K_z is defined as the coefficient of eddy diffusion in the vertical direction (i.e. the *vertical eddy diffusivity*). Coefficient K_x and K_y may be similarly defined for turbulent transport across planes perpendicular to OX and OY respectively. In the sea, K_z is usually in the range $0.1 - 10^3$ cm^2 s^{-1}, while K_x and K_y fall within the range $10^4 - 10^8$ cm^2 s^{-1}.

The general equation governing the concentration, c, of a particular constituent at any point in the sea may be written:

$$\frac{\partial c}{\partial t} + u \frac{\partial c}{\partial x} + v \frac{\partial c}{\partial y} + w \frac{\partial c}{\partial z} = \frac{\partial}{\partial x}\left(K_x \frac{\partial c}{\partial x}\right) + \frac{\partial}{\partial y}\left(K_y \frac{\partial c}{\partial y}\right) + \frac{\partial}{\partial z}\left(K_z \frac{\partial c}{\partial z}\right) + R \qquad (I.8)$$

where R denotes the rate of consumption (or production) of c within a small volume surrounding the point itself. The decay of a radioactive substance would be represented by R equal to $-\lambda c$, where λ is the decay constant. For a conservative property such as salinity, $R = 0$.

The above equation, which allows for both advection and turbulent mixing in three dimensions, is too complicated to be solved in its general form. In a particular problem some of the terms are likely to be small (compared with those represented the main processes) and can be neglected. These may include steady state solutions (i.e. $\partial c/\partial t = 0$) with:

(i) Horizontal flow and vertical mixing, for which equation I.8 reduces to:

$$u \frac{\partial c}{\partial x} = \frac{\partial}{\partial z} \left(K_z \frac{\partial c}{\partial z}\right) + R \qquad (I.9)$$

(ii) Horizontal flow and lateral mixing, for which equation I.8 reduces to:

$$u \frac{\partial c}{\partial x} = \frac{\partial}{\partial y} \left(K_y \frac{\partial c}{\partial y}\right) + R \qquad (I.10)$$

(iii) Radioactive decay and vertical mixing, for which equation (I.8) reduces to:

$$\frac{\partial}{\partial z} \left(K_z \frac{\partial c}{\partial z}\right) - \lambda c = 0 \qquad (I.11)$$

and if K_z is independent of depth:

$$K_z \frac{\partial^2 c}{\partial z^2} - \lambda c = 0 \qquad (I.12)$$

(iv) Vertical flow and vertical mixing, for which equation (I.8) reduces to:

$$w \frac{dc}{dz} = K_z \frac{d^2 c}{dz^2} + R \qquad (I.13)$$

or time-dependent solutions with

(i) Vertical mixing only, for which equation (I.8) reduces

$$\frac{\partial c}{\partial t} = \frac{\partial}{\partial z} \left(K_z \frac{\partial c}{\partial z}\right) + R \qquad (I.14)$$

again if K_z is independent of depth:

$$\frac{\partial c}{\partial t} = K_z \frac{\partial^2 c}{\partial z^2} + R \qquad (I.15)$$

(ii) Spreading of a patch by horizontal diffusion for which equation (I.8) reduces to:

$$\frac{\partial c}{\partial t} = \frac{1}{r} \frac{\partial}{\partial r} \left(K_r \frac{\partial c}{\partial r}\right) + R \qquad (I.16)$$

if the distance of any point from the centre is denoted by r and $K_x = K_y = K_r$.

Further considerations lead to introduction of box type models of the ocean when considering the overall distribution of a constituent. The large temperature gradient, high stability and very small coefficient of vertical eddy diffusion in the thermocline means that it acts as a partial barrier between water masses above and below it. In the simplest model, therefore, the world ocean is represented by two boxes or reservoirs, the first representing the surface layers to a depth of 100-200 metres and the second the deeper layers from this depth to the bottom, with the thermocline separating them. Complete mixing within each box is assumed to take place very rapidly but exchange between the two boxes takes place comparatively slowly. The concentration of a given property within a box is given by a single value (i.e. the mean concentration for the box) and the exchange between two boxes is specified using exchange-rate or transfer-rate constants. The rate of consumption or decay of a non-conservative constituent within a box is represented by a suitable parameter. A box model may be regarded as a finite difference analogue of the advection-diffusion equation I.3, which is expressed for continuously variable functions.

Bainbridge (1963) estimated, on the basis of a simple one-compartment model, that the mixing time for tritium in ocean surface water is about 3.5 years. Eriksson (1965) criticised this estimate because it emphasised tritium fallout data from continental stations for these North Pacific samples. He estimated that for a mixing depth of 75 metres a 22 year turnover time would be required for the mixing layer. He acknowledged, however, that turnover

times and mixing depths are interdependent and cannot be resolved with precision. Tamuly (1974) also supported a 14-35 year turnover rate, for the mixed layer in the Southern Ocean, this rate being variable with latitude.

Rooth and Ostlund (1972) suggested that vertical exchange is the least understood aspect of oceanic transport processes and that for optimal resolution in the determination of the parameters of a diffusive-advective boundary layer, the mean tracer life should be about one-tenth of the diffusion time scale. This means that tritium is an almost ideal tracer in oceanic thermoclines, where the characteristic diffusion timescales are currently thought to be ~ 300 years. Their paper on the penetration of tritium into the Atlantic thermocline shows how excellent results can be achieved by precise sample collection and data reduction. Eighteen Degree Water (EDW), a uniform water mass with minimal vertical variation in several parameters, is recognisable throughout the Sargasso Sea where tritium samples were collected. Uniform tritium concentrations of 8.3 ± 0.3 T.U. were observed just above the EDW. A temperature gradient (i.e. dT/dz where dz equaled 60 metres) versus temperature yielded an exponential temperature profile asymptotic to 2.3°C (i.e. dT/dz equaled 0 at 2.3°C). This was further supported by an exponential curve of temperature versus depth with a scale height of 420 metres and a temperature range $5^{\circ}C < T - 2.3^{\circ}C < 15^{\circ}C$ over which joint diffusion of tritium and temperature were indicated. Scale height is taken as that depth interval over which a measured parameter decreases by $1/e$. Assuming

a diffusive thermocline model where vertical diffusivity affects both the temperature field and the tritium distribution then plotting tritium concentration against temperature anomaly on logarithmic scales should yield a straight line. In fact, the data points were found to be distributed in not one but two straight lines. Their immediate conclusion was that the evolution of the tritium profile was not a laterally homogeneous process of downward diffusion but that, with a weakening of local vertical diffusion away from the Sargasso Sea gyre, lateral exchange or advection processes tended to become more effective. They suggested that the advective models of the thermocline, with quasi-horizontal exchange and circulation almost everywhere, have to be preferred over those built on laterally uniform vertical diffusion coefficients.

Via equation I.8 and assuming that the temperature distribution in the main thermocline is governed by a similar equation (except for the absence of the time dependence) and that the diffusion coefficients for heat and tritium are identical, a set of empirical relations were found to be an adequate description of their data. Local vertical exchange below the core of EDW was represented by a diffusion with a vertical exchange coefficient of $K_v = 0.20 \pm 0.03$ cm^2/sec. However, assuming a gross penetration of tritium due to a vertical diffusion process a vertical exchange coefficient of $K_v = 0.75$ cm^2/sec was deduced.

Begemann and Libby (1957) suggested that movement into the ocean depths is apparently quite slow. Bowen and Sugihara (1960), however, indicated that there was about three to four times as much ^{90}Sr below 100 metres as above. If the same ratio holds for tritium, a sizeable tritium reservoir could exist in the ocean depths. Indeed, several observers have recorded tritium at depths exceeding 1000 metres. Recently, Michel and Williams (1973) have performed tritium measurements on samples from the Antarctic Ocean. The high tritium concentrations found in certain deep water masses indicate an input of surface water into these masses in the last ten to twenty years.

Efforts to study directly the mechanics of the oceanic mixing processes are currently underway at several of the world's oceanographic research centres. The task is formidable, however, and no short route seems to lead to a quantitative model of vertical exchange, based on detailed knowledge of the processes. It is important to continue, in parallel, the pursuit of the large scale effects of the mixing processes. Until such understanding has been established, empirical representations of the eddy exchange effects have to be used in numerical models and in applications such as those in geochemistry or ecological problems.

I.5 AIMS OF RESEARCH.

From the discussion in the previous sections of this chapter, it is apparent that the measurement of tritium levels in various ocean water masses offers a fruitful field for future long term study. Not only may much immediate information be obtained from the tritium levels measured within the various ocean water masses but continued collection of tritium data by various workers will help to resolve the present lack of understanding of mixing and vertical-horizontal advection-diffusion processes.

Tritium cannot, as yet, be measured *in situ* so that samples are brought to the surface and returned to shore laboratories for analysis. This introduces the risk of sample contamination since ambient tritium levels can range from 10-100's T.U. while sample concentrations are rarely greater than 10 T.U. Such problems are significant in this study. The major aims of this research project are therefore:

(i) development of techniques for the extraction of pure, contaminant-free tritium samples from seawater,
(ii) construction and calibration of an electrolytic enrichment system for concentration of HTO in water samples,
(iii) construction of one stage methane synthesis systems and purification lines for conversion of water samples to methane,
(iv) optimisation and calibration of a gas proportional counter for determination of tritium levels in water

samples using internationally accepted standards, and

(v) use of the tritium levels in seawater, together with conventional hydrographic data, to deduce the physical structure of selected areas of the oceans.

CHAPTER II

SAMPLING AND ANALYTICAL PROCEDURES.

II.1 Introduction.

The extremely low concentrations of tritium in the hydrosphere (ca 10^{-18} T/H) necessitate specialised analytical techniques. In brief, the procedure consists of proper sampling, distillation to remove salts, electrolysis to concentrate heavy hydrogen, deuterium analysis before and after electrolysis, and radiometric measurement in a gas proportional counter.

II.2 Methods of Measurement of Tritium.

Neglecting reactor outputs, the highest concentrations of tritium observed in natural waters (i.e. in continental rains after thermonuclear tests) were around 1000 T.U. With present detection methods alone (either gas counting or mass-spectrometry) most natural tritium concentrations, which lie considerably below this maximum limit, cannot be determined directly. For example, with a clean mass-spectrometer employing an electron multipler to amplify the ion beam signal, the limit of sensitivity is still about 10^8 times higher than the maximum signal available from a tritium sample of natural concentration. Direct gas proportional counting of tritium is possible for concentrations as low as about 200 T.U. using a counting system of the kind to be described later. Thus, only for natural waters with highest tritium concentrations is direct counting suitable.

An increase in sensitivity by a factor of ten may be possible with larger volume high-pressure counters and mercury-wax shielding. Cloud chamber techniques (Fireman and Schwartzer, 1954) and internal Geiger-counting have limits of detection comparable to or higher than the system employed here. Neutron activation would produce ^{4}H but the half-life is of the order of microseconds (Schein et al, 1955 and 1956). The probable daughter, ^{4}He, is stable and would be present in immeasurably small quantities. Measurement of ^{3}He from the disintegration of ^{3}H has been considered by Clarke (personal communication, 1971) whereby ^{3}He is allowed to accumulate in very well degassed samples and then measured mass-spectrometrically. With a mass-spectrometer of detection limit around 10^{4} atoms, a 5 kg water sample and a sample storage time of about 1 year, tritium contents of approximately 0.001 T.U. could be measured.

In areas of expected high tritium concentrations (i.e. atomic reactors, heavy water plants, radioactive processing and disposal plants, etc.) other instruments have been developed which use various modifications of internal counting. Pittendrigh and Vousden (1954) developed a differential ionisation-chamber instrument which can operate with no significant error in a uniform gamma field. Gutman (1961) devised a Geiger-counter instrument for detecting traces of tritium oxide in air. Tritium steam is thermally decomposed over heated tungsten or magnesium to liberate tritium gas, which is separated from other gases by diffusion over a nickel or palladium tube. Ballard and Ely (1963) also developed a tritium oxide monitoring instrument with a Geiger-counter as detector. They, however, extracted water vapour

from the air with a dehumidifier and counted the water vapour directly in a heated flow-counter using a Geiger mixture of helium or helium/isobutane along with water vapour. Sannes and Bannville (1965) have developed a monitor with a spiral plastic scintillator for the detection of tritium. The classical detectors for tritium decay remain the ionisation chamber, the proportional counter, and the G-M tube although liquid scintillation detectors have been developed more recently and are now also becoming standard equipment. Liquid scintillation counting of tritium permits rapid analyses of aqueous samples but suffers the difficulty of incorporating aqueous samples into solvents at the temperatures required for good counting characteristics (Baxter et al, 1964). Compared to the electrolytic enrichment followed by scintillation counting, there is probably little difference when samples are not below 10 T.U. and this counting method is gaining widespread approval (Theodorsson, 1974). Geiger-counters have been used for counting tritium by introducing the tritiated gas directly into the counters. Proportional counting is preferred, however, because the pulses produced are linearly related to the β energy so that all other noise and contamination pulses can be discriminated out. Also, the pulses are not so large that they induce appreciable dead times. Hence proportional counters combine the advantages of simplicity, maximum sensitivity, and applicability to a wide range of counting gases. For accurate measurements the samples must be counted in the gaseous state (Wolfgang, 1963). The gas proportional counter is about an order of magnitude more sensitive than liquid scintillation instruments (Lal and Athavale, 1966; Sauzay and Schell, 1972). The samples can be counted as hydrogen

or can be converted to ethane, methane, or other hydrocarbons (see amongst others, Ostlund and Werner, 1962; Robinson, 1963; Bainbridge, 1965).

It remains clear, however, that the limit of detection of tritium is greater than the natural concentration of tritium in the environment and cannot be measured directly (Grosse et al, 1951). Even with the increase in tritium levels due to thermonuclear testing, the concentration of environmental tritium remains so low that its direct measurement is only rarely possible (Verhagen and Sellschop, 1963). The sample must be pre-enriched in tritium relative to protium prior to the counting operation.

Several methods have been developed, particularly since 1939, which permit the separation, or at least the concentration, of many isotopes (Moeller, 1954). Most of the procedures are physical in character because mass differences produce greater differences in physical than in chemical properties. Fortunately isotopic fractionation of hydrogen isotopes is the easiest of all to induce due to the large mass ratio for tritium to protium of 3:1 or 4:2 in the case of $HT:H_2$ or 20:18 for HTO to H_2O.

The partial demixing of gases in a temperature gradient is called thermal diffusion; the heavier isotopes are concentrated in cooler regions. The first experimental verification was provided by Chapman and Dootson (1917) but the degree of separation was not large with enrichment factors of only 1.06 - 1.09. A two stage thermal diffusion column for tritium enrichment has been described by Verhagen and

Sellschop (1965), whereby enrichments of x100 were obtained after 9 hours and x800 after 30 hours of operation. Roether (personal communication, 1971) also describes a thermal diffusion column with two stages and a storage volume in series. Tritium recovery exceeds 95% with overall enrichment of about x15.

In 1919 Lindeman presented theoretical arguments indicating that isotopes could be enriched by distillation since rates of escape of atoms or molecules from a liquid surface are generally inversely proportional to the square roots of their masses (Moeller, 1954). Preliminary concentration of heavy water has since been effected using the distillation technique. The separation factor 1.036, however, is rather small and multistage distillation techniques are therefore necessary for satisfactory enrichments (Becker, 1962). The major drawbacks to distillation as an enrichment process are the relatively long times required for enrichment (ca 28-50 days for 1 litre of water), the modest enrichment factors attained (ca x 6.3 - 15, respectively) and the poor reproducibility (Smith and Rawson, 1962). Following concentration by distillation, further reconcentration and volume reduction would be required for counting low activity tritium samples. Thermodynamically, hydrogen gas distillation is much more attractive than water distillation but the low boiling point of liquid hydrogen (-259^{o}C) requires use of highly specialised techniques and handling (Jacobs, 1968).

Gas chromatographic methods have been developed whereby suitable chromatographs can separate tritium-hydrogen mixtures. Hoy (1968) developed a palladium chromatograph

which can be used to detect fewer than 10 T.U. The method is rather complex but a 12 fold degree of enrichment can be attained with nearly complete recovery and high reproducibility (Borowitz and Gat, 1964). Besides the problem that for aqueous samples large quantities of water must be converted to hydrogen gas without fractionation, the method is tedious and time consuming since only 25-50 cc of gas can be enriched during a single operation lasting 30-60 minutes.

Electrolysis was first suggested as a means of isotope separation by Kendall and Crittenden in 1923 but was not confirmed until 1932 by Urey (1933). Various apparatus and procedures have been described. Ostlund and Werner (1962) described a cell similar to that developed earlier by Brown and Grummitt (1956). Large electrode surfaces were used with iron as cathode and nickel as anode. From a 250 ml sample, 50 mls were introduced into the electrolysis cell and approximately 0.6 g of sodium hydroxide added. When the volume had been reduced to 25 mls, after about 24 hours, an additional 25 mls of sample were introduced and the "periodic-addition" electrolysis continued. Following electrolytic enrichment, the sodium hydroxide was neutralised with carbon dioxide and the sample distilled. Brown and Grummitt (1956) performed their enrichment electrolysis in several stages, with distillation of the samples between stages to keep the concentration of hydroxide in the optimum range 1-20% w/w. Roether (personal communication, 1971) uses noble metal electrodes, a potassium sulphate electrolyte and a procedure similar to that of Ostlund and Werner. Metson (1969, 1973) improved the procedure by using a reservoir feed system and a motor driven variable output transformer.

The simplicity of electrolytic enrichment in which large volumes of water sample may be handled conveniently on a laboratory scale renders it the most attractive technique for pre-enrichment of natural samples and it was therefore adopted for this programme. Figure II.1 presents a flow diagram of sample analysis including the associated times involved and sample size at each step in the procedure.

II.3 Sampling.

Various procedures have been employed here to sample natural waters. Rainwater at Glasgow was collected directly into beakers situated near the laboratory and needed no supervision. Laboratory atmospheric samples were condensed onto a copper tube surrounded by a polyethylene funnel and immersed in a dewar of liquid nitrogen (Figure II.2).

In the case of ocean samples, two methods were used. Thirty litre Niskin bottles made of PVC were strung along a hydro-wire, each being separated from the other by a distance appropriate to the distribution of the water masses at each station. For the Pacific ocean samples, however, nine 30 litre Niskin bottles were after arranged around a rosette surface activated multiple sampler (SAMS). To each SAMS was fitted a salinity-temperature-depth (STD) probe and bottom pinger which, supported by a conducting cable, permitted continuous monitoring on deck. Electronic triggering from the surface closed the bottles at the desired depth. On deck, the seawater was withdrawn from the Niskin into various sample storage vessels. Dissolved oxygen samples were always drawn first, followed by those for tritium, stable iso-

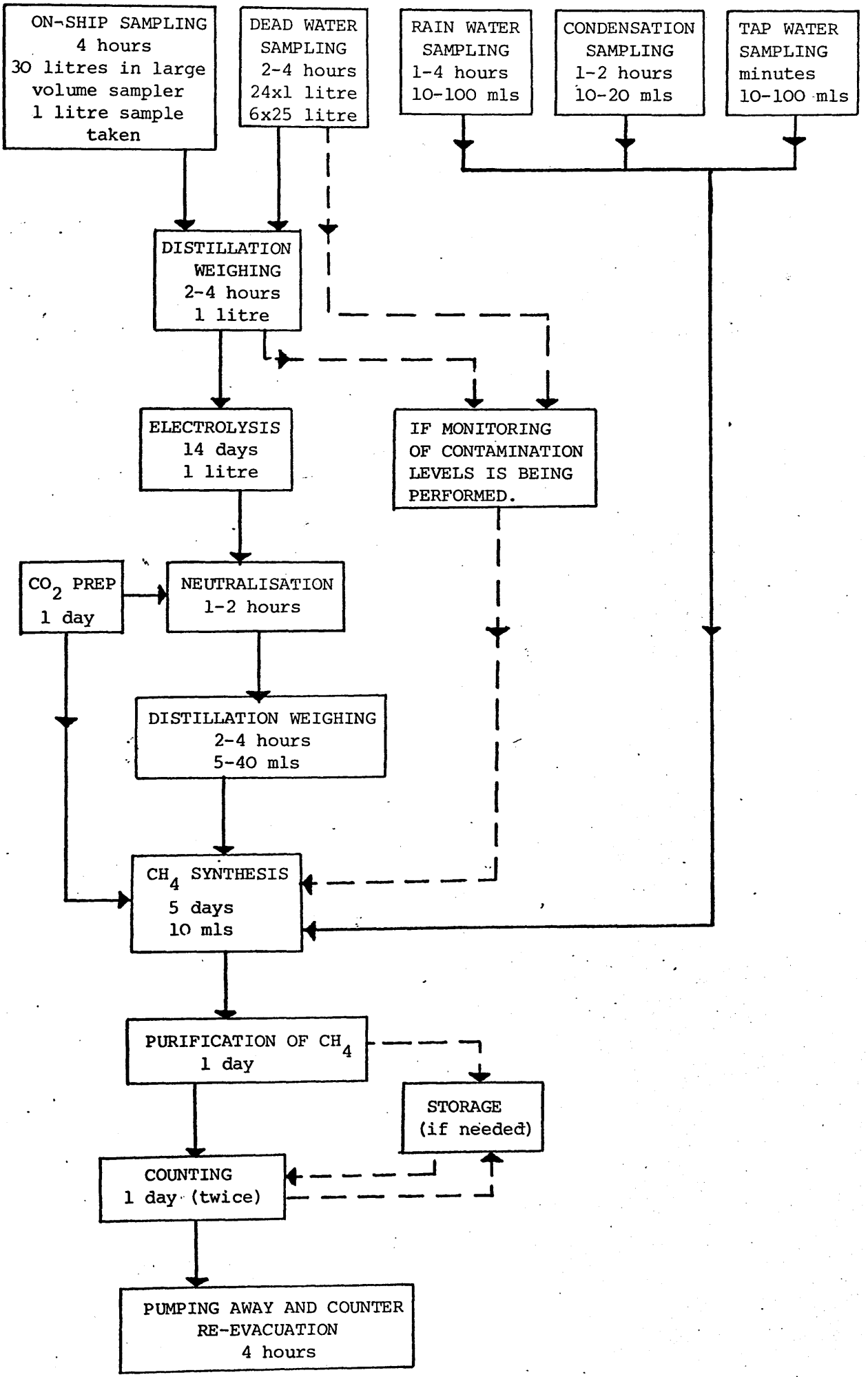

FIGURE II.1 FLOW DIAGRAM FOR TRITIUM ASSAY.

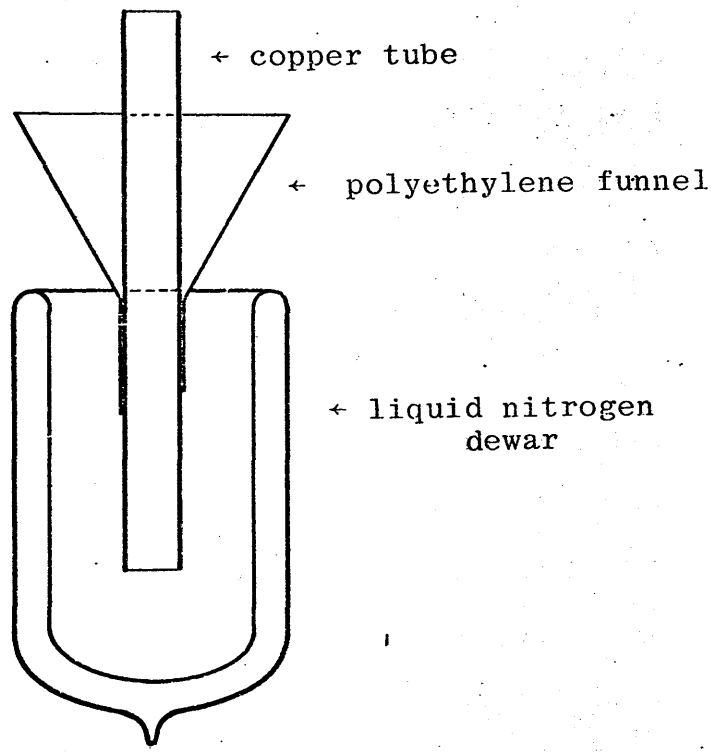

Figure II.2 Atmospheric Moisture Condenser.

tope, pH, salinity and nutrient analyses. Unfortunately the inclusion of concomitant collection of these auxiliary samples with each tritium sample was outwith the author's control as was the location of each station and sampling depths. Care is needed to ensure that no tritiated materials (luminous watches, paints, etc.) come into contact with the sample during collection. Ostlund (personal communication, 1971) described watch faces containing at least 25 m Ci tritium which released up to several thousand μ Ci tritium per year, and which upon contact with tritium-free water contributed several hundred T.U.'s of contamination within 10-60 minutes. Samples were drawn via a catheter attached to the Niskin bottle spigot so that the storage vessel filled from the bottom up. This water was discarded as a bottle rinse and then the container was refilled in the same manner and sealed securely allowing space for water expansion on warming. The water samples for this study were stored and transported in either (i) 1 litre amber glass bottles or (ii) 2.3 litre Winchesters (each with threaded bakelite caps forming a seal between the top of the glass bottle and the insert of the cap) or (iii) 1 litre ground-glass stoppered bottles. Finally, the caps or stoppers were all sealed securely with tape, wax or heat-shrink tape to prevent loosening and possible leakage of contents or exchange with the atmosphere.

II.4 Distillation.

Each 1 litre seawater sample is first distilled to dryness to separate out all salts and organic material. Figure II.3 shows the distillation apparatus which consists essentially of a 3 litre round-bottom flask set in a heating mantle with a quadruple-collection spray protector (to ensure complete separation of water from sea salts and solids). A vacuum-distillation head follows the Leibig condenser into a tared 1 litre round-bottom receiving flask. A drying tube containing silica gel is also connected to the vacuum-distillation head and an atmospheric pressure distillation is performed.

Since, during the subsequent electrolysis, the electrodes are extremely sensitive to corrosion from impurities, a 10 ml aliquot of each distillate is removed and the conductivity measured with a Pye Unicam Mel Conductivity Bridge using platinum electrodes. The maximum acceptable conductance value was 300 μ mho (Ostlund, personal communication) which corresponds to an impurity level of 180 ppm Total Dissolved Solids (TDS). Higher values cause rapid corrosion and severe deterioration of the electrodes during electrolysis. All samples, however, are well below these values in the region 10-185 μ mho (6-111 ppm TDS).

II.5 Electrolytic Enrichment.

The electrolysis is performed using the system shown in Figure II.4. An alkaline solution is electrolysed. Experience has shown that the concentration of hydroxide

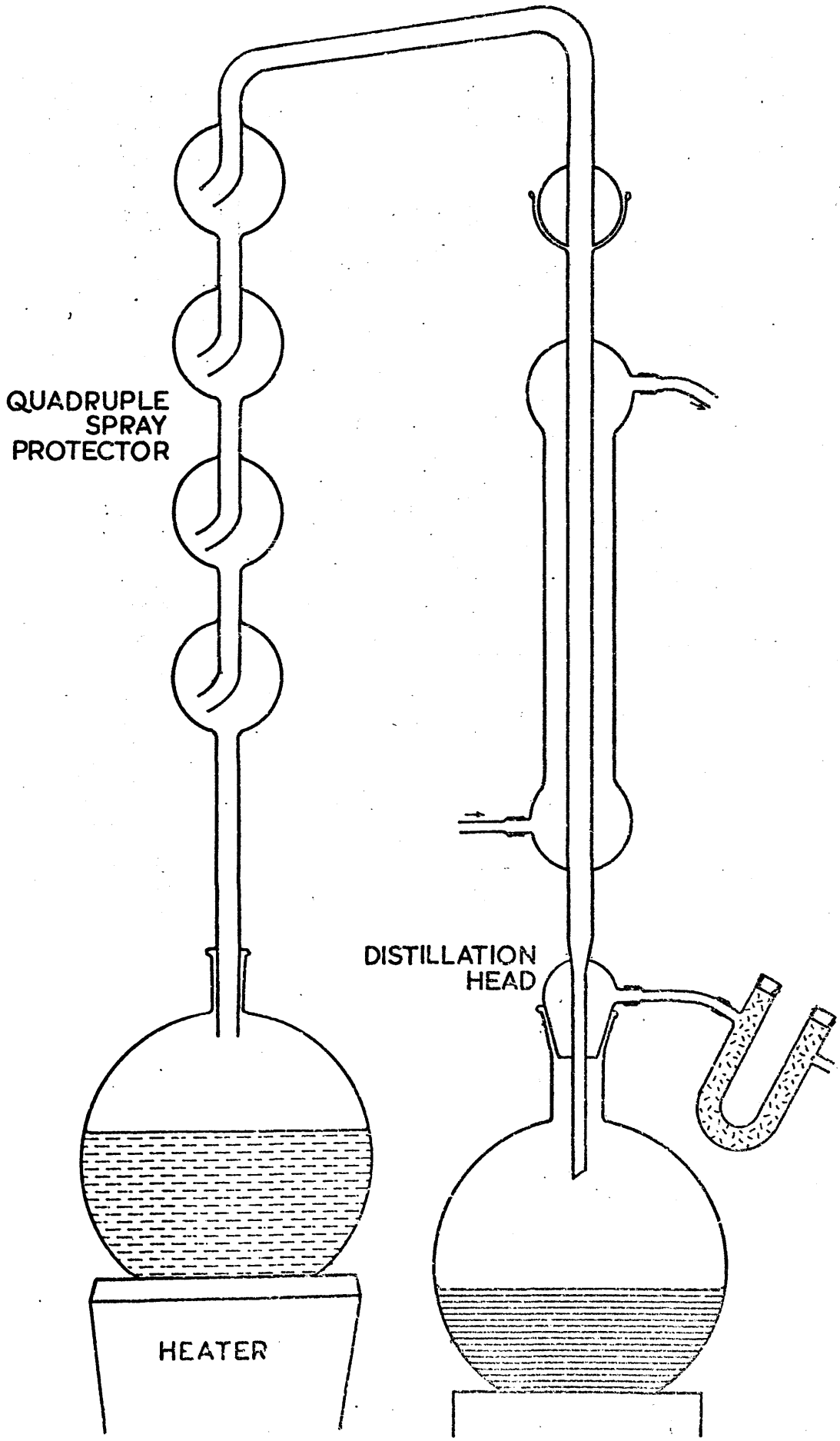

Figure II.3 Distillation Apparatus.

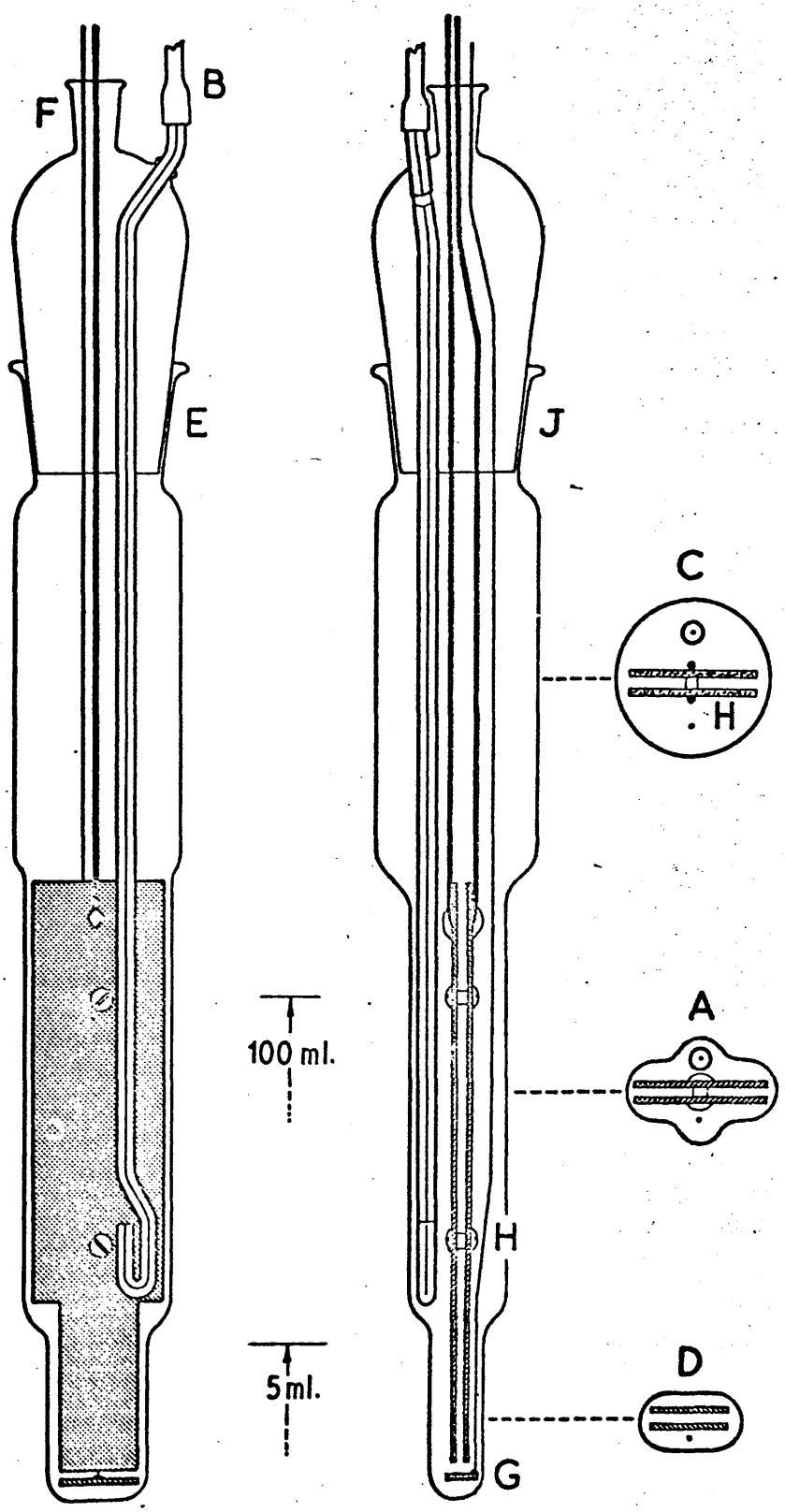

Figure II.4 Electrolysis cell and electrodes showing
A : middle cross-section and implosion channels; B : reservoir supply tube; C : upper cross-section; D : lower cross-section; E : B35 socket; F : B14 socket; G : probe placement; H : 3mm nylon spacers; J : Electrolysis head with B35 cone.

should be between 1-20% w/w if corrosion of electrodes is to be prevented. Recently, Theodorsson (1974) has investigated the limits within which the electrolyte concentration must be maintained to avoid corrosion of the electrodes. A decrease in initial hydroxide concentration increases the voltage needed to maintain the same constant current and therefore induces increased heat dissipation in the cell and hence temperatures rise. The higher temperature increases the rate of corrosion and Theodorsson concludes that this is possibly the main cause of the problem. At the final stages of electrolysis, current density is usually highest and the temperature will therefore reach its maximum. He again concludes that this particular temperature rise is probably the main cause of corrosion. Experience in the Glasgow laboratory is, however, in disagreement with Theodorsson's last conclusion. The electrolysis equipment, to be detailed elsewhere in this section, controls current density throughout the entire electrolysis, maintaining a constant level and in fact a decrease in heat dissipation occurs as electrolysis proceeds. Occasionally, during some electrolysis, corrosion of electrodes occurred during final stages but this cannot be attributed to thermal decomposition. The question remains unresolved but the corrosion phenomenon seems more likely related either to electrolyte concentrations exceeding 20% w/w or to TDS levels concentrating above 180 ppm. Tritium enrichments ranging from about x6-x20 with volume reduction factors between 10-1000 fold, however, have been obtained by electrolysis either in successive stages (Brown and Grummitt, 1956; Kaufman and Libby, 1954) or via periodic addition (Ostlund and Werner, 1962). Following the suggestion of Metson (1969), an improved design of electrolysis cell

and associated electronics makes it possible to reduce initial sample volumes of 2.5-1 litres to 10-1 mls in one cell, thus decreasing the manual workload per sample and improving accuracy by reducing the number of liquid transfers.

The electrolysis cell is a modification of a design previously described by Ostlund and Werner (1962) and Allen et al (1966). To provide a large electrode surface area within a small volume, the 60 cm^2 electrodes are located in a flattened glass tube portion of the cell. The cross-section 'A' shows "channels" which have been designed to avoid implosion by evacuation; these channels also greatly aid convection of the liquid during electrolysis. The lowest, narrowest part of the cell has a capacity of about 5 ml; the total volume below the index mark being about 100 ml. The electrodes, shaped to fit the taper of the cell, are separated by 3 mm nylon spacers. A sample tube, B, is turned upward at the end to prevent electrolytic gases entering and thus terminating the syphon action.

The reservoir and feeding system shown in Figure II.5, consist of the 1 litre round-bottom receiving flask containing the distilled sample and the reservoir feed head. This head is simply an internal funnel, the end of which is ground to an angle of 30^{o}, with a 4 mm bleed tap connected to a high purity argon source during electrolysis to prevent introduction of tritiated atmospheric contaminants.

The electrodes shown in Figure II.4 consist of a pure nickel anode, a mild steel cathode and an iron sensing probe and connecting wire. Experiments were conducted on various

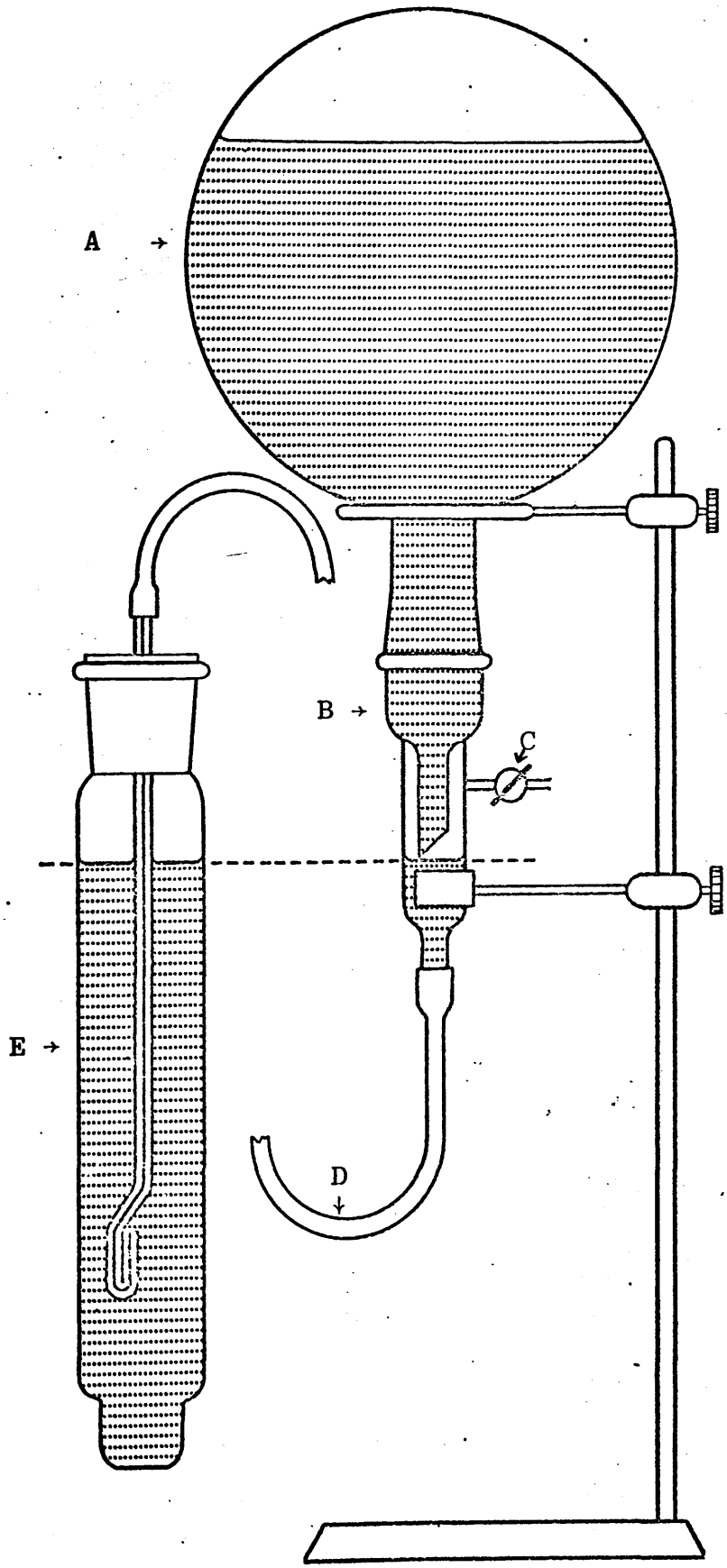

Figure II.5 The reservoir and feeding system showing A : Sample reservoir; B : B24 cone and reservoir feed head; C : 4mm bleed tap to high purity, dried argon; D : PVC tube; E : electrolysis cell.

electrode materials since preliminary electrolysis performed with 95% nickel anodes and mild steel cathodes failed through severe corrosion effects. Stainless steel cathodes were next constructed followed by 99% nickel anodes. Satisfactory results were obtained when electrodes of 99% nickel anodes and mild steel cathodes were used.

The metal electrodes and wire are initially degreased with trichloroethylene. The mild steel electrodes are given a high polish with fine steel wool pads until free from rust marks and blemishes. Following the investigations of Zutshi and Sas-Hubiki (1966) the cathodes are phosphate-coated. The mild steel electrodes are cleaned with hot detergent solution, dried, degreased with trichloroethylene and suspended in 5N phosphoric acid at 50^{o}C for 30 minutes. They are then washed with tritium-free water (see chapter III) rapidly dried, and stored in a closed container until required. The nickel anodes are also washed with hot detergent, dried and degreased with trichloroethylene before use. All copper wire connections to the electrodes are spot welded. 3mm nylon spacers separate each electrode and 6BA nylon screws and bolts maintain firm electrode pairs. The electrodes are stamped with an identifying mark and used repeatedly when sample activities are known to be comparable.

The sensing probe placement is critical to stable operation during electrolysis with maximum field effect experienced when the probe is parallel to the anode. Bubbles of the electrolytic gases, however, cause extreme instability in the main power supply and so produce a highly variable current density within the electrodes. With the probe

at right angles to the anode, the field effect is minimal but current density stability is maximised. Figure II.6 shows the relationship of probe placement and current density as a function of time.

The constant current density unit (CCDU) is a controlled output power supply. The probe registers fluctuations in the level of the electrolysing sample in the cell and the CCDU correspondingly adjusts the voltage to the main electrode plates so that a constant current density is maintained. Various safety features have been incorporated into the CCDU to prevent corrosion of the electrodes. Should either a short circuit occur or the current density exceed 200 m amps/cm^2, the units automatically shut down.

Following sample distillation, the tared 1 litre receiving flask is stoppered and reweighed. An electrode pair is selected and placed into an electrolysis cell. The electrolysis head and tube is fitted into the cell and sealed with black wax. 3.2 ml of a 40% NaOH solution (prepared from Na_2O_2 and tritium-free water in a high purity argon atmosphere) is syringed into the cell. The water sample is connected to the reservoir feed head which in turn is connected to the delivery tube. With the argon reservoir connected to the head, the syphon action is initiated and the entire sample and head adjusted to the appropriate 100 ml water level indicator. The unit is then clamped securely in a Perspex holding cage (Figure II.7). The NaOH concentration at this point is ~ 1% w/w. The electrodes and probe are connected to the CCDU and, since the electrolytic conductivity has a positive temperature coefficient, the cell

PROBE PLACEMENT VS. CURRENT DENSITY IN MAIN ELECTRODES.

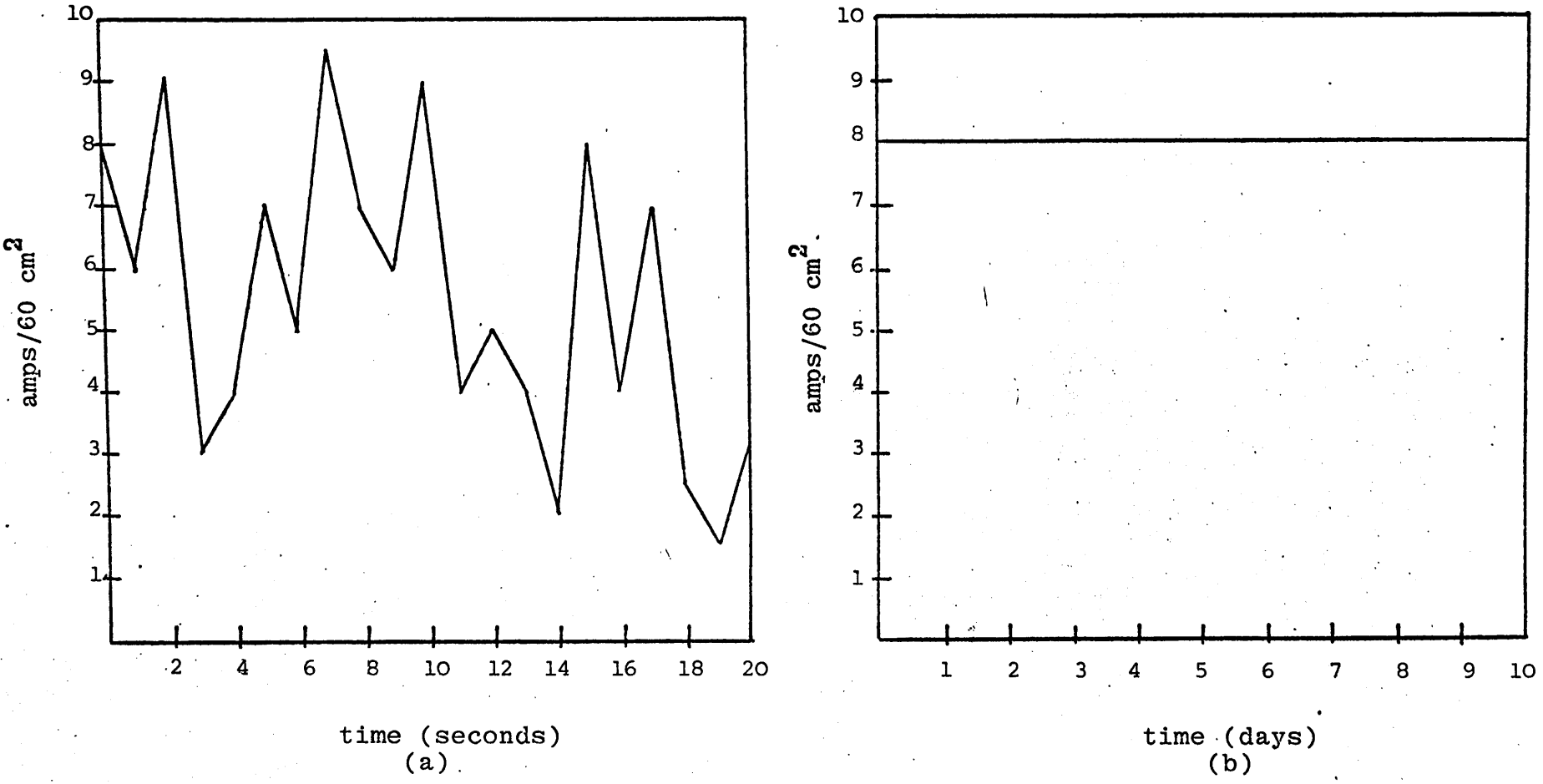

Figure II.6 Graph showing current density in main electrode plates as a function of probe placement (a) probe parallel to anode (b) probe perpendicular to anode.

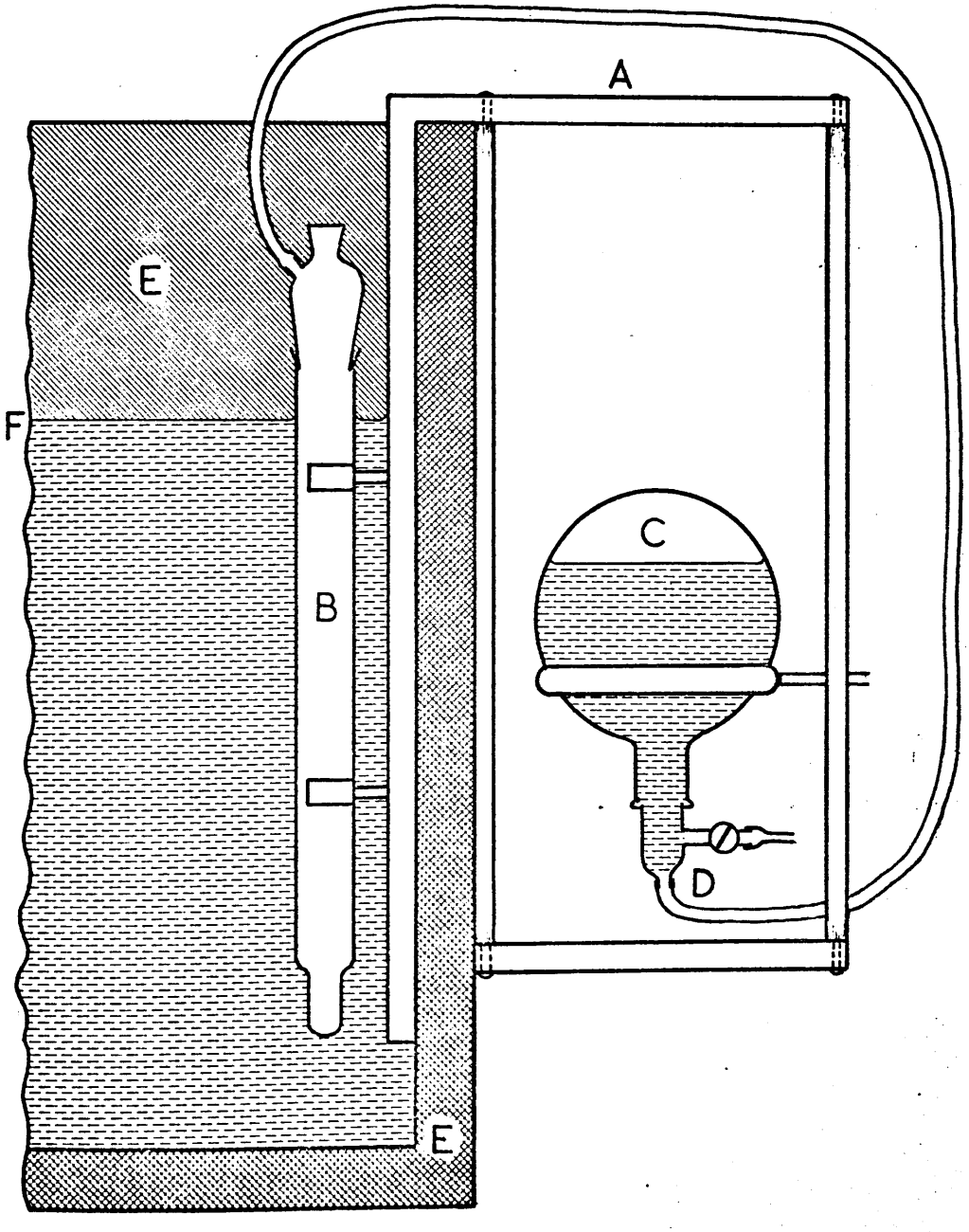

Figure II.7 Perspex holding cage (A) with electrolysis cell (B), reservoir flask (C) reservoir feed head (D), refrigerator wall (E) and water level (F).

is placed in a water bath at 10°C to prevent thermal run-away and loss of tritium. The water bath is in fact a top-loading freezer with ~ 12 ft^3 capacity, approximately two thirds filled with tritium-free water, covered with $\frac{1}{4}$-inch thick Perspex supporting a mechanical stirrer ensuring a homogeneous water bath temperature. The CCDU is then adjusted to deliver the maximum amperage (normally 8-10 amps). The sample is checked routinely to ensure that the electrolysis is proceeding correctly until the final volume reduction factor has been attained (normally 12-16 days). Figure II.8 shows the variation of current density, amperage, and volume of sample against time. A note is taken of the amp-hrs used during electrolysis.

With the electrolysis completed, the cell is removed from the holding cage and the delivery head plugged with a B10 and B14 stopper to reduce contamination risks. The sample is then neutralised with carbon dioxide prepared from marble chips heated to 1100°C. The carbon dioxide was studied both manometrically and mass-spectrometrically and was found to have a purity greater than 99%, to contain no water and to have a $\delta^{13}C$ value of -4.70% relative to PDB limestone (Fallick, personal communication). Furthermore, carbon dioxide prepared from marble chips in this manner has been used extensively as background gas for ^{14}C counting and has been shown (i) to have no radioactive content and (ii) to have less than 1 ppm electronegative impurities (Harkness, 1969; Stenhouse, 1972). Other materials could have been used (e.g. lead nitrate, Allen et al, 1966) but carbon dioxide neutralisation has the advantage that it converts the NaOH to Na_2CO_3 which is harmless to the electrodes and

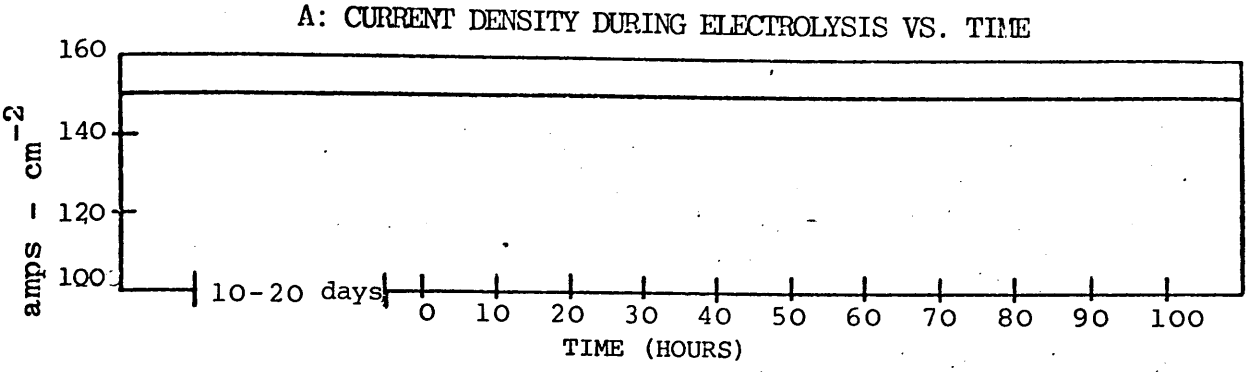

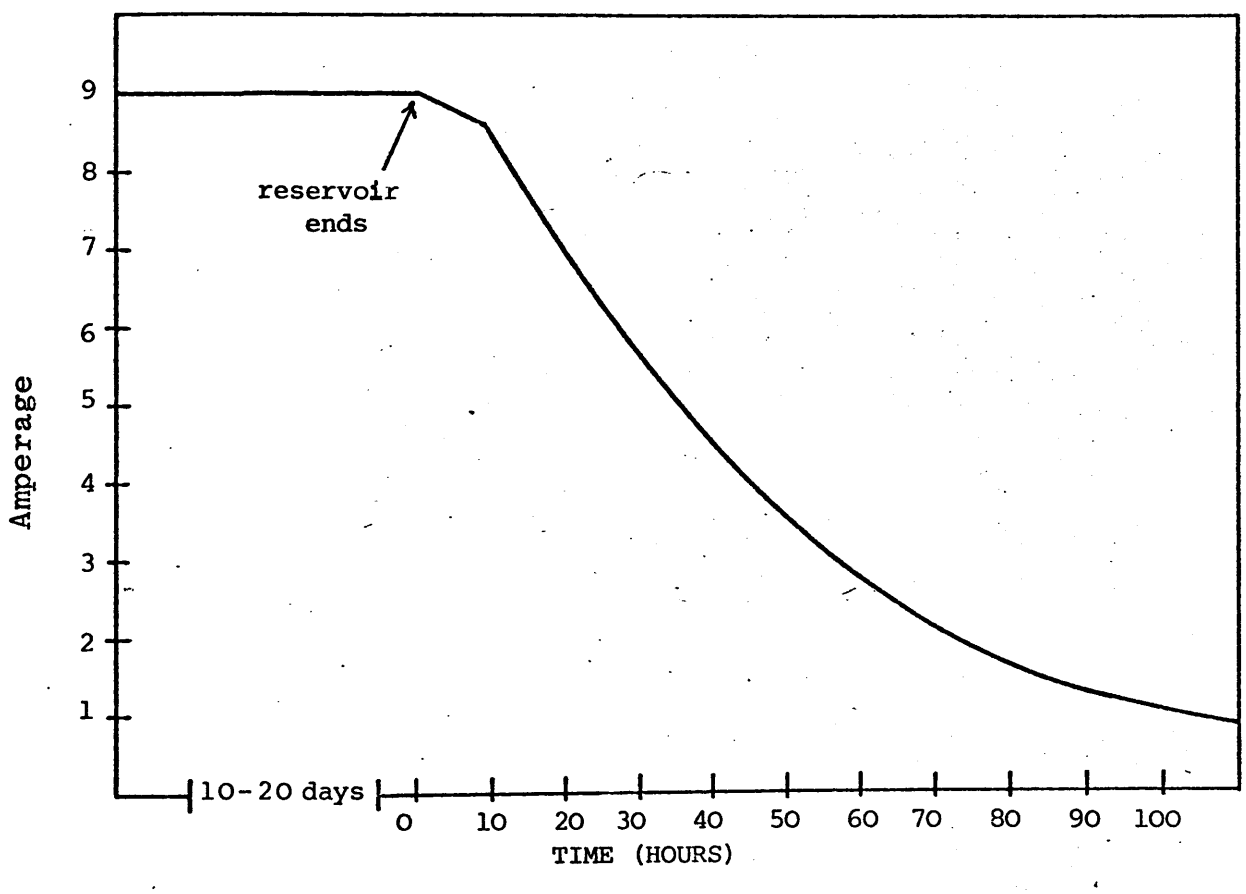

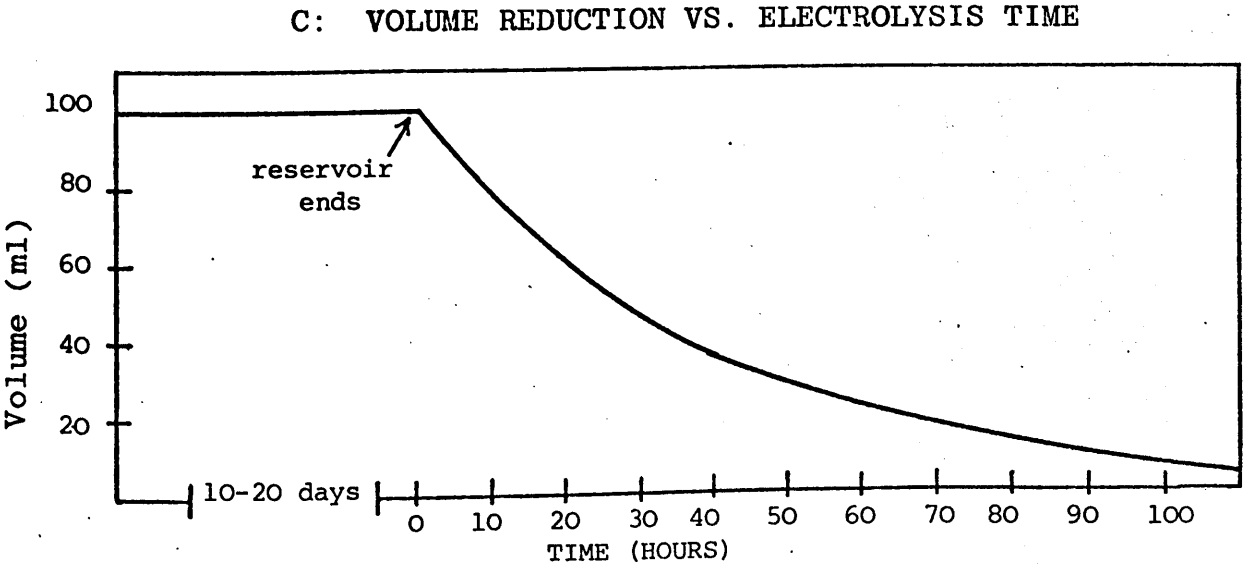

Figure II.8 A,B,C. Graphs showing A) current density B) main current to electrodes and C) volume reductions in cellas a function of electrolysis time.

is easily removed by washing with water. A clean Pasteur pipette connected to a length of plastic tubing is placed in the cell so that the tip of the pipette lies well below the level of the electrolysed sample. An excess of CO_2 (2-4 litre-atm) is condensed into a cold finger which is then connected to the plastic tubing. The carbon dioxide is allowed to warm and expand into the sample, neutralising the NaOH. A tared distillation ampoule (Figure II.9) is then connected to a B10/B14 adapter which is connected to the electrolysis head with black wax. The electrolysis cell is placed into a wire-wound furnace and the ampoule connected to the vacuum line (Figure II.10). The ampoule and cell are evacuated before liquid nitrogen is placed around the ampoule. The furnace is heated to 120°C and a vacuum distillation performed. When completed, the ampoule is removed, cleaned and reweighed. Vapour losses during final distillation were investigated but with recoveries consistently greater than 99% (Table II.1) were shown to be negligible. The final volume (V_f) and the initial electrolysis volume (V_i) yield the necessary volume reduction factor (V_f/V_i). Volume reduction factors calculated both from the measured initial volume and from ampere-hour initial volume agree within ±5% and normally within ±1-2% (Table II.2).

II.6 Methane Synthesis.

Hydrocarbon gases are well known for their remarkable radiometric counting characteristics with ideal long flat plateaux, low working voltages and low sensitivity to impurities. Acetylene and methane have been used for many years in counting of low activity natural carbon-14 (Schell, 1970).

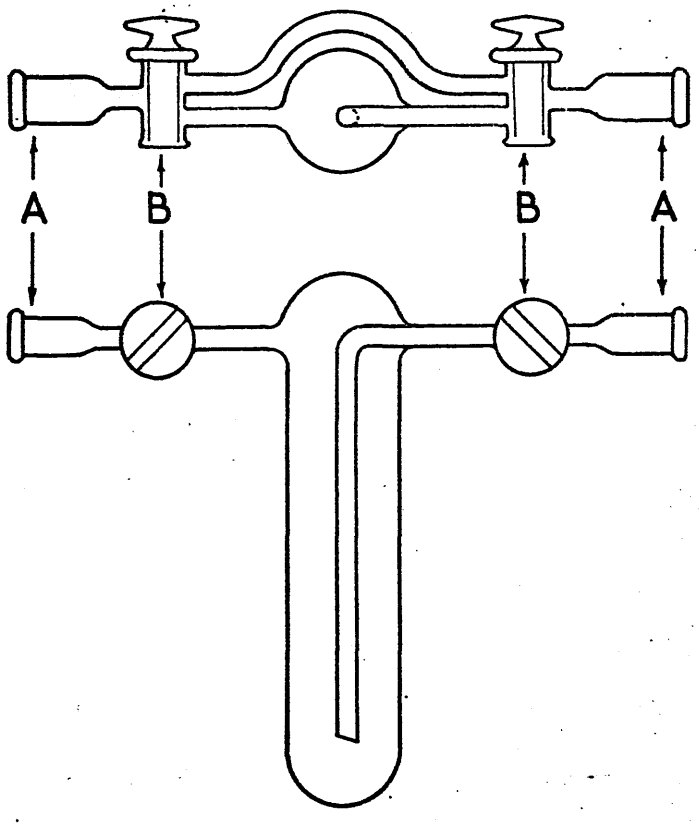

Figure II.9 Final distillation ampoule showing A: B14 cones and B: 4 mm double-oblique taps.

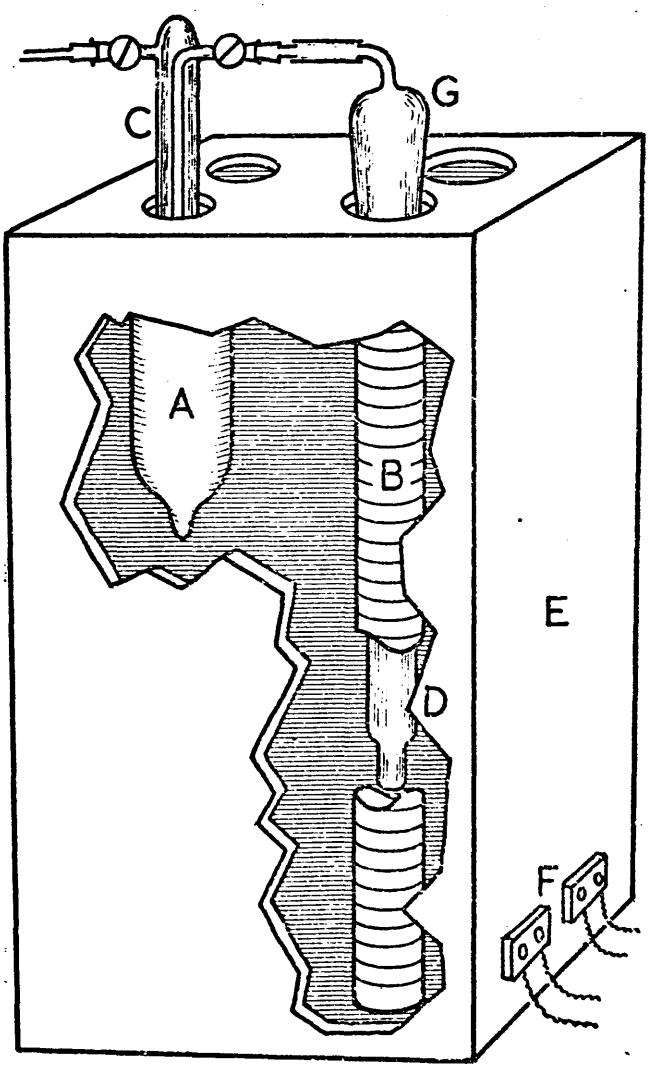

Figure II.10 Final distillation apparatus showing: A - liquid nitrogen B - wire-wound furnace, C - distillation ampoule, D - electrolysis cell and electrodes, E - asbestos board, F - electrical block connections, G - B34 to B14 adapter.

AMPOULE VAPOUR LOSSES - FINAL DISTILLATION

Run	Electrolysis cell H_2O initial weight (g)	Ampoule H_2O final weight (g)	% Recovery
1	8.31490	8.27499	99.52
2	7.06398	7.02272	99.42
3	7.27423	7.23175	99.42
4	6.84016	6.80404	99.47
5	6.79499	6.77036	99.64
6	6.84887	6.82052	99.59
7	6.57091	6.55103	99.70
8	5.60933	5.59223	99.70
9	7.63269	7.61907	99.82
	2σ=0.00005	2σ =0.00005	2σ =0.003

Mean Recovery = 99.59±0.14% (2σ)

TABLE II.1

COMPARISON OF VOLUME REDUCTION FACTORS

Run	Weighed $V_f/V_i \pm 2\sigma$ ($\times 10^{-3}$)	Calculated amp-hr $V_f/V_i \pm 2\sigma$ ($\times 10^{-3}$)	% deviation
1	9.68 ± 0.009	9.58 ± 0.09	0.97
2	20.41 ± 0.024	21.15 ± 0.025	3.95
3	18.94 ± 0.020	19.23 ± 0.020	1.52
4	42.94 ± 0.045	44.03 ± 0.045	2.55
5	14.78 ± 0.025	14.58 ± 0.025	1.42
6	10.07 ± 0.010	10.45 ± 0.010	3.77
7	21.10 ± 0.023	20.93 ± 0.023	0.80
8	11.75 ± 0.012	11.68 ± 0.012	0.61
9	19.28 ± 0.020	19.57 ± 0.020	1.49
10	21.98 ± 0.023	21.56 ± 0.023	1.96
11	33.59 ± 0.034	34.29 ± 0.034	2.09
12	31.51 ± 0.032	31.69 ± 0.032	0.57
13	20.51 ± 0.021	20.87 ± 0.021	1.73
14	21.39 ± 0.022	21.34 ± 0.022	0.24
15	16.57 ± 0.017	16.92 ± 0.018	2.12
16	11.05 ± 0.011	10.99 ± 0.011	0.55

Mean % Deviation = 1.65±1.09 (2σ)

TABLE II.2

Hydrogen is, in fact, the most common gas employed for tritium counting in the gas phase. The reduction of water to hydrogen is quick and simple. The use of hydrogen, however, presents various difficulties. In the Geiger region, double and triple pulse formation is possible, even with ethylene-argon counting mixtures. Counting of hydrogen in the proportional region is also difficult, due mainly to steep gas gain versus voltage characteristics and the ease of formation of negative ions.

Use of a hydrocarbon synthesised from water has the following advantages (i) superior counting characteristics particularly with regard to minimal effects of impurities; (ii) operation in the proportional region enabling possible background reduction via energy discrimination; (iii) higher tritium content per volume ratio since there are generally more than two atoms of hydrogen per molecule; (iv) satisfactory operation at pressures of several atmospheres. As a result, hydrocarbon counting allows counter filling with higher hydrogen content without unduly increasing the background or deteriorating counting characteristics.

The conventional approaches involve either conversion of water samples to hydrogen with subsequent counting in a mixture with a suitable hydrocarbon gas, or alternatively direct synthesis of a hydrocarbon gas having good counting characteristics. Both methods are practised in routine tritium analysis (Theodorsson, 1974; Ostlund, 1962; Bainbridge et al, 1961; Lal and Athavale, 1966).

The following reaction,

$$CO_2 + 4H_2 \xrightarrow{500^oC} CH_4 + 2H_2O \qquad (II.1)$$

(in the presence of a catalyst : 0.5% ruthenium-on-alumina)

was developed by Fairhall et al (1961) for the purpose of counting ^{14}C radioactivity as methane. Reaction (II.1), however, cannot be used directly in tritium assay as half the hydrogen is effectively wasted and isotopic fractionation effects are expected.

Anand and Lal (1964) succeeded in synthesising methane from water in a single stage. The main advantages of this method over that of ethane synthesis adopted earlier are fivefold: (i) the synthesised gas molecules contain four hydrogen atoms from the sample : this number is two in the case of ethane synthesis since four of the ethane hydrogens originate in cylinder ethylene; (ii) it is not necessary to prepare hydrogen first : the hydrogenation of carbon dioxide, using the sample hydrogen only, is performed with high yield in a single stage by the following equivalent reaction:

$$4Zn + CO_2 + 2H_2O \rightarrow CH_4 + 4ZnO \qquad (II.2)$$

(iii) the counting characteristics of methane are less sensitive to electronegative impurities than those of other gases (Burke et al, 1955); (iv) the water to methane conversion is rapid, quantitative, and non-hazardous (Fairhall et al, 1961); (v) methane is safe to handle, store, and count at high pressure in contrast to acetylene which tends to explode at pressures greater than 1.5 atm.

To avoid isotopic fractionation, the gas must be prepared in high yield. In addition it must be at least 99.99% pure with minimal electronegative impurities. In this study early investigations into the quantitative production of methane from water began using a 'flow system' similar to that described by Farmer (1972). The flow system had the advantage of being simple, cheap, and quick to construct. The only necessary modifications were the introduction of a smaller gas reservoir (10 litres), a zinc furnace following the ruthenium furnace and a sample inlet system between these furnaces (Figure II.11). The procedure consisted of loading the removable quartz tube with 300 g zinc and 50 g 0.5% ruthenium-on-alumina pellets, outgassing these materials at operational temperatures (425°C and 500°C, zinc and ruthenium, respectively) until a pressure less than 1 μ was attained, placing a 10% excess of carbon dioxide required for 100% conversion of water to methane based on equation (II.2), circulating the gas by an Austin diaphragm pump through the ruthenium furnace towards the zinc furnace, and finally, admitting the water sample from an ampoule through the water inlet system. Initial experiments revealed design flaws and material weaknesses; heat dissipated from the furnaces affected seals and taps of the sample inlet system and ampoule causing leaks. Asbestos board (½-inch thick) was placed between the inlet system and the furnaces and blowers were used to further dissipate heat. Various sealants and taps were considered. Rotary teflon taps and Edwards High Vacuum Silicone grease, however, were found capable of withstanding elevated temperatures while maintaining vacuum-tight seals. Water, when admitted through the inlet, passed immediately through the furnaces without

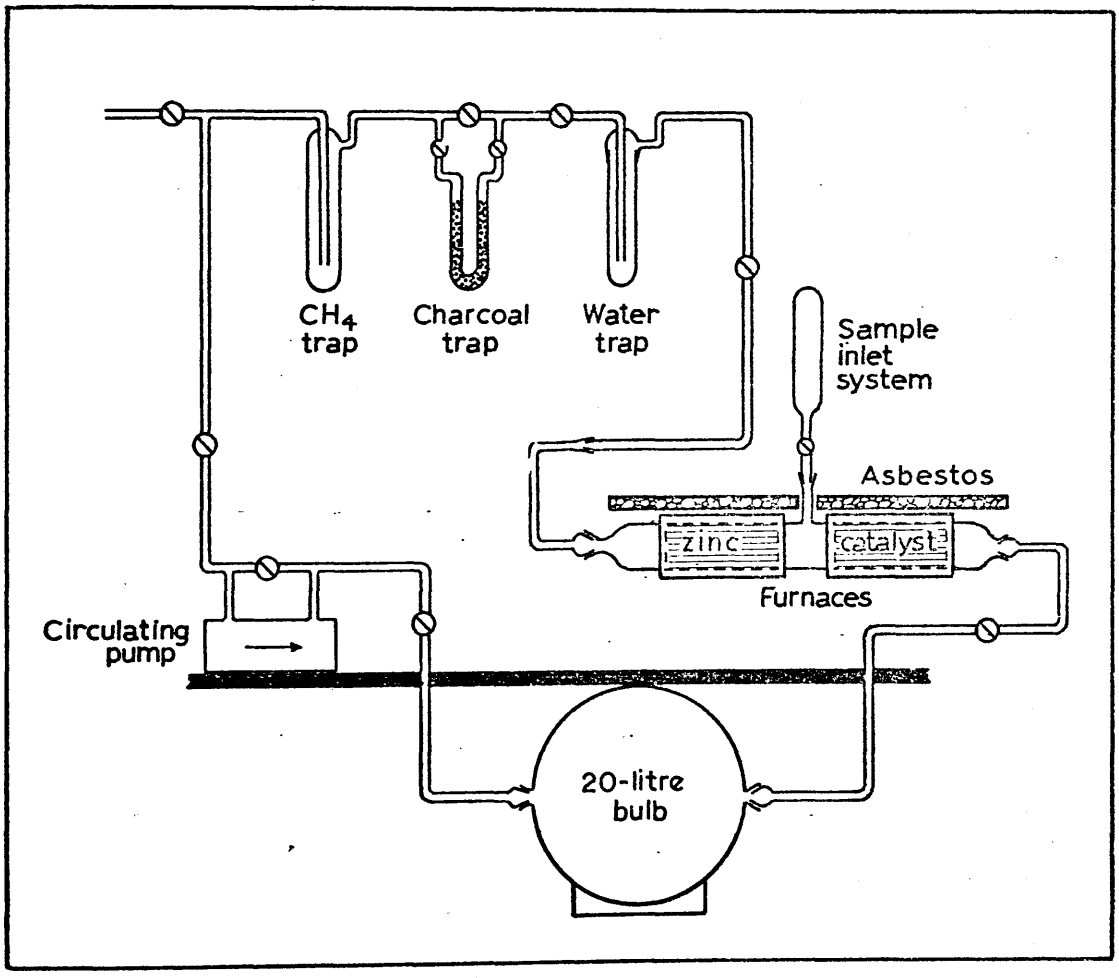

Figure II.11 Flow system for CH_4 synthesis.

reacting, condensing throughout the system. A ½-inch long section of 1 mm capillary tubing was added to the inlet system to restrict the flow of water, to cause water to enter as a vapour. No reaction occurred, however, and condensation of water continued. A more reactive agent for water reduction was sought. Magnesium, frequently mentioned as a useful chemical for water reduction (Ostlund, 1962; Allen et al, 1966; Theodorsson, 1974) was selected over other materials because of the high purity obtainable (99.7% minimum assay) and ease of outgassing adsorbed impurities. Magnesium unfortunately reacted with CO_2 at operational temperatures ($2Mg + CO_2 \rightarrow 2MgO + C$). Repeated experiments using zinc and varying operational procedures and conditions were performed to improve methane yields. Some methane was produced (ca 3-5% yields) when hot air blowers and heating tapes were used to warm large sections of the flow system. Wherever unheated sections of glass occurred, however, large-scale condensation of water was evident. It was decided therefore that unless the entire flow system could be heated to prevent condensation this method would be totally impracticable in converting water to methane and it was abandoned in favour of a reaction vessel which could sustain high temperature and pressure, thus eliminating condensation problems.

The reaction vessel and the vacuum line used for routine syntheses of up to 10 ml of water are shown in Figure II.12. Details of construction of the reaction vessel are given in Figure II.13. Two 33-inch stainless steel vessels of ~5.57 litre capacity were constructed from 3-inch by ¼-inch tubing with 8-inch diameter flanges at each end and a Hoke high-

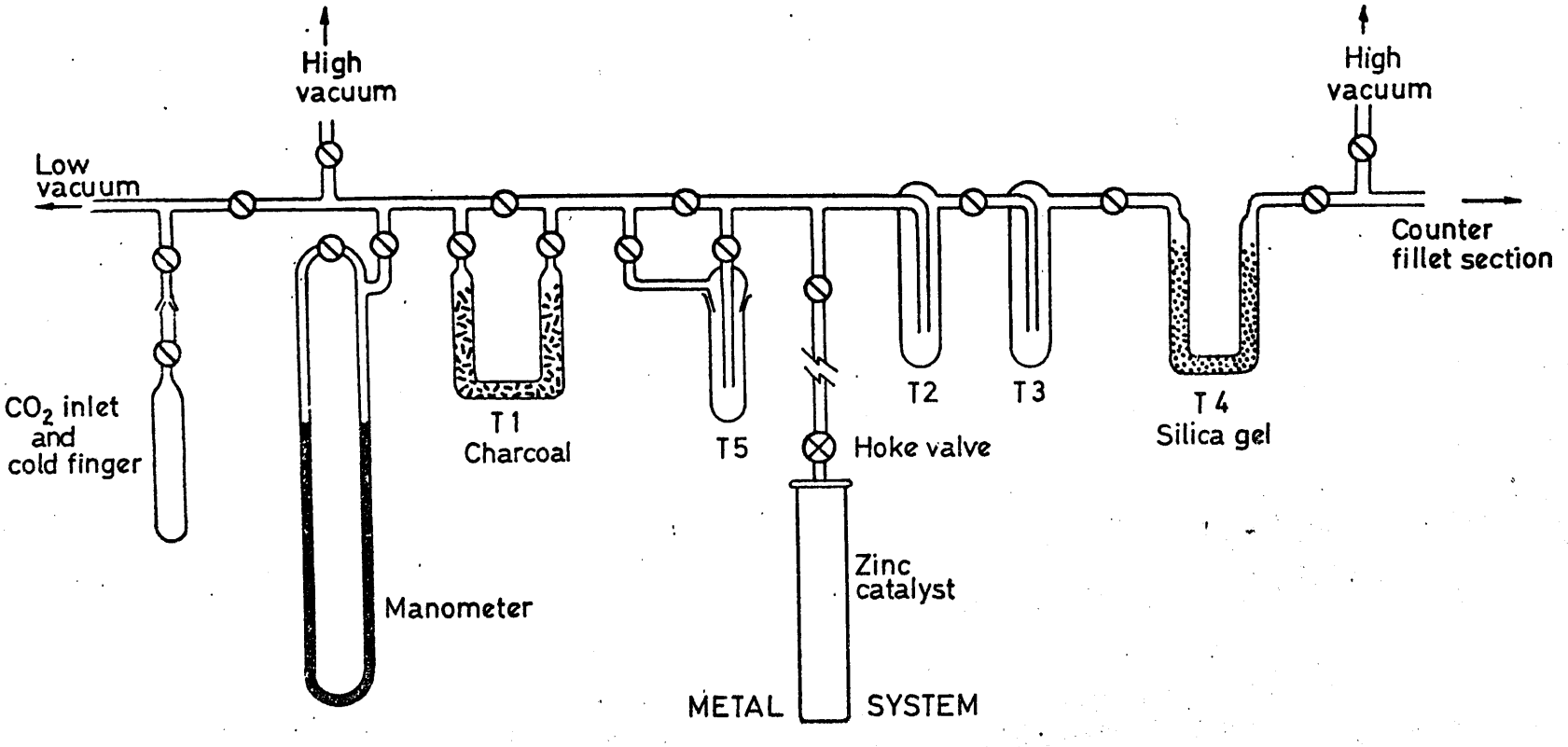

Figure II.12 Schematic diagram of the system used for methane synthesis and purification.

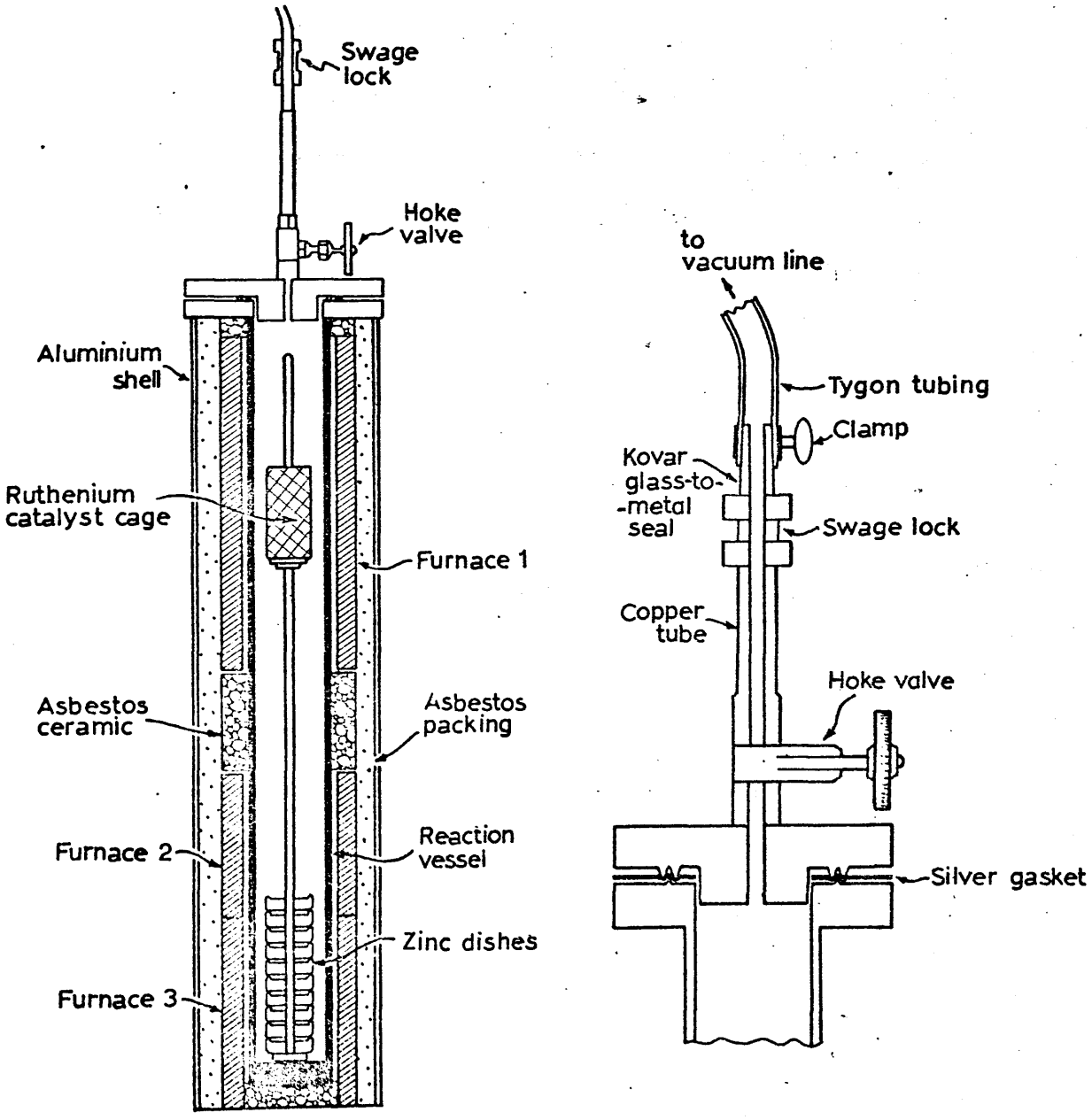

Figure II.13 A schematic diagram showing the details of the methane synthesis vessel. The sketch on the right shows details of the wide mouth cap with silver gasket and Hoke Bellows valve, capable of withstanding high pressure and temperature.

temperature high-pressure bellows valve welded on the outlet tubing. On the two facing flange surfaces at the top of each vessel were cut two sets of interlocking grooves to assist with formation of a vacuum-tight/pressure-tight seal. A pure silver gasket (0.01 inches thick) was placed between these grooves and torqued down to 25 ft-lbs by 6 one inch stainless steel bolts fitted through both flanges. In view of the high cost of silver, various alternative materials were envisaged and tested for use as gaskets including aluminium, bronze, copper, indium, lead, PTFE and Klingerit (a synthetic asbestos-neoprene composite material). Each gasket was able to provide a vacuum-tight seal except Klingerit which disintegrated under the sealing pressure. Indium and lead were eliminated from further consideration since temperatures between the flanges (ca 250-300^{o}C) approached or exceeded their melting points (327^{o}C and 157^{o}C, lead and indium, respectively). Of the remaining materials, all were capable of sustaining pressure-tight seals. At operating temperatures, however, these materials either outgassed or broke down. Bronze and copper were extreme examples, containing sulphur and producing H_2S. Aluminium was perhaps the most useful alternative material yielding little or no outgassing or contaminants but its performance was irreproducible. Although initially leak tested and vacuum-tight, when the aluminium was subjected to operating temperatures, the seals occasionally broke down and the aluminium became brittle. The results of these trials, using tritium-free water, are presented in Table II.3. Silver is evidently an ideal sealant and, although initially expensive has the compensation of being usable at least 4 times and being finally resaleable.

GASKET MATERIAL - ASSOCIATED BLANK COUNT RATE

ALUMINIUM

cpm ± 2σ	cpm ± 2σ
2.434 ± 0.06	4.902 ± 0.13
2.211 ± 0.06	5.170 ± 0.12
2.903 ± 0.07	2.779 ± 0.08
5.167 ± 0.12	2.908 ± 0.06
5.242 ± 0.11	2.245 ± 0.08
27.355 ± 0.41	1.785 ± 0.06
26.790 ± 0.42	10.987 ± 0.15
6.239 ± 0.15	10.960 ± 0.13

SILVER

cpm ± 2σ	cpm ± 2σ
2.331 ± 0.09	1.684 ± 0.10
2.550 ± 0.11	1.714 ± 0.07
1.805 ± 0.09	1.591 ± 0.10
1.834 ± 0.07	2.816 ± 0.12
1.712 ± 0.06	2.839 ± 0.07

PTFE

cpm ± 2σ	cpm ± 2σ
19.073 ± 0.26	1.646 ± 0.06
19.504 ± 0.25	2.784 ± 0.11
4.884 ± 0.15	5.084 ± 0.11
4.881 ± 0.13	5.081 ± 0.13

TABLE II.3

Each furnace consists of a 31-inch stainless steel case divided into 3 smaller and separately controlled heating regions. The upper furnace is designed to heat the ruthenium catalyst, which is functionally not highly temperature sensitive. Experience has shown that the catalyst will work quickly and quantitatively within the region of 350-600^{o}C. A 15-inch long heater region capable of reaching 600^{o}C was created by wrapping mineral-insulated heating cable around the stainless steel case. A 4-inch space separates this area from the lower heating region which is designed for the zinc reactant.

The reduction of water by zinc is extremely sensitive to temperature with quantitative reaction occurring only within the temperature range 425± 5^{o}C (c.f. melting point of zinc 429^{o}C). For this reason the zinc-heating furnace is sub-divided into 2 sections to enable more accurate control throughout the area. Two separate mineral-insulated heating cables were used in furnace construction. In addition, each furnace has its own mineral-insulated chromel-alumel thermocouple mounted centrally within its heating regime. The heating cables were successively wrapped in asbestos and 3 inches of high-temperature resistant insulation, the entire unit being enclosed in a $\frac{1}{8}$-inch thick aluminium shell in a supporting cage. Both furnace and thermocouple are connected to purpose built standard design temperature control units incorporating zero point switching.

Each reaction vessel is connected to the vacuum line which consists of a series of traps to purify the converted sample and to outgas the vessels. The presence of large

amounts of tritiated contaminants in the laboratory atmosphere requires that the most stringent outgassing procedures be followed. At the beginning of a synthesis, high purity argon is admitted to a pressure of 80-100 cm into the reaction vessel which is then opened and the spent zinc and ruthenium removed. The reaction vessel is resealed and the argon pumped off. All three furnaces are energised and the reaction vessel outgassed under high vacuum overnight. The reaction vessel is then cooled to ca 200°C and refilled with argon. Fresh zinc and ruthenium are placed into the reaction vessel which is then sealed. A normal charge consists of 300 g Analar zinc dust placed in 10 nickel dishes and 50 g 0.5% ruthenium-on-alumina pellets in a stainless steel cage. The argon is pumped away and glass trap T_5, surrounded with liquid nitrogen, is opened to the reaction vessel. The furnaces are energised and water condensed from the reactants into the glass trap. When the temperature in the lower furnaces reaches 425°C they are shut down and the high vacuum opened to the reaction vessel. The cold trap is isolated from the vacuum line and another night-long outgassing is continued. In the morning the pressure is routinely less than 1 μ and the upper furnace is shut down. The reaction vessel is closed off from the vacuum line and allowed to cool.

A water sample, previously distilled into an ampoule, is connected to the vacuum line and then to the fully outgassed reaction vessel. The region down to the Hoke valve is reduced to a pressure less than 1 μ. The reaction vessel is then opened and pressure measured to ensure that no leaks have occurred since final outgassing. A detachable cold

finger is filled with ~ 6.0 l-atm of ^{14}C-free carbon dioxide, made by heating acid-washed marble chips to 1100°C, and connected to the filling section of the vacuum line (Figure II.12). When the carbon dioxide filling section has been pumped to less than 1 μ, the bomb is opened and the water sample allowed to enter the reaction vessel. The carbon dioxide is expanded into the reaction vessel until a pressure of 90-100 cm is attained. This carbon dioxide filling normally represents a 10-20% excess over the stoichiometric requirement for 100% completion of reaction (II.2). The Hoke valve is shut and the furnaces energised to provide temperatures of 500°C and 425°C around the catalyst and zinc dust respectively: after an overnight heating, the reaction products are allowed to cool, then removed and methane is extracted using the vacuum line shown in Figure II.12.

The gases are initially allowed to expand into a liquid nitrogen-cooled charcoal-filled U-trap, T_1, which has previously been outgassed to less than 1 μ at 200°C. Any uncondensed gases are pumped off through the trap until the final pressure is less than 1 cm Hg. Liquid nitrogen is used to cool traps T_2 and T_3. The charcoal trap is warmed and the gases trapped into T_2 and T_3. Again the final pressure is normally less than 1 cm. The trapped gases are then left in close circuit with the liquid nitrogen-cooled trap T_4 containing high grade, radon-free silica gel (mesh size 12-28) which has been previously outgassed to less than 1 μ at 150°C. All the methane trapped in T_2 and T_3 is distilled to T_4 within two hours, leaving behind unconverted carbon dioxide in T_2 and T_3. Tests of distillation procedure were

performed using synthetic mixtures of carbon dioxide, methane and hydrogen. The results are presented in Table II.4 and in all cases recovery of methane is greater than 97%. Pure methane is then condensed into the stainless steel cold finger of the filling section to the gas proportional counter (Figure II.14) by warming T_4. The yields are found to be greater than 90% as estimated from the volumes both of carbon dioxide left unconverted and of methane produced (Figure II.15). No trace of water is usually detectable in T_2 and T_3 indicative of quantitative conversion.

After extraction of methane, high purity argon is filled into the reaction vessel to prevent entry of tritiated atmospheric contaminants. The normal reaction vessel outgassing procedure is continued.

One batch of catalyst is used in at least 15 successive experiments; fresh zinc dust is used each time. As commercially available ruthenium catalyst was found to contain about 4% water of crystallisation, it is degassed by heating under high vacuum before use.

By counting several methane samples prepared from tritium-free water immediately after synthesis of hot tritium samples, it was found that the memory of the reaction vessel is usually smaller than 6% (Table II.5). No detectable memory was observed when sample activity was less than 25 cpm; after enrichment, environmental samples rarely exceeded 5 cpm. Routinely, conversion of tritium-free water to methane preceded each sample and samples of similar tritium activity were synthesised in the same reaction vessel to

METHANE PURIFICATION TEST - PERCENTAGE RECOVERY

SYNTHETIC GAS MIXTURE			RECOVERED GASES			
CO_2	CH_4	H_2	CO_2		CH_4	
(cm)	(cm)	(cm)	cm	%	cm	%
20.0	42.7	-	20.0	100	42.0	98
20.0	66.2	-	20.0	100	66.0	100
20.3	62.0	9.1	19.9	99	60.1	97
20.5	25.0	24.3	20.1	98	24.5	98

Mean Recovery of Methane = 98.25 ±1.26% (2σ)

TABLE II.4

(Pressure readings accurate to ± 0.1 cm (2σ))

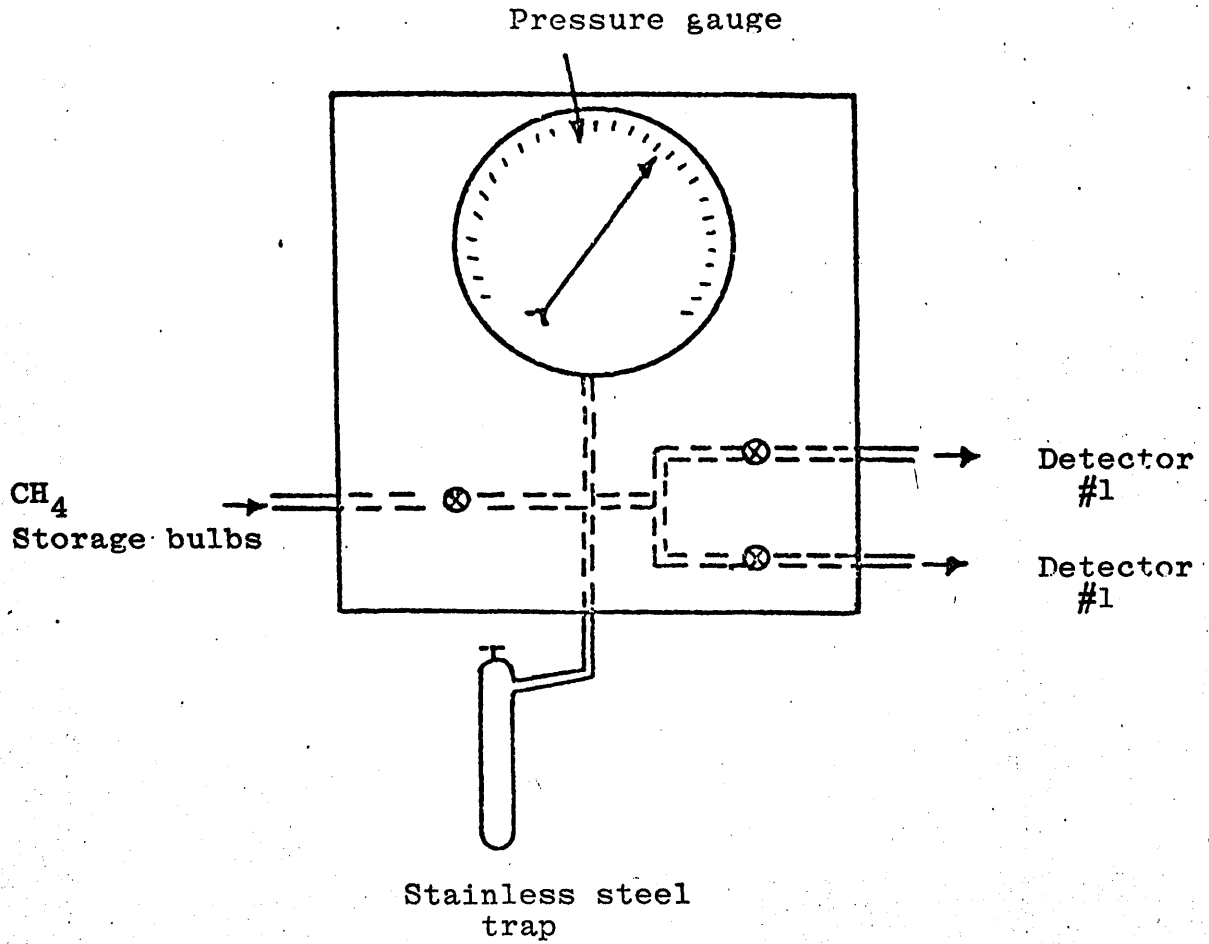

FIGURE II.14 COUNTER FILLING SECTION.

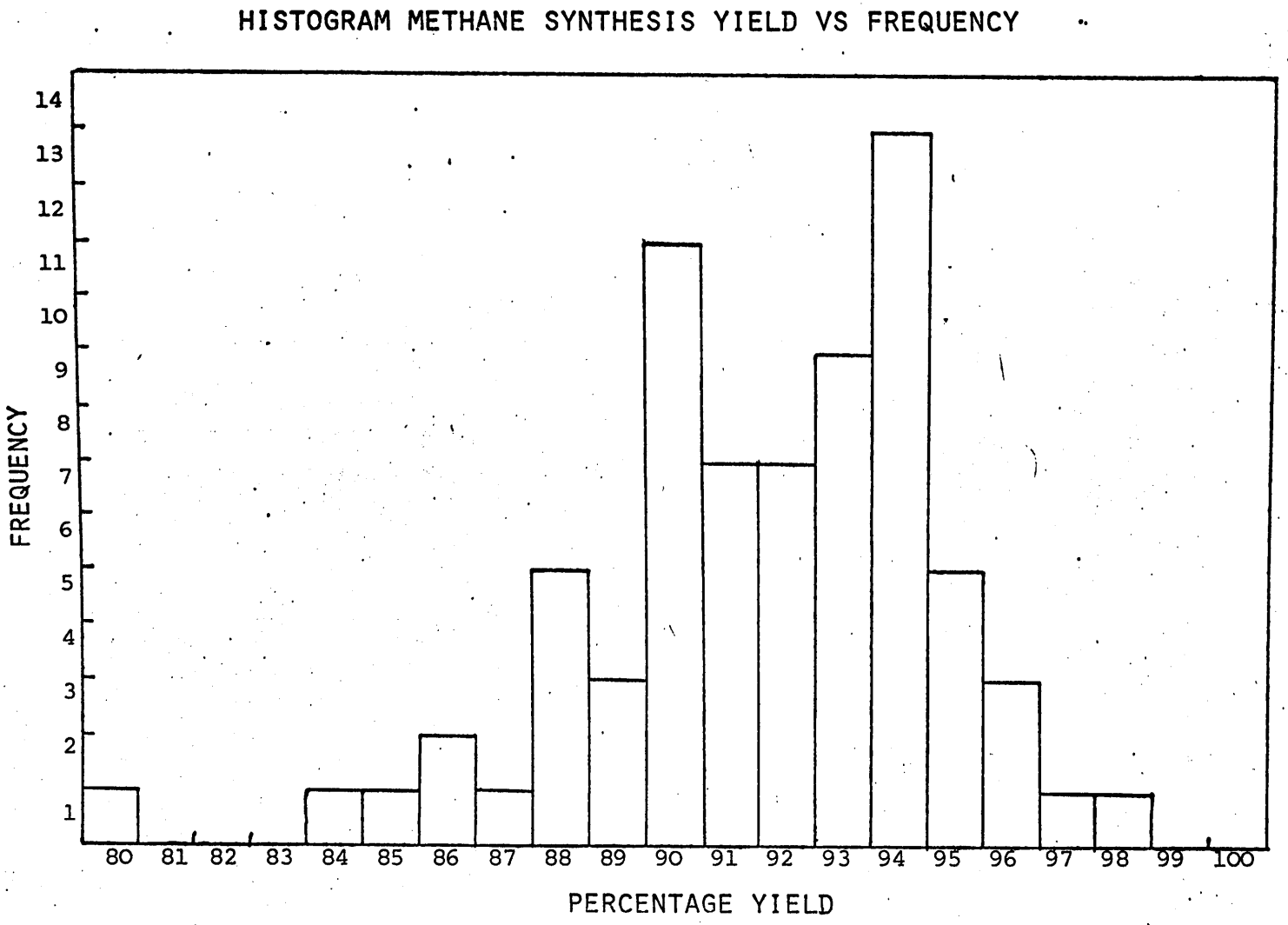

Figure II.15 Histogram showing the distribution of the percentage yield obtained from methane synthesis.

MEMORY EFFECT - REACTION VESSELS

LEFT REACTION VESSEL			RIGHT REACTION VESSEL		
Hot Tritium sample (cpm above bkgd ±2σ)	Proceeding Blank sample (cpm above bkgd ±2σ)	Memory (% ± 2σ)	Hot Tritium sample (cpm above bkgd ±2σ)	Proceeding Blank sample (cpm above bkgd ±2σ)	Memory (% ± 2σ)
182.57 ± 1.19	9.72 ± 0.31	5.32 ± 0.16	40.02 ± 0.51	1.09 ± 0.10	2.72 ± 0.25
95.79 ± 0.72	4.95 ± 0.24	5.17 ± 0.25	88.08 ± 0.72	1.06 ± 0.08	1.20 ± 0.09
60.69 ± 1.00	2.45 ± 0.16	4.04 ± 0.26	16.82 ± 0.29	*	N.M.D.
12.69 ± 0.31	*	N.M.D.	23.97 ± 0.25	*	N.M.D.
27.37 ± 0.30	*	N.M.D.	27.31 ± 0.30	*	N.M.D.
27.05 ± 0.30	0.36 ± 0.09	1.33 ± 0.33	9.37 ± 0.21	*	N.M.D.
16.07 ± 0.29	*	N.M.D.	1143.00 ± 2.0	58.29 ± 0.66	5.10 ± 0.06
27.23 ± 0.03	0.82 ± 0.11	3.01 ± 0.40	644.00 ± 2.0	44.44 ± 0.61	6.90 ± 0.09
12.44 ± 0.20	*	N.M.D.	7.14 ± 0.16	*	N.M.D.
16.25 ± 0.29	*	N.M.D.	10.62 ± 0.25	*	N.M.D.
4754.00 ± 2.0	72.11 ± 1.0	1.52 ± 0.01	16.23 ± 0.31	*	N.M.D.
10.65 ± 0.25	*	N.M.D.			

TABLE II.5

* - no measurable increase in background.

N.M.D. - no memory detected.

eliminate problems of contamination through memory effects.

II.7 Gas Storage and Counter Filling Sections.

A series of ten 5 litre pyrex glass bulbs provide the storage facilities which are necessary if there is a delay in recounting a sample or if short-lived radioactive contaminants (e.g. ^{222}Rn, $t_{\frac{1}{2}}$ = 3.825d) are believed to be present. Contamination due to short-lived radionuclides was investigated by storing several samples for long periods (ca 2-3 months) after determining their initial count rate following purification. The results presented in Table II.6 demonstrate no difference between initial and final count rates. Therefore it is assumed that there is no introduction or presence of short-lived radionuclides in the analytical procedure. To minimise transfer losses due to the finite vapour pressure of methane at liquid nitrogen temperatures (10 mm at -196°C, Weast, 1970), each storage bulb has a cold finger attached. Each bulb is evacuated to less than 1 μ prior to filling and a manometer in the storage frame monitors the bulb filling pressures.

The counter is routinely filled to a pressure of 5 atm through the all-metal system shown in Figure II.14. The detector is first pumped below 1 μ over a period of about 1 hour. The valve to the detector is closed and the 100 ml stainless steel trap is cooled by liquid nitrogen. Both the counter filling system and sample storage section or silica gel trap T_4 are isolated from vacuum. The sample gas is distilled into the metal trap. The filling section is then isolated from the vacuum rack by a bellows valve and the

DETERMINATION OF THE PRESENCE OF SHORT-LIVED RADIONUCLIDES.			
SAMPLE	INITIAL COUNT RATE (cpm ± 2σ)	FINAL COUNT RATE (cpm ± 2σ)	STORAGE TIME (days)
1	3.01±0.10	3.02±0.11	79
2	5.44±0.13	5.55±0.14	92
3	3.45±0.10	3.43±0.11	94
4	4.76±0.13	4.86±0.12	38

TABLE II.6

methane expanded into the counter. The counter filling pressure is adjusted to 5 atm by returning excess methane to a storage bulb or by pumping away. The filling pressure can be read to an accuracy of 0.2 psi (± 0.25%), (Farmer, 1972). The counter valve is closed and the remaining methane condensed into the storage bulb or pumped away.

All sample activities are normalised to a constant filling temperature of 18°C since temperature variations of 10°C have occasionally been experienced. A thermometer probe within the counter shield monitors the filling temperature. The 0.5 litre detector contains approximately 0.4 g hydrogen for a 5 atm fill of methane at 18°C. Thus, in theory, the absolute minimum weight of sample water required prior to conversion to methane is 3.5 g. Because of small losses in gas preparation and methane distillation, however, an excess is necessary. Normally when there is a sufficient quantity of water sample available, a 10 ml portion is used for the conversion to methane. It should be noted that by filling the counter to the same pressure with each gas and by normalising tritium activities to 18°C, sample and standard activities can be directly compared without recourse to absolute counter volume or absolute activity measurement.

II.8 Tritium Counting System.

The counting system employed has been described by Sharp and Ellis (1965). The sample detector is a 0.5 litre internal gas proportional counter supplied by Beckman Instruments Inc., California. Two detectors can be accommodated

within the concentric wall multiple anode anticoincidence counter but only one is involved in this research project. The whole assembly is encased within an aged lead shield (J. Girdler and Co., London). Counter electronics, anti-coincidence system and power supply are of Beckman design. A block diagram of the counting system is shown in Figure II.16.

(a) Detector, guard and shielding assembly.

The detector was machined from a solid ingot of OFHC (oxygen free high conductivity) copper providing a 1.8 cm thick copper wall which acts as a very clean inner lining to the shield (Figure II.17). The interior surface of the detector is electroplated with pure nickel to absorb any alpha particles from the copper and to eliminate memory effects occasionally observed with pure copper cathodes. The outside of the detector is also nickel plated. Stainless steel wire (diameter 0.001 inches) stretched to 90% of its elastic limit constitutes the anode. Satisfactory vacuum and pressure holding performances are obtained by using teflon as insulator material and by sealing the endplates of the detector with O-rings. The detector can be operated at gas filling pressures of up to 10 atm methane.

Both inner and outer walls of the guard counter are heavy wall OFHC copper pipe with a combined wall thickness of 2.5 cm. Thus, including the detector wall, there is over 4 cm OFHC copper shield liner surrounding the sample volume. The increase in efficiency of interception of mu-mesons producing gamma showers in the shield is due to the close fitting guard counter within the shield. The outer sleeve of the guard is easily removable allowing inspection and cleaning

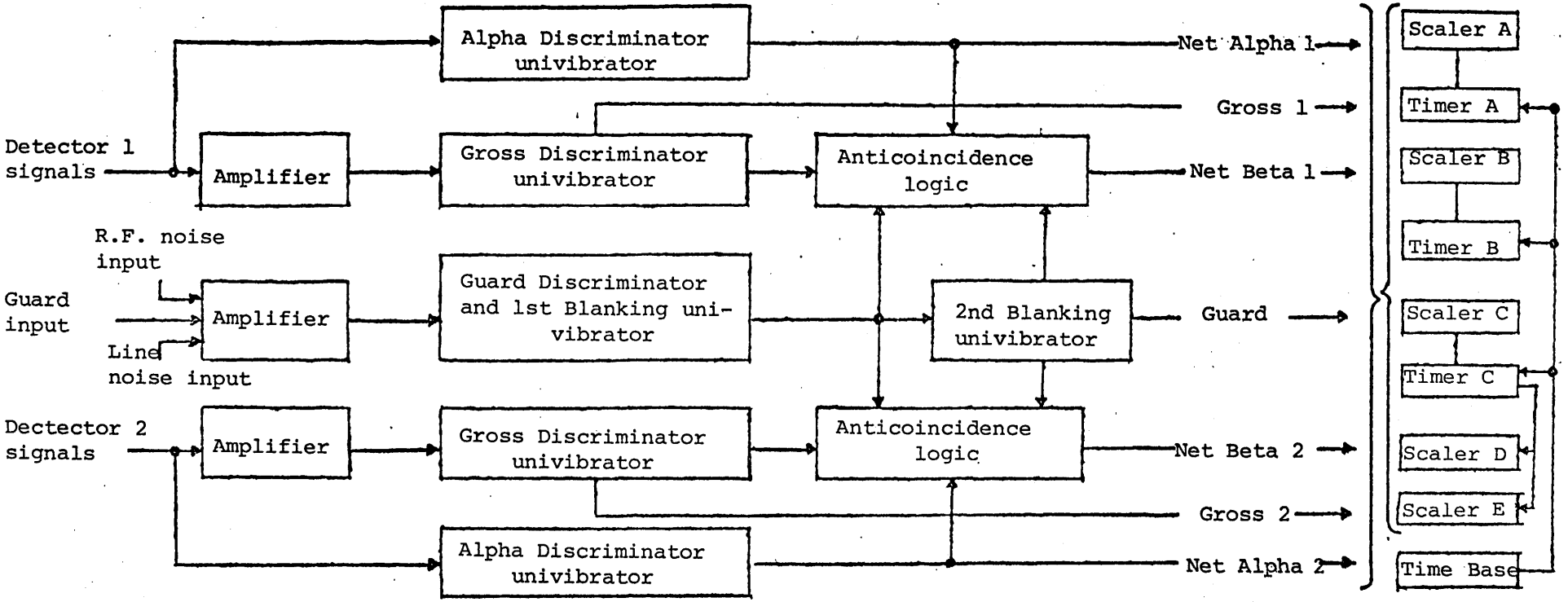

Figure II.16 Block Diagram of Counting Electronics.

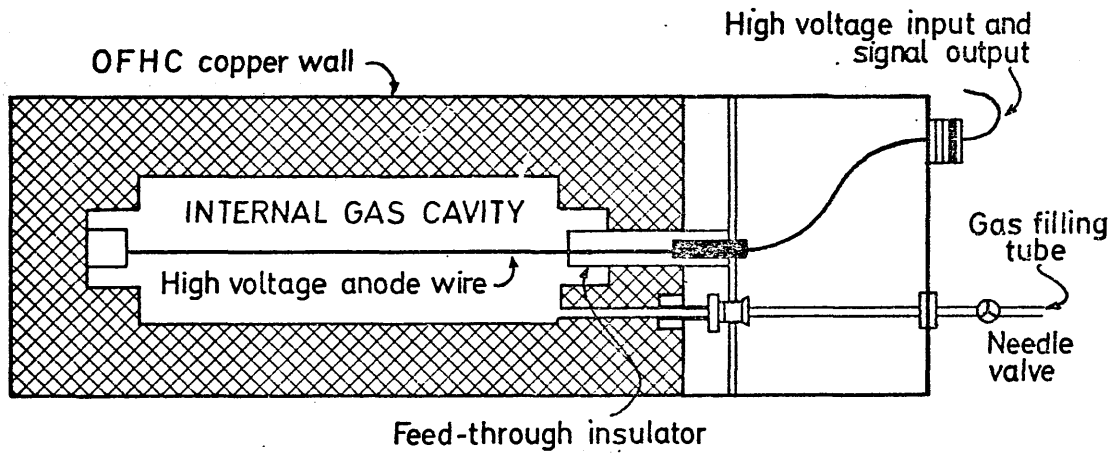

Figure II.17 Cross-section diagram of sample detector.

of the anode wire assembly.

The guard counter is filled to 80 cm Hg with inactive methane. Each fill has a lifetime of 6-8 months. To ensure that the guard channel is at least as sensitive to noise as the detector channel, both are operated within the proportional region. This effectively cancels simultaneous pulses in both channels.

The external shield is constructed of 4-inch thick aged lead, known to be relatively free from natural radioactivity and fission products. Its overall dimensions are 16" x 16" x 36", with a total weight of 2910 lbs. Close fitting lead plate doors which open freely on thrust bearings are fitted at each end of the shield. Ready access to the counter unit is thus provided.

The background count rate of the system largely represents the sum of the following components:

(i) alpha and beta radiation from radioactive contamination of the counter material,

(ii) ionising particles, mainly cosmic-ray mu-mesons producing gamma secondaries in the lead shield which are not effectively cancelled by anticoincidence (Sharp and Ellis, 1965),

(iii) neutron-induced events,

(iv) Compton-, photo-, and pair electrons produced by γ-particles in the counter wall and in the gas.

Twenty to forty per cent of the background count rate is believed to arise from gamma ray interactions in the counter

walls producing recoil electrons which interact with the counting gas (i.e. the "wall effect"; Oeschger, 1963). Guard and detector combined in a single unit have been designed by Oeschger to reduce the wall effect. The Beckman system, however, compensates for the increase in background by a reduction in dead volume.

(b) Electronic and power supply.

Seven data outputs are provided from the main electronics; net alpha counts, gross unguarded counts and net beta counts for each detector, and guard counts (Figure II.16). Any of the seven outputs can be read from the five available scalers. A high energy and low energy register would be more appropriate for the net alpha and net beta channels, respectively, since the division between these registers is based on energy discrimination and not ionising radiation. An adjustable upper level discriminator sets the triggering point between the beta and alpha channels. Four of the five scaler units are linked to automatic data printers which print out every 30 minutes allowing examination of data for statistical reproducibility.

Noise elimination and control is one of the most important features of the electronic design. The guard consists of two 500 microsecond blanking circuits which were set to trip at 0.4 millivolts by using a pulse height generator. If more than 2 ionising events occur within 500 microseconds, the guard is effectively paralysed and unable to remove any spurious counts by anticoincidence logic. The power line and a radio-frequency pick up antenna are coupled into the anti-coincidence circuit to eliminate environmental electrical

noise. The lower discriminator was adjusted to trip at 0.5 millivolts. This ensures that the anticoincidence circuit is more sensitive to noise than the detectors.

A circuitry test programme is built into the main electronics unit. Three internal test pulses simulate detector pulses at the detector inputs, mu-meson pulses coincident at the detector and guard inputs, and alpha pulses at the detector inputs. Using the 7 data outputs and 5 scalers, a 105 step test programme can thoroughly check every circuit board in a few minutes.

The high voltage power supply provides 3 channels separately adjustable between 1000 and 10,000 volts.

II.9 Counter Characteristics.

(a) Optimum operating conditions.

The optimum working conditions for measurement of tritium were determined essentially by maximising the parameter commonly referred to as the "figure of merit", E^2/B defined as the sample counting efficiency squared divided by the background count rate (Sharp and Ellis, 1965). If the sensitivity for a 95% accurate detection of tritium by gas proportional counting is defined as 'that amount of tritium required to raise the background count rate by twice its root mean square deviation (i.e. $2\sqrt{N}/t$, where N equals the total number of counts obtained during t, the total counting time)' then decreasing the background count rate will correspondingly reduce the counting efficiency, and hence increase the counting time necessary to achieve the desired

accuracy. For low level samples, the figure of merit is directly proportional to the number of samples which can be counted per week to this given statistical accuracy.

After filling the counter with 5 atm tritiated methane, the upper discriminator was adjusted to place all counts into the net β channel; the gas was pumped away, refilled with tank methane (described in the next section) and an overnight background count rate determined. This procedure was repeated for 17 different discriminator positions; the net α/net β ratio being taken at the beginning and end of each experiment using an external ^{137}Cs source. These results are presented in Table II.7 and shown graphically, in Figure II.18 A,B,C.

The figure of merit rises to a maximum value in a plateau region between net α/net β ratios of 5.0 to 9.0 with an apparent maximum value at ~ 7.0. The background count rate tends to rise slowly from 1.0 to 1.5 cpm thereafter rising rapidly to a maximum over 6.5 cpm; concomitant is a decrease in net α/net β ratios from 20 to 6. Overall efficiency for detection of tritium decreases continually with increasing net α/net β ratios. Using an external ^{137}Cs source, the net α/net β ratio equal to 7.0 ± 0.2 was selected as the best compromise between minimum background count rate and maximum efficiency. The figure of merit lies within the plateau maximum region, the background count rate is less than 1.5 cpm and the detection efficiency is greater than 93%. Furthermore this ratio is well within the operating voltages of the power supply (ca 6.0 to 6.6 kV, depending upon the quality of the synthesised methane).

DETERMINATION OF THE FIGURE OF MERIT.

POSITION	BACKGROUND β (cpm)	BACKGROUND α (cpm)	EFFICIENCY (%)	NETα/NETβ	E^2/B
1	2.51	3.70	98.77	3.12	3882
2	2.20	2.71	98.72	3.96	4430
3	0.90	5.02	51.37	20.00	2921
4	6.55	0.99	100.00	0.55	1530
5	0.95	3.67	64.00	15.70	4308
6	2.28	2.29	98.62	3.64	4230
7	1.38	3.31	88.97	8.46	5730
8	1.84	2.60	98.40	4.75	5251
9	1.50	3.51	91.50	7.58	5581
10	2.03	3.04	97.45	4.88	4682
11	1.33	3.79	79.50	10.37	4732
12	1.11	3.81	59.38	15.89	3190
13	1.56	3.58	91.58	8.29	5381
14	1.60	3.14	95.45	6.06	5694
15	1.52	3.66	86.23	9.67	4882
16	1.46	3.22	90.35	8.68	5598
17	1.32	3.42	93.08	6.90	6575

TABLE II.7

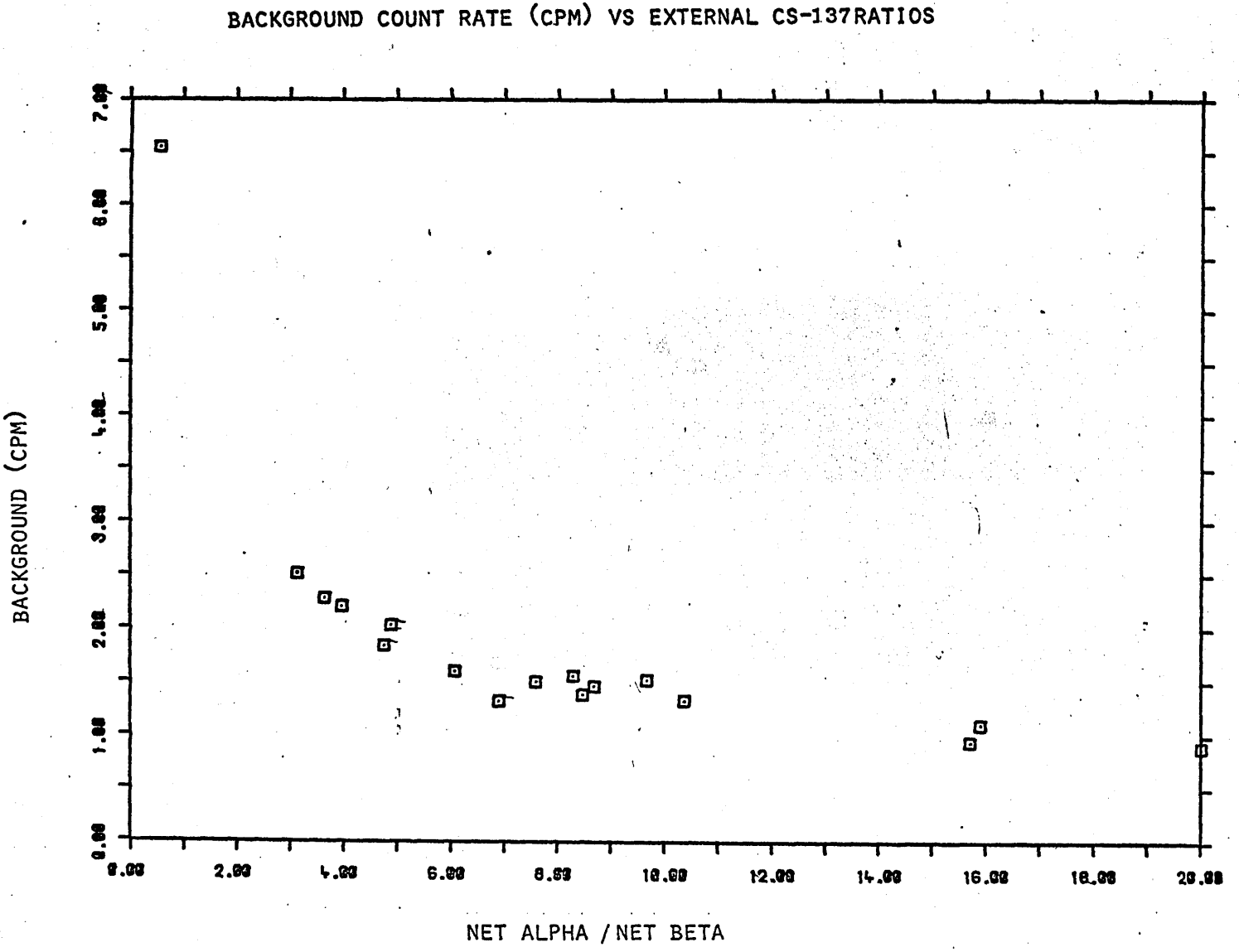

Figure II.18A The backround count rates in cpm of the net β channel from different discriminator positions. The expected deviations due to $\pm 2\sigma$ errors are shown by the square boundary surrounding each point.

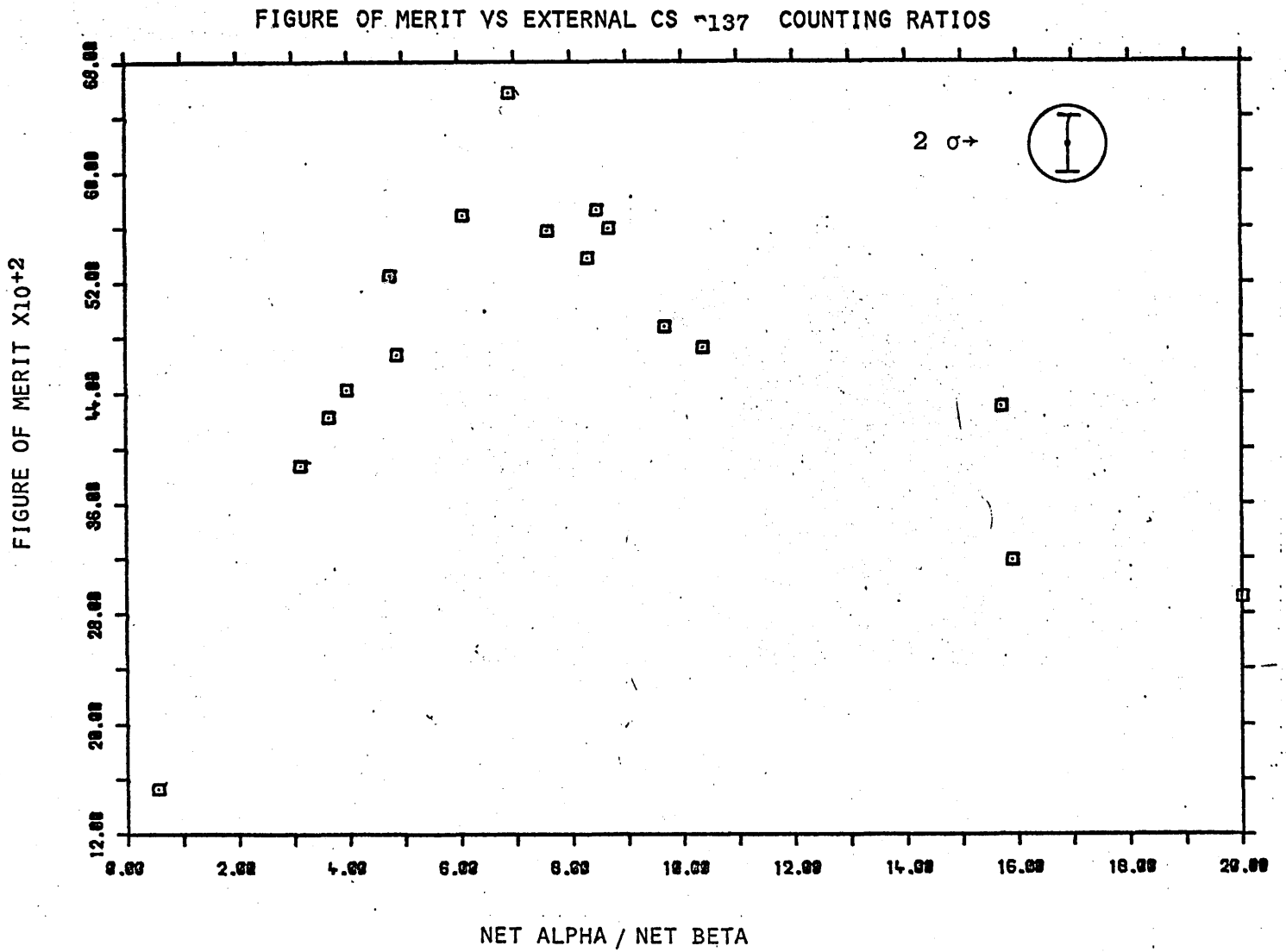

Figure II.18B The figure merit obtained from different discriminator positions. The expected deviation due to a $\pm 2\sigma$ error for the figure of merit and net α/netβ are shown in the upper left side figure of the graph.

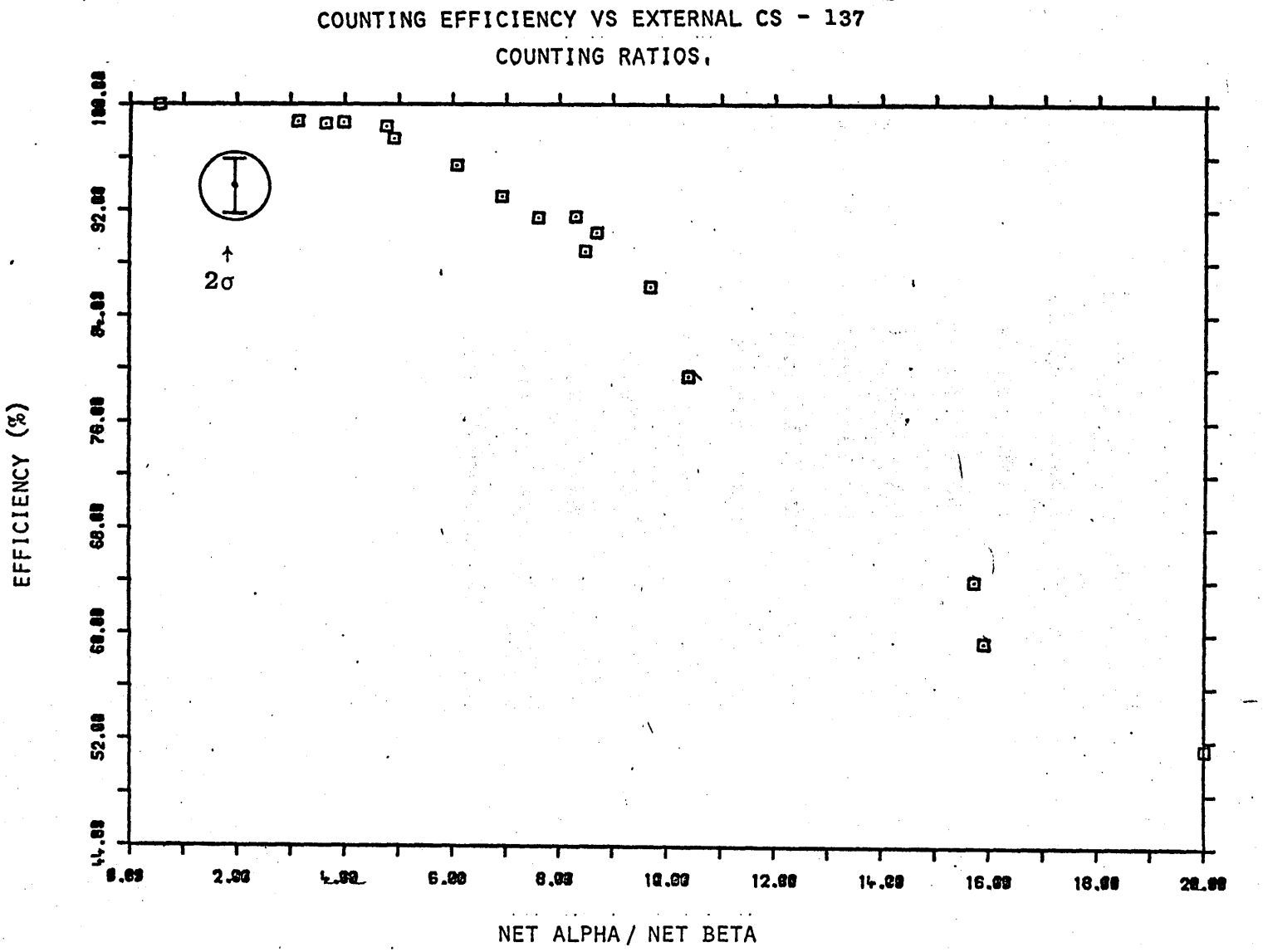

Figure II.18C The counting efficiency for the detection of tritium with different discriminator positions. The expected deviations due to a ±2σ error for the counting efficiency and net α/netβ are shown in the upper left side figure of the graph.

(b) Plateaux.

All initial calibration procedures were performed using "pure tank" methane obtained from Beckman Instruments Ltd., Glenrothes. This source of inactive methane has been shown to be free from radioactive contamination and capable of producing excellent agreement with methane synthesised from inactive materials in the laboratory (Baxter, 1969; Ergin, 1969; Farmer, 1972). Detector plateaux are monitored using an external ^{137}Cs source to increase the count rate and improve statistics. The detector plateaux are commonly 1000 volts in length with slopes less than 0.5% per 100 volts (Figure II.19). Guard plateaux are 500 volts to 1000 volts long with a slope less than 1% per 100 volts. At the routine filling pressures of 5 atm for the detector and 1.05 atm for the guard counter, working voltages are approximately 6.3 kV and 4.2 kV respectively. The optimum detector filling pressure was selected as 5 atm for the following reasons:

(i) the high voltage power unit is unstable at the continuous operating voltages (>8kV) required for higher filling pressures (Ergin, 1969),

(ii) a filling pressure of 5 atm is in accord with the production rate and handling capacity of the gas preparation system.

(c) Operating voltages.

To compare count rates of different sample gases, it is necessary to operate at a constant gas gain (i.e. constant electron multiplication factor). Trace quantities of electronegative impurities in the counting gas decrease the electron multiplication and hence alter the distribution and amplitude of pulses in adjacent energy channels. Methane is

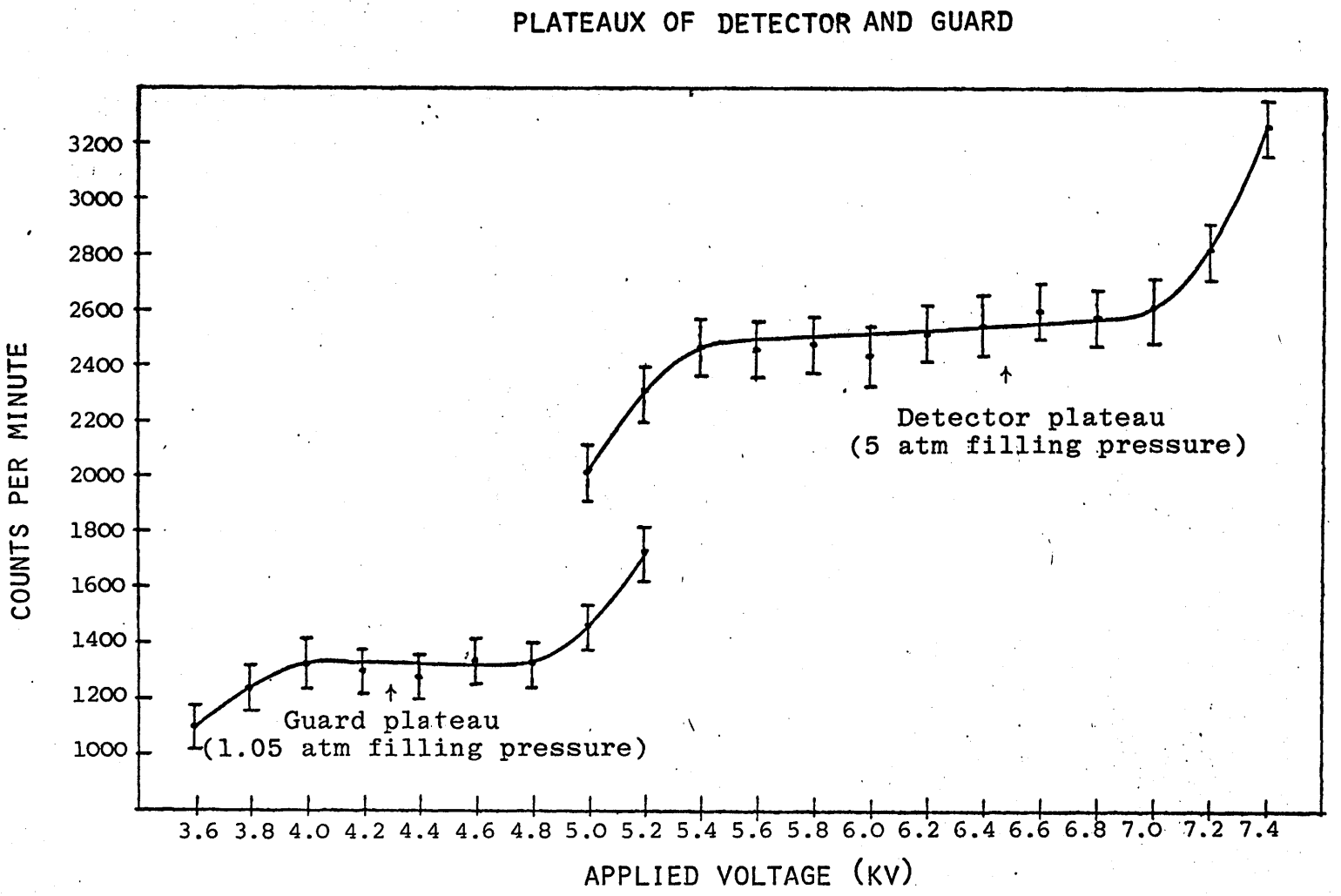

Figure II.19 Graph showing sample count rate, using an external ^{137}Cs source, in guard and detectors as a function of voltage.

much less susceptible to this effect than most gases but small variations in gas purity are unavoidable. Adjustment of the operating voltage compensates for any variation in gas purity. The operating voltage is determined by observing the distribution of counts, produced by an external ^{137}Cs source, in the net β and net α channels as the applied high voltage is increased (Figure II.20). The upper discriminator is set so that all pulses less than 18 keV are recorded in the net β channel. The voltage where the ratio net α/net β equals 7.0 is chosen as the operating voltage. For routine filling pressures the operating voltage is in the range 6.3±0.1 kV.

(d) Background data.

Background measurements are made weekly with a minimum of 4000 counts recorded per run. The "tank" methane supplied by Beckman is used as the background gas. Inactive gases prepared from marble, anthracite and inactive "tank" carbon dioxide have yielded data in agreement with those of "tank" methane (Baxter, 1969; Ergin, 1969; Farmer, 1972).

An inverse linear relationship is evident between the background count rate and barometric pressure. At high pressures, the physical resistance of the atmosphere to the passage of cosmic-ray derived particles is greater than at low pressures. Hence, periods of high atmospheric pressure correspond to low background count rates and vice versa. Atmsopheric pressure, continuously recorded by a laboratory barograph, ranged from 980 mb to 1040 mb during the total period of sample counting. The mean barometric pressure is calculated for each sample counting period.

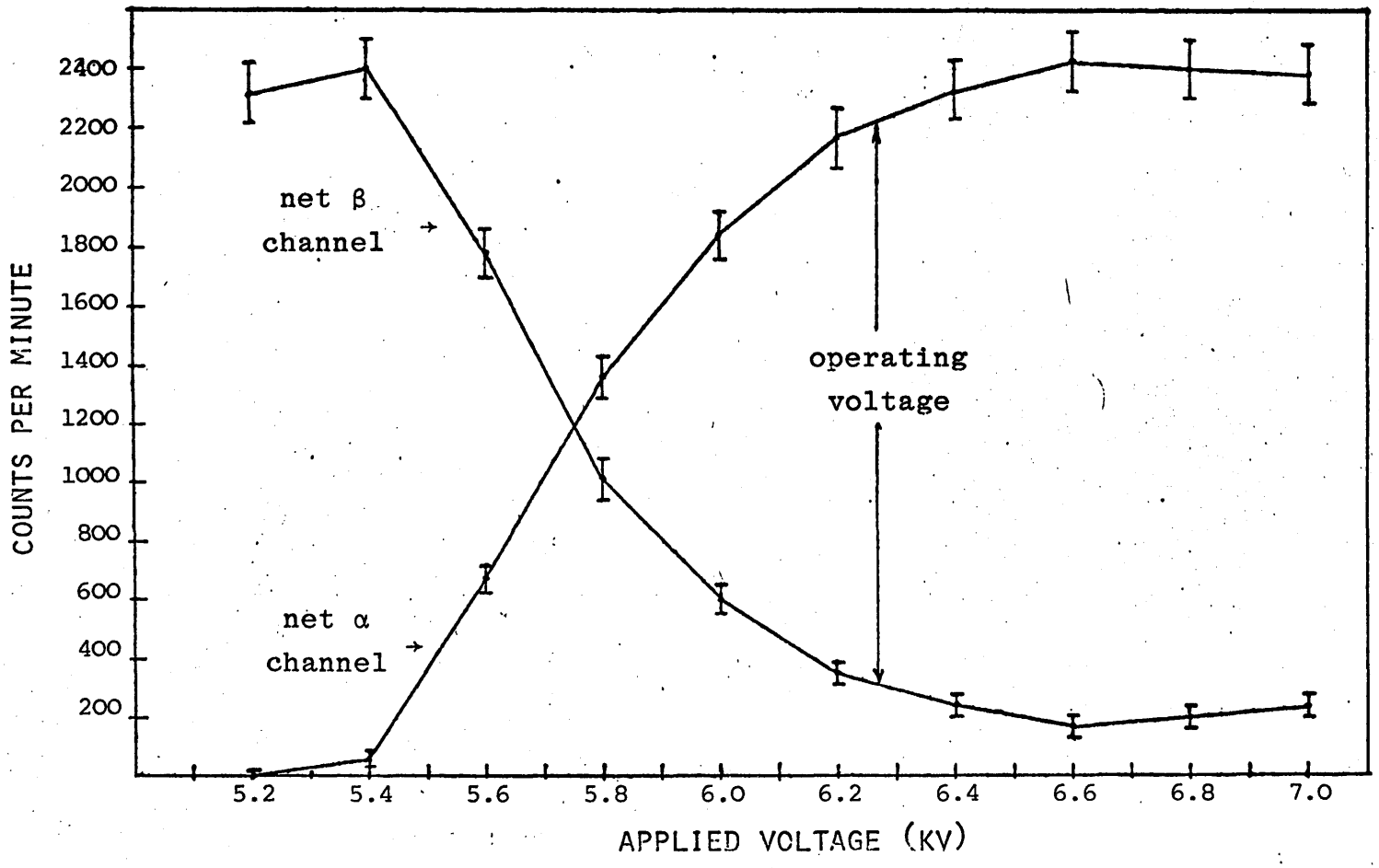

Figure II.20 Graph showing the distribution of counting rates in the netα and net β channels, obtained from an external ^{137}Cs source, as a function of detector voltage.

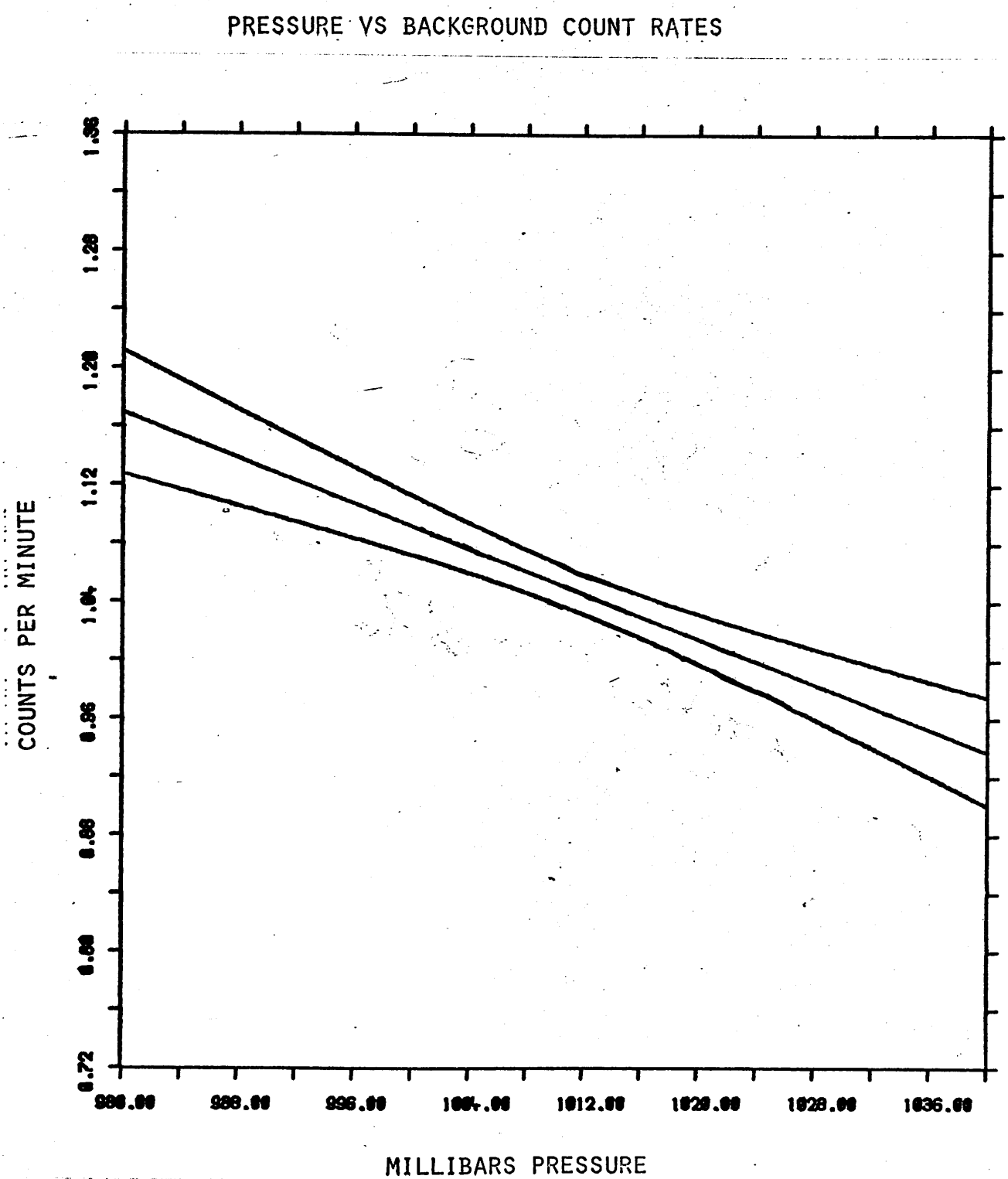

Figure II.21 Graph of variation in background count rate with atmospheric pressure showing the best fit least-squares regression straight line with associated 95% confidence interval.

The linear regression for any series of data was calculated by computer analysis using the method of least squares fit. Figure II.21 shows such an analysis for the period September 1971-November 1973. The background count rate is 0.991 ± 0.002 cpm at 1020 mb with a rate of change -0.004 cpm/mb at 5 atm filling pressure. The corresponding calculations are detailed in Appendix 3.

A small increase in background count rate has been observed since November 1973, the mean count rate rising to 1.111 ± 0.004 cpm at 1020 mb. This increase may reflect an enhanced cosmic-ray flux or may have resulted from minor modifications of the counting equipment. Regular monitoring of the background allows the gas counting programme to be divided into periods determined by the statistical agreement between series of background measurements. The critical parameter, however, is not the background count rate but is the analytical blank count rate. This, as will be seen in the next chapter, is considerably greater than background. Thus the slight variation in background count rate since November 1973 is of negligible importance.

CHAPTER III.

CALIBRATION AND STANDARDISATION

III.1 Contamination and Blank Values.

Preceding any discussion of equipment performance and/or results, it is necessary to give a detailed account of problems encountered with contamination and blank values. Personal discussions with both Ostlund (University of Miami) and Roether (University of Heidelberg) emphasised the importance of maintaining a low-level tritium environment for tritium assay, particularly within a department of Chemistry in which radiochemical investigations including tritium were being conducted during this investigation. Indeed, one particular laboratory which occasionally uses microcurie levels of tritium is less than 100 feet distant from the low-level laboratory. To ascertain the magnitude of tritium levels within the laboratory, atmospheric moisture was condensed from air using a large polythene funnel surrounding a 2' x ½" copper tube placed into liquid nitrogen (Figure II. 2). In less than 2 hours, 10-20 mls of water were collected. Using the same procedure, atmospheric moisture present in the nearest tritium laboratory was also collected. In addition, several atmospheric precipitation samples were collected into open beakers during storm activity at various distances away from the Chemistry Department to reduce risk of local tritium contamination.

These samples were collected during construction of the tritium laboratory so that synthesis to methane and subsequent gas counting were impossible. A Hewlett Packard Tri-Carb Liquid Scintillation counter which was calibrated for tritium was used for these measurements. A liquid scintillation cocktail specifically designed for water analysis was prepared as follows : a mixture of 40 g naphthalene (spectral grade), 200 mg $(CH_3)_2$POPOP, 4 g PPO, 100 ml methanol, 20 ml ethylene glycol was diluted to 1 litre with dioxane. Table III.1 presents the tritium levels for rain water, tap water, the low-level tritum laboratory and the nearest tritium laboratory.

BACKGROUND LEVEL OF TRITIUM

Low-level lab. (TU's ± 2σ)	Nearest tritium lab (TU's ± 2σ)	Rainwater (TU's±2σ)	Tap water (TU's± 2σ)
299 ± 46	5397 ± 46*	136 ± 31	181±28
339 ± 46*	2486 ± 57	127 ± 27	143±12
136 ± 31+	998 ± 55+	125 ± 30	
129 ± 27+		87 ± 24	

+, * - samples collected on same day

TABLE III.I

It is probable, from these observations, that levels of tritium in the low-level laboratory can occasionally be enhanced by contamination from the adjacent radiochemical laboratory. This potential tritium contribution plus contamination from the general ambient atmosphere could therefore introduce relatively large amounts of tritium to both blanks and samples, the latter being 1-3 orders of magnitude lower in their tritium content. However, by taking extreme care during the analytical procedure, these contamination effects can be maintained at insignificant levels.

Discussions with Otlet (Atomic Energy Research Establishment, Harwell) ensued, since similar but more extreme problems had been encountered at his laboratory through its very close proximity to the atomic reactor. Since the cost of reproducing the complex double-door, dehumidifying-atmospheric scrubbing system employed at Harwell proved prohibitive, it was decided that an inert atmosphere dry box, continuously flushed with dried, high purity argon and containing drying agents (silica gel), be constructed (Figure III.1). This system would ensure a tritium-free environment for storage, preparation and measurement of various chemicals, standards, and samples used in this research.

To determine blank values, tritium-free water was obtained from the unmanned Newton-on-Trent pumping station near Lincoln, England. Carbon-14 determination ascertained this water to be in excess of 25,000 years old. An independent measurement of the tritium content was performed by the International Atomic Energy Agency, Vienna, yielding a value of $-0.20 \pm 0.24(2\sigma)$ T.U. suggesting this water to be at least

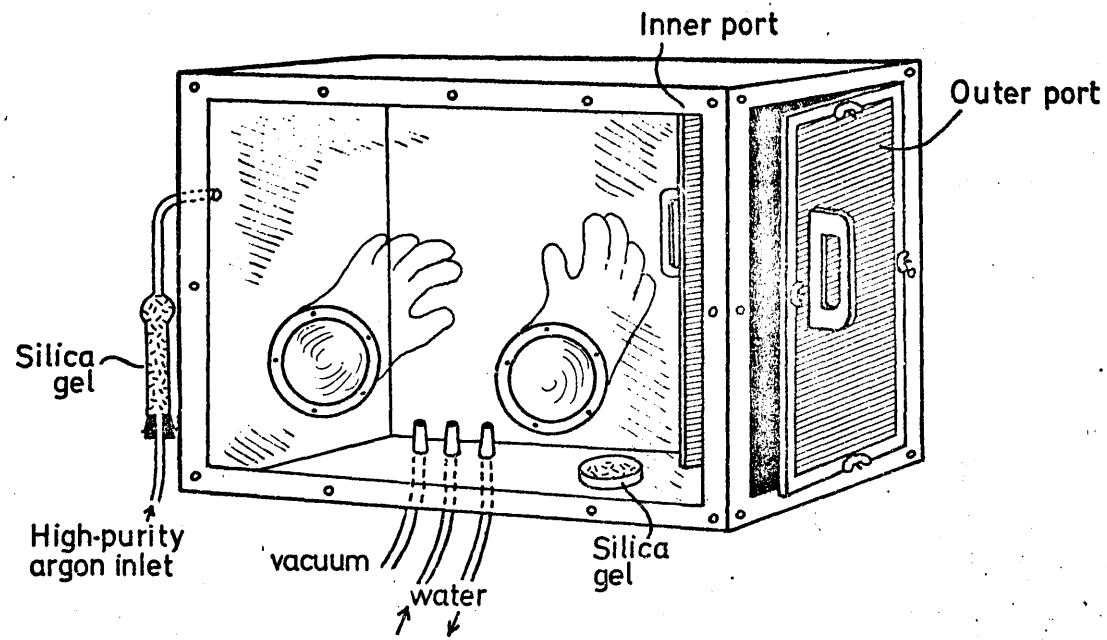

Figure III.1 Inert atmosphere dry box.

as inactive as the "dead" water of I.A.E.A.

After completion of the analytical system at Glasgow, tritium-free water was converted to methane, counted, and initially produced variable count rates averaging ~11 cpm (Table III.2). The major period of data acquisition occurred during the final stages of this research after a lower and more constant blank count rate of ~2.5 cpm was obtained (Table III.3). Blank determinations are normally performed in each bomb essentially simultaneously. Although somewhat variable, the blank counting rates exhibit a remarkable correlationship between reaction vessel and date of synthesis. Figure III.2 demonstrates this marked linearity of contamination between reaction vessels. Each point represents the count rate derived from tritium-free water concurrently synthesised in each reaction vessel. The difference between the average blank counting rates obtained from the tritium-free water during the initial and final periods of this research could reflect (i) improved technique gained by experience, (ii) contamination of the tritium-free water used during the initial period of this research or (iii) continuous and gradual outgassing of the stainless steel of the reaction vessels prior to attainment of final and stable blank counting rates. Since the minor modifications of technique were considered unlikely to influence blank levels and as the I.A.E.A. cross-check implied that no contamination of the tritium-free water had occurred, the former two possibilities seem considerably less valid than the third, namely the continual reduction of tritium-rich hydrogen outgassing from the stainless steel of the reaction vessels.

INITIAL PERIOD BLANK DETERMINATIONS-CONCURRENT SYNTHESIS	
Left Bomb (cpm ± 2σ)	Right Bomb (cpm ± 2σ)
2.39 ± 0.09	2.50 ± 0.10
3.20 ± 0.11	3.39 ± 0.09
5.20 ± 0.13	4.39 ± 0.13
6.10 ± 0.11	6.10 ± 0.14
6.29 ± 0.14	6.20 ± 0.15
8.20 ± 0.17	8.00 ± 0.18
9.00 ± 0.16	8.00 ± 0.19
9.80 ± 0.18	10.40 ± 0.18
10.00 ± 0.18	11.00 ± 0.22
10.50 ± 0.21	11.60 ± 0.19
16.00 ± 0.20	12.50 ± 0.20
12.29 ± 0.13	14.00 ± 0.21
13.50 ± 0.22	15.80 ± 0.22
18.00 ± 0.25	16.00 ± 0.32
19.19 ± 0.29	20.79 ± 0.27
25.19 ± 0.29	24.79 ± 0.26
10.92 ± 6.23 = Mean value (cpm ± 2σ) = 10.97 ± 6.24	

TABLE III.2

FINAL PERIODS BLANK DETERMINATION			
cpm ± 2 σ	cpm ± 2 σ	cpm ± 2 σ	cpm ± 2 σ
3.95 ± 0.08	2.06 ± 0.08	2.49 ± 0.09	3.16 ± 0.10
3.92 ± 0.11	2.49 ± 0.08	2.66 ± 0.09	3.25 ± 0.11
2.70 ± 0.09	1.94 ± 0.08	1.61 ± 0.08	2.21 ± 0.09
2.40 ± 0.10	1.92 ± 0.08	1.68 ± 0.08	1.79 ± 0.08
1.96 ± 0.08	1.80 ± 0.09	1.57 ± 0.07	1.96 ± 0.08
2.92 ± 0.10	2.73 ± 0.10	3.21 ± 0.10	
Mean value (cpm ± 2σ) = 2.45 ± 0.70			

TABLE III.3

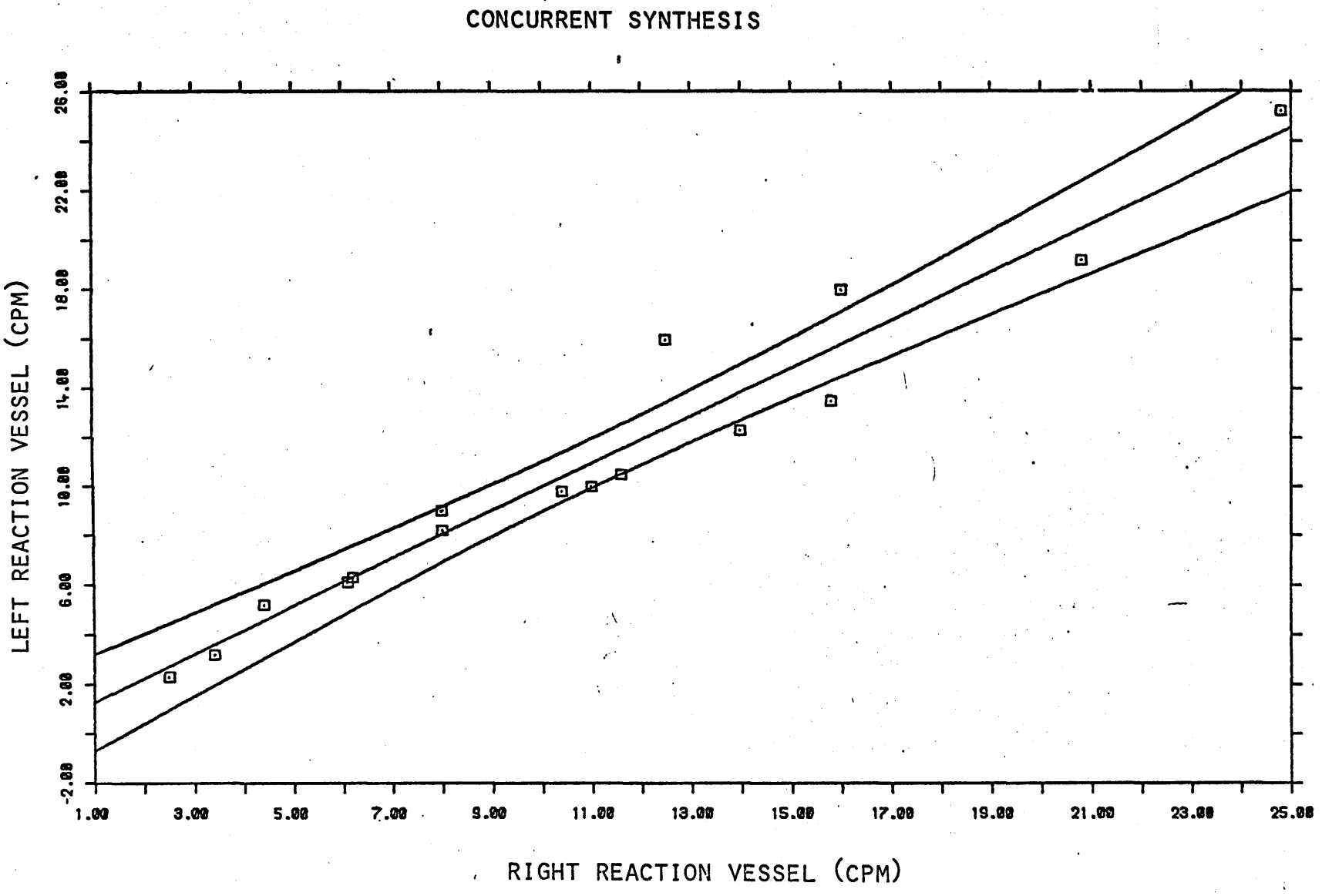

Figure III.2 Blank count rate in cpm for each reaction vessel determined during concurrent synthese. The expected deviation due to a $\pm 2\sigma$ error in count rates is shown by the square boundary surrounding each point. The best fit least-squares straight line is bounded by the associated 95% confidence interval.

Adsorption of a gas onto a solid surface can take place by two principal methods, namely by physical or chemical adsorption (chemisorption). In physical adsorption the gas molecules are attracted to the surface by Van der Waal's forces and the heat of adsorption is low (less than 10 kcal/mole). In chemisorption actual chemical combination, (involving a sharing or exchange of electrons) occurs between the gas molecules and those of the solid. Here the heat of adsorption is much higher (20-200 kcal/mole). The quantity of gas adsorbed at constant temperature on a given surface increases with the pressure of gas in the gas phase. The relation between the quantity adsorbed and the pressure at constant temperature is called an adsorption isotherm.

In any vacuum system which has reached equilibrium and in which leaks have been eliminated, the pressure depends on the total outgassing of the system and the pumping speeds of the vacuum pumps:

$$p = Q/S \text{ in torr} \qquad \text{(III.1)}$$

where Q is the outgassing rate in torr litre per second (torr $1.s^{-1}$) and S is the pumping speed in $1.s^{-1}$. Strictly speaking, this formula is true only for a discrete part of the system where molecular flow prevails and where one can consider a volume into which gas is evolved from surfaces and out of which gas flows due to pumping. The rate of outgassing of a material is expressed in torr litre per second per square centimeter (torr $1.s^{-1}cm^{-2}$) and the total outgassing of a system will be made up of the sum of the outgassing rates of each material present multiplied by its area. Frequently the pressure will depend on the outgassing of a large area

of material with a low outgassing rate, e.g. the chamber wall, or a small area of material with a high outgassing rate, e.g. a gasket or a component inside the system.

In general the pressure in a pumped vacuum system will slowly decrease with time due to reduction of the outgassing rate of the materials as gas is removed. This is because the rate depends on the surface coverage or on the concentration of gas dissolved in the material. Figure III.3 shows a typical plot of log outgassing rate against log time (Elsey, 1975b). As can be seen, the outgassing rate of a material at constant temperature reduces as the pumping time increases. The pumping time is usually expressed in hours. Outgassing rates may be presented in either graphical or tabular form. The plots of log outgassing rate against log time have negative slopes and are usually linear. In tabular form, the outgassing rate after a specified pumping time is quoted with the slope of the log-log plot for the same time. The outgassing rate is given the symbol K with a subscript indicating the pumping time. The slope is given the symbol α and the negative sign omitted. A typical statement is:

K_{10} stainless steel 5×10^{-10} torr $l.s^{-1}$ cm^{-2};

α_{10} stainless steel 1.0.

A contribution to the outgassing of the vessel walls and other components of a vacuum system is made by gas diffusing out of the bulk of the material. If, in fact, the gas diffuses right through the material from the outside, the process is called permeation. For 2 mm stainless steel exposed to a partial pressure of 4×10^{-4} torr of hydrogen (i.e. atmospheric concentration, Weast, 1968) concentration changes

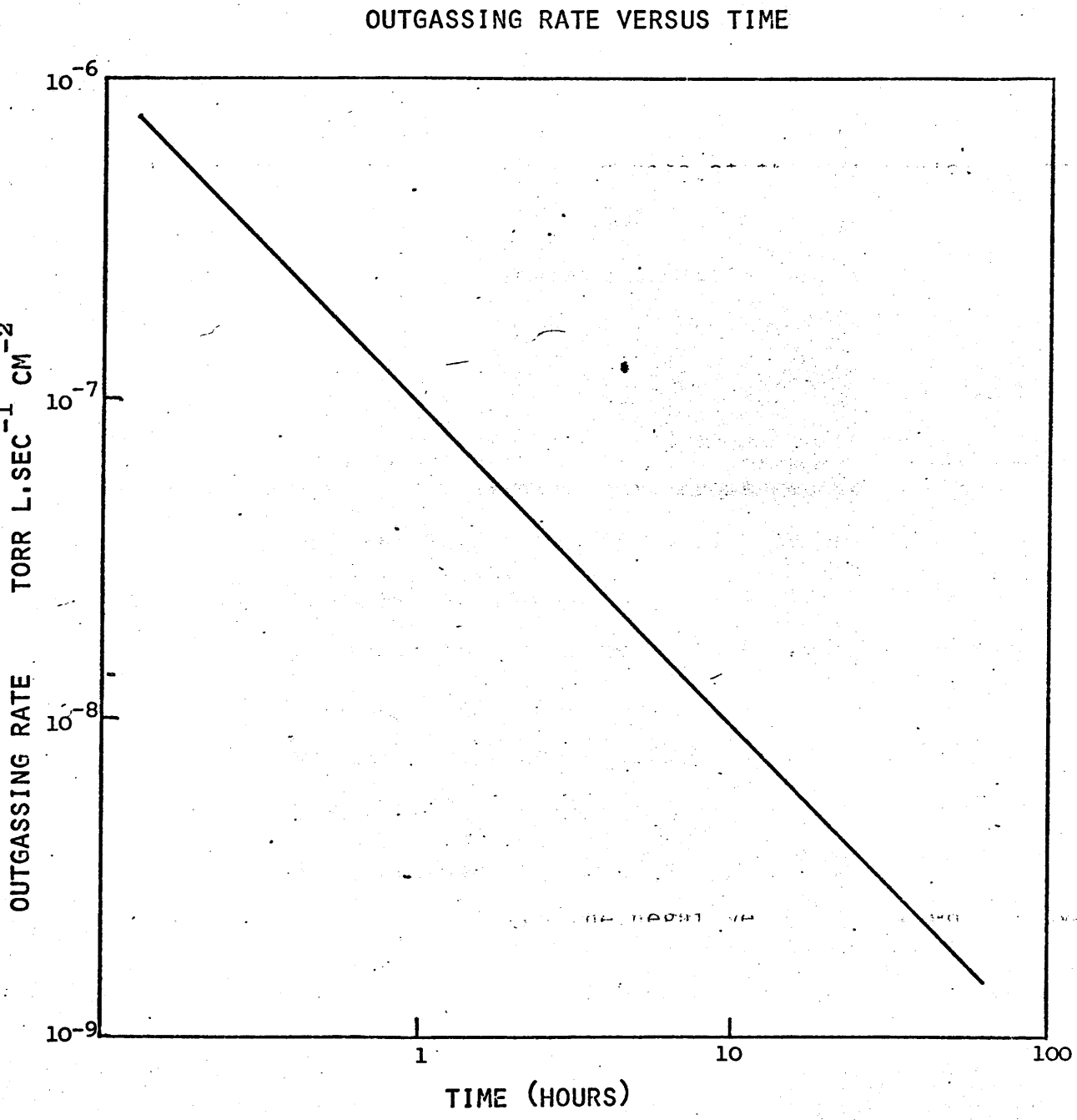

FIGURE III.3 Typical outgassing rate plot.

at room temperature are negligible. However, the normal bakeout, by virtue of the greatly enhanced diffusion constant at elevated temperatures, will modify this conclusion to the extent of establishing near-equilibrium permeation rates. Any attempt to reduce the outgassing rate below about 10^{-16} torr $l.cm^{-2}s^{-1}$ is pointless (Calder and Lewin, 1967).

According to Fick's law of diffusion, gas flow in a solid is proportional to the concentration gradient of the gas in the solid. Thus:

$$q = -D\ dc/dx \qquad \text{(III.2)}$$

where q is the gas flow across unit cross-section in unit time in the x direction. D is the diffusion coefficient and dc/dx is the concentration gradient. The minus sign indicates that the gas flow is in the opposite direction to the concentration gradient. Diffusion is an activated process and the diffusion coefficient increases with temperature according to the equation

$$D = D_o \exp(-E/RT) \qquad \text{(III.3)}$$

where E is the activation energy for diffusion.

Diffusion is a slow process and in the condition before equilibrium is achieved Fick's second law of diffusion applies:

$$D \frac{\delta^2 c}{\delta x^2} = \frac{\delta c}{\delta t} \qquad \text{(III.4)}$$

For the boundary condition of a vessel wall which is thick enough to be considered semi-infinite and which has an initial uniform gas concentration C_o, Lewin (1965) determined the outgassing rate after a pumping time t to be given by:

$$q_t = C_o D^{\frac{1}{2}} (t)^{\frac{1}{2}} \qquad \text{(III.5)}$$

Stainless steel contains large amounts of hydrogen which dissolves in the metal during manufacture. Chemical analysis by Calder and Lewin (1967) gave 5 cm^3 hydrogen per 100 g stainless steel or, equivalently, C_o = 0.3 torr 1.cm^{-3} with indication that C_o may have been even higher. With the reaction vessels employed in this study (ca 30 kg each) this amounts to a minimum 1500 cm^3 hydrogen. In stainless steel at room temperature, D is high enough for diffusion of hydrogen to limit the pressure attainable and yet low enough to prevent the concentration of the gas in the metal being significantly depleted in a reasonable time (Elsey, 1975b). D varies exponentially with temperature so to improve the outgassing either D can be lowered (e.g. drastically by immersing the metal in liquid helium), or the gas concentration in the metal can be depleted more quickly by raising the metal to a high temperature (e.g. $D_{300}(H_2$ stainless steel) = 3.5 x $10^{-8} cm^2 s^{-1}$ and $D_{1000}(H_2$ stainless steel) = 8.7 x $10^{-5} cm^2 s^{-1}$, Elsey, (1975b)). Calder and Lewin (1967) presented the following Table III.4 giving the effectiveness of intermediate temperatures and theoretical times for reaching an outgassing rate of 10^{-16} torr 1.$s^{-1} cm^{-2}$ for 2 mm thick stainless steel with C_o = 0.3 torr 1.cm^{-3} of hydrogen (~0.22 x 10^{-3} l-atm cm^{-3} of hydrogen). This outgassing rate corresponds to 1.47 x 10^7 molecules H_2/second diffusing from the walls of the reaction vessels. The percentage of tritium is not known. The bakeout is complicated by the two-stage outgassing procedure described in Chapter II. Furthermore, the reduction of water to hydrogen during methane synthesis at elevated temperatures and pressures causes hydrogen to redissolve into the steel walls of the reaction vessels and prolong the

t(sec)	D($cm^2 sec^{-1}$)	T(^oC)
1.0×10^6 (11 days)	3.5×10^{-8}	300
8.6×10^4 (24 hours)	3.8×10^{-7}	420
1.1×10^4 (3 hours)	3.0×10^{-6}	570
3.6×10^3 (1 hour)	9.0×10^{-6}	635

TABLE III.4 Bakeout times of 2 mm thick sheet at various temperatures for $q = 10^{-16}$ torr $1.cm^{-2}$ sec^{-1}

eventual total outgassing of the steel (Elsey, personal communication). Even if no hydrogen is reintroduced into the steel, at least 1 - 11 days of continuous outgassing would be required to decrease the outgassing rate to 10^{-16} torr $l.s^{-1}cm^{-2}$ based on 2 mm stainless steel outgassing data. The generalisation of the above considerations to materials of various thickness (e.g. 6 mm stainless steel reaction vessels) is that thicker material must be degassed for a longer period, approximately proportional to the square of the thickness (or, alternatively, at a correspondingly higher temperature), to give the same outgassing rate and will exhibit a lower (inversely proportional to thickness) permeation rate for atmospheric hydrogen (Calder and Lewin, 1967).

The surface condition of the stainless steel further obscures the outgassing rates. Jones et al (1973) suggest that after normal vacuum bakeout the surface of the steel is coated with a thin film of graphite, which itself is a strong absorbent of gases. This theory is supported by information published recently by Lambert and Comrie (1974). During several early methane syntheses, a large production of carbon was noted, examined by electron microscopy and determined to be filaments of pyrolytic carbon formed by dissolution of carbon into the steel (Baird, personal communication).

Table III.5 taken in part from Elsey (1975b) shows variations in outgassing rates for different stainless steels. The complex mechanisms of outgassing are not well understood. Contributions to outgassing come from surface desorption and from the bulk. Which predominates depends on the state

Material	K_1 torr $l.s^{-1}cm^{-2}x10^{10}$	α_1	K_{10} torr $l.s^{-1}cm^{-2}x10^{10}$	α_{10}
Mild steel	5400	1	500	1
Mild steel (slightly rusty)	6000	3.1	130	1
Mild steel (Chromium plated polished)	100	1	9.0	-
Mild steel (aluminium spray coated)	600	0.75	100	0.75
Steel (chromium plated fresh)	70.5	1	5.8	1
Steel (chromium plated polished)	91	1	8.0	1
Steel (nickel plated fresh)	42.4	0.9	4.94	0.9
Steel (nickel plated)	27.6	1.1	2.33	1.1
Steel (chemically nickel plated fresh)	83	1	7.05	1
Steel (chemically nickel plated polished)	52.2	1	4.6	1
Steel (descaled)	3070	0.6	2950	0.7
Stainless steel	-	-	14	1.6
Stainless steel	1750	1.1	210	0.75
Stainless steel	900	0.7	200	0.75
Stainless steel ICN 472 (fresh)	135	0.9	14.7	0.9
Stainless steel ICN 472 (sanded)	82.8	1.2	10.4	0.8
Stainless steel NS22S (mech. polished)	17.1	0.5	4.6	0.7
Stainless steel NS22S (electro. polished)	42.8	1.0	4.28	1.0
Stainless steel NS22S	144	1.3	13.5	1.9
Zinc	2210	1.4	322	0.8

TABLE 5 : Outgassing rates for various metals.

of the surface. However, the surface of common materials is an undefined mixture and it is probable that the process is controlled more by impurities such as carbon and oxides than by the base material or the gases desorped (Elsey, 1975a). The detailed factors which control the outgassing rates of materials need further investigation. The present evidence, however, suggests that this outgassing process is perhaps the single most important cause for the high and variable blank count rates especially during the early stage of this work when extensive carbon production occurred during several methane syntheses. The stainless steel surface must certainly have been affected, altering the outgassing rate and producing a variable blank count rate. Continual use of the reaction vessels, and gradual outgassing of the stainless steel have eventually brought the blank count rate to its present and stable value of 2.45 ± 0.70 cpm. The variation of blank counting rates within the same bulk sample of tritium-free water possibly reflects minor contributions from ambient tritium.

The analytical procedure is monitored periodically for tritium contamination. An aliquot of tritium-free water is removed before and after distillation, synthesised to methane and counted. The remainder of the sample is electrolytically enriched, neutralised, distilled, synthesised to methane and counted. As Table III.6 demonstrates, no apparent systematic introduction of tritium occurs during the analytical procedures with the exception of the synthesis. Within experimental error, tritium-free water exhibits a constant counting rate throughout the entire analytical procedure with tritium contamination appearing to occur during

MEASUREMENT OF THE BLANK COUNTING RATE CONTAMINATION THROUGHOUT ANALYTICAL PROCEDURE.

Sample	Distillation		Electrolytically Enriched
	before (cpm ±2σ)	after (cpm ±2σ)	(cpm ± 2σ)
1	4.53 ± 0.10	4.28 ± 0.13	N.D.
2	9.36 ± 0.16	9.24 ± 0.15	9.62 ± 0.19
3	7.94 ± 0.17	8.12 ± 0.14	8.24 ± 0.17
4	N,D.	6.10 ± 0.14	5.96 ± 0.13
5	N.D.	22.27 ± 0.26	22.44 ± 0.29
6	8.23 ± 0.15	7.91 ± 0.15	8.34 ± 0.16
7	N.D.	6.13 ± 0.12	6.26 ± 0.15

N.D. - not determined.

TABLE III.6

the methane synthesis. Although blank values yield appreciable counting rates, it is sufficient to monitor fluctuations in the blank by performing tritium-free water analyses before and after each sample assay, further ensuring that no memory effect is experienced between samples. In addition, concurrent synthesis of tritium-free water in the second reaction vessel whenever possible allows accurate evaluation of contamination levels within each sample.

III.2 Storage.

Slow continuous contamination of both standards and tritium-free water has also been examined. Several 1 litre ground glass-sealed bottles were filled with tritium-free water and stored in the laboratory atmosphere for a period of 18 months. One bottle was used in the determination of blank counting rates and opened repeatedly in the laboratory for removal of small aliquots. Measurements made at I.A.E.A., Vienna showed that for this sample the tritium level increased marginally to 0.54 ± 0.24 ($\pm 2\sigma$) T.U. while no increase was recorded in that of the unopened sample. It was concluded that contamination of samples would be negligible if stored in a properly sealed container. This conclusion was substantiated by Roether (personal communication, 1971) who described the unpublished results of Sonntag and Munnich. Tritium contamination and water loss from various container materials and seals were measured as a function of time. Ground glass-sealed bottles were found best for sample storage, with no measurable evidence of contamination. Further measurements were performed after increasing the size both of the stopper and air space in sample bottles.

In each case a decrease in performance of the storage vessel was found. Bowen and Roether (1973) concluded that samples stored in polyethylene bottles take up tritium during storage by diffusion of ambient moisture through the walls. As described in Chapter II, whenever possible, small-necked ground glass-sealed bottles were used for the collection and storage of samples. If this was not possible, glass bottles with threaded bakelite caps were used with the stipulation that some additional sealing agent be employed (i.e. heat shrink plastic tape or melted wax). In either case, the vessel would be nearly completely filled, with space only to allow for water expansion thus keeping air space minimal.

III.3 Enrichment Factors.

(a) Fundamental formulae.

The extent of enrichment of the heavy hydrogen isotopes must be known to calculate the initial tritium concentration. The necessary relations and data supporting the separation of protium, deuterium, and tritium are given by Kaufman (1953). For completeness they will be reviewed here.

Suppose we have a water sample of V ml containing P moles of protium, D moles of deuterium and T moles of tritium; then, for any one, the fractional decrease in the water phase during electrolysis is $\frac{d(P,D,T,)}{P,D,T,}$. These quantities can be regarded as fitting the following equation:

$$d(\ln P) = \alpha d(\ln D) = \beta d(\ln T) \qquad \text{(III.6)}$$

where α and β are known as separation factors and α is independent of deuterium concentration (Farkas, 1937). It is assumed

that β is not a function of tritium concentration. Upon (i) integrating equation III.6 from the initial condition represented by subscript i to the final condition, (ii) considering that P>>D>>T, (iii) assuming molal volumes, V, do not depend appreciably on the hydrogen isotopes (Kirshenbaum, 1951) i.e. that the molar volumes of H_2O and D_2O are equal, and (iv) using α and β as average values of these factors during electrolysis, we derive:

$$\ln \frac{V}{V_i} = \alpha \ln \frac{D}{D_i} = \beta \ln \frac{T}{T_i} \qquad \text{(III.7)}$$

which on rearranging yields:

$$\frac{V}{V_i} = \left[\frac{D}{D_i}\right]^{\alpha} = \left[\frac{T}{T_i}\right]^{\beta} \qquad \text{(III.8)}$$

If the fractional recoveries of protium (V/V_i), deuterium (D/D_i), and tritium (T/T_i) are denoted R_v, R_d, and R_t respectively, formula (III.8) becomes:

$$R_v = R_d^{\alpha} = R_t^{\beta} \qquad \text{(III.9)}$$

By using X's for the molar fractions of the isotopes in question, equation (III.8) can be transformed to:

$$X_t^i = X_t \cdot \frac{V}{V_i} \left[\frac{X_d^i}{X_d} \frac{V_i}{V}\right]^{\alpha/\beta} \qquad \text{(III.10)}$$

Equation (III.10) shows which quantities have to be known for the determination of an unknown assay of tritium in a sample of natural water. By following and calibrating the deuterium enrichment, that for tritium can be derived, and the entire electrolytic enrichment procedure tested against the theoretical results obtained from Bigeleisen (1962). Experience has shown that even this is not necessary, as the linearity and reproducibility of tritium enrichment versus volume

reduction is quite satisfactory. Even when one measures the D/H ratios in the electrolysed samples to gauge the degree of enrichment, better accuracy is hardly achieved in practice (Ostlund and Werner, 1962). It was therefore decided to measure the tritium enrichment versus volume reduction of standard solutions and whenever possible, to monitor both separation factors by additional measurement of deuterium content. Hence, the reliability of the electrolytic procedure could be checked.

(b) Deuterium enrichment.

Deuterium enrichments are normally determined on a D/H mass-spectrometric isotopes instrument. However, non-availability of such an instrument enforced development of a new technique in collaboration with Ritchie (University of Glasgow) using the available equipment.

Measurement of D/H ratios in water samples is now performed routinely by mass-spectrometric analysis of the ratio of $(^1H_2{}^{16}O)^+$ to $(^1H^2D\ ^{16}O)^+$ ion intensities using an A.E.I. MS902S double-focussing mass-spectrometer which has a maximum static resolving power of 100,000 (or 10 ppm). The ions are detected by a high gain electron multiplier. The signal produced is displayed on a switched attenuating collector meter which provides a wide dynamic range for the relative intensities of measured ions. A function switch provides that the accelerating voltage may be switched from either low to high mass ion positions. These low and high mass ion positions are precisely adjusted to 1 ppm via a decade resistance box. By alternating the function switch between these mass ion

positions, sequential measurement may be taken.

The ion source and vacuum system are initially baked out at 200°C for 3 days to reduce memory effects. After cooling, the ion source filament is switched on for 2 hours to obtain constant temperatures (150°C). A 1 ml sample is introduced via a 5ml Quickfit flask, frozen by liquid nitrogen, and evacuated by an oil diffusion pump. The isolated sample is allowed to warm, expanding into a 2 litre flask, which is fed into the ionisation chamber and left to flush through the instrument at least one hour before taking any measurements, further reducing risk from memory effects. The sample pressure in the ionisation chamber is adjusted to 1.5×10^{-6} torr. With the accelerating voltage set at 8 kV, a trap current of 500 μA and an electron voltage of 45 eV, the magnet current is adjusted to measure $(^{1}H_{2}\ ^{16}O)^{+}$ ions on the collector meter. Source tuning is adjusted for maximum ion intensity.

It was expected that in addition to the peak from $(^{1}H^{2}D^{16}O)^{+}$ (m/e = 19) contributions from $(^{1}H_{3}\ ^{16}O)^{+}$ would occur (the latter in fact always larger than the former but resolvable under high resolution). With the static resolving power of the instrument adjusted to ~12,000, the m/e = 19 region shows, in addition, two less intense peaks (< 10% intensity of the $(^{1}H_{3}\ ^{16}O)^{+}$ ion) with some slight overlap to adjacent ion peaks. With the resolving power increased to ~ 30,000 interference to the $(^{1}H^{2}D^{16}O)^{+}$ ion is minimal. Beyond 30,000 resolving power, sensitivity is severely reduced with meter fluctuations unreadable. Furthermore, synthetic solutions containing known concentrations of D_2O

were prepared and analysed to ensure correct instrument set-up and operation. Table III.7 presents the resulting data with the expected and observed D/H ratios. Analyses of these spiked samples immediately defined the $(^{1}H^{2}D^{16}O)^{+}$ ion peak and D/H ratios were determined.

With low and high ion mass positions adjusted to give about half-scale deflection on the readout meter (eliminating any non-linearity effects), readings are then taken over a period of 30 minutes and the entire procedure repeated for each sample.

MASS-SPECTROMETRY CALIBRATION FOR D/H MEASUREMENT

	D/H Ratios	
	Calculated (ppm±2σ)	Measured (ppm±2σ)
I	8160 ± 100	8255 ± 180
II	5780 ± 100	5770 ± 220
III	4140 ± 100	4010 ± 121

TABLE III.7

(c) Determination of enrichment factors.

To determine the enrichment factors, 20 solutions prepared from tritium-free water, heavy water and tritiated water were electrolysed. Tritiated water standards were obtained from the International Atomic Energy Agency, Vienna, while 99.79% heavy water was purchased from BDH Ltd. V_i and V were obtained by weighing; X_d and X_d^i were measured mass spectrometrically; X_t^i was calculated; and X_t measured in the methane counting apparatus. The nature of the reservoir addition procedure does not exactly fulfil the requirements of equations (III.8) and (III.10) which are valid for batch electrolysis where the entire sample reacts. In applying them to the reservoir addition electrolysis, it must be remembered that only part of the sample participates in the reaction. Various adaptations are possible. It is common to transform the enrichment factors (Ostlund and Lundgren, 1964) so that equation (III.9) becomes:

$$R_v = R_d^{\alpha'} = R_t^{\beta'} \qquad \text{(III.11)}$$

which can further be transformed to (Metson, 1969):

$$R_t = TP^{-1} \qquad \text{(III.12)}$$

where T is the tritium enrichment factor (T/T_i) and P^{-1} is the volume reduction factor (V/V_i);

and equation (III.10) becomes:

$$X_t^i = X_t \cdot \frac{V}{V_i}\left[\frac{X_d^i}{X_d}\,\frac{V_i}{V}\right]^{\alpha'/\beta'} \qquad \text{(III.13)}$$

Bigeleisen (1962) showed theoretically that α/β could not be expected to be constant but that $\ln \alpha / \ln \beta$ is fundamentally constant. Therefore,

$$\ln \beta' / \ln \alpha' = \eta' \qquad \text{(III.14)}$$

In Table III.8 are given the results obtained from the synthetic solutions. The data support the conclusions that η' is a constant. The function thus is best expressed by

$$\eta' = \log \beta' / \log \alpha' = 1.37 \pm 0.07 \qquad \text{(III.15)}$$

Furthermore, as equation (III.7) suggests, a log-log graph of volume reduction factors versus tritium enrichment factors should be linearly related with slope equal to β and should therefore provide a calibration curve for further electrolytic enrichments. For convenience, the volume reduction factor is inverted and referred to, in this thesis, as the volume enrichment factor. The graph for tritium enrichment versus volume enrichment of the data presented in Table III.8 is shown in Figure III.4. A noticeable deviation from linearity occurs when volume enrichment factors exceed 100 fold. All samples, however, require tritium enrichment factors of 40 - 60 fold corresponding to volume enrichment factors well below this region of non-linearity. Indeed, if only those points with volume enrichment factors less than 100 fold are considered and a straight line drawn, a correlation coefficient of 0.989 is calculated compared with 0.971 for all data points.

The correlation coefficient is associated with the probability that a given set of data fits a particular mathematical relationship. The high probability of fit (maximum value equals + 1.0 or - 1.0) gives confidence to the

Calibration of tritium enrichment and determination of the apparent fractionation factors.

Samples	V_i ($g\pm 2\sigma$)	V_f ($g\pm 2\sigma$)	X_d^i ($ppm\pm 2\sigma$)	X_d ($ppm\pm 2\sigma$)	X_t^i ($cpm\pm 2\sigma$)	X_t ($cpm\pm 2\sigma$)	α'	β'	β'/α'	η'
1	985±1	3.91±0.001	-	-	1.86±0.10	165.90±1.5	-	5.41	-	-
2	992±1	6.96±0.001	-	-	0.93±0.10	71.60±1.0	-	8.29	-	-
3	1015±1	19.23±0.001	-	-	0.36±0.02	13.50±0.26	-	11.60	-	-
4	1036±1	12.48±0.001	-	-	0.35±0.02	18.60±0.30	-	9.71	-	-
5	1030±1	44.78±0.001	-	-	0.35±0.02	3.96±0.16	-	4.35	-	-
6	1030±1	44.78±0.001	-	-	0.35±0.02	4.07±0.13	-	4.52	-	-
7	574±1	8.43±0.001	-	-	0.35±0.02	15.27±0.29	-	9.30	-	-
8	574±1	8.43±0.001	-	-	0.35±0.02	14.27±0.29	-	8.09		
9	1030±1	13.52±0.001	-	-	0.35±0.02	15.78±0.31	-	8.48	-	-
10	973±1	11.41±0.001	-	-	0.18±0.02	10.64±0.25	-	12.32	-	-
11	981±1	19.05±0.001	2200±38	46470±639	36.77±0.70	1140±2	4.42	7.77	1.76	1.38
12	977±1	3.10±0.001	3010±57	223690±4410	36.77±0.70	4751±2	3.98	6.44	1.62	1.35
13	988±1	33.49±0.001	2780±36	33400±716	36.77±0.20	636±2	3.77	6.35	1.68	1.39
14	982±1	31.12±0.001	419±57	5380±172	0.33±0.02	6.11±0.21	3.84	6.47	1.69	1.39
15	962±1	24.62±0.001	380±61	6044±70	0.33±0.02	7.38±0.18	4.08	6.57	1.61	1.34
16	998±1	29.45±0.001	360±61	4596±121	0.18±0.02	3.22±0.16	3.53	5.51	1.56	1.35
17	991±1	32.73±0.001	260±57	3555±220	0.18±0.02	3.78±0.50	4.29	9.32	2.17	1.53
18	1016±1	15.23±0.001	260±57	7840±180	0.18±0.02	7.78±0.18	5.29	9.56	1.81	1.36
19	1015±1	12.32±0.001	260±57	11000±230	0.18±0.02	9.96±0.21	6.62	11.08	1.67	1.27
20	962±1	23.73±0.001	-	-	0.17±0.02	3.97±0.29	-	6.72	-	-

MEAN VALUES $\pm 1\sigma$ $\alpha' = 4.42\pm0.97$ $\beta' = 7.48\pm2.23$ $\alpha'/\beta' = 1.73\pm0.18$ $\eta' = 1.37\pm0.07$

TABLE III.8

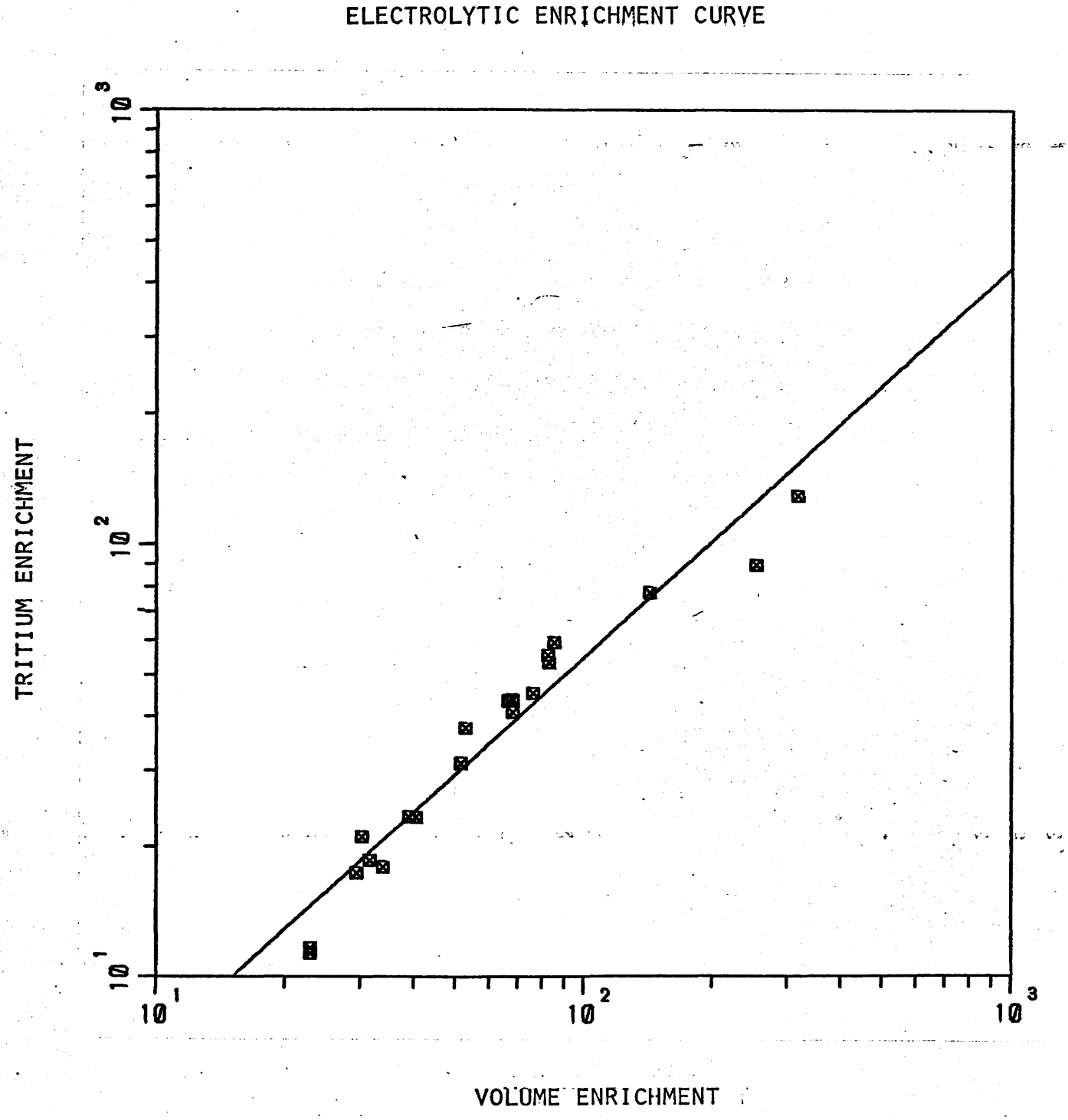

Figure III.4 Graph showing all tritium standard electrolyses with the best fit least-squares straight line. The expected deviation due to a $\pm 2\sigma$ error in tritium or volume enrichment is shown by the square boundaries surrounding each X symbol.

log-log representation of the data. The electrolytic calibration curve (Figure III.5) presents this line and the associated 95% confidence interval error bars for the best fit least-squares straight line as a whole and is used to evaluate tritium enrichment factors for further sample assays.

(d) Recovery and reproducibility.

Metson (1969), while concluding that a complete theoretical comparison of sample addition methods is difficult, derived tritium recovery equation (III.16) which when used in conjunction with equation (III.17) predicts, via equation (III.18), that the overall recovery of tritium should be higher with continuous addition methods.

$$R_1 = \frac{V_r}{V_f} \left[\beta - (\beta - 1) \exp - (1/\beta) \left(\frac{V_t}{V_r} - 1\right) \right] \quad \text{(III.16)}$$

$$R_2 = \left[\frac{V_f}{V_r}\right]^{1/\beta_1} \quad \text{(III.17)}$$

$$R = R_1 R_2 \quad \text{(III.18)}$$

He considered the electrolysis to be performed in two stages with firstly the total volume (V_t) being reduced to the intermediate or reacting volume (V_r), which remains constant by continuous addition and secondly V_r being reduced to final volume (V_f). It was assumed that $\beta = \beta_1$. Equation (III.15) was used primarily to investigate the influence of V_r on R_1 which increases exponentially as V_r increases but small gains in recovery must be balanced against practical considerations (e.g. the maximum electrolyte concentration is dictated by

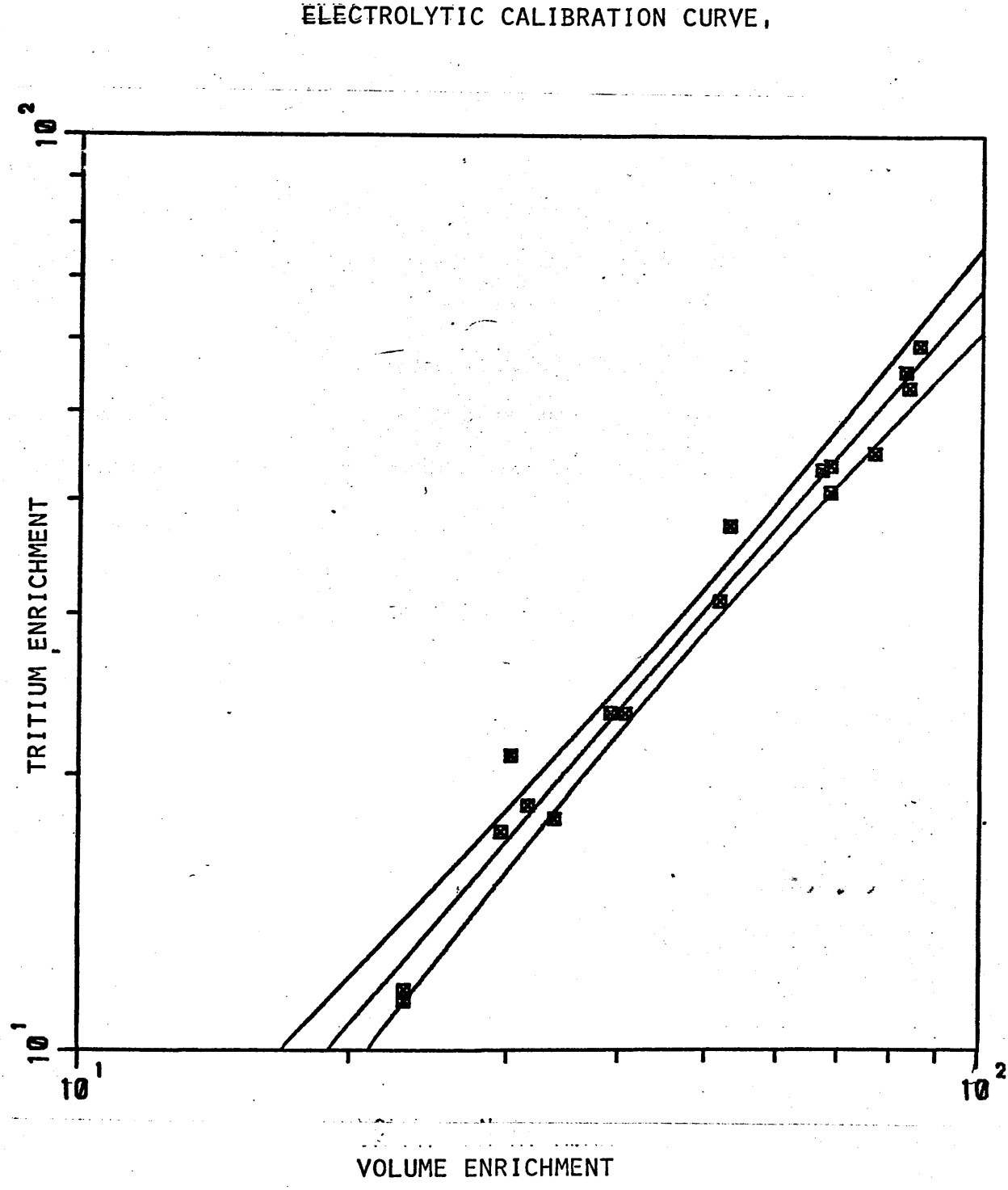

Figure III.5 The tritium calibration curve for determination of tritium enrichment factors for different degrees of volume enrichment (<100 fold). The expected deviations due to a $\pm 2\sigma$ error in tritium or volume enrichment are shown by the square boundaries surrounding each X symbol. The best fit least-squares straight line is bounded by the 95% confidence interval of the line used as a whole.

the final volume, V_f, and it is advantageous to keep V_r as low as possible to improve the electrolyte conductivity). Figure III.6 (in which V_t = 1000 mls, V_r = 5 mls, $\beta = \beta_1 = 10$, and which includes curves for R_2 and overall recovery, R) shows that as the volume V_r becomes large the rate of increase falls progressively. Metson then experimentally confirmed the hypothesis that better recoveries are obtained by continuous addition than by discrete addition with mean values of 61.0 ± 2.0% (2σ) versus 53.0 ± 2.0% (2σ) respectively.

Several solutions were electrolysed under similar conditions to determine the reproducibility of tritium recovery between different cells and the data are presented in Table III.9. A mean tritium recovery of 62.3 ± 1.5% (2σ) was obtained. Replicate analyses are included and these further demonstrate the reproducibility of the electrolytic procedure. Table III.10 presents an independent check of tritium recovery using the D_2O tracer method. The agreement of tritium recovery between these methods is well within experimental error (± 5%). It was therefore concluded that an independent determination of the tritium recovery by using additional deuterium measurement was unnecessary in routine determinations.

During electrolysis the gases bubbling through the liquid and escaping from the system carry away both water vapour and spray. The overall recovery is therefore reduced by these loss mechanisms. The influence of vapour pressure and spraying was investigated by Ostlund and Werner (1962)

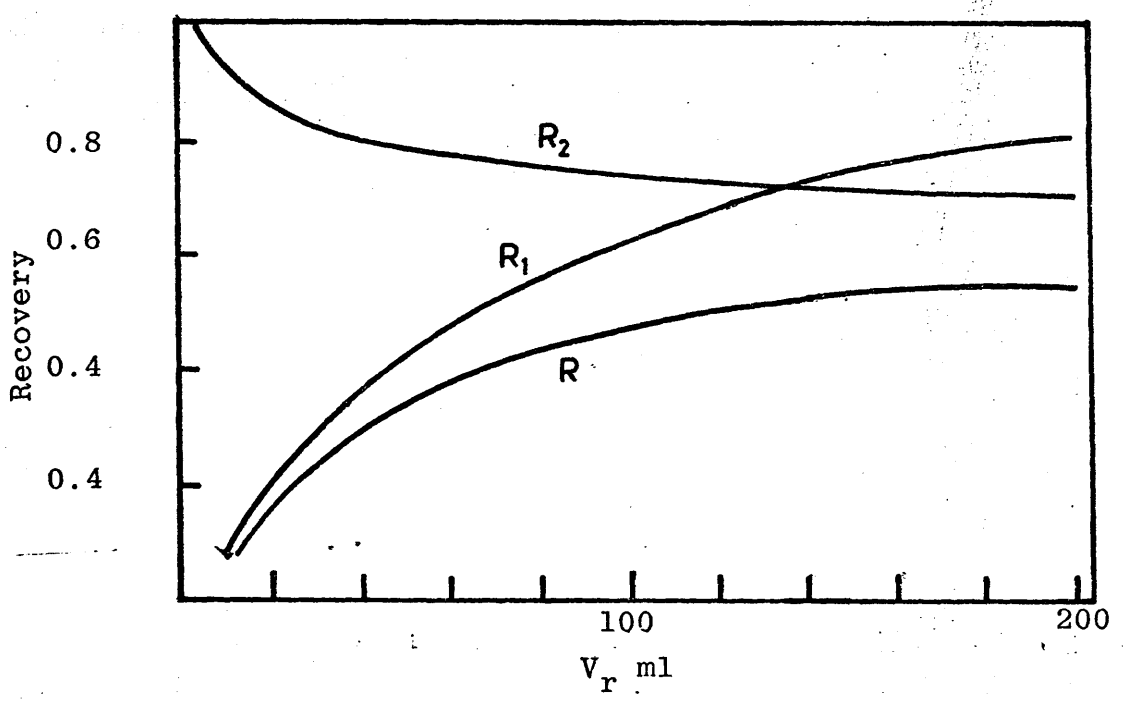

Figure III.6 Variation of recovery with change in reacting volume, V_r, for V_f = 5 ml, V_t = 1000 ml and $\beta = \beta_1 = 10$: R_1 = theoretical tritium recovery for continuous sample addition (V_r constant); R_2 = theoretical tritium recovery when V_r is electrolysed to final volume V_f and $R = R_1 R_2$ = over-all recovery.

REPRODUCIBILITY - TRITIUM RECOVERY BETWEEN CELLS

SAMPLE	CELL	VOLUME ENRICHMENT FACTOR ± 2σ (P)	TRITIUM ENRICHMENT FACTOR ± 2σ (T)	TRITIUM RECOVERY $R=TP^{-1}$ ± 2σ (%)
1	3	46.7 ± 0.05	29.0 ± 1.0	62.10 ± 2.14
2	7	49.5 ± 0.06	31.1 ± 1.0	62.83 ± 2.20
3	1	47.6 ± 0.05	29.6 ± 1.0	62.18 ± 2.10
4	2	46.0 ± 0.05	28.5 ± 1.0	61.96 ± 2.18
5	8	48.5 ± 0.05	30.3 ± 1.0	62.47 ± 2.06
6	6	49.3 ± 0.05	30.0 ± 1.0	60.85 ± 2.03
7	10	46.8 ± 0.05	28.5 ± 1.0	60.90 ± 2.14
8	8	59.6 ± 0.06	38.0 ± 1.0	63.76 ± 1.68
9	10	55.9 ± 0.06	35.0 ± 1.0	62.61 ± 1.79
10	8	45.9 ± 0.05	28.0 ± 1.0	61.00 ± 2.18
11	6	50.5 ± 0.06	31.0 ± 1.0	61.39 ± 1.98
12	10	61.9 ± 0.11	40.0 ± 1.0	64.62 ± 1.62
13	5	52.0 ± 0.01	32.0 ± 1.0	61.54 ± 1.92
14^{+}	8	67.2 ± 0.11	43.0 ± 1.0	63.99 ± 1.49
15^{+}	10	50.2 ± 0.05	31.0 ± 1.0	61.75 ± 1.99
16*	10	38.9 ± 0.04	23.0 ± 1.0	59.13 ± 2.57
17*	5	66.9 ± 0.11	43.0 ± 1.0	64.28 ± 1.50
18^{-}	8	48.2 ± 0.04	29.5 ± 1.0	61.20 ± 2.00
19^{-}	2	66.7 ± 0.11	43.0 ± 1.0	64.47 ± 1.50

Mean averages ± 2σ = 52.5 ± 8.2, 32.8 ± 5.8, 62.26 ± 1.46.

+,*,-, represent replicate analysis.

TABLE III.9

Sample	α' factor	β' factor	Volume enrichment factor $\pm 2\sigma$ (P)	Deuterium enrichment factor $\pm 2\sigma$ (D)	Tritium enrichment factor $\pm 2\sigma$ (T)	Tritium $R=TP^{-1}$ (%)	Recovery D_2O method $R=R_D^{\alpha'/\beta'}$ (%)
1	4.42	7.77	51.5 ± 0.05	21.1 ± 0.5	31.0 ± 0.2	60.19	60.25
2	3.98	6.44	315.2 ± 0.34	74.3 ± 2.0	129.2 ± 0.7	40.99	40.94
3	3.77	6.35	29.5 ± 0.03	12.0 ± 0.3	17.3 ± 0.1	58.64	58.62
4	3.84	6.47	31.6 ± 0.03	12.8 ± 1.8	18.5 ± 1.3	58.54	58.49
5	4.08	6.57	39.1 ± 0.04	15.9 ± 2.6	22.4 ± 1.5	57.29	57.19
6	3.53	5.51	33.9 ± 0.03	12.5 ± 2.2	17.9 ± 2.2	52.80	52.77
7	4.29	9.32	30.3 ± 0.03	13.7 ± 3.1	21.0 ± 3.6	69.31	69.39
8	5.29	9.26	66.7 ± 0.07	30.2 ± 6.7	43.2 ± 4.9	64.77	63.59
9	6.66	11.08	82.4 ± 0.08	42.3 ± 9.3	55.3 ± 6.3	67.11	67.14

TRITIUM RECOVERY BETWEEN METHODS

TABLE III.10

and applied to the calculation of the true electrolytical enrichment factors α_o and β_o. No real improvement was achieved in the calculation of tritium recovery and it was subsequently assumed that water loss is identical in both sample and recovery cells. This assumption was adopted by Bainbridge and O'Brien (1962), Metson (1969) and others and has been employed throughout this research. The cells, of identical construction, are energised by Constant Current Density Units and run in a water bath of controlled temperature, so that any change in operating conditions will be negligible.

CHAPTER IV.

DISCUSSION OF EASTERN TROPICAL PACIFIC OCEAN DATA.

IV.1 Introduction.

The complex interplay of physical, chemical and biological processes necessitates, in the full description of the oceanography of any region, consideration of as many and as wide a range of tracers as possible. In general, the overall picture is synthesised from the work of several different groups of workers, falling roughly into the three categories mentioned above. The work reported in this chapter was undertaken as a contribution towards the understanding of the oceanography of the eastern tropical Pacific. Measurements were made on both conservative and non-conservative properties in the hope that the relative importance of various processes could, to some extent at least, be distinguished. Samples were collected at 12 stations during cruise T-AGOR 3-73-1 of U.S.N.S. Bartlett in March 1973 from Callao, Peru to Acapulco, Mexico. The relevant portion of the ship's track is shown in Fig. IV.1. Appreciation of the full significance of the tritium results is, however, dependent on these incorporated into a general scheme emerging both from analyses of samples, taken at the same locations, for other tracer parameters (e.g. $\delta^{18}O$, ^{228}Ra, ^{226}Ra, ^{222}Rn, ^{210}Pb) and from previous work in the same area.

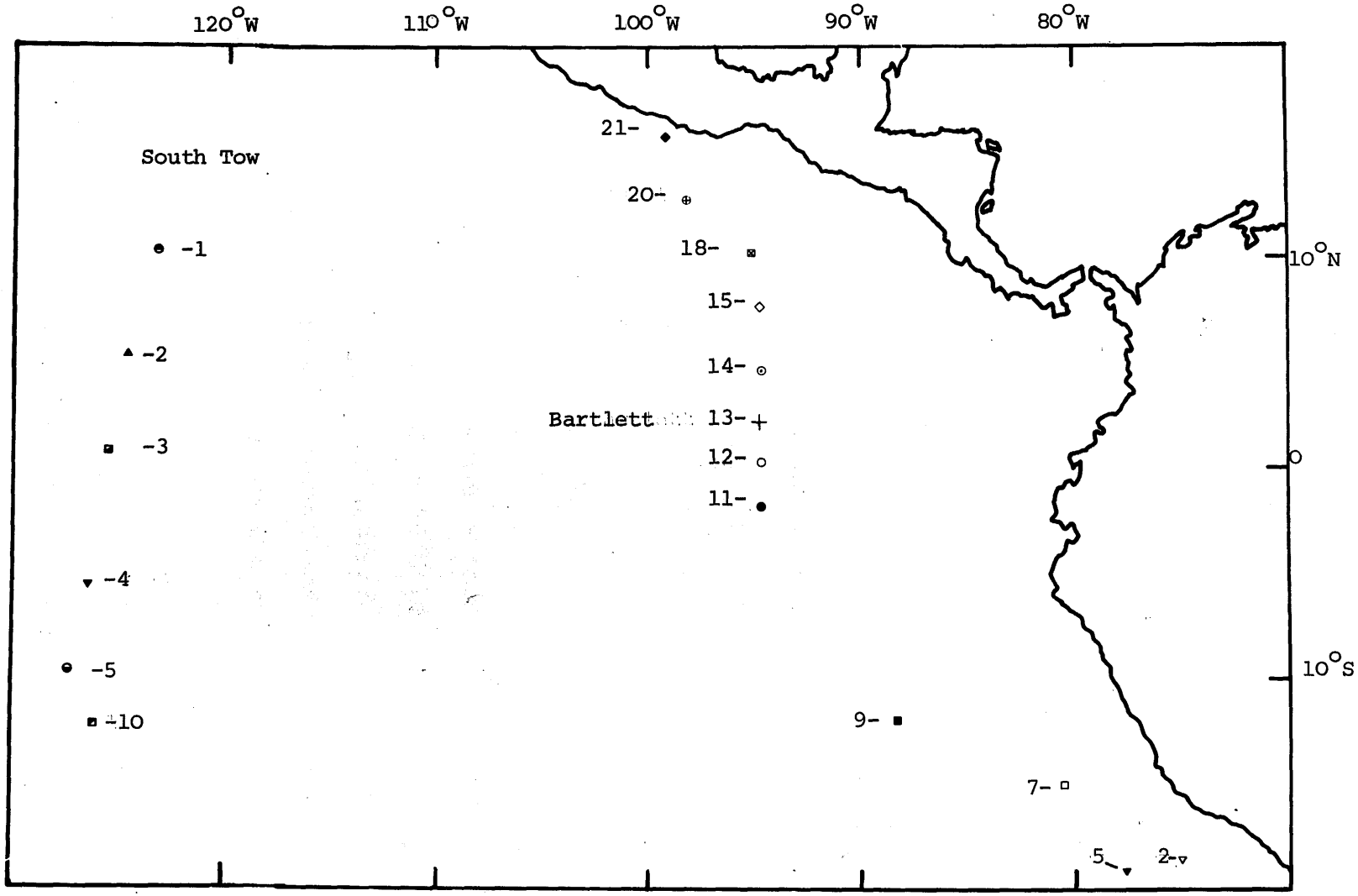

Figure IV.1 Position of Bartlett and South Tow stations in the equatorial Pacific Ocean.

IV.2 General Oceanography.

A rather brief outline of the general oceanography of the equatorial Pacific, with emphasis on the eastern tropical Pacific, will now be given so that the specific station analyses which follow can be placed in a wider context.

Unfortunately, compared to the other major oceans, remarkably little is known about the general circulation of the Pacific, although great strides forward have been taken in recent years, particularly through the works of Reid (1965) on Intermediate Waters, of Tsuchiya (1968) on the Upper Waters and of those involved in the recently reported 'Scorpio' Expedition transoceanic cruises of U.S.N.S. Eltanin (Warren, 1973; Reid, 1973).

(a) Equatorial Pacific Ocean - Upper Layers.

The equatorial region extends across the mid-latitudes of the Pacific Ocean from 20^{o}N to 20^{o}S. The currents flow mainly in an eastward or westward direction with small north-south perturbations superimposed on them. Wind stress has a very strong influence on the currents (Warren, 1970). Here, the upper layers will be considered as the top 1,000 metres or so.

The northernmost current of the equatorial system is the westward flowing North Equatorial Current (NEC), extending from 10^{o}N to 20^{o}N. In the east, this current receives water from the California Current, which turns

westward after flowing south along the coast of North America. This flow is a source of water of high tritium content and is also augmented from the North Pacific Gyre as the NEC flows westward. Water of much lower tritium content is added from the Equatorial Countercurrent (ECC), which flows in an easterly direction on the southern border of the NEC. Water from the north and south are added in approximately equal volumes (Sverdrup et al, 1942). The NEC can be considered a transition zone between the high-tritium North Pacific waters and low-tritium South Pacific waters. The higher concentrations in the north reflects the input of bomb-produced tritium fallout.

In the equatorial zone (especially in the NEC), several salinity maxima and minima occur. Under the NEC lies a salinity minimum at a σ_t (the density at the given temperature and salinity and at one atmospheric pressure) of 26.8. This water mass is Sub-Arctic Intermediate Water (SAIW), which extends to about 15°N. Above this minimum at a σ_t of about 26, is a second smaller salinity minimum, the shallow salinity minimum of the North Pacific, which extends almost to the equator (Reid, 1973). The source of the northern shallow minimum is at approximately 40°N, 140°W (Montgomery and Stroup, 1962). From there the water flows under the more saline but less dense waters of the sub-tropical and equatorial North Pacific. An equivalent shallow salinity minimum is also found in the equatorial South Pacific.

Above the shallow minimum in the north is found a salinity maximum at a σ_t of 24.25. This maximum is not

found beyond the boundary of the NEC and ECC. The source for the maximum is in the North Pacific Gyre at about 30^{o}N. The situation is similar in the South Pacific except that the water in the gyre is more saline and forms closer to the equator.

South of 8^{o}N lies the Equatorial Countercurrent (ECC). The ECC is an eastward-flowing current extending from 5^{o}N to 8^{o}N. It receives most of its water from water accumulated in the western Pacific by the wind-driven North and South Equatorial Currents. Thus, its water is a mixture of high and low tritium components from the NEC and SEC respectively. The South Equatorial Current extends from about 4^{o}N across the equator beyond 10^{o}S. Most of its water is derived from the South Pacific, especially from the eastern boundary current flowing along the coast of South America (Wooster, 1970). It receives water of moderate tritium content from the ECC. Another smaller countercurrent is found at approximately 10^{o}S, though its exact position is not well known. Its location has been noted by several expeditions and varies from 5^{o}S to 10^{o}S (Tsuchiya, 1970). Its presence is indicated by a salinity minimum with values between 34.0 and 34.9 $^{o}/_{oo}$. The source of the current is believed to be in the western south Pacific.

The NEC, ECC and SEC complete the classical picture of the equatorial current system but in recent years two further components have been identified. In order of discovery these are the Equatorial Undercurrent (EUC) or Cromwell Current, at the equator beneath the SEC, and the

South Equatorial Counter Current (SECC) at 10^{o} - 12^{o}S. Reid (1959) located the SECC as a geostrophic flow. This current had not previously been recognised as it is narrow and weak. With the introduction of this SECC it is now necessary to refer to the earlier recognised ECC as the North Equatorial Counter Current (NECC). These surface currents are shown in Figure IV.2.

Under the SEC at the equator flows the Equatorial Undercurrent. The undercurrent runs almost the entire length of the Pacific Ocean (Cromwell et al, 1954). Its core usually lies from 100-300 metres below surface and extends through a vertical distance of 100-200 metres. The EUC is almost as large in volume transport as the North or South Equatorial Undercurrents (Pickard, 1963).In the summer of 1952 a study at 150^{o}W included current measurements by free drifting drogues at and below the surface at 3^{o}S, on the equator and at 7^{o}N. The resultant data proved that near the equator and embedded in the SEC was an eastward flowing current at between 70 - 200 metres depth (Montgomery and Stroup, 1962). Knauss (1966) discerned details of the EUC as a thin ribbon, only 0.2 km thick but 300 km wide, extending from about 2^{o}N - 2^{o}S and in length extending certainly from 150^{o}W to 92^{o}W and perhaps even flowing further east. It does appear to be connected with the NECC (Rotschi, 1970). As with the thermocline, the undercurrent is found at shallower depths in the eastern Pacific ocean due to the large-scale horizontal circulation and upwelling.

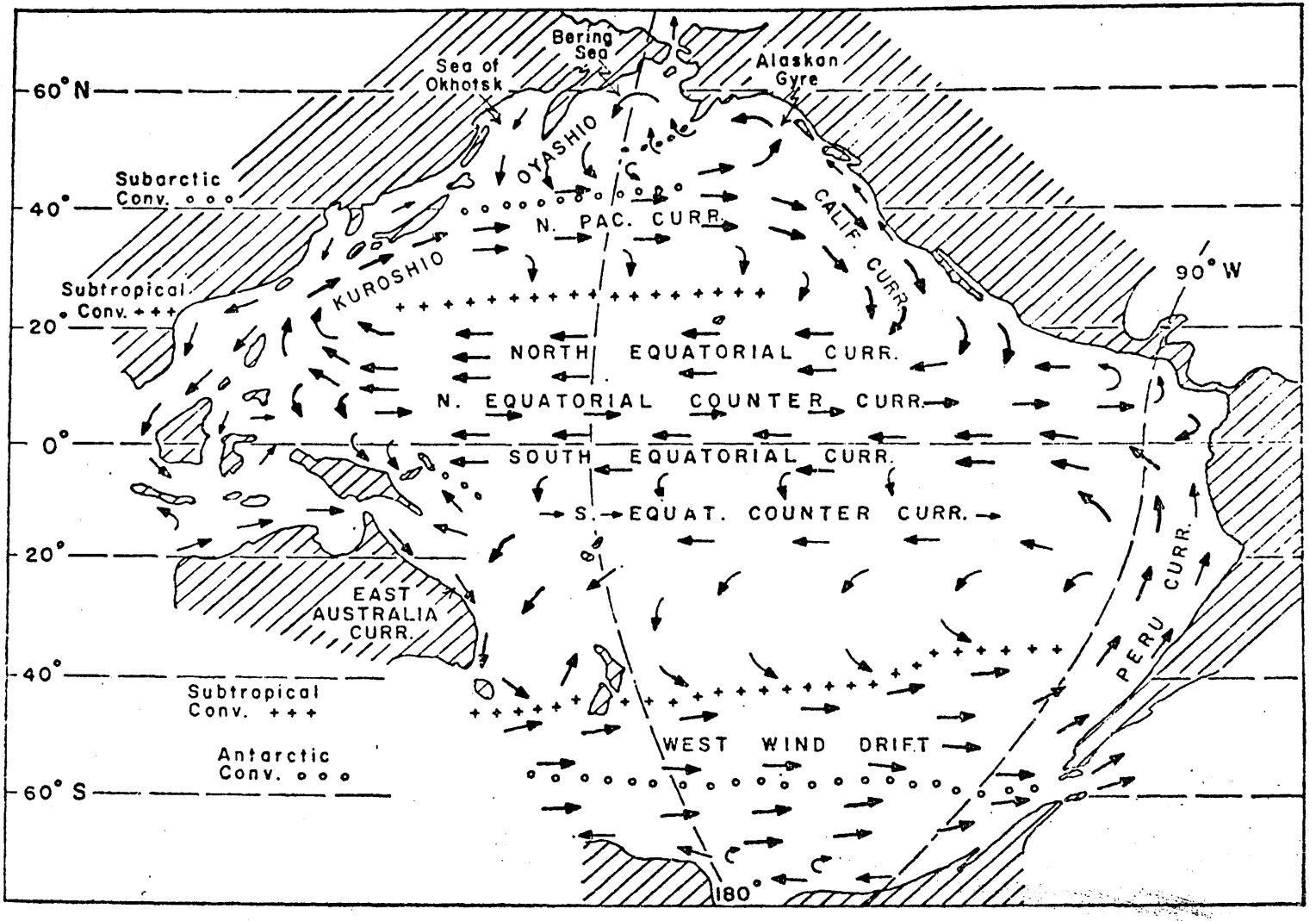

Figure IV.2 Surface currents of the Pacific Ocean (after Pickard, 1963).

In the east, the sub-Antarctic tongue at 600-1000 metres depth is distinguished by its low salinity ($34.6^{o}/_{oo}$ and less) and is clearly illustrated on Reid's (1965) chart of salinity distribution on the 125 cl/t isanostere (surface of constant specific volume anomaly). Off the coast of northern South America, the circulation in the upper layers is dominated by the Peru-Chile current system. This area was studied in some detail (Gunther, 1936) and has since been subjected to intensive investigation by Peruvian and Chilean scientists because of the economic and environmental problems caused by the phenomenon known as 'El Nino'. However, the complexity of current designations and our ignorance of this large and complicated system of surface and subsurface circulation requires that its taxonomy be carefully and systematically revised (Wooster, 1970). Accordingly, the simple description of Idyll (1973) will be adopted. Idyll recognises four components as listed below, the first two being northerly flowing, the other two southerly;

(i) Coastal Current - this flows next to the shore and is seldom more than 200 metres in depth.

(ii) Oceanic Current - further out to sea than (i), this current may be as deep as 700 metres or more and contains sub-Antarctic water. It has also been called the Humboldt Current, particularly in early work.

(iii) Peru Countercurrent - this is a warm subsurface current which flows between (i) and (ii). Rarely exceeding 300 metres in depth, yet only occasionally reaching the surface, it represents the eastern limb of an anti-cyclonic movement. From November to March, it is most pronounced

and is situated about 500 km offshore.

(iv) Peru undercurrent - underneath all three flows this deeper southward migrating current is characterised by relatively high salinity but low dissolved oxygen. It has been studied by Wooster and Gilmartin (1961).

The latter three currents should contain little, if any, tritium. The Coastal Current, however, should contain less than 4 T.U., larger values indicating incursions of North Pacific water.

An interesting feature of the Peru-Chile current system is the disruption of the general stream in the coastal belt resulting in upwelling or inversion of the surface layer near the mainland coast. Upwelling is usually attributed to the influence of the component of the wind stress, pointing equatorward, parallel to the coastal boundary. In terms of simple Ekman theory, the offshore transport and therefore the upward flux of water from below, is directly proportional to the component of the wind stress and inversely proportional to the Coriolis parameter. The processes of upwelling are thus associated with certain definite regions, depending to a large extent on atmospheric circulation. Off the Peruvian coast the low latitude and high trade wind stress combine to produce a zone of intense divergence with consequent strong and prolonged upwelling. These replenishing waters bring with them characteristics of the depth from which they originated, resulting in low salinities and temperatures but high nutrient content. These latter two properties are extremely conducive to production of anchovies and, indeed, these waters support

the largest single species fishery in the world (Kasahara, 1970), providing some 22% of the total world catch (Idyll, 1973). According to Gunther (1936), the evidence of isotherm and isohalines suggests that upwelling is generally restricted to the upper 200 metres with occasional deeper excursions in certain localities (e.g. Callao and Caldera). The same author estimates the breadth of the zone of upwelling to vary between 5 and 30 miles, but points out that this is extremely narrow compared with the breadth of the region influenced by upwelled water. Also, perhaps surprisingly, upwelling is not always seen to be in immediate contact with the coast.

Under normal conditions, the southernmost extension of the Peru Countercurrent is within a few degrees of the equator but, given certain meteorological regimes which result in relaxation of the trade wind system, the north flowing wind driven currents abate and allow the warm Countercurrent to penetrate further south, with disastrous results for the cold water fish population. This episodic phenomenon is known as 'El Nino'. The theory of a seven year periodicity has been largely discredited but does give an indication of the time-scale involved. The economic and ecological consequences can be severe.

(b) Equatorial Pacific Ocean - Lower Layers.

Much less is known about the deep circulation of the Pacific than about that in upper layers. In the dynamical theory of deep-water circulation by Stommel's group (Stommel, 1958; Stommel and Arons, 1960), a broad cyclonic

gyre exists with an upward flux of water into the thermocline balanced by deep input of bottom water from the Antarctic. The deep western boundary current predicted by this model has been observed by Reid et al (1968) and studied in some detail during the 'Scorpio' Expedition (Warren, 1973).

In the eastern Pacific, the cold Antarctic Bottom Water is not observed in the Chile and Peru Basins because the Chile Ridge forms a natural barrier between these more northerly basins and the Bellinghausen Basin in the south. Apart from Antarctic Bottom Water, which along with its mixtures with Pacific Water fills the southern basins below about 3500 metres, all other deep watersfound in the Pacific are considered to be secondary masses (in the technical sense of the term). In general, they are distinguished by high uniformity of hydrological features. In the scheme given by Muromtsev (1963), these deep waters are formed by mixing of Pacific water proper and water arriving from the Indian Ocean (via Australia) and the Atlantic Ocean (via the Drake Passage). Two regimes are recognised by Muromtsev (1963) in the South Pacific, identified both by depth and other characteristics. The South Pacific Upper Deep Water is typified by temperatures in the range 2-2.5^{o}C, salinities of 34.61 - 34.66$^{o}/_{oo}$ and dissolved oxygen concentrations of 2.81 - 3.84 ml/l corresponding to 42 - 48% saturation. This water is formed in northern tropical latitudes by mixing of equatorial intermediate and underlying waters and spreads southward to 65.5^{o}S at depths of approximately 2000 metres. In contrast, the Lower Deep

Water with temperatures of 1.7 - 2.0°C, salinities of 34.63-34.73 °/oo and dissolved oxygen concentrations of 3.5 - 4.2 ml/l (48 - 57% saturation) in the south, is formed in high southern latitudes. The higher oxygen concentrations are a reflection of the Antarctic component of this mass.

However, as mentioned earlier, the equatorial currents lie between the North Pacific water with its high tritium content and the South Pacific water with its low tritium content and this asymmetry can therefore be used effectively to monitor the input of North and South Pacific water to the equatorial systems.

IV.3 Hydrographic features.

In this section the hydrographic features observed at Bartlett Stations, 3,5,7,9,11,12,13,14,15,18,20 and 21 will be described; discussion will be in relation both to the general oceanography given in section IV.2, and to the water mass structure revealed by selected data from other investigations in the same region. Unfortunately, a very limited choice of suitable tritium observations is possible; South Tow Series Station 1-5, and 10 have been selected using as selection criteria:

(i) a reasonable geographical proximity so as to approach uniform hydrological structure,

(ii) relatively recent station occupation in order to minimise time dependent changes,

(iii) sampling of complete water column and high precision assay of relevant parameters.

Station locations are given in Table IV.1 and are indicated in Figure IV.1. The South Tow series (Scripps Institution of Oceanography) was conducted in 1972; station data have been reported by Michel (1974) and Michel and Suess (1975). Of course, due to local differences, considerable caution must be exercised in such comparisons.

Unfortunately, a final report of the Bartlett cruise containing corrected hydrographic data is not as yet available. The following sources of data have been used:

(i) on-board direct measurement of salinity, temperature and dissolved oxygen. Salinities were measured using a Bisset-Berman Corporation Model 6220 Portable Laboratory Salinometer calibrated with IAPO Standard Sea Water; the precision of analysis was ± 0.005% (Daxter, personal communication). Temperatures were measured using conventional reversing thermometers and oxygen determinations carried out using a micro-Winkler titration (Fallick, 1975).

(ii) SAMS probe STD data, both uncorrected and corrected for observed temperature, salinity and probe characteristics (Moore, personal communication). The probe printout gives temperatures to 0.01°C and salinities to 0.01°/oo.

The hydrographic results are presented in Tables IV.2 - IV.11 for the previously mentioned Bartlett Stations. Potential temperatures (θ) were calculated from the polynomials of Bryden (1973). The depth distributions of temperature, salinity, and where available, the dissolved oxygen concentration have been plotted in Figures IV.3 - IV.5. In these profiles the South Tow data (Michel, 1974)

CRUISE	STATION NUMBER	LATITUDE	LONGITUDE
Bartlett T-Agor 13-73-1	3	18°57.0'S	75°03.1'W
Bartlett T-Agor 13-73-1	5	19°16.7'S	77°56.4'W
Bartlett T-Agor 13-73-1	7	15°23.6'S	80°42.3'W
Bartlett T-Agor 13-73-1	9	11°08.8'S	88°14.9'W
Bartlett T-Agor 13-73-1	11	2°00.8'S	94°33.8'W
Bartlett T-Agor 13-73-1	12	0°16.8'N	94°30.2'W
Bartlett T-Agor 13-73-1	13	2°02.3'N	94°34.1'W
Bartlett T-Agor 13-73-1	14	4°33.5'N	94°27.1'W
Bartlett T-Agor 13-73-1	15	7°24.7'N	94°29.9'W
Bartlett T-Agor 13-73-1	18	9°59.3'N	95°03.7'W
Bartlett T-Agor 13-73-1	20	12°36.0'N	98°10.0'W
Bartlett T-Agor 13-73-1	21	15°39.1'N	99°19.1'W
South Tow	1	10°18.0'N	123°10.0'W
South Tow	2	5°13.0'N	124°32.0'W
South Tow	3	0°28.0'N	125°31.0'W
South Tow	4	4°59.0'S	126°25.0'W
South Tow	5	9°59.0'S	127°22.0'W
South Tow	10	12°37.0'S	126°00.0'W

TABLE IV.1

Location of oceanographic stations used in discussion of oceanography of eastern tropical Pacific.

SAMPLE	DEPTH (m)	SALINITY (°/oo)	TEMPERATURE (°C)	POTENTIAL TEMPERATURE (θ)	DISSOLVED OXYGEN (ml/l)	TRITIUM UNITS (TU±2σ)
3-2-1	7	35.587	24.46	24.46	4.58	2.30 ± 0.22
3-2-4	32	35.170	20.20	20.19	4.71	1.80 ± 0.20
3-2-5	62	34.907	17.59	17.58	4.19	1.40 ± 0.16
3-2-6	91	34.933	14.78	14.77	2.55	0.93 ± 0.15
3-2-7	120	34.888	14.30	14.28	0.94	N.D.
3-2-8	195	34.852	12.83	12.80	0.46	0.65 ± 0.14
3-2-10	476	34.564	8.33	8.29	1.03	0.35 ± 0.14
3-2-11	705	34.452	5.77	5.68	1.43	0.11 ± 0.13
3-2-12	936	34.493	4.55	4.49	1.63	B.D.L.
3-1-1	1203	34.529	3.66	3.57	1.75	B.D.L.
3-1-4	1470	34.582	2.95	2.84	2.28	B.D.L.
3-1-5	1981	34.657	2.25	2.11	2.67	B.D.L.
3-1-6	2468	34.703	1.91	1.73	3.31	0.35 ± 0.14
3-1-7	2949	34.694	1.80	1.57	3.45	B.D.L.
3-1-8	3445	34.689	1.77	1.50	3.54	B.D.L.
3-1-10	3692	34.686	1.74	1.44	3.75	B.D.L.
3-1-11	3971	34.684	1.74	1.41	3.66	B.D.L.
3-1-12	4031	34.684	1.73	1.40	3.77	B.D.L.

TABLE IV.2

N.D. = Not determined. B.D.L. = Below detection limit.

Hydrographic properties at Bartlett Station 3.

SAMPLE	DEPTH (m)	SALINITY ($^{o}/_{oo}$)	TEMPERATURE (^{o}C)	POTENTIAL TEMPERATURE (θ)	DISSOLVED OXYGEN (ml/l)	TRITIUM UNITS (TU±2σ)
5-3-A	50	35.212	19.31	19.30	-	0.67 ± 0.21
5-1-1	279	34.765	10.85	10.81	0.44	0.31 ± 0.13
5-1-4	406	34.662	8.90	8.86	0.25	
5-1-5	529	34.566	7.36	7.31	1.03	
5-1-6	774	34.493	5.52	5.45	0.97	
5-1-7	1027	34.518	4.36	4.28	1.68	
5-2-A	1200	34.534	3.49	3.40	1.75	
5-1-8	1348	34.559	3.35	3.25	1.95	
5-1-10	1677	34.589	2.75	2.63	2.37	
5-1-11	1988	34.624	2.32	2.18	2.53	
5-1-12	2315	34.642	2.05	1.86	3.10	
5-2-B	3200	34.686	1.76	1.48	3.47	
5-2-C	3600	34.677	1.76	1.47	3.59	
5-2-D	3900	34.683	1.70	1.38	3.68	
5-2-E	4100	34.681	1.73	1.39	3.56	

TABLE IV .3

Hydrographic properties at Bartlett Station 5.

SAMPLE	DEPTH (m)	SALINITY (°/oo)	TEMPERATURE (°C)	POTENTIAL TEMPERATURE (θ)	DISSOLVED OXYGEN (ml/l)
7-3-1	52	35.066	17.78	17.78	4.96
7-3-4	151	34.790	12.70	12.68	0.23
7-3-5	297	34.754	10.99	10.95	0.53
7-3-6	496	34.565	8.09	8.03	0.53
7-3-7	895	34.502	4.83	4.74	1.45
7-3-8	1095	34.518	4.02	3.92	1.93
7-3-10	1241	34.542	3.55	3.44	2.39
7-3-11	1491	34.577	2.94	2.82	1.84
7-3-12	1739	34.610	2.51	2.37	2.39
7-1-4	2088	34.641	2.03	1.89	2.74
7-1-5	2692	34.667	1.81	1.61	3.58
7-1-6	2995	34.669	1.80	1.57	3.41
7-1-7	4496	34.682	1.79	1.40	3.40
7-1-8	4594	34.682	1.80	1.39	3.17
7-1-10	4617	34.680	1.80	1.39	3.40
7-1-11	4631	34.679	1.80	1.39	3.31
7-1-12	4651	34.680	1.80	1.39	2.81
7-1-1	4669	34.684	1.80	1.39	3.34

TABLE IV.4

Hydrographic properties at Bartlett Station 7.

SAMPLE	DEPTH (m)	SALINITY ($^{o}/_{oo}$)	TEMPERATURE (^{o}C)	POTENTIAL TEMPERATURE (θ)	DISSOLVED OXYGEN (ml/l)	TRITIUM UNITS (TU±2σ)
9-1-1	7	35.46	26.45	26.45	4.75	3.58 ± 0.38
9-2-A	30	35.53	23.55	23.54	3.13	
9-2-B	60	35.07	15.34	15.35	2.00	
9-2-C	90	34.55	14.03	14.02	0.23	
9-2-D	130	34.92	12.98	12.97	0.59	
9-1-4	204	34.86	11.95	11.93	0.45	
9-2-E	230	34.85	11.72	11.69	0.57	
9-1-5	398	34.72	9.82	9.76	0.36	
9-1-6	498	34.63	8.41	8.35	0.53	
9-1-7	597	34.58	7.09	7.02	0.81	
9-1-8	791	34.52	5.41	5.33	0.81	
9-1-10	984	34.52	4.51	4.42	1.64	
9-1-11	1237	34.56	3.54	3.43	1.87	
9-1-12	1483	34.59	2.93	2.80	2.19	
*9-XBT-1	3950	34.673	1.78	1.39	-	
*9-XBT-2	4050	34.681	1.78	1.39	-	
*9-XBT-3	4250	34.682	1.81	1.40	-	

TABLE IV .5

Hydrographic properties at Bartlett Station 9

* XBT data (Moore, personal communication)

SAMPLE	DEPTH (m)	SALINITY ($^{o}/_{oo}$)	TEMPERATURE (^{o}C)	POTENTIAL TEMPERATURE (θ)	DISSOLVED OXYGEN (ml/l)	TRITIUM UNITS (TU±2σ)
11-2-A	30	35.03	22.10	22.09	3.91	4.32 ± 0.19
11-1-A	40	35.12	-	-	2.12	
11-1-B	80	35.06	22.02	22.00	1.68	
11-1-C	100	34.99	14.11	14.09	1.48	
11-2-B	140	34.95	13.49	13.47	1.34	
11-2-C	165	34.91	12.82	12.79	0.40	
11-2-D	265	34.77	10.52	10.48	0.08	
11-1-E	405	34.61	7.64	7.60	0.83	
11-2-E	550	34.55	6.00	5.95	1.35	

TABLE IV.6

Hydrographic properties at Bartlett Station 11.

SAMPLE	DEPTH (m)	SALINITY ($^{o}/_{oo}$)	TEMPERATURE (^{o}C)	POTENTIAL TEMPERATURE (θ)	DISSOLVED OXYGEN (ml/l)	TRITIUM UNITS (TU±2σ)
12-1-A	18	34.95	20.37	20.37	2.94	4.86 ± 0.23
12-2-A	70	35.10	16.22	16.21	2.19	
12-1-B	100	35.03	14.99	14.97	1.92	5.09 ± 0.20
12-1-C	168	34.90	12.83	12.80	0.36	1.86 ± 0.18
12-2-D	350	34.73	9.84	9.79	0.16	
12-1-D	424	34.64	8.18	8.13	0.50	0.78 ± 0.16
12-1-E	560	34.57	6.72	6.66	0.89	
12-2-E	730	34.54	5.36	5.29	1.38	

TABLE IV.7

Hydrographic properties at Bartlett Station 12.

SAMPLE	DEPTH (m)	SALINITY ($^{o}/_{oo}$)	TEMPERATURE (^{o}C)	POTENTIAL TEMPERATURE (Θ)	TRITIUM UNITS (TU$\pm 2\sigma$)
13-1-A	43	35.09	18.61	18.60	5.31 ± 0.44
13-2-A	50	35.10	18.26	18.25	
13-1-C	87	35.01	15.56	15.54	
13-1-D	120	34.97	14.16	14.14	
13-2-B	150	34.95	13.66	13.64	
13-1-E	195	34.88	12.66	12.63	
13-2-C	280	34.76	10.27	10.23	
13-2-D	430	-	8.42	8.37	

TABLE IV.8

Hydrographic properties at Bartlett Station 13.

SAMPLE	DEPTH (m)	SALINITY ($^{o}/_{oo}$)	TEMPERATURE (^{o}C)	POTENTIAL TEMPERATURE (θ)	TRITIUM UNITS (TU±2σ)
14-1-A	30	33.75	26.12	26.11	5.35 ± 0.24
18-1-A	20	33.73	27.89	27.88	
20-TAP	2	33.75	29.33	29.33	16.96 ± 0.58
20-1-2	67	33.70	27.95	27.94	

TABLE IV.9

Hydrographic properties at Bartlett Stations 14, 18, and 20.

SAMPLE	DEPTH (m)	SALINITY ($^{o}/_{oo}$)	TEMPERATURE (^{o}C)	POTENTIAL TEMPERATURE (θ)
15-1-A	39	33.64	27.05	27.04
15-1-B	70	34.70	17.11	17.10
15-1-C	95	34.76	14.18	14.16
15-2-A	123	34.84	13.10	13.08
15-1-D	175	34.78	12.12	12.09
15-2-B	208	34.75	11.51	11.48
15-2-C	280	34.68	10.28	10.24
15-1-E	350	34.64	9.29	9.25
15-2-D	465	34.57	5.72	5.66

TABLE IV.10

Hydrographic properties at Bartlett Station 15.

SAMPLE	DEPTH (m)	SALINITY ($^{o}/_{oo}$)	TEMPERATURE (^{o}C)	POTENTIAL TEMPERATURE (θ)
21-2-A	20	33.85	-	-
21-1-A	35	33.99	27.04	27.03
21-1-B	60	34.53	19.13	19.12
21-1-C	100	34.80	13.75	13.73
21-1-D	170	34.79	11.83	11.80
21-2-B	280	34.71	10.42	10.38
21-1-E	350	34.63	9.08	9.04
21-2-C	500	34.56	7.22	7.16
21-2-D	660	34.55	5.75	5.68
21-2-E	900	34.56	4.42	4.35

TABLE IV.11

Hydrographic properties at Bartlett Station 21.

have been included. The station key given in Figure IV.3 will be used throughout this chapter, except where otherwise stated. Excluding some surface scatter of the South Tow data, the temperature and salinity profiles are seen to be reasonably uniform at all stations, so that the existence of a common hydrological regime may be broadly assumed; detailed interstation differences will be discussed later. The gross features of :

(i) high gradients in upper layers,

(ii) regularity in the deep water,

(iii) a strongly developed main thermocline,

(iv) an intermediate salinity maximum,

(v) a shallow oxygen maximum

are all as expected.

Elucidation of the upper water structure has been facilitated by study of logarithmic depth plots. The top 100 metres or so are Peru Surface Water, distinguished from more northerly Equatorial Surface Water by its lower temperatures but higher salinities. This difference reflects a greater excess of evaporation over precipitation than in the equatorial belt. Oxygen concentrations typically decrease rapidly with depth below the mixed layer. Underneath, down to 400 - 500 metres lie South Subtropical Subsurface Waters containing the oxygen minimum. Oxygen concentrations at the minimum are quite uniform indicative of high biological consumption; no variation in depth of the minimum with latitude is apparent. The intermediate waters in the depth range 400-1400 metres are characterised by the salinity minimum layer. Formed in the Antarctic

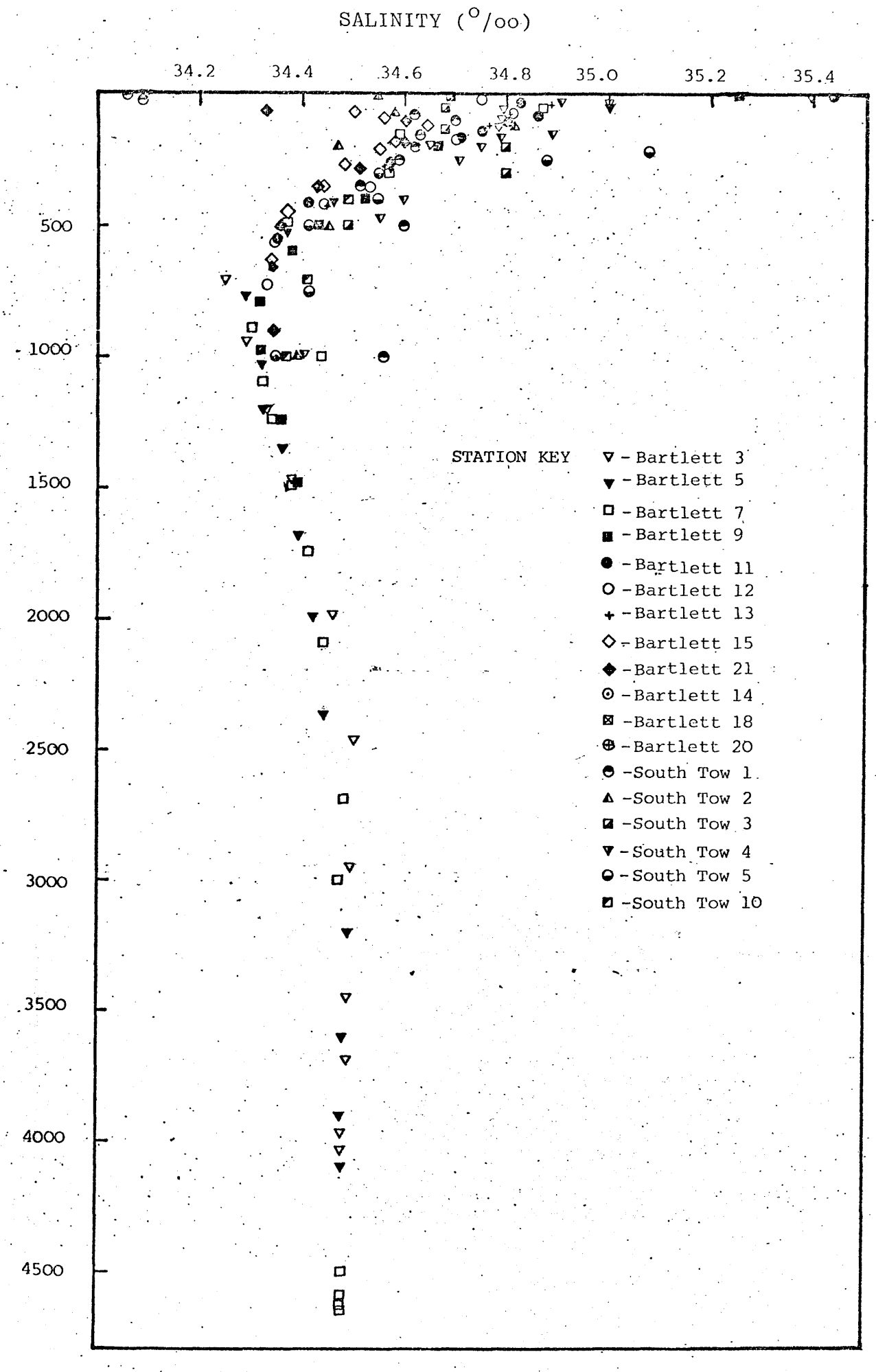

Figure IV.3 Salinity versus depth at eastern tropical Pacific stations.

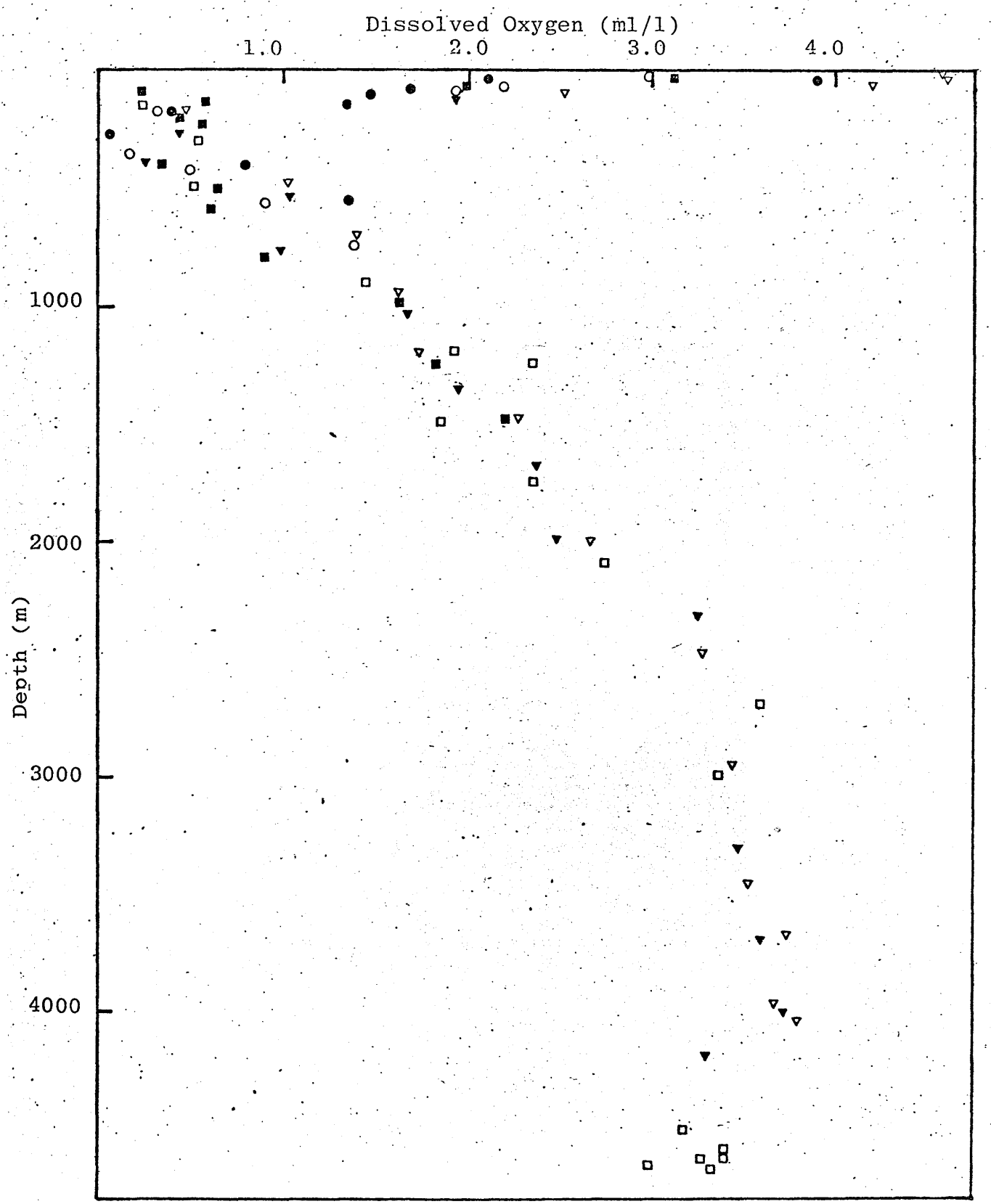

Figure IV. 4 Dissolved oxygen vs depth at Eastern Tropical Pacific Stations.

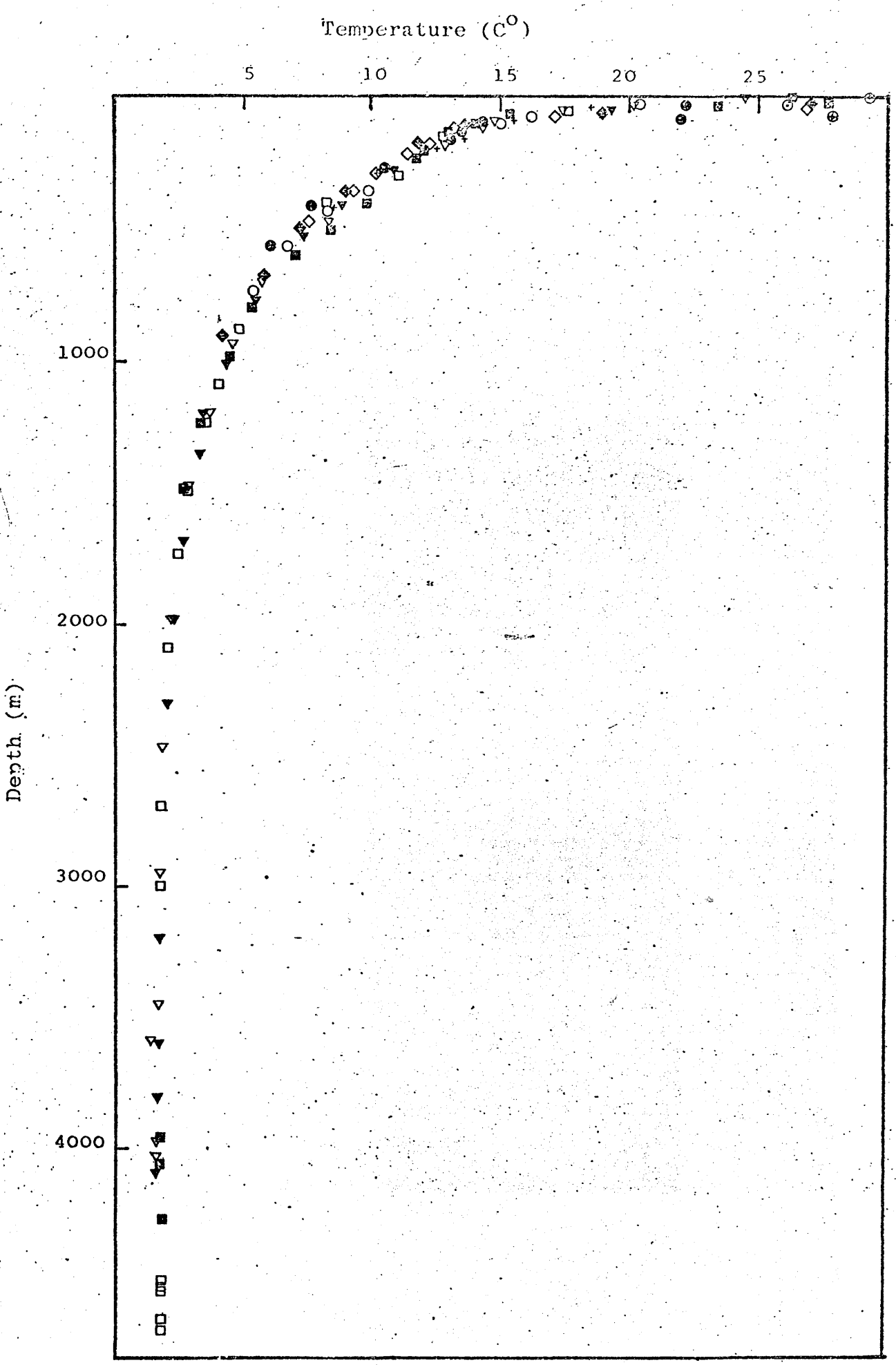

Figure IV.5 Temperature versus depth at eastern-tropical Pacific stations.

convergence zone by mixing of surface and subsurface waters and advected northwards, the South Pacific Intermediate Water gradually loses its identity by vertical mixing with shallower and deeper layers and eventually merges laterally with southward flowing intermediate waters in low latitudes. The erosion of the salinity minimum, and so of the intermediate core, as the equator is approached can be clearly seen in the profiles of Figure IV.6 in which the salinity scale has been expanded by omission of the surface layers. The South Tow series, separated by the dashed line, clearly shows this erosion. The depth to which intermixing with intermediate waters influences the Deep water is at least 2000 metres. There is some indication of a mid-depth salinity maximum at ~ 2500 metres at Bartlett Station 3 but discussion of this feature is reserved until later. The corresponding temperature plot (Figure IV.7) shows relatively uniform thermal structure through the main thermocline. Dissolved oxygen concentrations increase more or less linearly with depth (Figure IV.8). Muromtsev (1963) used the $2^{o}C$ isotherm to divide deep waters in the region of interest into South Pacific Upper Deep Water and underlying Lower Deep Water. The former, originating in northern tropical latitudes, shows low oxygen concentrations, the saturation increasing linearly with depth. The latter is formed in high southern latitudes and has an enhanced rather constant oxygen concentration. Neither Antarctic Bottom Water ($0.24^{o}C < T < 0.85^{o}C$) nor any of its mixtures with Pacific Bottom Water ($1.0^{o}C < T < 1.6^{o}C$) are seen this far north in the eastern basins. The water mass structure outlined above is nicely illustrated in a θ-S plot of the entire water column as

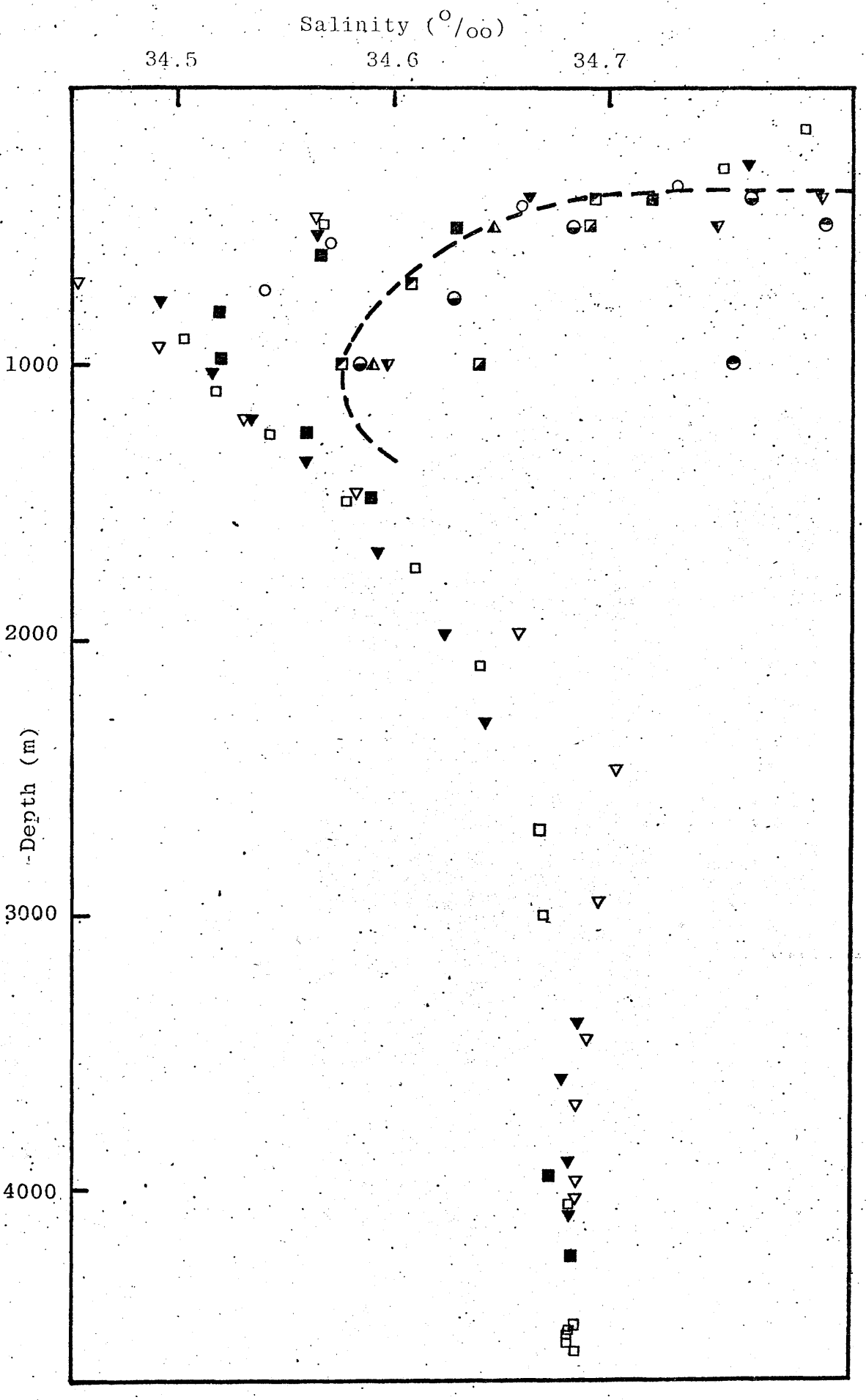

Figure IV.6 Subsurface salinity profile at eastern tropical Pacific Stations.

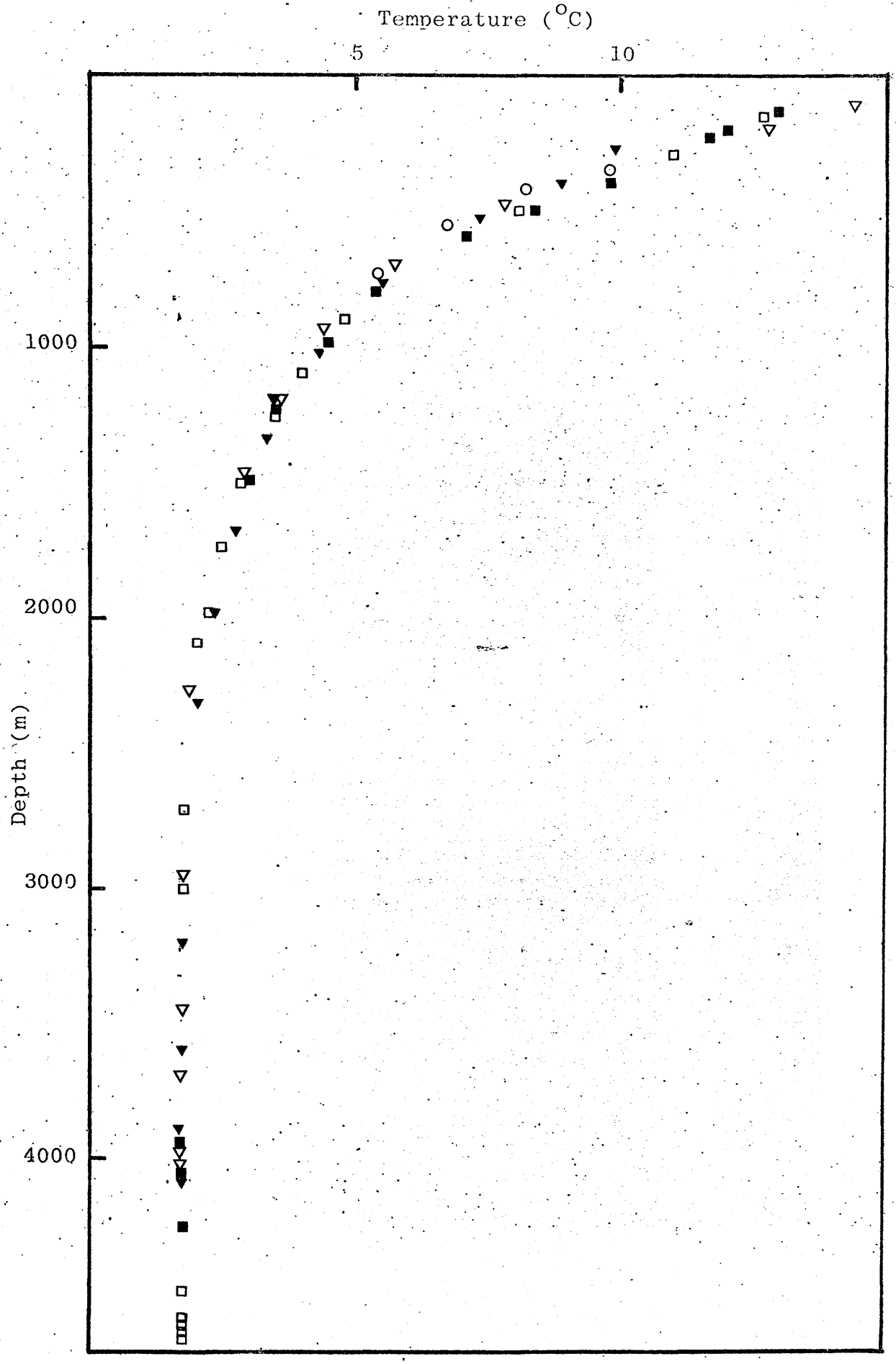

Figure IV.7 Subsurface temperature profile at eastern tropical Pacific Stations.

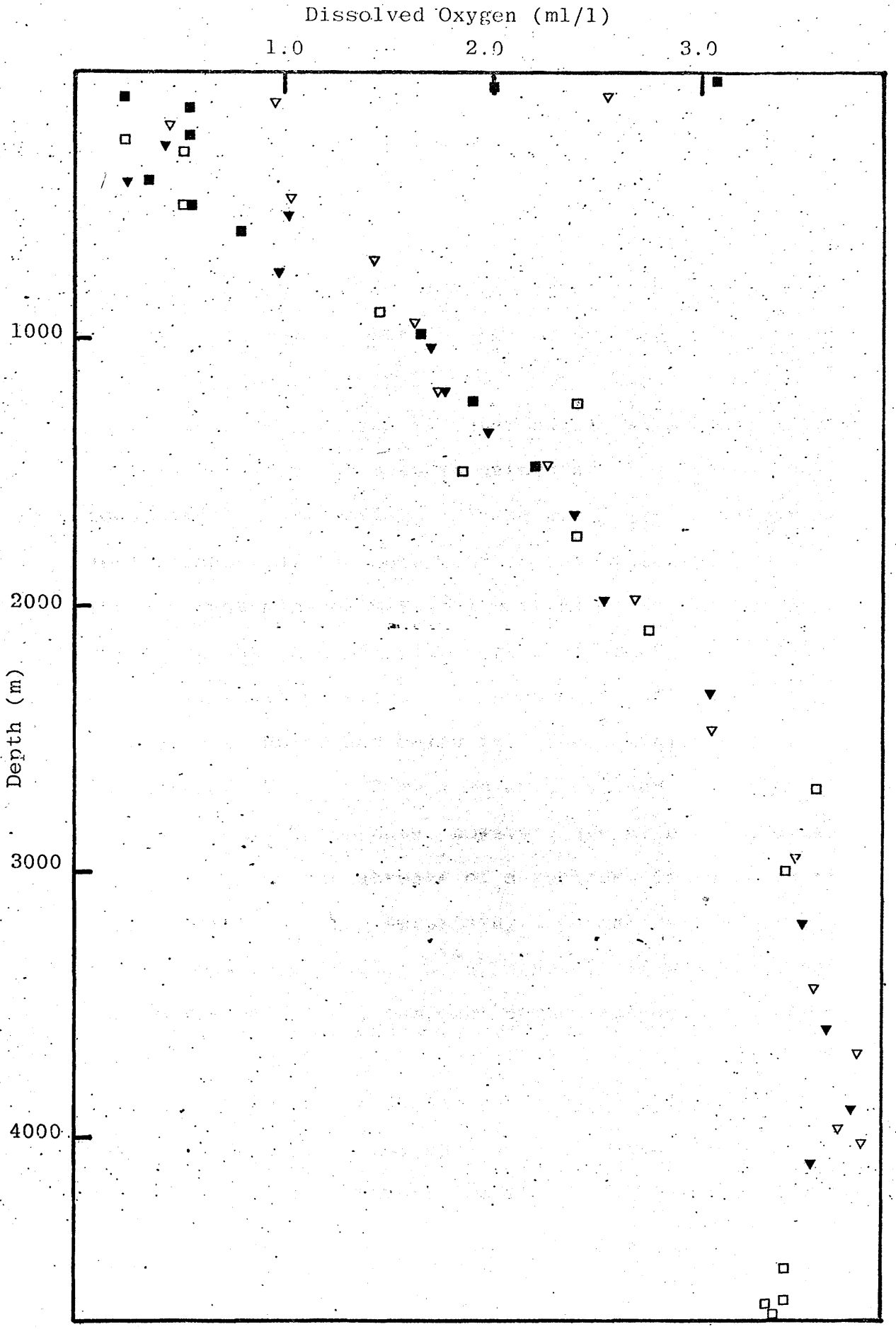

Figure IV.8 Subsurface dissolved oxygen profile for eastern tropical Pacific Stations.

presented in Figure IV.9. In particular, the three component types beneath the subsurface water can be observed to mix along smooth curves, with the degree of mixing and direction of intermediate flow clearly indicated by interstation differences.

To aid analysis of mixing processes in the abyssal waters, the Θ -S diagram for the deep layers below about 1000 metres is given in Figure IV.10. The effect of latitudinal differences in intermediate water salinities is obvious, with the deepest waters at all stations being considerably more uniform; there are thus two linear Θ-S loci connecting the intermediate and bottom waters. The apparent mid-depth salinity at Bartlett Station 3 corresponding to a salinity core centred at about 2500 metres is again observed and appears to influence the samples both above and below it. The salinity probe data for Bartlett Station 3 were re-examined and no maximum could be discerned. These data, however, are at best accurate to $\pm 0.01^{o}/_{oo}$ so the absence of a recorded increase in the deep water is not too surprising. Anomalous tritium concentrations (see IV.4), $\delta^{18}O$ values (Fallick, 1975) and radium values (Moore, personal communication) are also observed at ~2500 metres at Bartlett Station 3. The consistent influences on the neighbouring samples seen in the salinity profile are not apparent. The view that this is a local transitory effect (Fallick, 1975) cannot be ruled out and is supported by Thomson and Turekian (1976) who observed no anomalous behaviour of ^{210}Pb and ^{210}Po at this depth at Bartlett Station 3. However, the entire water

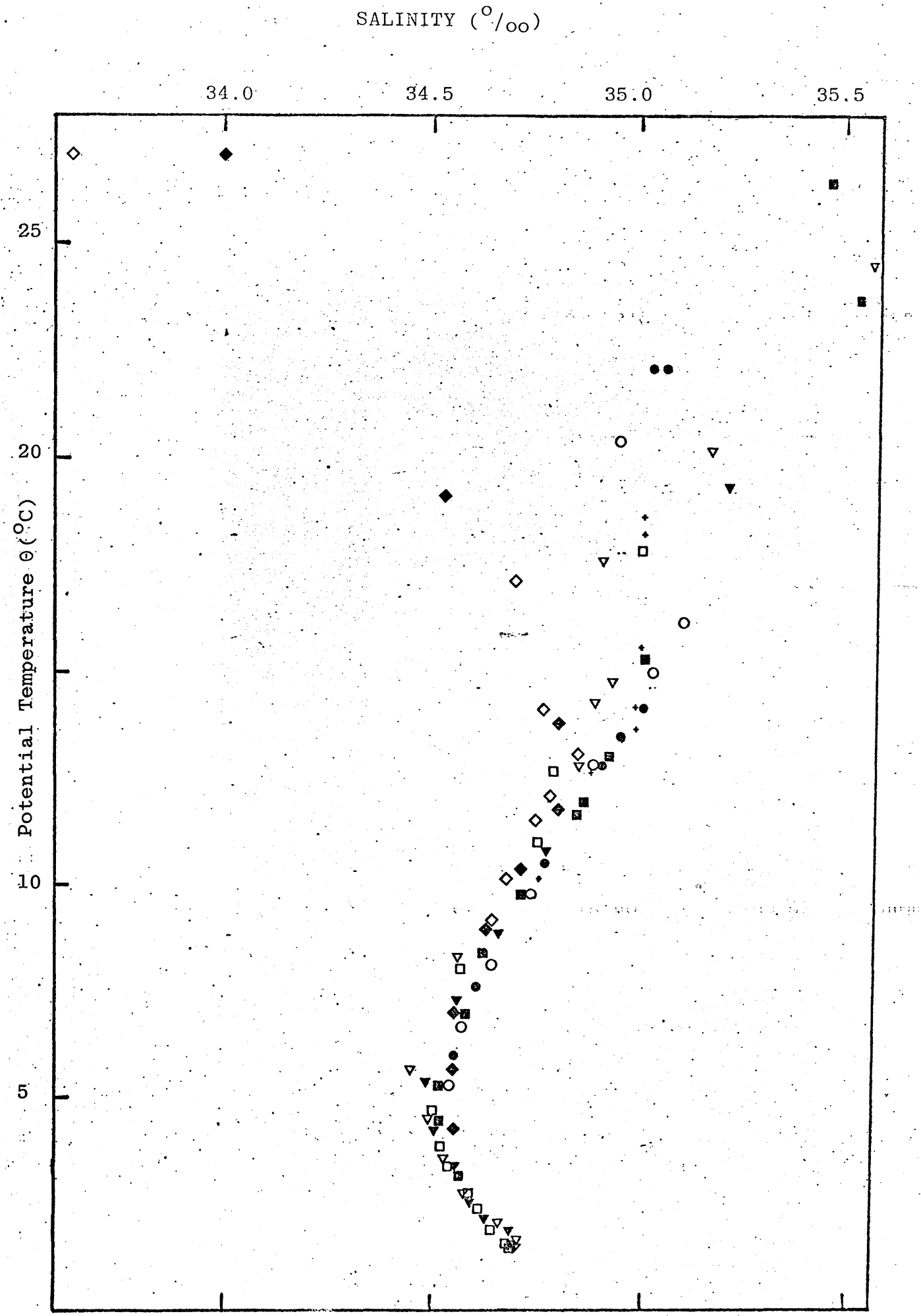

Figure IV.9 Entire plot θ-S for eastern tropical Pacific Stations.

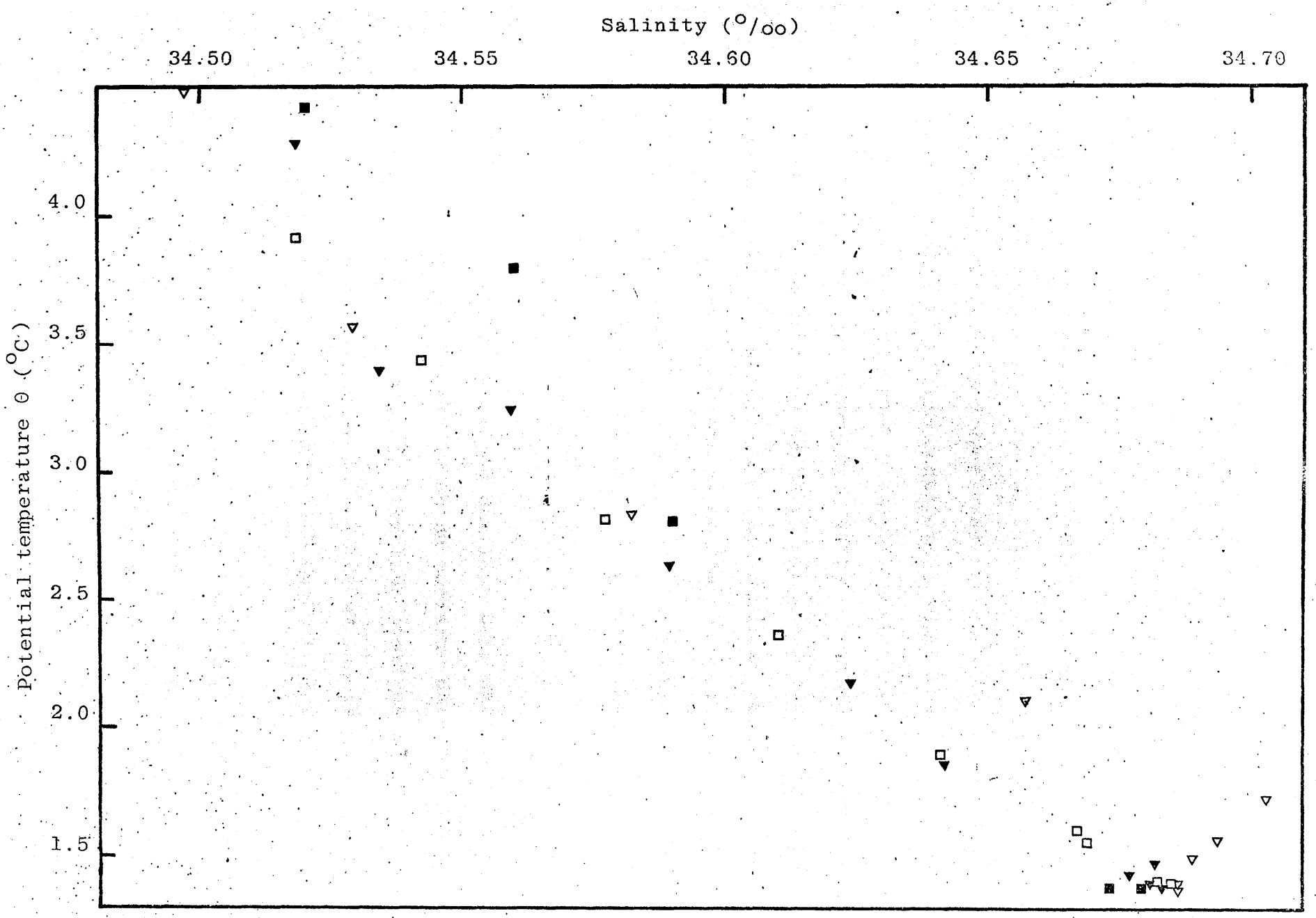

Figure IV.10 θ-S plot for eastern tropical Pacific deep water.

column at Bartlett Station 3 exhibits anomalous behaviour of ^{210}Pb and ^{210}Po. ^{210}Pb shows a depletion relative to ^{226}Ra at all depths and ^{210}Po appears to be deficient relative to ^{210}Pb. Thomson and Turekian (1976) suggest that, since Bartlett Station 3 is in a region where productivity is estimated to be 200 - 400 g organic carbon per square metre per year due to intense upwelling, the high productivity and upwelling are responsible for the marked excursions from radioactive equilibrium. It should be noted, however, that plots of their salinity data also show this salinity anomaly. It is therefore not certain at this time whether the anomaly represents a real phenomenon indicative of a significant but transient current or alternatively is the consequence of a mistrip of the sampling device as viewed by Moore (personal communication). The latter explanation, however, is inconsistent with the salinity profile.

The uniformity of the Bartlett Deep water can be observed from Table IV.12 which contains data for 13 assays of bottom water for the four stations 3,5,7 and 9, the mean salinity being $34.681 \pm 0.006\,^{o}/_{oo}$ (2σ) and the mean potential temperature $1.39 \pm 0.01\,^{o}C$ (2σ). From Figure IV.11 it is clear that, except for the three anomalous salinity values of Bartlett Station 3 (circled), all results for station 3,5,7 and 9 can be represented by a single line, indicating simple mixing between two component types, viz. Intermediate and Deep Water. Error bars corresponding to $\pm 0.005\,^{o}/_{oo}$ in salinity and $\pm 0.001\,^{o}C$ potential temperature have been affixed to these points.

SAMPLE	DEPTH (m)	POTENTIAL TEMPERATURE (θ)	SALINITY ($^{o}/_{oo}$)
3-1-11	3971	1.41	34.684
3-1-12	4031	1.40	34.684
5-2-D	3900	1.38	34.683
5-2-E	4100	1.39	34.681
7-1-7	4496	1.40	34.682
7-1-8	4594	1.39	34.682
7-1-10	4617	1.39	34.680
7-1-11	4631	1.39	34.679
7-1-12	4651	1.39	34.680
7-1-1	4669	1.39	34.684
9-XBT-1	3950	1.39	34.673
9-XBT-2	4050	1.39	34.681
9-XBT-3	4250	1.40	34.682
MEAN AVERAGES $\pm 2\sigma$ =		1.39±0.01	34.681±0.006

TABLE IV.12

Bottom water hydrographic characteristics at Bartlett Stations 3,5,7 and 9.

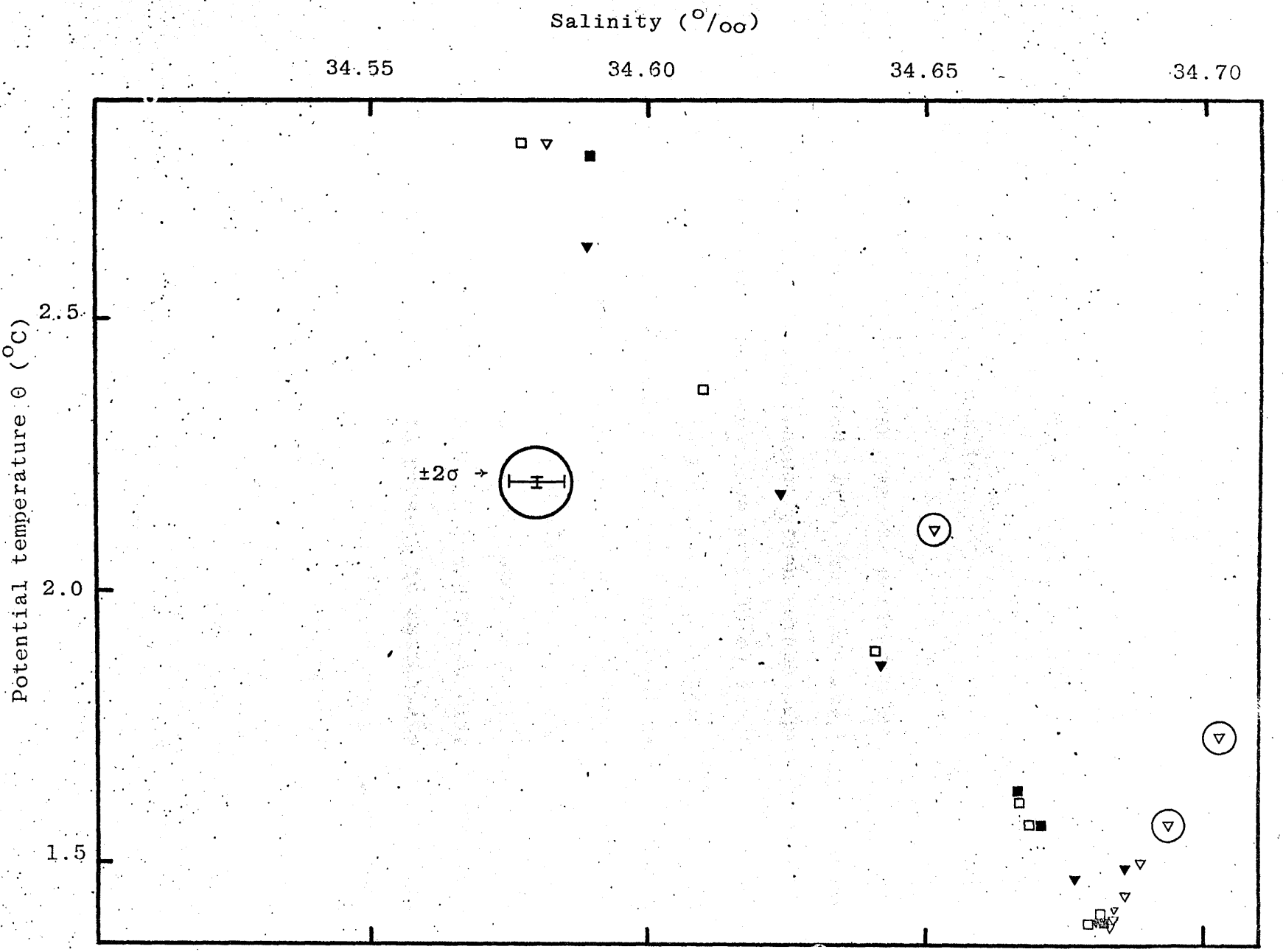

Figure IV.11 θ-S for Bartlett Stations Deep Water.

The Deep Water distinction referred to earlier was, as stated, based on the 2°C isotherm and on oxygen concentrations. The evidence for this from the Bartlett samples is presented in the potential temperature versus dissolved oxygen plot shown in Figure IV.12. There is obvious inter-station consistency.

IV.4 Tritium Features.

The tritium measurements performed on the Bartlett samples are presented, with the South Tow Series, in two modes (i) tritium concentration versus depth (provided sufficient data points are available) and (ii) tritium concentrations within specific σ_t values. The σ_t values, calculated from the equation of state of seawater (Wang and Millero, 1973), are presented in Table IV.13. The apparent lack of adequately spaced stations and samples per station precludes the possibility of such in-depth studies as Rooth and Ostlund (1972) or Michel and Suess (1975). However, sufficient detail is present to assimilate this additional information into the regional oceanography of the area and the geophysical processes occuring therein.

As seen from the South Tow profiles (Figure IV.13A to F) proceeding southwards through the complex equatorial zone, the more southerly stations (4,5 and 10) exhibit, largely as expected, a decrease in tritium concentrations with respect to depth. At South Tow 4,5, and 10, tritium concentrations drop sharply below the thermocline similar to the South Tow 1 profile taken north of the equator.

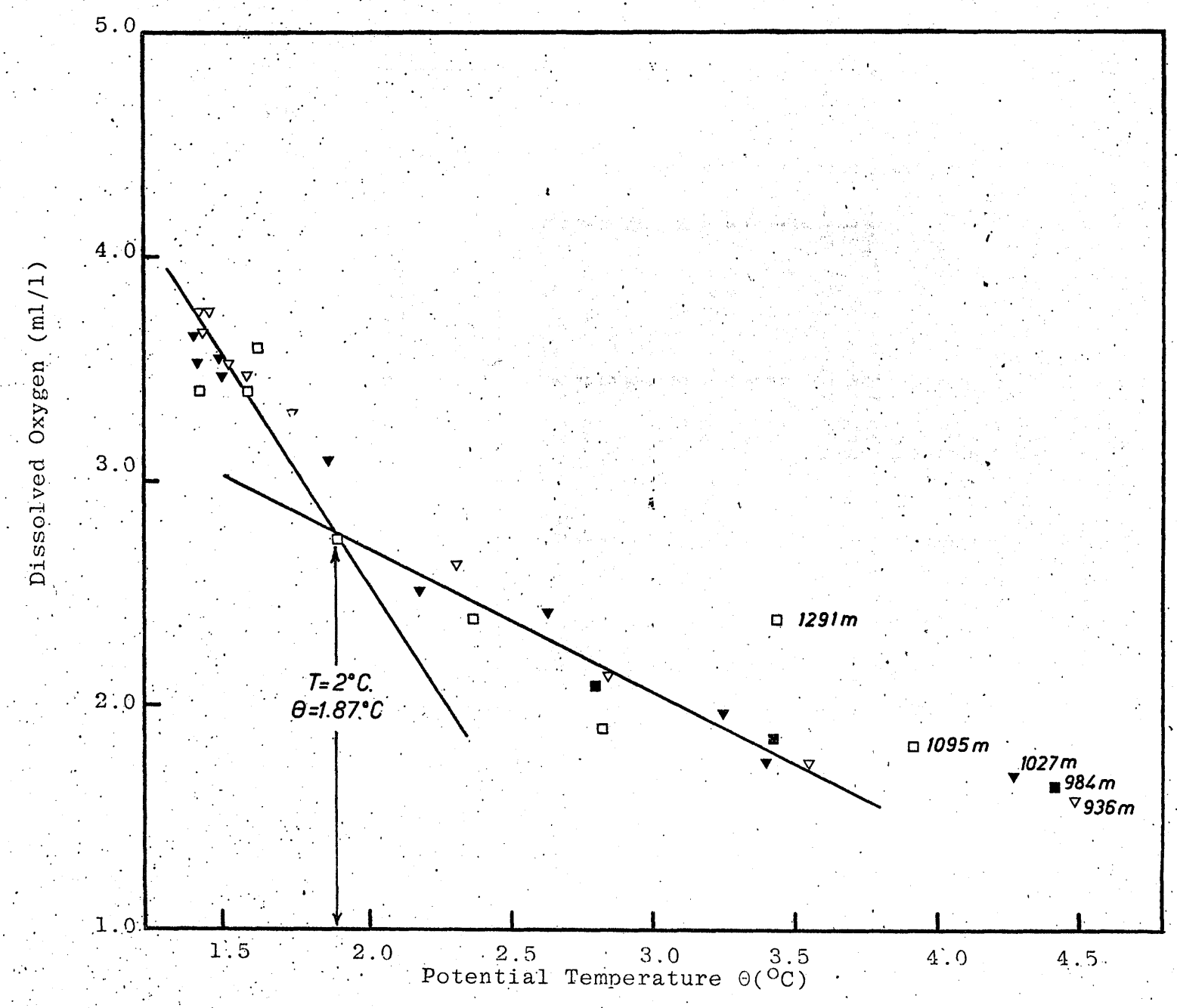

Figure IV.12

Potential temperature versus dissolved oxygen for Bartlett deep water samples.

BARTLETT SAMPLE	σ_t	TRITIUM CONCENTRATION (T.U.±2σ)	DEPTH (m)
3-2-1	23.648	2.30 ± 0.22	7
3-2-4	24.392	1.80 ± 0.20	32
3-2-5	25.113	1.40 ± 0.16	62
3-2-6	25.467	0.93 ± 0.15	91
3-2-7	25.837	N.D.	120
3-2-8	26.150	0.65 ± 0.14	194
3-2-10	26.786	0.35 ± 0.14	476
3-2-11	27.041	0.11 ± 0.13	705
3-2-12	27.224	B.D.L.	936
3-1-1	27.366	B.D.L.	1203
3-1-4	27.479	B.D.L.	1470
3-1-5	27.613	B.D.L.	1981
3-1-6	27.676	0.35 ± 0.14	2468
3-1-7	27.681	B.D.L.	2949
3-1-8	27.680	B.D.L.	3445
3-1-10	27.683	B.D.L.	3692
3-1-11	27.676	B.D.L.	3971
3-1-12	27.675	B.D.L.	4031
5-3-A		0.67 ± 0.21	50
5-1-1	26.393	0.31 ± 0.13	279
9-1-1	22.931	3.58 ± 0.38	7
11-1-A	24.232	4.32 ± 0.19	30
12-1-A	24.645	4.86 ± 0.23	18
12-1-B	26.015	5.09 ± 0.20	100
12-1-C	26.368	1.86 ± 0.18	168
12-1-D	26.984	0.78 ± 0.16	424
13-1-A	25.207	5.31 ± 0.44	43
14-1-A	22.076	5.35 ± 0.24	30
2(-TAP	21.037	16.96 ± 0.58	1

N.D. = Not determined - B.D.L. = Below detection limit

TABLE IV.13

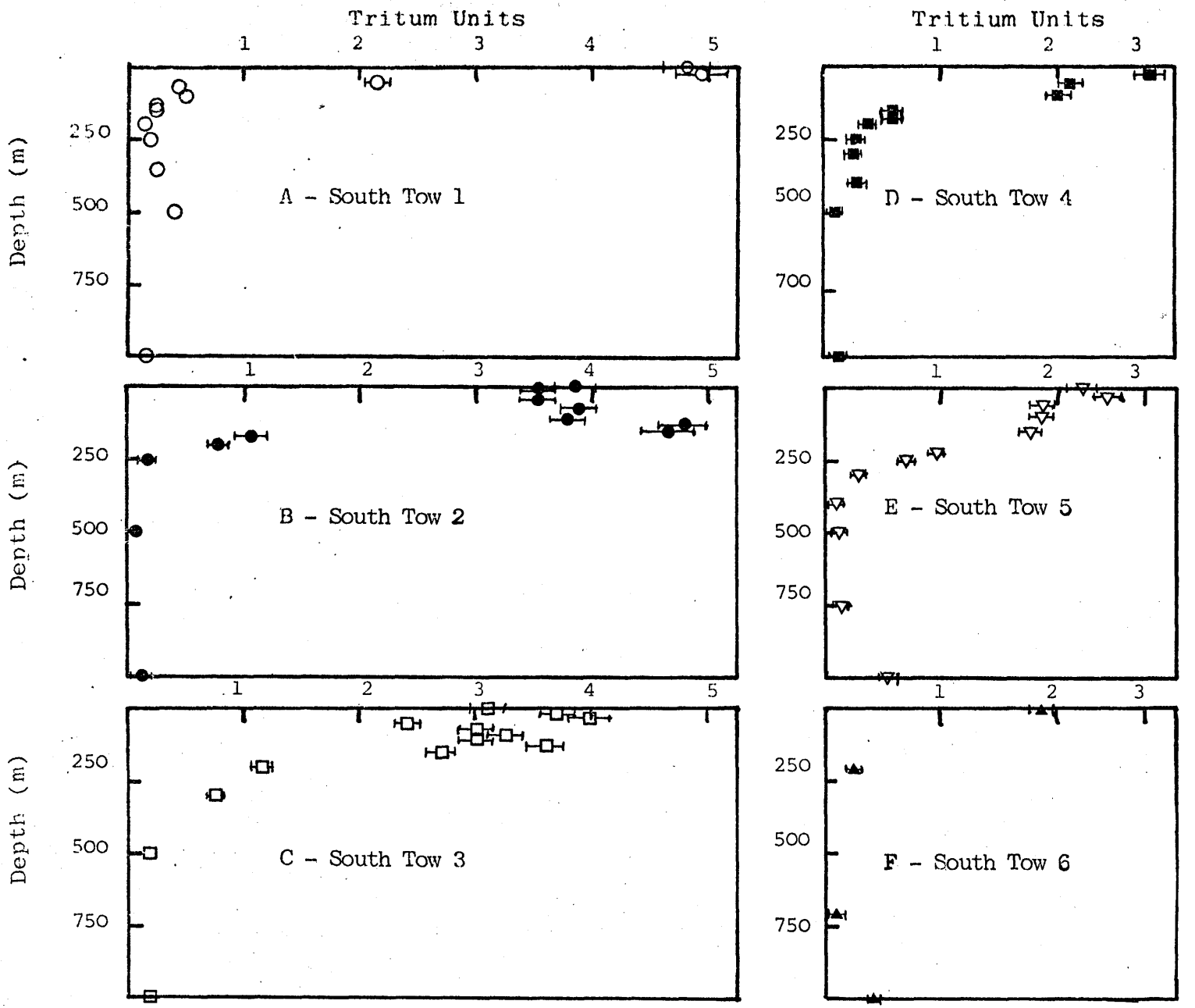

Figure IV.13 South Tow tritium concentration (± 1 σ) versus depth profiles.

As indicated previously, the SECC is represented by water with a salinity between 34.0 - 34.9$^{o}/_{oo}$. The only waters with salinities in this range are below the thermocline. Most samples can be considered to be representative of the SECC. These features are repeated at Bartlett Station 3 (Figure IV.14). It should be noted that the highest tritium concentration found in any profile was 2.78 T.U. at South Tow 4. Michel (1974) considers 3.4 T.U. to be an upper limit for tritium in the South Pacific and that any water masses sampled in the equatorial system with tritium concentrations greater than 4 T.U. have a significant input of water from the North Pacific. The more complex situations are presented in Figure IV.13 B and C with these profiles being within the NECC and EUC, respectively. It is apparent that very strong tritium gradients exist within these water columns indicating that water levels within a few metres of one another have different sources and are not well mixed. Of the four samples analysed at Bartlett Station 12, a very similar situation exists (Figure IV.14), particularly when compared with South Tow 3 (Figure IV.13C).

In addition to the similarities between these two Bartlett Stations and their South Tow counterparts, analysis on constant σ_t surfaces continue to show remarkably close correlations. As pointed out by Tsuchiya (1968), Michel (1974) and Michel and Suess (1975) isanosteric and σ_t surfaces show a shallowing towards the east, coupled with increased salinities and tritium concentrations on each surface. In Figures IV.15 - IV.17, the σ_t surfaces of 25, 26 and 27 are shown respectively. The σ_t surface of

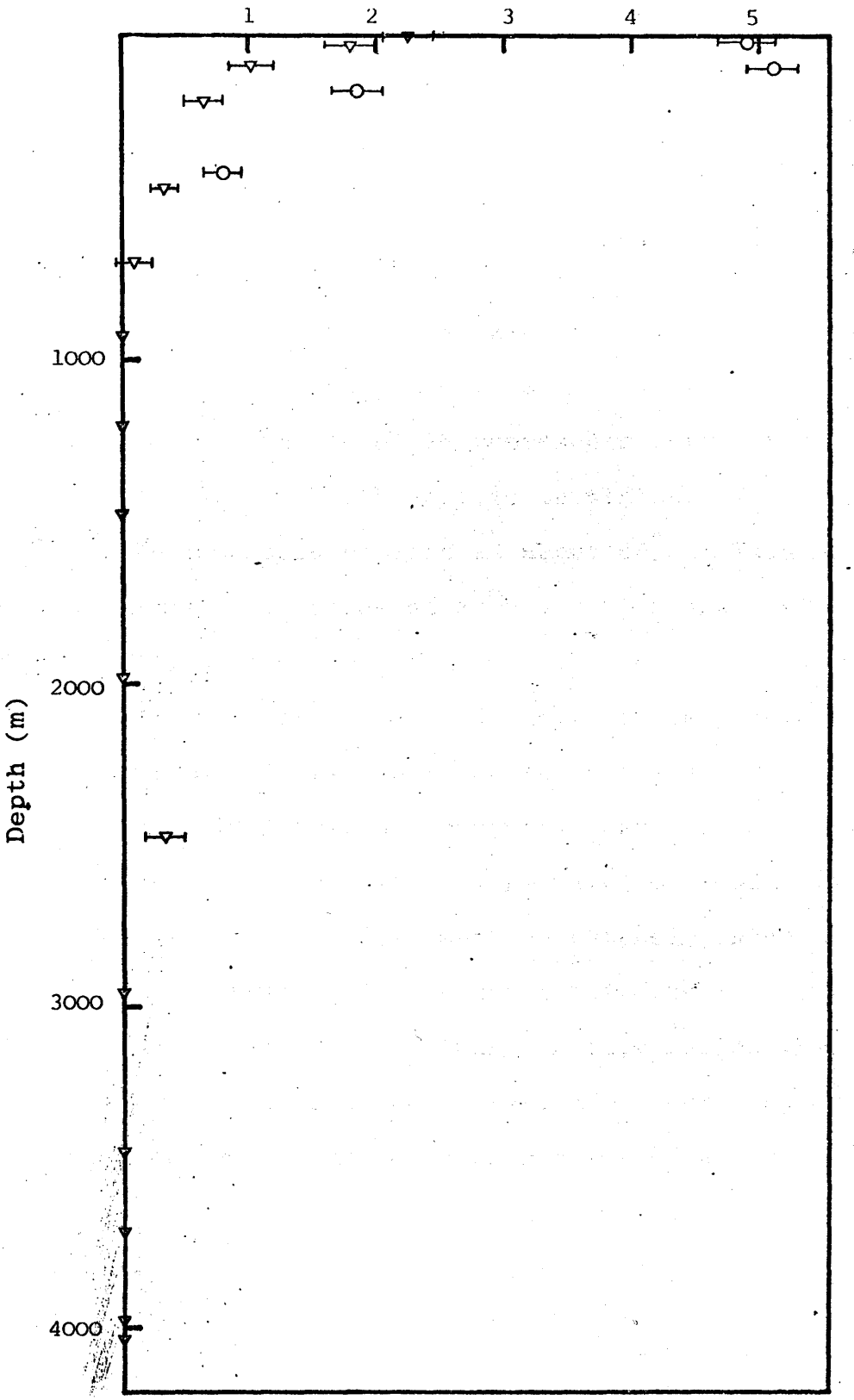

Figure IV.14 Tritium concentration ($\pm 2\sigma$) versus depth profiles for Bartlett Stations 3 and 12.

25 represents water which outcrops in both the North and South Pacific at latitudes of about 30°. This surface sinks to about 200 metres at 20°N and remains 100 -150 metres deep throughout most of the equatorial region. This is the density surface on which the subsurface tritium and salinity maxima are found in the NECC and the EUC. As expected, this surface occurs at shallower depths eastwards with increasing tritium and salinity values; Bartlett Station 3 perhaps shows a slight salinity decrease possibly indicative of upwelling. The σ_t surface of 26 represents water which outcrops in the sub-Arctic North Pacific in winter. It reaches the surface in the South Pacific at about 45°S. This surface sinks to about 300 metres at 20°N and 20°S and rises to a depth of 200 metres throughout the rest of the equatorial system. In the North Pacific, tritium concentrations are highest in the sub-Arctic where salinities are lowest. As salinities increase, tritium concentrations decrease, indicating that mixing occurs with saline water of lower tritium concentration along this surface (Michel, 1974). Bartlett results along this surface suggest that the influence of upwelling is perhaps more dominant in this region than in the South Tow region and that water, after deriving its salinity and tritium maxima in the north, mixes with the SECC water being upwelled, reducing the salinity and tritium values. The σ_t surface of 27 represents water which reaches the surface at about 60°S in the South Pacific. This isoline sinks to about 800 metres at 50°S and remains between 600 - 800 metres deep throughout most of the Pacific. Again, as with the σ_t of 26, tritium concentrations are greater but salinities are similar. The position of this surface at

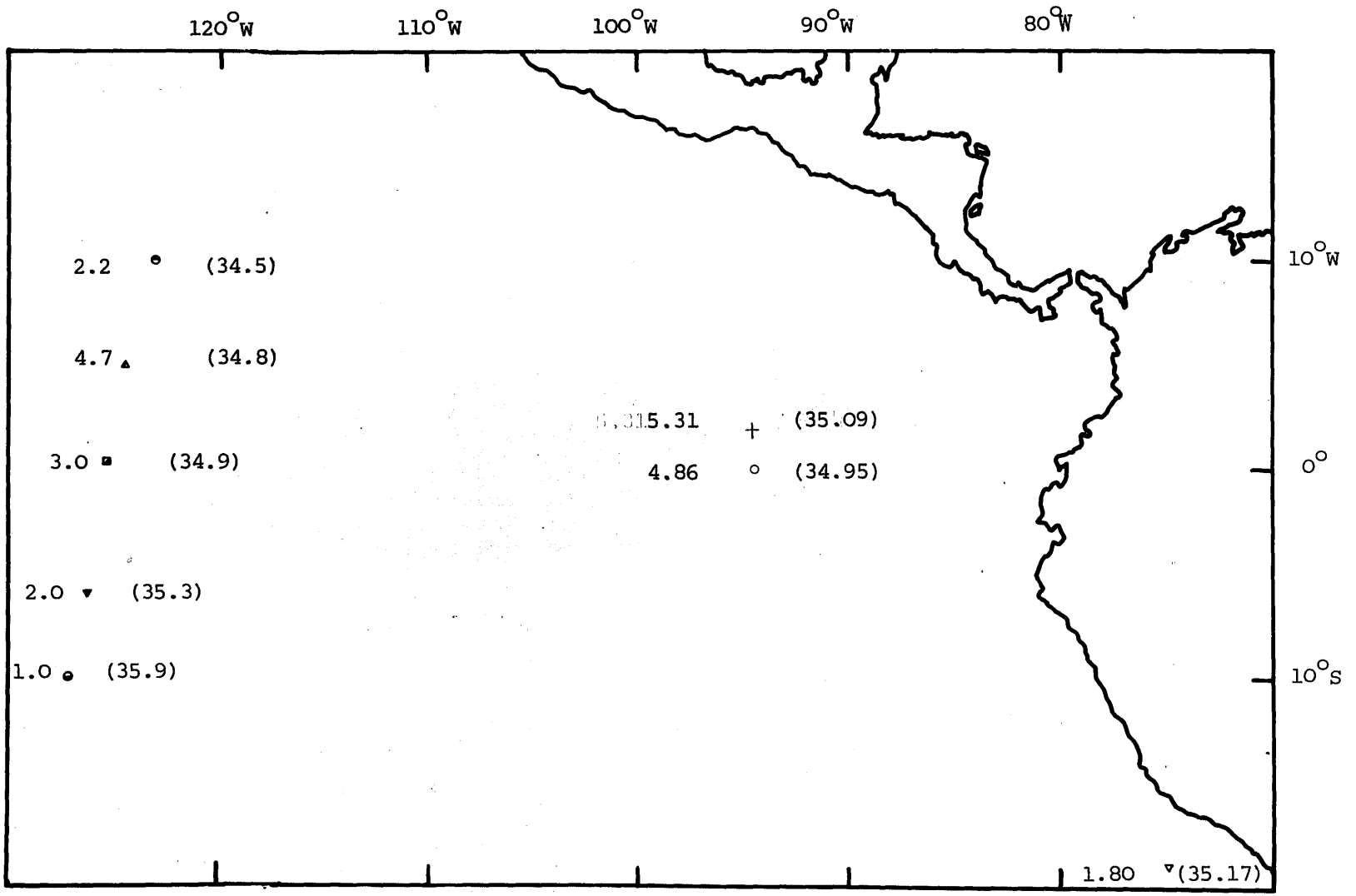

Figure IV.15 Tritium concentration on a σ_t surface of 25 . Salinity is in Parentheses.

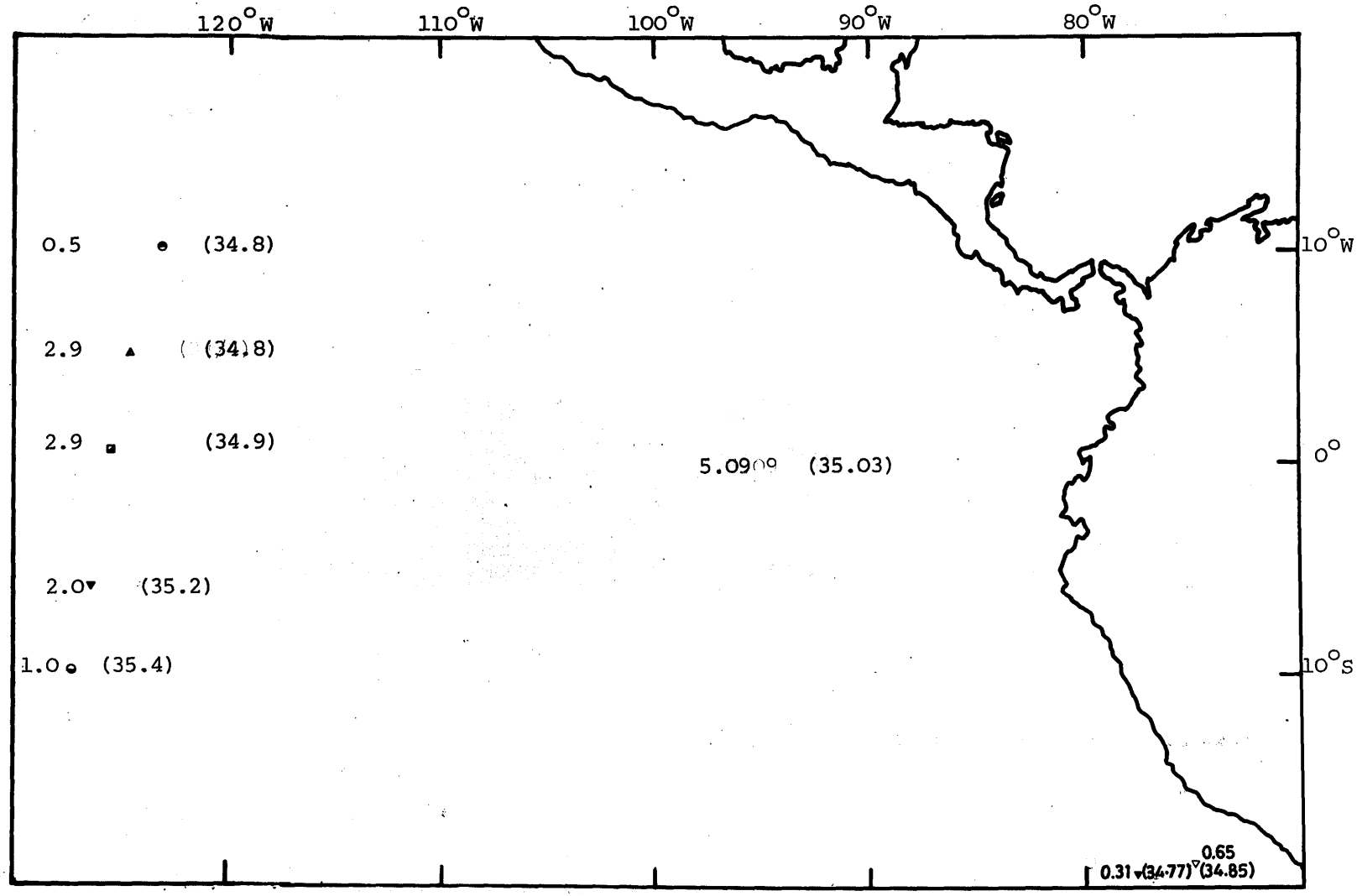

Figure IV.16 Tritium concentrations on a σ_t surface of 26 . Salinity is in parentheses.

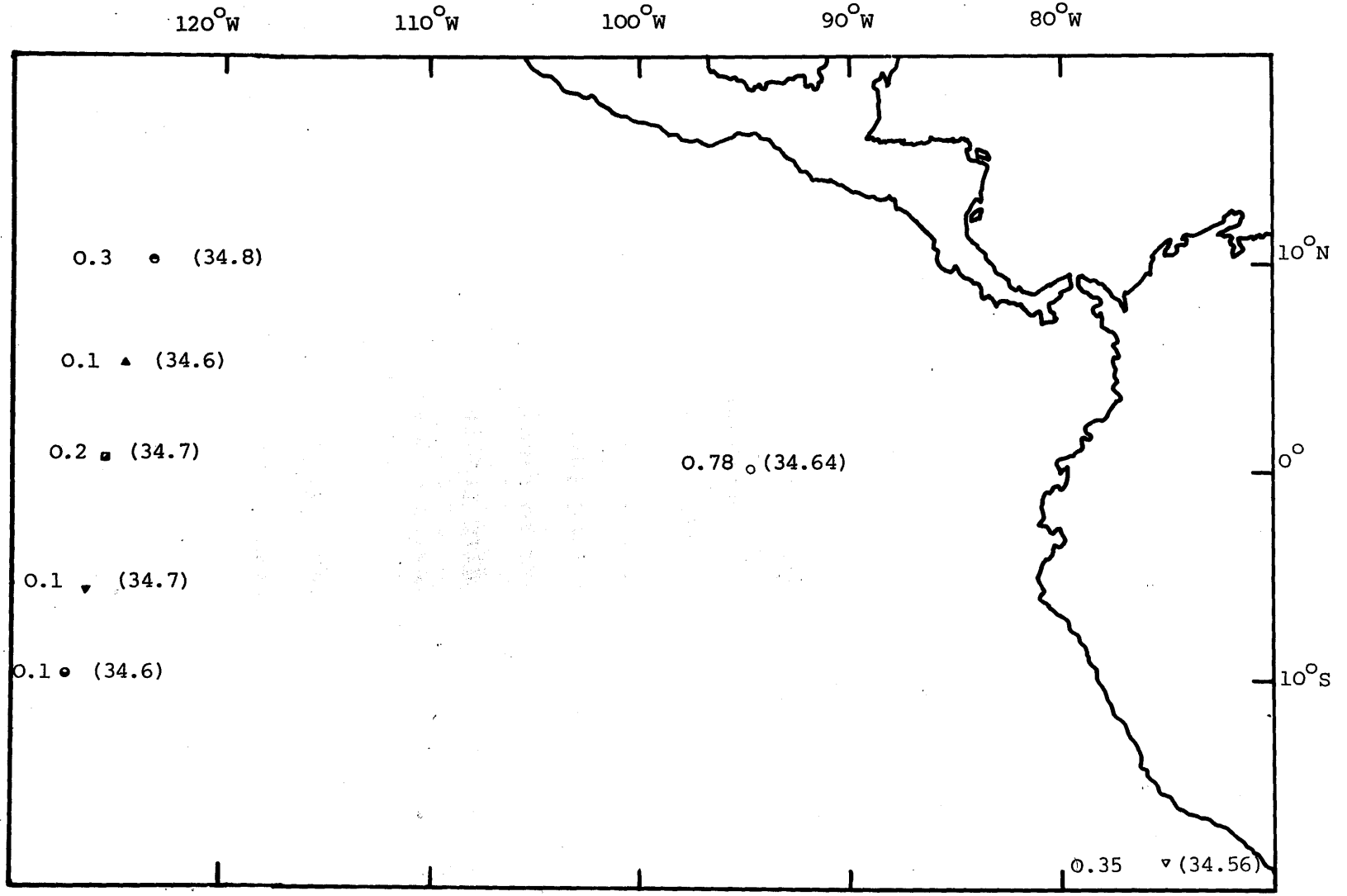

Figure IV.17 Tritium concentrations on a σ_t surface of 27. Salinity is in parentheses.

400 - 500 metres deep for the Bartlett Stations corroborates the occurrence of upwelling in this region. A final plot of tritium concentrations in the surface layer is made with the assumption that samples with σ_t values less than 23 are representative of surface conditions (Figure IV.18). Correlation with the South Tow series is excellent with a constant decrease in tritium levels reflecting continuous mixing and losses of tritium into other subsurface water masses. By addition of these data points to the tritium contours established by Michel and Suess (1975) and by recalling that since 1966 the tritium inventory has remained essentially constant, it is evident that these contours continue smoothly into the eastern tropical Pacific (Figure IV. 19). The apparent increase of the tritium gradient southwards, along with higher tritium values, is consistent with the highly tritiated California Current flowing southward and turning west, forming part of the NEC. Penetration of high tritium values south of the equator is perhaps surprising but surface mixing with the eastward flowing NECC could account for these observations.

A temperature anomaly plot versus temperature, using a 60 metre depth interval suggests for the four Bartlett Stations with complete XBT data, an asymptotic temperature of 11.2°C (Figure IV.20). The logarithmic plot of T-11.2°C versus depth does not, however, exhibit much linearity, except in the upper 100 metres or so, with a scale height of 50 metres (Figure IV.21). Indeed, below 100 metres, Bartlett Station 3 deviates greatly from the general linear trend. Both observations are perhaps not surprising in

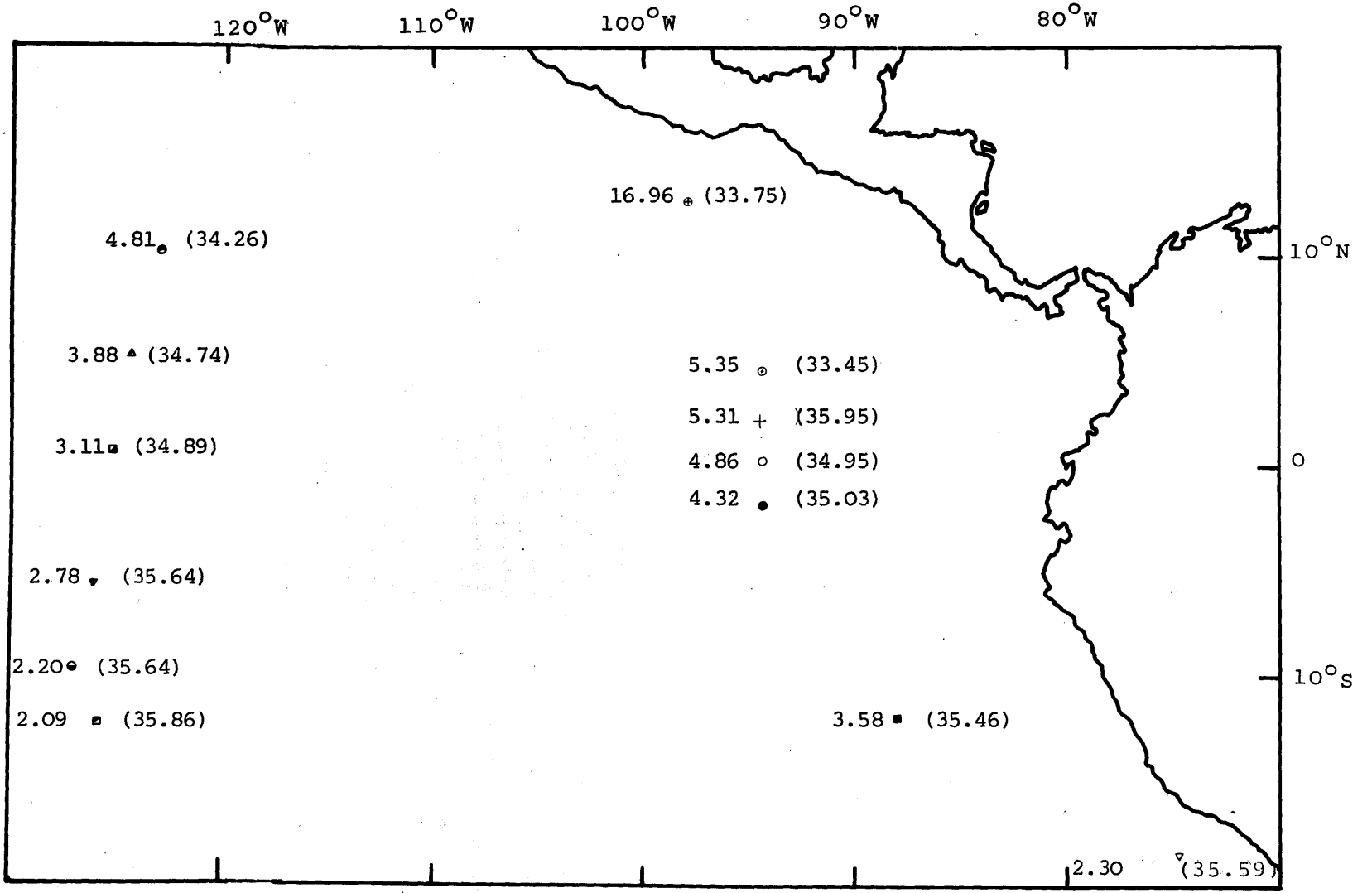

Figure IV.18 Surface tritium concentrations. Salinity is in parentheses.

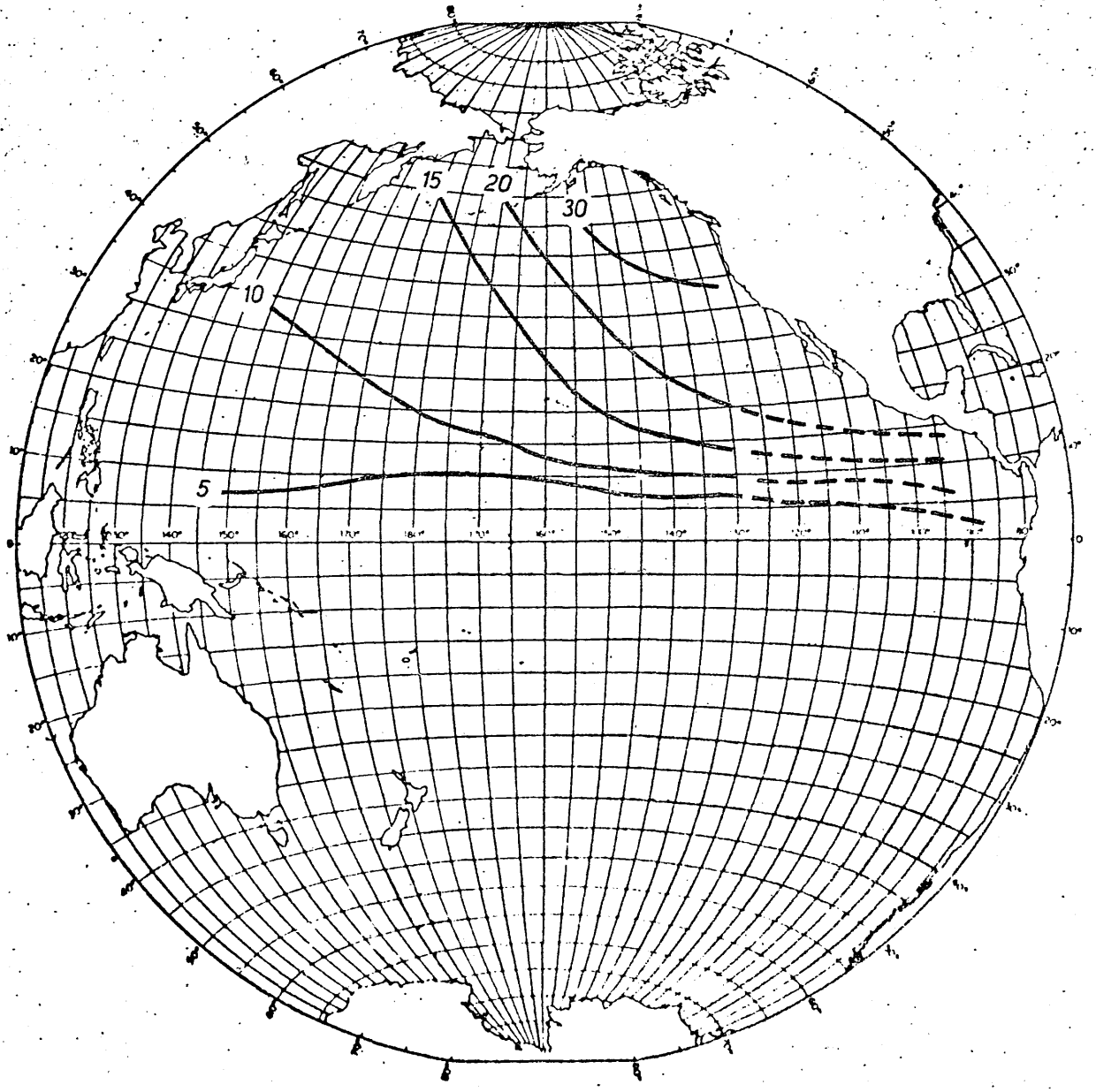

Figure IV.19 Average tritium distribution in the surface seawater of the Pacific Ocean. A north-south asymmetry is present because of the higher input of tritium in the northern latitudes. The east-west asymmetry is a result of deeper mixing in the western Pacific and the flow of surface currents.

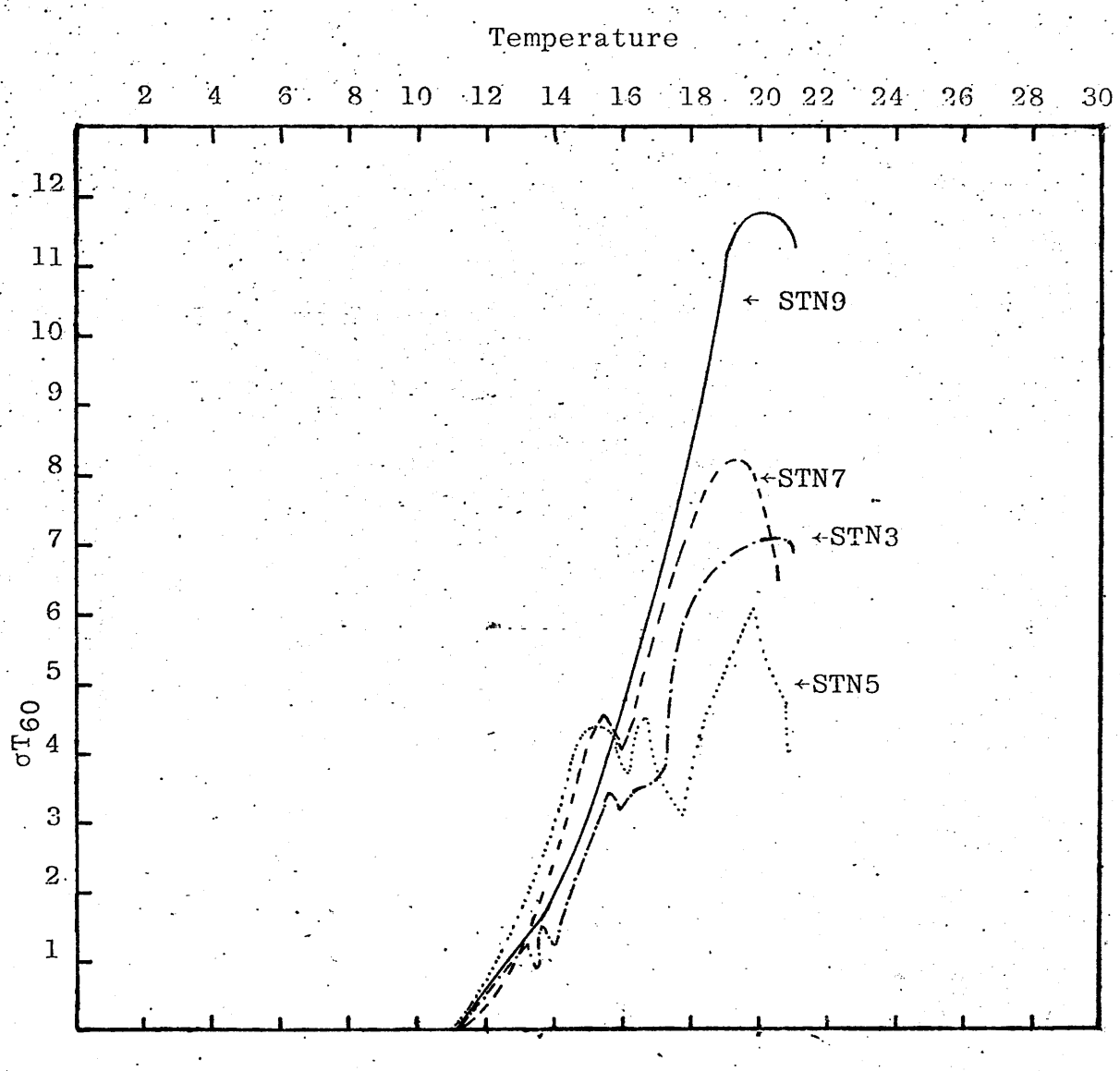

Figure IV.20 Temperature gradient versus temperature for Bartlett Stations 3,5,7 and 9.

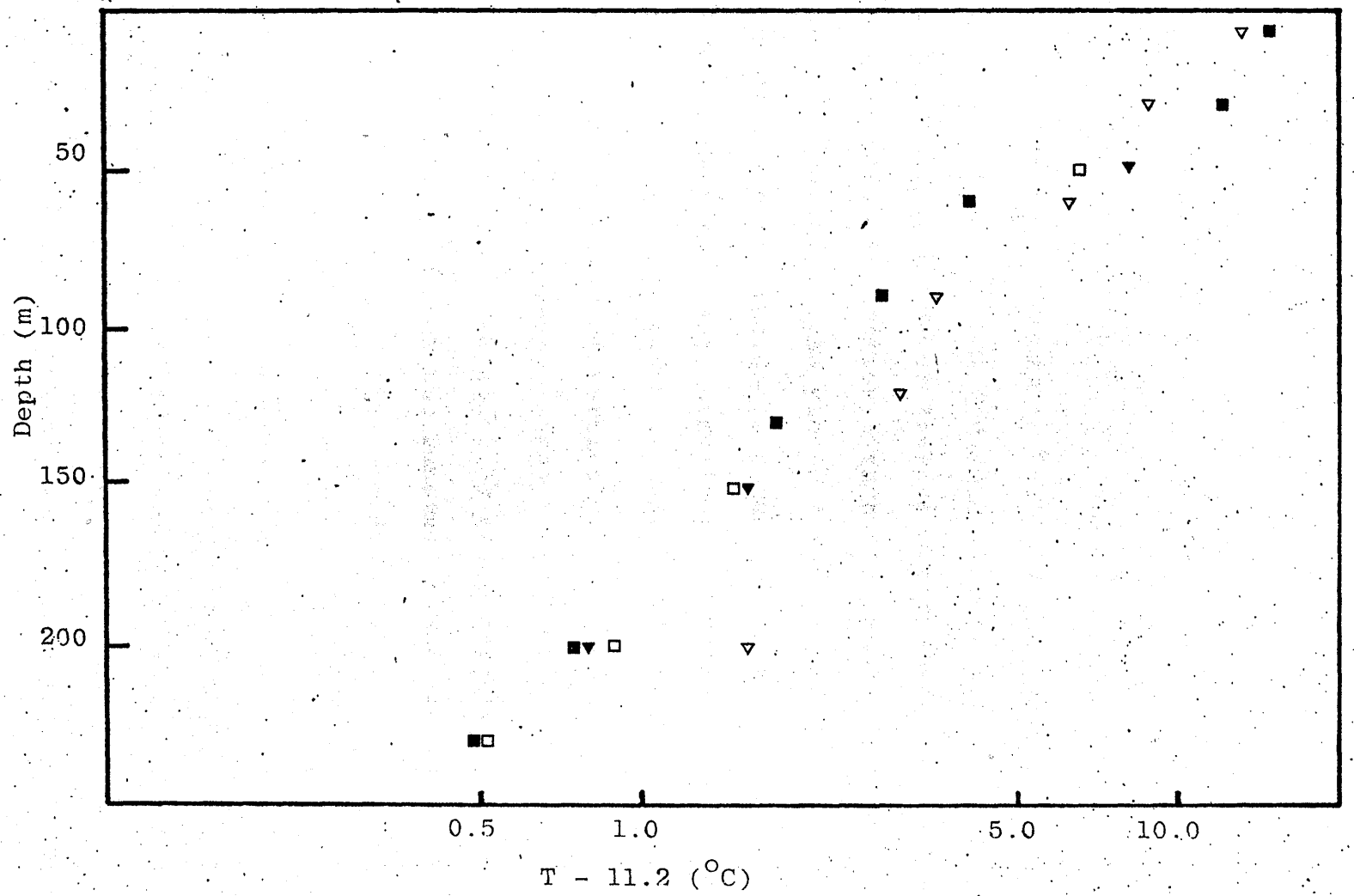

Figure IV.21 Approximate exponential subrange for Bartlett Stations 3,5,7 and 9 profiles.

view of the extreme horizontal circulation present throughout the equatorial Pacific and of the upwelling known to occur most intensely closest to the Peru-Chile coast (i.e. Bartlett Station 3). Calculation of vertical eddy diffusivity constants using equation (I.12) in the form (Trier et al, 1972):

$$K_v = \left(\frac{z}{\ln(C_1/C_2)}\right)^2 \lambda \qquad \text{(IV.1)}$$

yields the values shown in Table IV.14, assuming gross penetration of tritium due to vertical diffusion. The joint exponential decrease of tritium and temperature with depth supports this assumption within the upper 200 metres of Bartlett Station 3 and yields a K_v = 0.397 cm^2/sec. The vertical eddy diffusion is close to values obtained from tritium data by other investigators (Roether et al, 1970; Rooth and Ostlund, 1972; Roether, 1974), and is well below previous estimates of vertical eddy diffusion obtained by other methods (Veronis, 1969). Even an upper limit of K_v of 0.9 cm^2/sec, obtained by considering all the uncertainties, is below the generally accepted value of 1-2 cm^2/sec for K_v (Michel and Suess, 1975). The results indicate that the effects of vertical processes on the structure of the thermocline have been overestimated. Lateral factors may exert stronger influence than was generally believed and could even dominate. This must certainly apply to Bartlett Station 12 where subsurface tritium and salinity maxima exist (i.e. large scale horizontal circulation) and which yields a K_v of 1.555 cm^2/sec.

The surface tritium values were analysed in an attempt to estimate the turnover or removal times of the upper mixed

Bartlett Station 3 from depth (m)	to depth (m)	K_v (cm^2/sec)
7	32	0.186
7	62	0.220
7	91	0.154
7	195	0.397
7	476	1.112
7	705	0.945
195	705	1.477
195	476	3.693
476	705	0.702

TABLE IV.14

layer waters using a balance equation (Bainbridge, 1963; Eriksson, 1965; Tamuly, 1974) in conjunction with rainfall tritium recorded for Howard AFB (IAEA,1973) as a representative station. A land based station near the Panama Canal, Howard AFB, might not ideally represent eastern tropical Pacific rainfall concentrations. Schell and Sauzay (1973), however, have shown that rainfall tritium concentrations at marine stations between 20°N to 20°S average 15 T.U. (10 - 20 T.U.) in agreement with Howard AFB (14.20 T.U.). Given this assumption, the equation relating tritium input and removal is as follows:

$$\frac{dN}{dt} = I - RN - \lambda N = I - aN \qquad \text{(IV.2)}$$

where N is the concentration of tritium in the mixed layer in T.U.; I is the input or rate of deposition of tritium into the 100 metre depth mixed layer (Bathen, 1972) in T.U. $year^{-1}$, λ is the decay constant of tritium (0.056 $year^{-1}$), R^{-1} is the turnover or removal time of tritium through the mixed layer, in years, and $a = (\lambda + R)$ or $(a - \lambda)^{-1} = R^{-1} = \tau_o$. I, the tritium input by precipitation only to the ocean surface mixed layer of 100 metres depth, is calculated from the relationship.

$$I = \frac{P.TUP}{10^4} \qquad \frac{T.U.}{year} \qquad \text{(IV.3)}$$

where P is the mean annual precipitation in cm/year over the ocean and TUP is the tritium concentration, T.U., in precipitation. The value of I is input by rain only and does not include molecular exchange. Higher inputs of tritium by several orders of that by precipitation to the ocean surface by vapour-exchange were suggested by models in

recent times (Eriksson, 1965; Craig and Gordon, 1965; Taylor, 1968; Gat, 1970). In calculations by Michel and Suess (1975) molecular exchange is assumed to add twice as much tritium as precipitation, and therefore all rainfall values are multiplied by 3 to obtain the total input I. A steady-state is assumed between tritium input and removal (Tamuly, 1974) and equation (IV.2) yields:

$$I - aN = 0 \qquad \text{(IV.4)}$$

A straight-forward substitution into equation (IV.4) gives τ_o of 15-4 years depending upon latitude (Table IV.15). No errors have been calculated since the assumption of molecular exchange and representative rainfall data can yield only approximate residence times. However, these residence times appear to be in agreement with previously cited τ_o's. The latitude dependence exhibited by the residence time strongly reflects the influence of upwelling in the more southern Bartlett stations and horizontal circulation and mixing in the northern Bartlett Stations. Montgomery (1959) using salinity distributions suggested residence times of subtropical surface waters to be 6-12 years; by inventory methods Eriksson (1965) proposed a mean residence time of 22 years; Houtermans' (1966) tentative interpretation of tritium results in the Pacific Ocean surface waters indicated an upper limit τ_o of 12 years; Pritchard et al (1971) predicted residence times of surface waters of the world ocean to be 10 years; Goldberg et al (1971) considered the residence time of a relatively non-reactive chemical element (i.e. Na^+, Cl^-, K^+) in the mixed layer for the world ocean to be about 20 years when only physical

Bartlett Station	Residence Time (τ_o) (years)	Latitude
14	14.84	$4^{o}33.5'N$
13	14.64	$2^{o}02.3'N$
12	12.53	$0^{o}16.8'N$
11	10.33	$2^{o}00.8'S$
9	7.79	$11^{o}08.8'S$
3	4.33	$18^{o}57.0'S$

TABLE IV.15

mixing processes cause removal of the element to deeper waters; while Tamuly (1974) estimated 14-35 years residence times dependent on latitude. It is again not surprising that the residence times decrease in a southerly direction (i.e. more rapid mixing is occurring due to upwelling).

IV.5 Summary.

Taken as a whole, the hydrographic results obtained from the Bartlett cruise are in general accord with the known oceanography of the eastern tropical Pacific. The temperature structure is uniform over the region, apart from near-surface variations caused by local meteorological and heat budget differences. The shallow and intermediate waters display salinity distributions compatible with orthodox views on both the ocean-atmosphere interactions and the prevailing current systems. The bottom waters are typical of those found in basins north of the complex ridge system patterning the ocean floor off Chile. Only in the deep water of Station 3 is a feature observed which is at variance with the expected salinity, tritium and radium distributions. At this location, there is an apparent core of high salinity water at ~ 2500 metre depth which has a consistent influence on both deeper and shallower layers. A similar relationship with tritium has not been found. The $\delta^{18}O$ results of Fallick (1975) confirm the general hydrological regime presented and indicate that homogeneity of the deep water is violated at ~2500 metres depth but the effect on neighbouring samples is not observed. The deep water distinction on the basis of dissolved oxygen concen-

tration (Murmomtev, 1963) is confirmed.

Regions of joint tritium and temperature diffusion have been found to exist but at shallower depths and smaller depth intervals. Within the equatorial Pacific, lateral exchange dominates any vertical processes and leads to unusually high K_v values. Near 20^oS, vertical processes act, at least within the upper 200 metres, yielding K_v of 0.397 cm^2/sec. Below 200 metres upwelling plays a dominant role in the distribution of properties yielding high K_v's, shallower σ_t surfaces and lower salinities. Tritium values still reflect residual higher levels from original input north of the equator. However, for Bartlett Station 3 below 200 metres, lateral advective processes seem unlikely to dominate whereas intense upwelling (which is known to occur in this region) seems the more likely explanation of the observations. High values of K_v are found below 200 metres with a maximum K_v of 3.693 cm^2/sec between 200 - 500 metres. Furthermore, the shallowing of the σ_t surfaces is in accord with this mechanism and is supported by recent ^{210}Pb and ^{210}Po studies (Thomson and Turekian, 1976) on Bartlett Station 3 and 9 samples, demonstrating marked differences in their profiles versus depth with a depletion of ^{210}Pb and ^{210}Po from radioactive equilibrium at Bartlett Station 3 due to intense upwelling and high organic productivity.

The calculated residence times also support upwelling occurring in the southern Bartlett Stations. The latitude dependence exhibited by the residence times is proportional to the horizontal circulation, mixing and upwelling observed

in the eastern equatorial Pacific. Furthermore, these residence times (4-15 years) agree with current estimates for surface waters (6-35 years).

CHAPTER V.

MEASUREMENTS FROM ANTARCTIC WATERS.

V.1. Introduction.

The structure of this chapter will parallel that of Chapter IV for both have much the same purpose in attempting to present the results obtained from seawater samples within a general framework of the oceanography, both physical and chemical, of the appropriate region. Thus, a short introduction to the main features of the general system will be given, followed by a rather more specific account of the hydrology at the individual station. Finally, the tritium results will be analysed in the light of the preceding section. There are, however, several points of contrast with Chapter IV. Firstly, the oceanography of the Antarctic is much more complex than that of the eastern tropical Pacific; some of the reasons for this will be mentioned in section V.2. Secondly, samples have been obtained and analysed from a single station only.

In Chapter IV it was seen that understanding the Peru-Chile current system, a critical problem to the fishing industries of the coastal states, was dependent upon the knowledge of the oceanographic and meteorological regimes both to the north and south of the zone usually affected most strongly by 'El Nino'. The Antarctic is another geographical location on which increasing emphasis is being focussed by marine scientists. The Committee on Polar

Research (1974) has drawn attention to four areas considered as being especially significant there:

(i) weather and climate modifications;

(ii) an ecologically sound strategy for disposal of waste and radioactive by-products;

(iii) an ecologically efficient long term use of the region's fisheries; and

(iv) the improved prediction of local weather, sea and ice conditions.

V.2 General oceanography of the Antarctic Region.

Whether or not the water surrounding the continent of Antarctica constitute an 'Ocean', in the sense that there are Atlantic, Pacific and Indian Oceans, is a matter of some debate. Certainly, the waters are totally bounded only by the continent to the south and *could* be described as the southernmost extensions of the three oceans mentioned. However, for the purposes of this chapter, the terms *'Antarctic Ocean', 'Southern Ocean'* etc. will be used in the generally accepted manner to describe these waters whose northern boundary is somewhat arbitrarily fixed at the Antarctic Polar Front. One of the most important features of the region is that it is the only place where waters of the Pacific, Atlantic and Indian Oceans all converge and intermix freely. This mixing is greatly enhanced by the prevailing oceanographic and atmospheric conditions causing a higher degree of uniformity of water properties in the major basins to the north than would otherwise be the case.

It is generally agreed that the circumpolar region plays a crucial role in determining many characteristics of other areas of the ocean. Prominent among early reports describing the general structure and circulation pattern of the Southern Ocean is the work of Deacon (1933, 1937, 1963 and others) based on the 'Discovery' Expeditions. Several other Discovery Reports are also important (e.g. Clowes, 1938; Sverdrup, 1933). However, in several instances, direct reading of these early publications has not been possible since they are rather obscure foreign reports but by common consent contain original ideas or observations. These have been referenced with an asterisk, maintaining a description consistent with the bulk of the literature (e.g. 'Wust, 1938*'). Most of the major early references have been gathered by Gordon (1971) in a recent review and will not be listed here. The basic hydrology and current system are greatly influenced by (i) climatic conditions, and (ii) bottom topography. In the tropical and subtropical ocean regions, there is strong stratification of the upper water column so that the deep ocean has only limited interaction with surface layers, principally by eddy diffusion and gentle upwelling through the thermocline. However, at high latitudes, the extremely cold atmosphere and lack of strong stratification permit deep vertical convection and overturning to occur, resulting in the water column instability typically found in the Antarctic. South of 65^{o}S, the prevailing winds are easterly, blowing parallel to the coast of the continent due to katabatic effects (Killworth, 1973). The induced surface current is therefore mainly to the west, with a southward component. North of 65^{o}S, westerlies prevail, with a maximum at 53^{o}S

(Deacon, 1963), causing an eastward flow with a small transport northwards. Where the two wind systems meet there is divergence and around 65°S is the Antarctic Divergence zone (Figure V.1). Here, deep water upwelling occurs replacing the wind-driven surface layers. This upward flux is extremely important for the oceanography of the region, causing the warm salty deep water to be exposed to the intense cold of the atmosphere. Therefore, the divergence will be somewhat variable, being dependent on atmospheric circulation. In the region of maximal westerlies, the cold, dense northward flowing Antarctic Surface Water (ASW) meets warmer, less dense, southward flowing subantarctic water, consequently sinking below it and resulting in high surface temperature gradients in this area. A frontal system develops and there is intense vertical mixing. The Antarctic Convergence, the original name of this feature, is less frequently used since both convergent and divergent features are observed. It is more commonly known as the Polar Front Zone and marks the northern limit of the Antarctic Ocean as previously defined. Some 2° - 4° of latitude wide (Gordon, 1971), the Polar Front Zone is a more permanent feature than the Antarctic Divergence. The well mixed, turbulent water mass formed near the surface migrates northwards at intermediate depths, the temperature minimum disappearing as a result of mixing, but the low salinity remains and is the characteristic by which this Antarctic Intermediate Water (AAIW) is identified further north. At the surface, north of the Front, Subantarctic Surface Water flows towards the equator until, at ~ 40°S, it meets the southward flowing subtropical surface water in a region of convergence (the Subtropical Convergence).

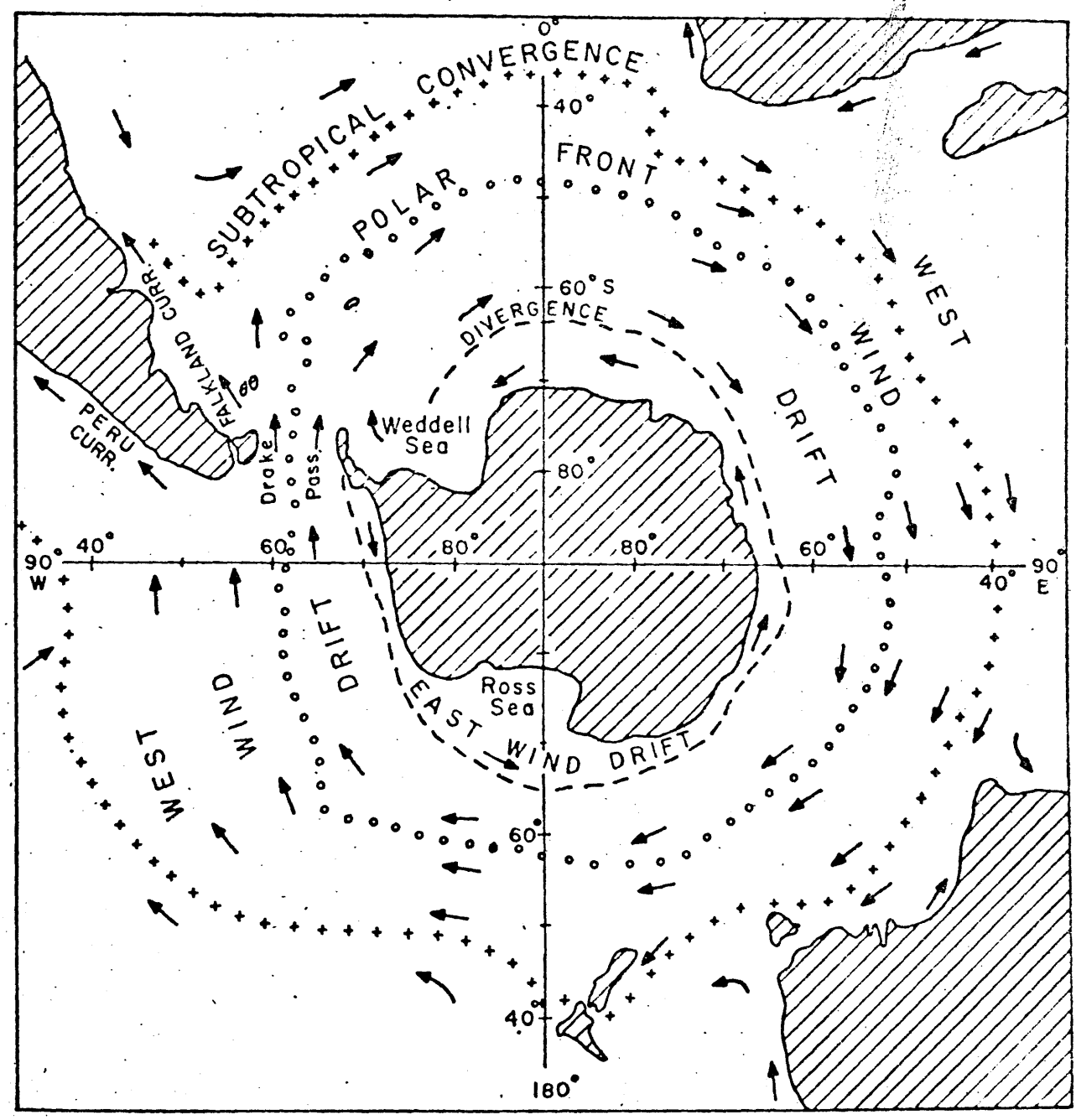

Figure V.1 Southern Ocean-surface circulation and mean positions of the subtropical convergence, Polar Front and Antarctic Divergence (after Pickard, 1963).

Surface waters sink, joining the northward flowing AAIW.

Warm, high salinity deep water flows into the Antarctic from all three major ocean basins to the north. The North Atlantic Deep Water (NADW) has a particularly high salinity due to its Mediterranean component. These waters mix with the northward flowing intermediate current and, at the Polar Front, rise over the zonal Circumpolar Deep Water (CDW) until reaching the Antarctic Divergence where they are brought close to the surface, joining in formation of surface waters. Southward flowing surface water at latitudes greater than $65^{o}S$, upwelling Deep Water and intensely cold water from the continental shelf mix to form a very dense water which plunges down the continental slope, entraining further Deep Water as it sinks. The production of this Antarctic Bottom Water (AABW) is believed to occur in several geographical areas close to the continent (e.g. the Weddell Sea, the Ross Sea and off the Adelie coast). Flowing northwards under the Deep Water, the interaction of the AABW with topographic features of the sea floor is believed to contribute to the upwelling of Deep Water at the Polar Front Zone.

The connecting link between the aforementioned two modes of circulation (i.e. surface/intermediate and deep/bottom) is the Antarctic Circumpolar Current (ACC) (Wyrtki 1961). The Polar Front, strongly coupled to the ACC, is frequently associated with the axis of the Current. In Figure V.2 an attempt has been made to illustrate the structure around Antarctica. Although conditions are not meridionally uniform, particularly with regard to Bottom

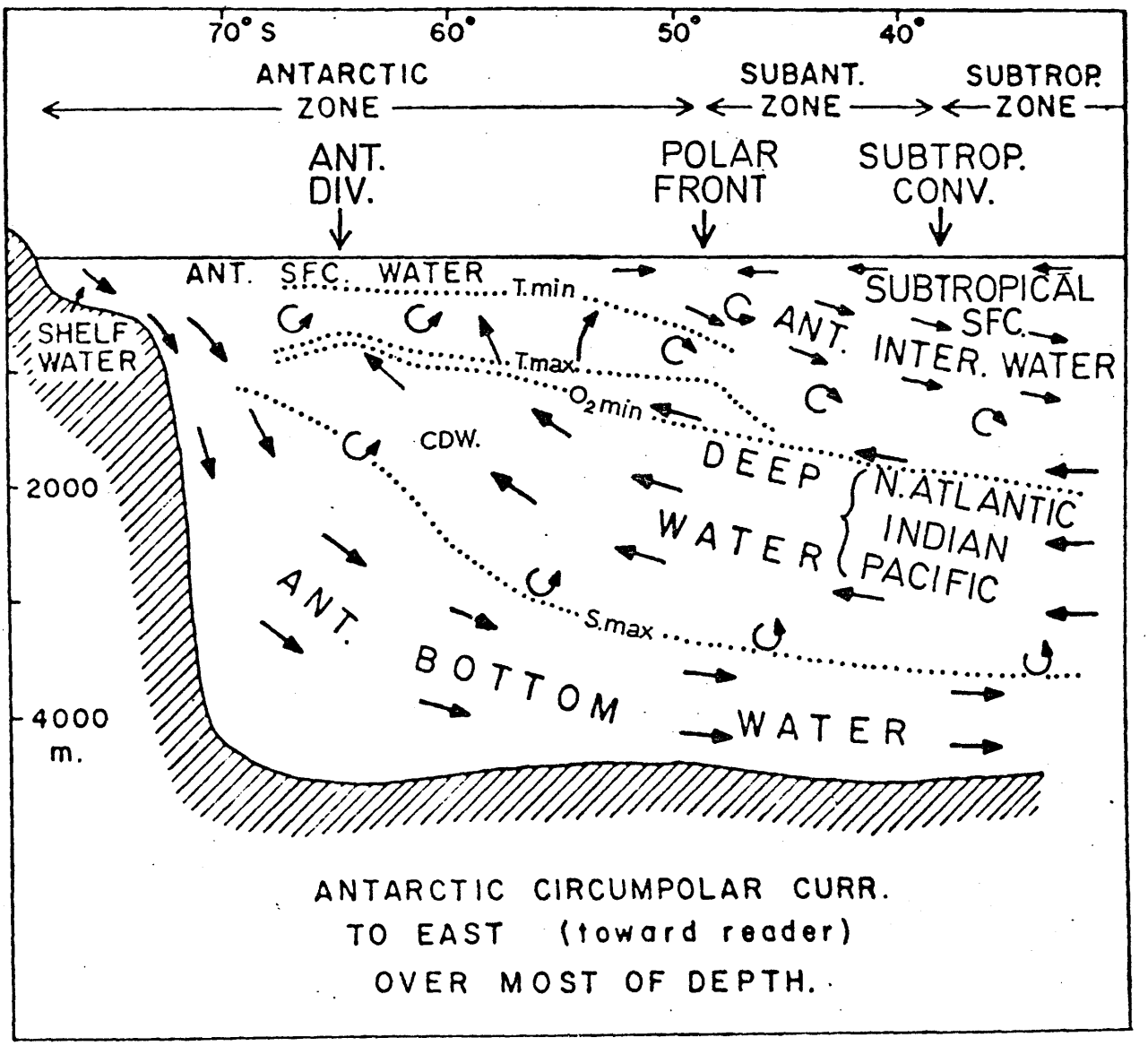

Figure V.2 Schematic of vertical components of the circulation in the Southern Ocean and prominent hydrographic features.

Water formation, and the asymmetrical nature of the coastline together with the existence of a complex bottom topography produces important longitudinal differences, the main features are represented.

The circumpolar current system, comprising a zonal flow, a meridional flow and the source of deep water in the Weddell Sea, dominates the deep-ocean circulation. These Antarctic currents provide the link between the world's major oceans. Antarctic convection sends equatorwards both the sheetlike AAIW and also the abyssal AABW. In terms of mass transport, the ACC is the largest ocean current in the world (Devine, 1972). It has been assigned an absolute transport of 200-250 sv (1sv = 1 sverdrup = 10^6 m^3 s^{-1}) by both Callahan (1971), using geostrophic calculations, and Reid and Nowlin (1971), using direct current-meter observations. The ACC has the unique distinction, compared to other major currents, of the absence of meridional barriers (Munk and Palmen, 1951). However, the suggestion that the ACC is basically a zonal flow (Hidaka and Tsuchiya, 1953) is impossible due to its forced flow through the narrow Drake Passage and then past the blocking South Antilles Arc (Stommel, 1957). The ACC is deflected by at least five different ridge systems as it flows around Antarctica. That no single theory accounts fully for the features peculiar to the region where the ACC flows should not diminish the importance of the ACC in both Antarctic and global oceanography.

A second major important problem is that of the dynamics and mode of formation of the AABW. Water mass analysis shows

that the bottom water over a large fraction of the world ocean originates in the waters surrounding Antarctica. Water from this region reaches northward to 40^{o} - 45^{o}N in the western Atlantic and strongly influences both Indian and Pacific bottom circulations (Wust, 1936* and 1957*). Chung (1971) mapped the penetration of AABW in the western Pacific basins. Various mechanisms of formation of AABW have been proposed over the years. Brennecke (1921*) and Mosby (1934*) first postulated that cold, high-salinity water forms at the surface in winter by the freezing of ice, subsequently mixes with deeper, warmer and more saline water at the edge of the continental shelf and thereafter sinks to the bottom. Further work by Deacon (1937) and Wust (1938*) suggested that the majority of the AABW is formed in the Weddell Sea. Recent studies have shown that other sources of AABW exist, the Ross Sea (Jacobs et al, 1970) and off the Adelie coast (Gordon and Tchernia, 1972) being the best documented.

Fofonoff (1956) drew attention to the fact that due to the non-linearity of the equation of state for seawater, when two water types of different temperatures and salinities mix, the mixture produced may be more dense than either of the original types and may therefore sink (a phenomenon known as *cabbeling*). This can be easily illustrated on a T-S diagram. Noting that there are no observations of unmixed shelf water at great depths, Fofonoff further proposed that bottom water is formed principally in shallow water and that the critical shelf water salinity interval was 34.51 - $34.56^{o}/_{oo}$. This was redefined by Gill (1973), by considering the depth of mixing, to 34.465 - $34.515^{o}/_{oo}$. Within this

salinity range, the shelf water overlying warm deep water is prevented from sinking by its heavier mixtures. Foster (1972) has shown that cabbeling instability can enhance the downward flux of shelf water. Other physical processes which may play a part in bottom water formation include cooling of the coastal current shelf water by the vast ice shelves (Seabrooke et al, 1971), wind-driven sinking (Killworth 1973) and sinking as a result of horizontal and vertical circulation within the Weddell Sea (Gill, 1973). However, absolute rates of formation of AABW have not been determined directly, but many indirect estimates exist. Care must be exercised in discussing these, as some are based on the amount of bottom water produced in the Weddell Sea, some on that produced all around Antartica and some on the northward flux of bottom water in the Atlantic or Pacific Ocean. Values predicted for the amount of Bottom Water formed around the coast of Antarctica vary according to the physical mechanism postulated and the proposed subsequent mixing with deep water as the dense water slides down the continental slope to the bottom. The ratio of deep water to altered shelf water is generally taken as 2:1 and 3:1 depending on the measured parameter. Wyrtki (1961) calculated from heat budget considerations that 11.5 sv of sinking water could be formed by thermohaline processes over the entire Weddell Sea; Killworth (1973) considered wind-driven sinking and obtained 20 sv only by including the entire coastline of Antarctica, the Weddell Sea value being considerably smaller. Gill (1973), using a model of the vertical and horizontal circulation within the Weddell Sea with the final mixture containing 25 - 30% shelf contribution and dilution effects, arrived at 6 - 9 sv of AABW being formed. This could be in-

creased to 10 - 15 sv by including the Ross Sea. Seabrooke et al (1971) concluded that alteration of shelf water of the Antarctic coastal current as it comes in contact with the underside of the Filchner and Ronne Ice Shelves is a determining factor, yielding a 2:1 mixing ratio deduced from preformed nutrient data and 5 sv of Bottom Water. Using a 35% shelf-water contribution, Baranov and Botnikov (1964) estimated that 20 sv leaves the Weddell Sea. Wright (1969, 1970) calculated a northward flux of AABW in the Atlantic of 5 sv while Warren and Voorhis (1970) obtained a value of 12.9 sv for the Pacific. Very much greater values have occasionally been suggested for the Atlantic. Le Pichon et al (1971) calculated geostrophic velocities and estimated the transport in the Southern Argentine Basin to be 90 sv. Edmond (1973) has supported this using dissolved silicate distributions, obtaining 101 sv. With such diverse formation mechanisms and variable range of flux estimates, there is obviously much room for criticism. Therefore Solomon (1974) has pointed out that the Weddell Sea area assumed by Wyrtki (1961) includes a sizeable fraction that is ice-covered, that Munk's (1966) estimate is invalid because not all melting ice forms AABW. The mechanism of Seabrooke et al (1971) has been discredited by Gill (1973) since the ice shelves cannot conduct away the necessary heat to allow the required cooling of the coastal current.

V.3 Hydrographic Features.

Samples from the waters around Antarctica were obtained from Cruise 47 of U.S.N.S. Eltanin during 1971 by

Dr. J.M. Edmond of M.I.T. The 2.5 litre samples were stored in glass winchesters with hard-plastic screw-on caps and sealed in wax. An extensive sampling programme by the author, planned for Cruise 56 (1973), was not carried out as the vessel was withdrawn from active service. Tritium samples (4) were only collected at Eltanin Station 47-1308. Additional hydrographic data from three other Eltanin stations have, however, been included to extend coverage of this region. The station locations are listed in Table V.1. All hydrographic data are given in Jacobs et al (1974); additional measurements on Cruise 47 were performed by Edmond and have been obtained through his courtesy. These data will be shown in graphical form only and will not be tabulated. Unlike the Pacific Ocean results discussed in Chapter IV, those reported in this Chapter do not belong to a uniform hydrological regime. This is illustrated in the widely varying profiles of the hydrographic parameters. Cruise 47 Stations 1284, 1308 and 1314 are located in the Indian sector of the Antarctic Ocean, and Station 1270 in the subtropical zone of the Indian Ocean. This distinction is immediately evident from the water mass structure in Figures V.3, V.4 and V.5 showing the depth distributions of temperature, salinity and dissolved oxygen concentration, respectively. Unless otherwise stated, the station key given in Figure V.3 will be used throughout this Chapter. Station 1270 is situated very near the Subtropical Convergence. Thus the surface waters are warm, highly saline and have large dissolved oxygen concentrations. The salinity and oxygen profiles reflect the extreme uniformity of the upper 600 metres; the salinity within $0.15^{o}/_{oo}$ of the surface

CRUISE	STATION	LATITUDE	LONGITUDE
47	1270	$40^{o}34.9'S$	$90^{o}56.3'E$
47	1284	$64^{o}03.9'S$	$80^{o}34.4'E$
47	1308	$54^{o}56.0'S$	$82^{o}38.7'E$
47	1314	$54^{o}26.2'S$	$69^{o}43.8'E$

TABLE V.1

Antarctic Sampling Station Locations.

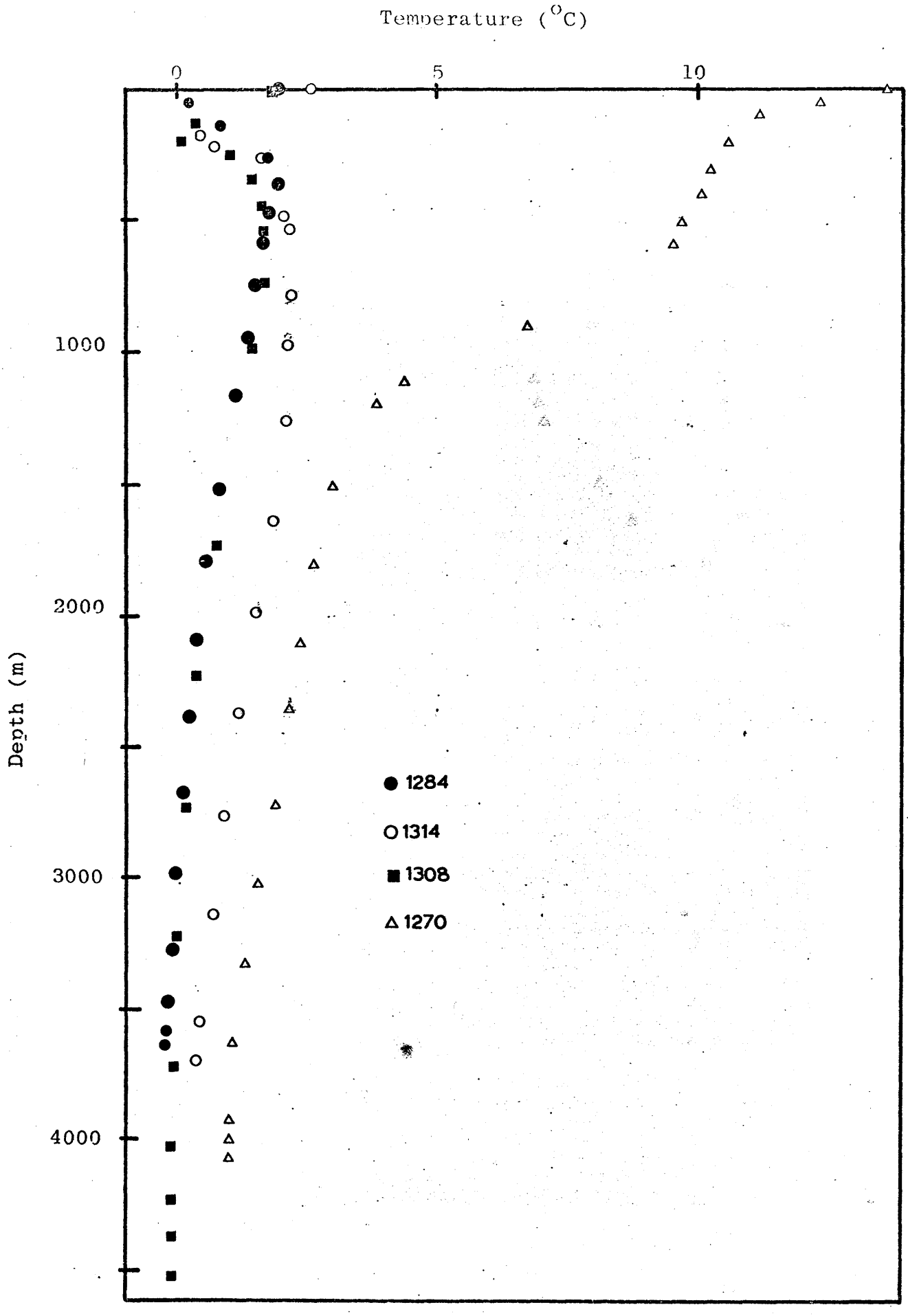

Figure V.3 Temperature versus depth at cruise 47 stations.

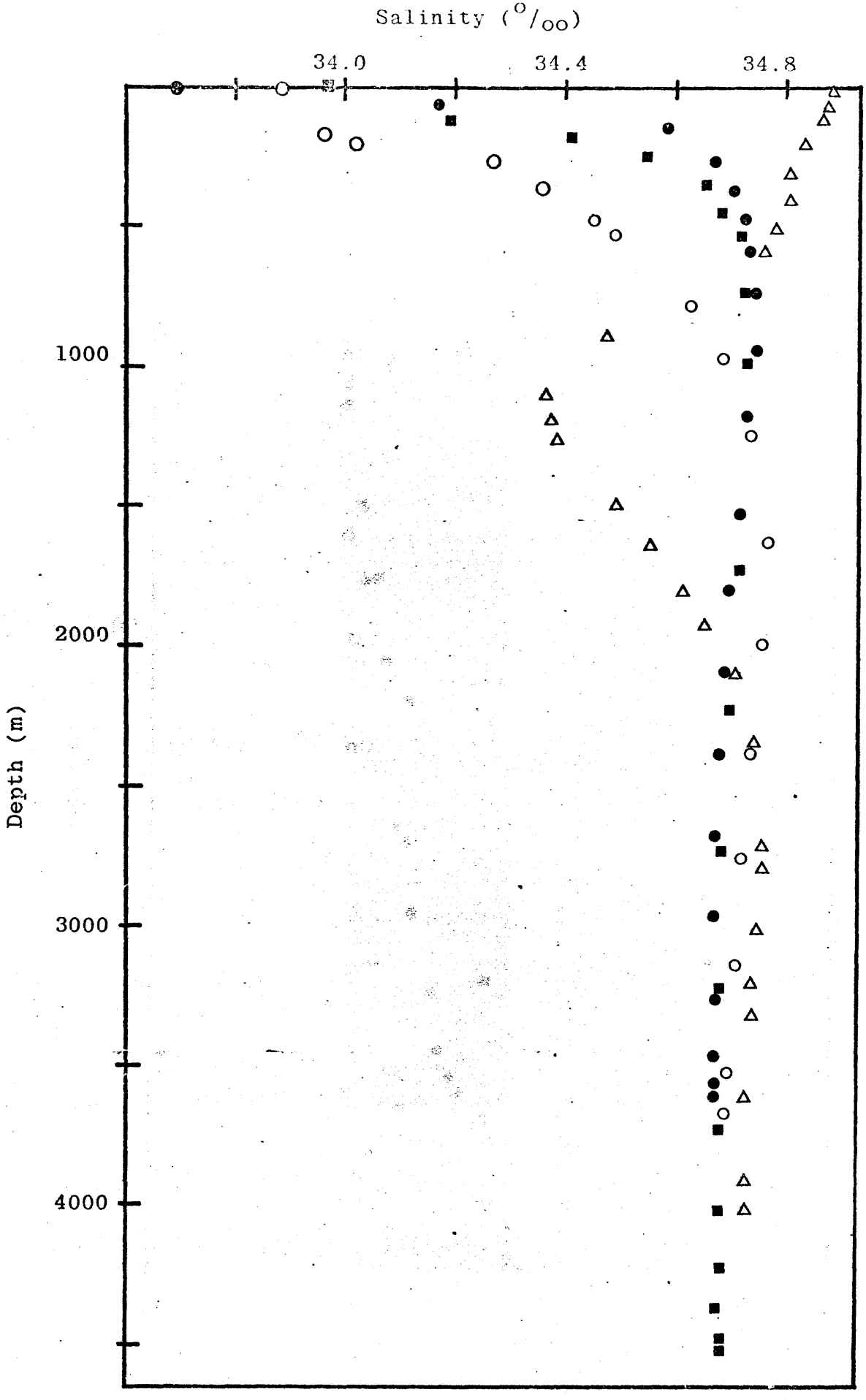

Figure V.4 Salinity distribution at Cruise 47 stations.

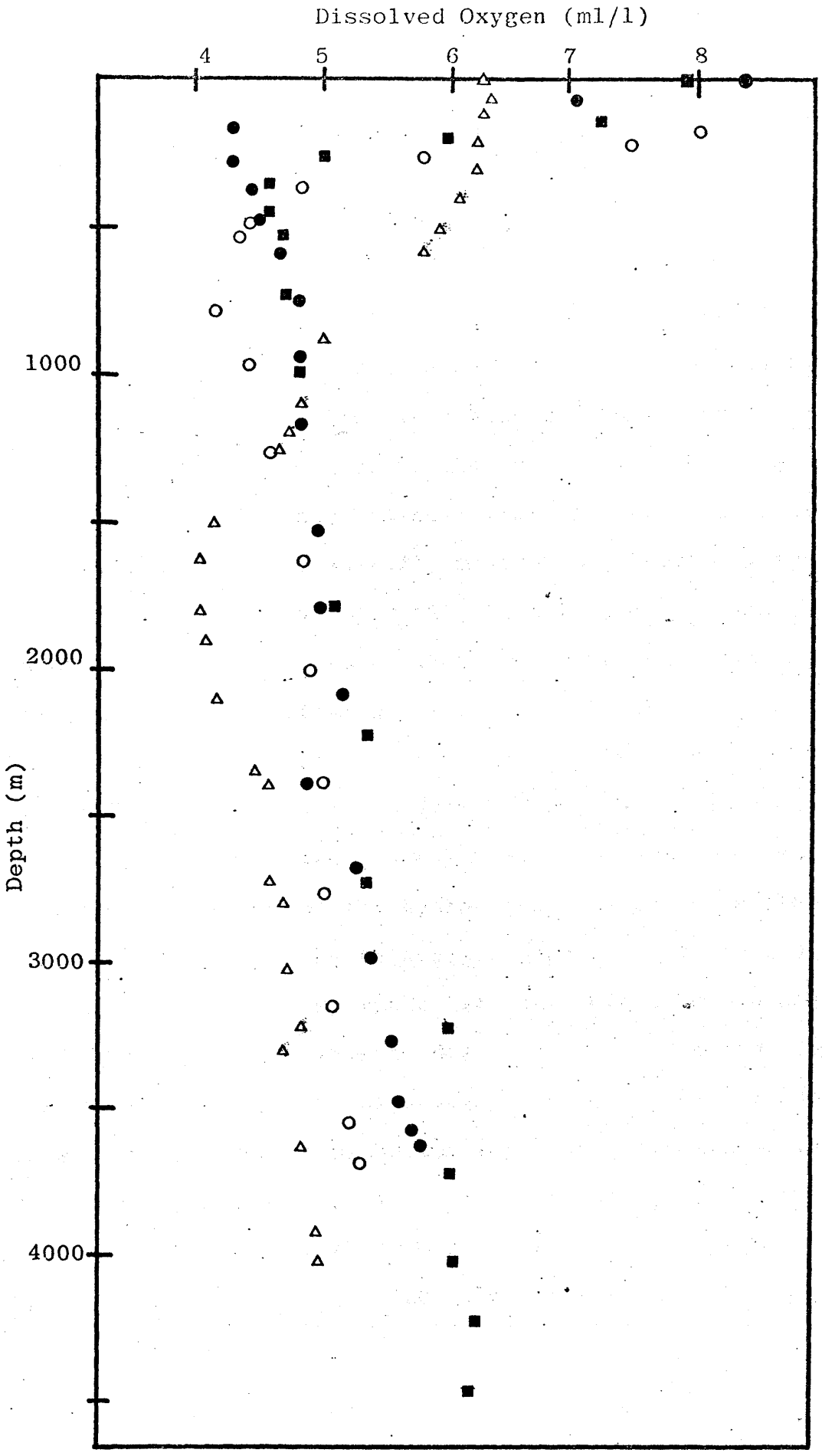

Figure V.5 Dissolved oxygen distribution at Cruise 47 Stations

value and the dissolved oxygen concentrations within 0.20 ml/l. This is caused by sinking surface waters in the Convergence zone as the northward flowing subantarctic and southward flowing subtropical waters meet. Below this layer lies a pronounced salinity minimum of $34.36^{o}/_{oo}$ at the core depth ~ 1100 metres. Oxygen concentrations are high (4.14 - 4.60 ml/l) but the water is much colder ($3^{o}C < T < 7^{o}C$) than that at shallower depths. Clearly, this is AAIW formed at the Polar Front being advected northwards. Below the Intermediate Water lies warm, highly saline Indian Deep Water with its core indicated by the salinity maximum of $\sim 34.76^{o}/_{oo}$ about 2750 metres. The characteristic dissolved oxygen minimum is observed in this mass at 1600 - 1700 metres depth. This water mixes with similar water from the North Atlantic and Pacific to become incorporated into the ACC. Stations 1284, 1308 and 1314 are separated from 1270 by the Polar Front zone and the Mid-Indian Ridge system. While 1270 illustrates subtropical aspects of the hydrography, these three stations are more typical of the Antarctic proper. Stations 1308 and 1314, being of comparable latitude, might be expected to display similar parameter distributions. The profiles show this not to be the situation. Fallick (1975) reasoned this to be the result of bottom topography variations in the area. Station 1314 lies just off, and to the west of, the Kerguelen Plateau whereas 1308 is situated over a local topographic depression to the east of the Plateau. The greater depth at this Station is supported by the profiles. Station 1284, further south by $\sim 10^{o}$ latitude and intermediate in longitude, is much closer to Antarctica and shallower than 1308 and 1314 since it overlies the gentle rise con-

necting the Kerguelen Plateau to the continent. Antarctic Surface Water at ~2-3°C moves northwards from the Divergence. A well-developed subsurface temperature minimum, above 200 metres, forms since the stations are south of the Polar Front where the minimum layer rapidly descends, contributing to AAIW formation. The Deep Water being brought near to the surface south of the Antarctic Divergence at 65°S, is clearly demonstrated by the depths at which the characteristic oxygen minimum, temperature and salinity maxima layers are found. Table V.2 gives estimates of the appropriate depths of each feature but these are somewhat inaccurate and intended for illustration purposes only. The observed trends, moving southwards, are a shallowing of the oxygen minimum, temperature and salinity maxima layers. The θ-S plot for the entire water column is given in Figure V.6 and identity of deep water at 1270 with much shallower water further south is apparent. Several interesting points emerge from subsurface samples shown in Figure V.7 and the deep and bottom water plot of Figure V.8. Although the salinity profile (Figure V.4) and the temperature profile (Figure V.3) show deep 1314 samples slightly more saline and warmer than those of 1284 and 1308, the θ-S diagrams show that the deepest water at 1270, the deep water at 1314 and the deep water above ~2800 metres (i.e. $\theta > 0^{\circ}C$) at 1284 and 1308 have a common origin (viz Circumpolar Deep Water). Figure V.8 indicates that at 1284 and 1308 there is an underlying bottom water of nearly constant salinity (34.67-34.68 $^{o}/_{oo}$ and potential temperature range - 0.5 to 0.0°C. The rapid increase in oxygen concentrations in these layers observed in Figure V.5 represent AABW, with the oxygen content reflecting the

Station	1270	1314	1308	1284
Latitude	40°34.9'S	54°26.2'S	54°56.0'S	64°03.9'S
Temperature maximum (metres)	-	650	500	350
Salinity maximum (metres)	2750	1650	1050	800
Oxygen minimum (metres)	1600	650	400	200

TABLE V.2

Depths of Prominent Hydrographic Features at Cruise 47 Stations.

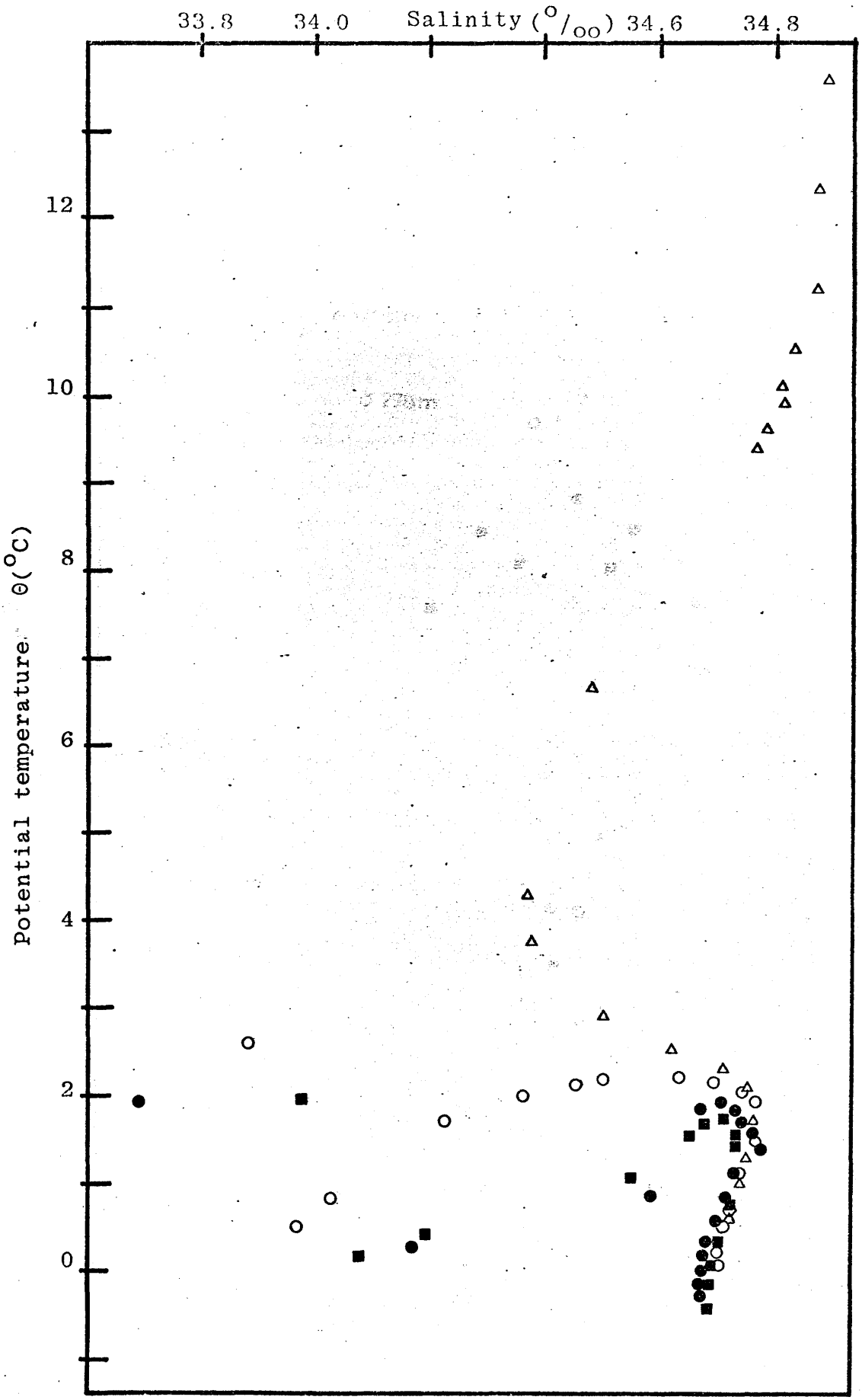

Figure V.6 Θ-S plot for complete water column.

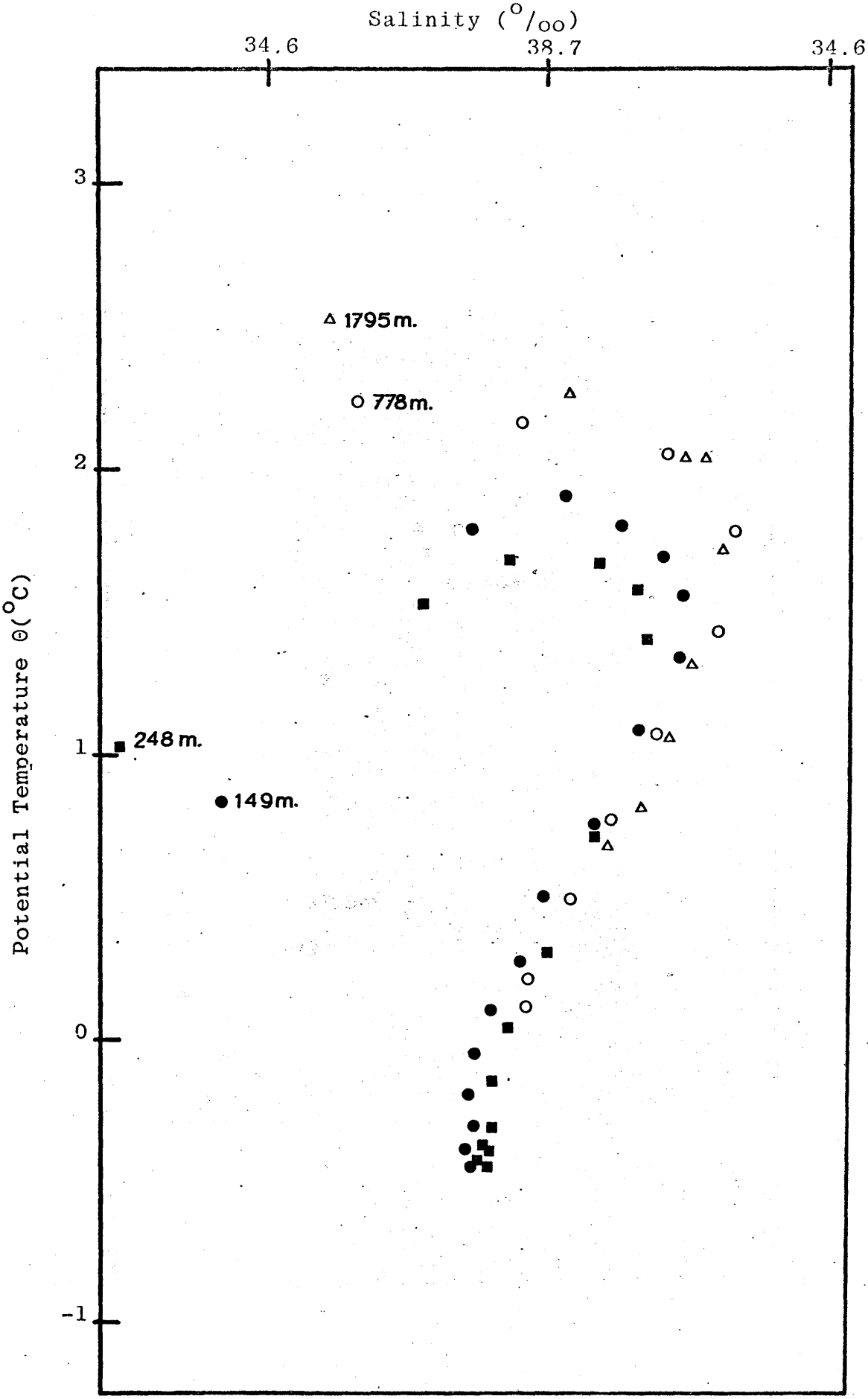

Figure V.7 Subsurface θ-S plot of Cruise 47 stations.

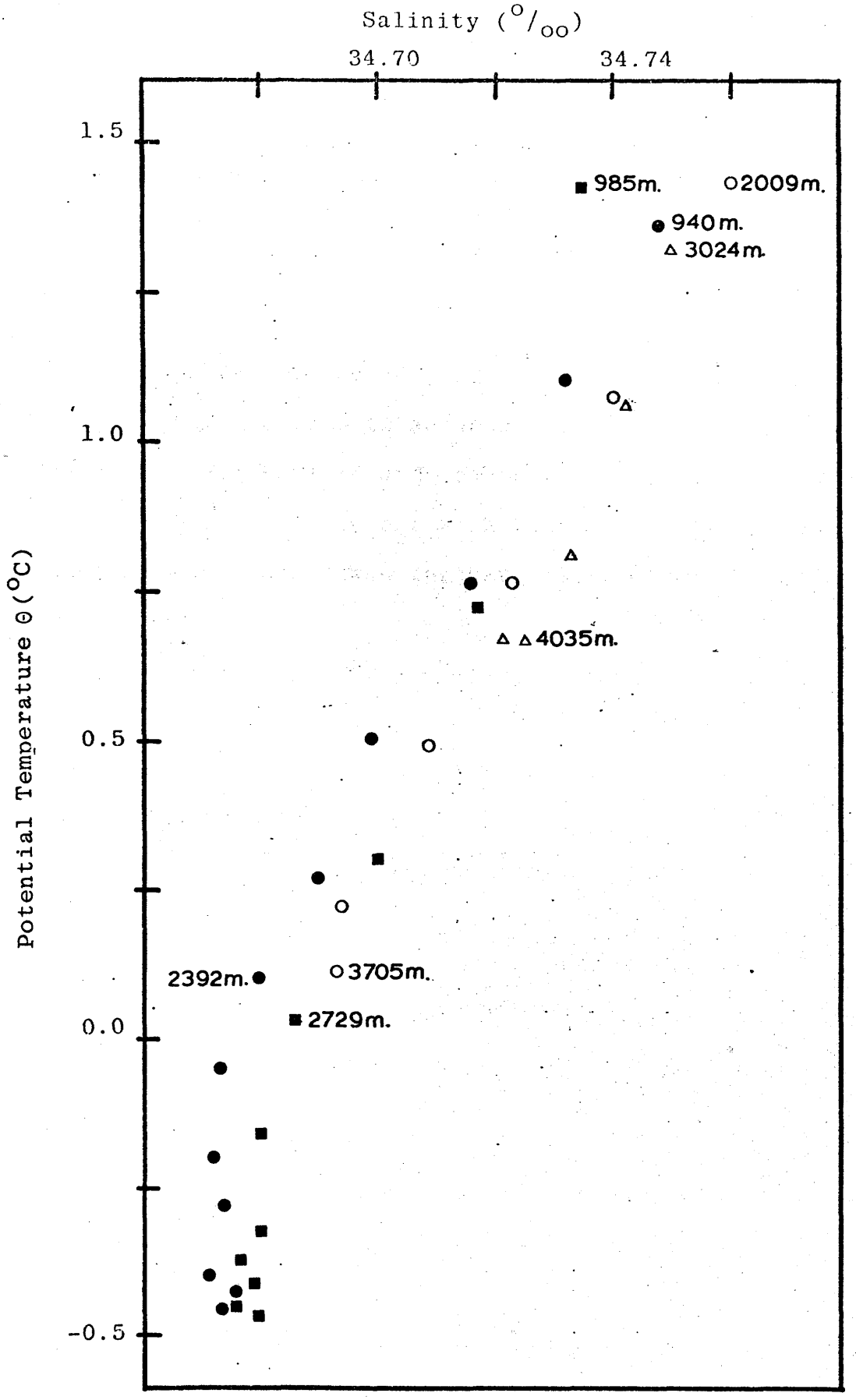

Figure V.8 Θ-S for Deep and Bottom Waters.

recent atmospheric contact of the shelf component. The absence of AABW at 1314 has been attributed to topographic effects associated with the Kerguelan Plateau; its appearance at 1308 indicates the arrival of AABW either from the south or the east (Fallick, 1975). The ranges of values of hydrographic parameters describing these various water masses are in good accord with accepted literature values (e.g. Gordon, 1971; Hufford and Seabrooke, 1970) and the basic structure is in agreement with that deduced from more complete sections taken further east (Gordon, 1972).

V.4 Tritium features.

Tritium measurements in the Southern Ocean have been regrettably few in number. There was a significant rise in tritium concentrations in rain waters (following the testing of fusion bombs (Taylor, 1966), but no pre-bomb tritium analyses were performed on sea water from this region. The few post-bomb surface seawater measurements indicate tritium concentrations in the order of 0.5 - 1.5 T.U. (Dockins et al, 1967). Several other profiles taken in the Southern Ocean gave similar results (Michel, 1974, Michel and Suess, 1975; Tamuly, 1974). It should be noted that increases in tritium concentrations following nuclear testing were much less pronounced in the southern hemisphere than in the northern hemisphere. As previously discussed, this region can be expected to show overturn of surface waters and mixing of tritium to great depths. High latitudes often shown penetration of bomb-produced radionuclides deeper into the ocean than at lower latitudes because of the extreme winter cooling (Munnich and Roether, 1967; Volchok et al, 1971).

Unfortunately, in this study only four samples were analysed from the Antarctic region but these do represent all the tritium samples collected at 1308. It is fortuitous that these samples were taken at surface, intermediate and bottom depths. The tritium data are presented in Table V.3 with other hydrographic data. The 2 metre sample is clearly ASW with the high tritium value reflecting its contact with the atmosphere. Highest tritium values are in the mixed

Depth (metres)	Tritium Units (T.U.± 2σ)	Temperature (°C)	Salinity (°/oo)	θ (°C)	Dissolved Oxygen (ml/l)	σ_t
2	1.86 ± 0.32	1.93	33.979	1.93	7.89	27.182
2729	B.L.D.	0.20	34.686	0.04	5.36	27.863
4479	0.35 ± 0.17	-0.13	34.679	-0.45	6.22	27.874
4529	0.38 ± 0.21	-0.13	34.680	-0.45	6.28	27.875

B.L.D. - Below Limit of Detection

Tritium Measurement of 1308 Samples.

TABLE V.3

layer and are in excess of 1 T.U. This is well demonstrated by the inclusion of our data with that of Tamuly (1974), Michel (1974) and Michel and Suess (1975) as presented in Figure V.9 showing surface seawater tritium concentrations. The tritium content of the 2729 metre sample is below the limit of detection. This observation therefore is indictive of water of long residence time (i.e. time since atmospheric contact) and is therefore CDW produced by the mixing of North Atlantic, Indian and Pacific Deep Waters (all of which have residence times far in excess of 100 years). Thus this sample is composed primarily of deep water with long residence times compared to the half-life of tritium, and little or no residual tritium is therefore observed. The lower oxygen concentration and high salinity value support the conclusion that this sample is CDW, as does its position in Figure IV.8. Depth-tritium profiles taken from Tamuly (1974) and shown in Figure V.10 corroborate the existence of an intermediate depth interval containing little or no tritium associated with the CDW. Lying below the CDW are the two deepest samples (4479 and 4529 metres, respectively). These exhibit the homogeneous properties consistent with AABW (Figure IV.8). That these samples contain tritium is hardly surprising and suggests that recently formed AABW (i.e. since the introduction of nuclear detonations) has reached this region of Antarctica. The tritium data therefore suggest that within the Southern Ocean there exists a mixed surface layer containing high tritium concentrations followed by an intermediate depth interval containing little or no tritium. That tritium is found only in the deepest layer (i.e. AABW) indicates

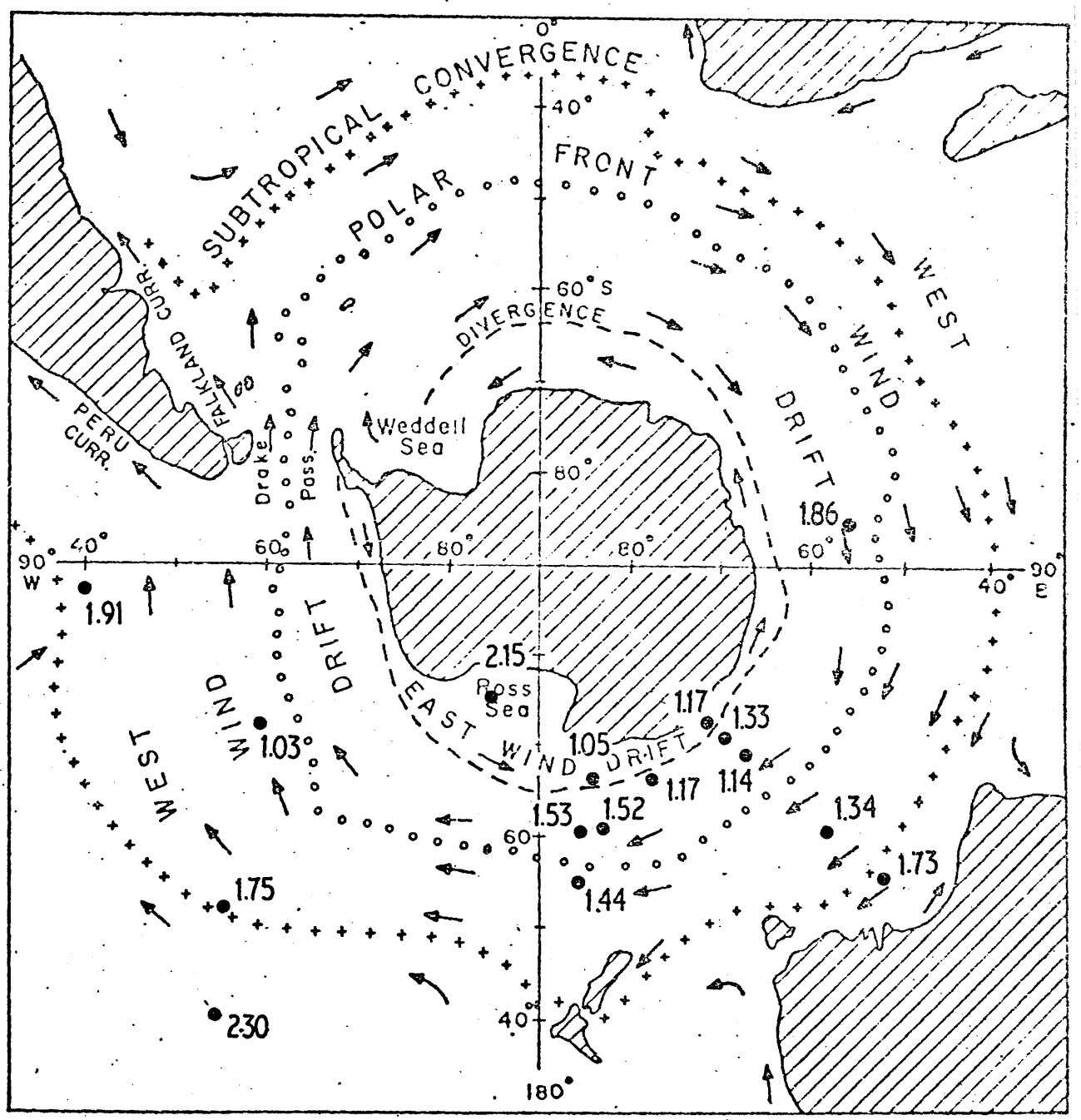

Figure V.9 Surface tritium concentrations in T.U.

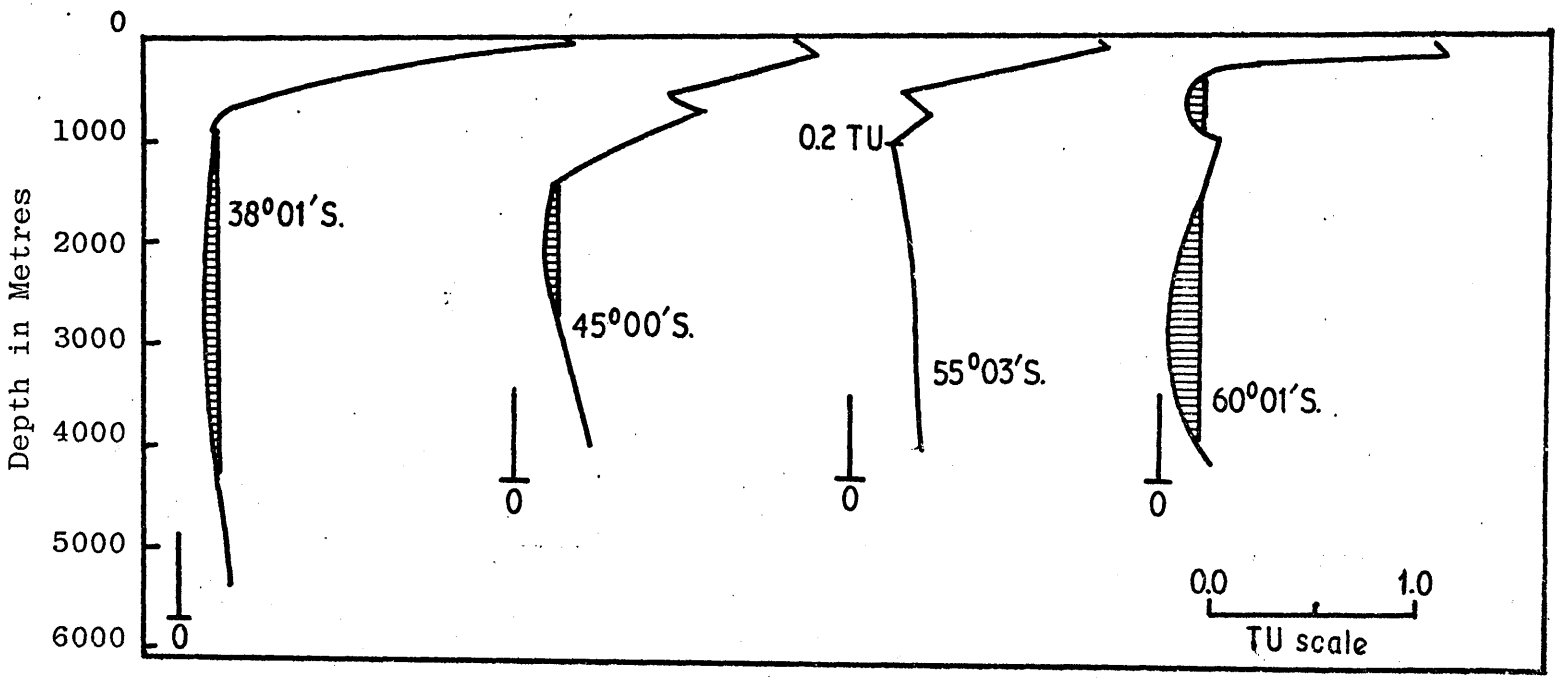

Figure V.10 Depth-tritium profiles at four Southern Latitudes (after Tamuly, 1974).

that ASW must mix with deeper water and by cabbeling, produce AABW. These conclusion fit the observed tritium data and are further supported by Tamuly (1974), Michel (1974) and Michel and Suess (1975).

Thus the tritium results obtained in this study, though few in number, indicate major features of Antarctic oceanography and are confirmative of previously existing theories of water structure.

APPENDIX 1.

```
C THIS PROGRAM CALCULATES SIGMA-T (THE CONVENTIONAL DENSITY), THE THERMOSTERIC
C ANOMALY, VT (THE CONVENTIONAL SPECIFIC VOLUME), AND THE "SURFACE" ANOMALY
C OF SPECIFIC VOLUME (ALPHA(S,T,O)) USING THE METHOD OF WANG AND MILLERO
C (JGR, 1973) AND THE APPROPRIATE SALINITY AND TEMPERATURE DATA.  SAMPLE NAME
C DEPTH AND TRITIUM CONCENTRATION CAN ALSO BE ENTERED.
      IMPLICIT REAL*8 (A-H,O-Z)
      INTEGER DEPTH
      DIMENSION NAME(3)
      WRITE(6,10)
   10 FORMAT(4X,'SAMPLE',5X,'DEPTH',2X,'SALINITY',2X,'TEMP(C)',2X,'SIGMA
     1-T',6X,'THERMOSTERIC ANOMALY',6X,' SPECIFIC VOLUME (VT)', 2X
     2'ALPHA(S,T,O)','TRITIUM UNITS')
      1 READ(5,20)(NAME(J),J=1,3), SALT, TEMP, DEPTH, TU
   20 FORMAT(3A4, F8.0, F10.0, I10, F10.0)
      IF(SALT.LE.0.0) GO TO 60
      S=SALT
      T=TEMP
      C=1.8030D-5*T-8.164D-7*T*T+1.667D-8*T*T*T
      B=1.0-4.7867D-3*T+9.8185D-5*T*T-1.0843D-6*T*T*T
      A=(4.5316842620*T-0.5459391107*T*T-1.9824839871D-3*T*T*T
     1  -1.438030609D-7*T*T*T*T*T)*(1/(T+67.26))
      SO=-0.09344586324+0.814876576925*S-4.8249614030-4*S*S
     1  +6.767861356D-6*S*S*S
C CALCULATES SIGMA-T THE CONVENTIONAL DENSITY
      ST= A+B*SO +C*SO*SO
C CALCULATES DELTA(ST)  THE THERMOSTERIC ANOMALY (MAMAYEV,1975) WHICH
C IS ALSO KNOWN AS THE "SURFACE" ANOMALY OF SPECIFIC VOLUME.
      DST=0.02736-((ST*1.0D-3/(1+ST*1.0D-3))
C CALCULATES A(STO) THE SPECIFIC VOLUME AS A FUNCTION OF TEMP. AND SALT.
      ASTO=0.9726+DST
C CALCULATES VT THE CONVENTIONAL SPECIFIC VOLUME
      VT=1D6/(ST+1D3)-0.9D3
      WRITE(6,40)(NAME(J),J=1,3), DEPTH, S, T, ST, DST, VT, ASTO
   40 FORMAT(1X,3A4,3X,I4,3X,F6.3,4X,F5.2,4X,F6.3,9X,F12.8,17X,F10.6,6X,
     1F12.10)
      GO TO 1
   60 STOP
      END.
```

```
C THIS PROGRAM CALCULATES THE CONCENTRATION OF TRITIUM (IN TU'S) FOR ANY
C SAMPLE GIVEN THE COUNTS, TIME, BLANK VALUES, THE TRITUM ENRICHMENT
C FACTORS AND OTHER RELEVANT DESCRIPTIVE INFORMATION.  CORRECTION FOR
C RADIOACTIVE  DECAY AND ASSOCIATED TWO SIGMA ERRORS ARE CALCULATED.
C ALL VALUES ARE CALCULATED WITH A TWO-SIGMA ERROR BAR.
C COUNTER FILLING TEMPERATURE CORRECTION ADJUSTED TO 18 DEGREES C.
C A SECOND COUNT RATE IS NOT REQUIRED.

      DIMENSION NAME(100,3), CR2(100),T1(100), T2(100), CR1(100),
     1  SCR1(100, SCR2(100), ACT1(100), ACT2(100),
     2  ACTAVE(100), BLNK(100), TE1(100), TIME(100), DEPTH(100),
     3  A1(100), A2(100),STE1(100)
      DIMENSION ERR1(100), ERR2(100), FT(100)
      REAL LAMDA
      INTEGER TIME, DEPTH, T1, T2, CR1, CR2
      READ (5,10) N
   10 FORMAT (12)
      READ(5,20) ((NAME(I,J),J=1,3), CR1(I), T1(I), CR2(I), T2(I),
     1  TE1(I), BLNK(I), TIME(I), DEPTH(I), STE1(I),FT(I),I=1,N)
   20 FORMAT(3A4, 2I5, I6, I5, F5.1, F6.0, 2I5, 2F5.2)
      LAMDA=(0.693)/(12.262*365)
      SBBOC=0.150
      SBEOC=0.150
C SET UP LABELLED COLUMNS
      WRITE(6,30)
   30 FORMAT(/,5X),'SAMPLE',3X,'DEPTH',3X,'TU1',3X,'TU2',3X,
     1 'TU AVE',3X,'CPM 1',3X,'CPM2')
      DO 40 I=1,N
      Y=CR1(I)
      T=T1(I)
      SCR1(I)=Y/T
      Z=SQRT(Y)
      A1(I)=(Z/T)*2.0
C COUNTER FILLING TEMPERATURE CORRECTION ADJUSTED TO 18 DEGREES C.
      IF(FT(I).LE.0.0) FT(I)=18.0
      FT(I)=FT(I)
      TEMP=273.0+FT(I)
      CORFAC=TEMP/291.0
      CSCR1=CORFAC*SCR1(I)
      SA1=CSCR1*SQRT((A1(I)/SCR1(I))**2.0)
      B1=CSCR1-BLNK(I)
      SAB=SQRT((SA1*SA1)+(SBBOC*SBBOC))
C CORRECTS FOR TRITIUM ENRICHMENT FACTOR
      C1=B1/TE1(I)
      SABC=C1 *SQRT(((SAB/B/**2)+((STE1(I)/TE1(I)**2))
C CORRECTION FACTOR FOR RADIOACTIVE DECAY AND CONVERSION TO TRITIUM UNITS
      X=EXP(-LAMDA*TIME(I))*0.026
      D1=C1/X
C CALCULATES ERROR OF SAMPLE ACTIVITY IN TU'S
      ERR1(I)=SABC/X
C CONVERTS SAMPLE ACTIVITY TO FULLY CORRECTED TU ACTIVITY
      ACT1(I)=C1/X
      IF(CR2(I).LE.0.0) GO TO 40
      Y=CR2(I)
      T=T2(I)
      SCR2(I)=Y/T
      Z=SQRT(Y)
      A2(I)=(Z/T)*2.0
C COUNTER FILLING TEMPERATURE CORRECTION ADJUSTED TO 18 DEGREES C.
      CSCR2=CORFAC*SCR2(I)
      B2=CSCR2-BLNK(I)
      SAB2=SQRT((SA2*SA2)+(SBBOC*SBBOC))
```

```
C CORRECTS FOR TRITIUM ENRICHMENT FACTOR
      C2=B2/TE1(I)
      SABC2=C2*SQRT(((SAB/B2)**2)+((STE1(I)/TE1(I))**2.0))
C CORRECTION FACTOR FOR RADIOACTIVE DECAY AND CONVERSION TO TRITIUM UNIT
      D2=C2/X
C CALCULATES ERROR OF SAMPLE ACTIVITY IN TU'S
      ERR2(I)=SABC2/X
C CONVERTS SAMPLE ACTIVITY TO FULLY CORRECTED TU ACTIVITY
      ACT2(I)=C2/X
      AVESCR=(CSCR1+CSCR2)/(2.0)
      AVCPM=(AVESCR-BLNK(I))/(TE1)
      ACTAVE(I)=AVCPM/X
   40 CONTINUE
      WRITE(6,50)((NAME(I,J),J=1,3), DEPTH(I), ACT1(I), ACT2(I),
     1 ACTAVE(I), SCR1(I), SCR2(I), ERR1(I), ERR2(I), A1(I),
     2 A2(I), I=1,N)
   50 FORMAT(/,2X,3A4,I5,2F8.2,F10.3,2F8.3,/,19X,2F8.2,10X,2F8.3)
      STOP
      END
```

APPENDIX 3.

```
C THIS PROGRAM IS A LINEAR LEAST SQUARES REGRESSION FIT WITH A
C CONFIDENCE INTERVAL ESTIMATE FOR THE LINE AS A WHOLE USING THE METHODS
C AS DESCRIBED IN THE NBS SPECIAL PUB-300 V1 "PRECISION MEASUREMENT AND
C CALIBRATION".  THE CONFIDENCE INTERVAL ESTIMATE (+OR- W) IS NORMALLY
C TAKEN TO BE 95% AND IS DETERMINED BY THE F VALUE SUPPLIED WITH EACH
C DATA SET, WHICH ITSELF IS DETERMINED BY THE NUMBER OF (X,Y) DATA
C POINTS (N), WHERE F(2,N-2) IS THE VALUE SELECTED FROM THE F TABLE.
C
C THE INITIAL PROGRAM READS THE NUMBER OF DATA PAIRS (X,Y) CONTAINED IN
C EACH DATA SET AS N AND THEN ALLOWS THE DIMENSION OF THE XY ARRAY TO BE
C AUTOMATICALLY SET AND CARRIED THROUGH TO EACH SUBROUTINE.  THE THREE
C SUBROUTINES ARE CALLED MAIN, WHICH PERFORMS THE LINEAR REGRESSION CAL-
C CULATIONS WHILE THE REMAINING TWO SUBROUTINES ARE RESERVED FOR PLOTTING
C AND ARE DESCRIBED IN THE PROCEEDING PARAGRAPH.
C
C TWO SUBROUTINES ARE AVAILABLE FOR PLOTTING PURPOSES WITH VARIABLE
C OPTION.  THE FIRST IS A LINEAR PLOT OF THE REGRESSION CURVE AND IS
C SELECTED WHENEVER IPLOTS IS GREATER THAN ZERO (SUBROUTINE PLOTER).
C THE SECOND IS A VARIABLE LOG-LOG OR LOG-LINEAR PROGRAM (SUBROUTINE
C LGPLOT). THIS SUBROUTINE WILL BE SELECTED WHENEVER LPLOTS IS LESS
C THAN ZERO WITH THE FOLLOWING OPTION--
C    A) IF LPLOTS EQUALS -1, AXES WILL BOTH BE LOGARITHMIC
C    B) IF LPLOTS EQUALS -2, Y-AXIS LOGARITHMIC, X-AXIS LINEAR
C    C) IF LPLOTS EQUALS -3, Y-AXIS LINEAR, X-AXIS LOGARITHMIC
C
C DIRECTIONS FOR ADJUSTING THE SIZE OF EACH PLOTTING FIELD ARE DESCRIBED
C WITHIN EACH PLOTTING SUBROUTINE.
C
C THE SUBROUTINES IF SELECTED FOR A GIVEN SET OF DATA WILL--
C    A) PLOT THE DATA POINTS FOR THIS SET,
C    B) PLOT THE COMPUTED BEST STRAIGHT  LINE, AND
C    C) PLOT THE CONFIDENCE INTERVAL ESTIMATE FOR THE LINE AS A WHOLE
C THE PRINT-OUTS WILLBE IN COLUMNS (USING THE APPROPRIATE VALUES OF THE
C DATA AS DETERMINED BY SELECTION OF THE VARIOUS SUBROUTINE OPTIONS).
C THUS COLUMNS WILL BE, 'X OBSERVED (OR LOG X)', 'Y OBSERVED (OR LOG Y)'
C 'Y CALCULATED', 'THE DEVIATION', 'THE ERROR ON THE LINE (W)', AND THE
C 'DATE OF THE DATA', IF ENTERED IN COLUMNS 73-80 AS IDENFICATION.
C
```

```
C IF SKIPMN IS GREATER THAN ZERO, MAIN SUBPROGRAM IS SKIPPED AND ONLY THE
C PLOTTING SUBROUTINE IS CALLED.  POINTS ARE PLOTTED WHILE NO LINE NOR
C ERROR BARS ARE DRAWN
C
C ---DECK SET UP---
C
C FOLLOWING THE PROGRAM DECK, THE DATA DECK IS SET UP AS FOLLOWS--
C    A) CARD 1 CONTAINS N, THE NUMBER OF X-Y DATA PAIRS (I3 FORMAT).
C    B) CARD 2 CONTAINS THE F VALUE (F19.0 FORMAT), IPLOTS (COLUMN 20,
C       I1 FORMAT), LPLOTS (COLUMN 29-30, I2 FORMAT), AND SKIPMN (COLUMN
C       40, I1 FORMAT).
C    C) CARD 3 CONTAINS YT, THE TITLE OF THE Y-AXIS, CONTAINING UP TO 20
C       ALPHA-NUMBERIC CHARACTERS WITHIN THE FIRST 20 COLUMNS; XT, THE
C       TITLE OF THE X-AXIS, CONTAINING UP TO 20 ALPHA-NUMERIC CHARACTERS
C       WITHIN THE SECOND 20 COLUMNS (21-40); AND HT, THE HEADING FOR
C       THE GRAPH CONTAINING UP TO 20 ALPHA NUMERIC CHARACTERS IN THE
C       THRID 20 COLUMNS (41-60).
C    D) CARD 4 TO N EACH CONTAINS AN X-Y DATA PAIR IN 2F10.0 FORMAT.
C    E) IF ANOTHER SET OF DATA IS TO FOLLOW, REPEAT DATA DECK SEQUENCE,
C       STEPS A TO D.
C    F) PLACE BLANK CARD AT END OF DATA DECK TO TERMINATE PROGRAM.
C
C THIS PROGRAM ESTABLISHES THE DIMENSION FOR THE ARRAY XY(N,2) WHICH IS
C THEN CARRIED THROUGH TO THE MAIN CALCULATION SUBPROGRAM AND TO EACH
C PLOTTING SUBPROGRAM.
C
      IMPLICIT READ*8 (S)
      INTEGER SKIPMN
      DIMENSION XY(200)
      DIMENSION XY(200), Y(200)
      DIMENSION YT(5), XT(5), HT(5)
      COMMON /PLT PGM/ X,Y,B0,B1,SXX,SSY,AVE X,F,   YT,XT,HT,SKIPMN,
     1 LPLOTS, IPLOTS, INDEX
      INDEX=0
    8 READ(5,10) N
   10 FORMAT(I3)
      IF(N.EQ.0) GO TO 15
      CALL MAIN1(XY,N)
      GO TO 8
   15 IF(INDEX.EQ.1) CALL MOVE (0.0,0.0,0,0)
      STOP
      END

      SUBROUTINE MAIN1(XY,N)
      IMPLICIT REAL*8 (S)
      INTEGER P, SKIPMN
      DIMENSION XY(N,2)
      DIMENSION YT(5), XT(5), HT(5)
      DIMENSION X(200), Y(200), YC(200), DEV(200),IDENT(200)
      COMMON /PLT PGM/ X,Y,BO,B1,SXX,SSY,AVE X,F, YT,XT,HT,SKIPMN,
     1LPLOTS, IPLOTS, INDEX
      READ(5,5) F, IPLOTS, SKIPMN
C ENTER IPLOTS IN COLUMN 20, ENTER LPLOTS IN COLUMN 29-30, ENTER SKIPMN
C IN COLUMN 40
    5 FORMAT(F19.0, I1, 8X,I2,9X,I1)
      READ(5,11) YT,XT, HT,((XY(I,J),J=1,2),I=1,N)
   11 FORMAT(15A4/(2F10.0))
      IF(SKIPMN.GT.0) GO  TO 65
```

```
      SX=0
      SY=0
      SXY=0
      SXSY=0
      SX2=0
      SY2=0
      DO 20 I=1,N
C CONVERTS ARRAY XY TO X-ARRAY AND Y-ARRAY
      X(I)=XY(I,1)
      Y(I)=XY(I,2)
      XI=X(I)
      YI=Y(I)
C CONVERTS DATA TO APPROPRIATE LOG OR LINEAR SCALE DETERMINED BY LPLOTS
      IF(IPLOTS.EQ.1) GO TO 19
      IF(LPOLOTS.EG.0) GO TO 19
      IF(LPLOTS + 2) 16,18,17
   16 X(I)=ALOG10(XI)
      XI=X(I)
      GO TO 19
   17 X(I)=ALOG10(XI)
      XI= X(I)
   18 Y(I)=ALOG10(YI)
      YI=Y(I)
   19 SX=SX+XI
      SY=SY+YI
      SXY=SXY+XI*YI
      SX2=SX2+XI*XI
      SY2=SY2+YI*YI
   20 CONTINUE
      AVE X=SX/N
      AVE Y=SY/N
      SXSY=SX*SY
      SSXY=SXY-SXSY/N
      SSX2=(SX*SX)/N
      SXX=SX2-SSX2
      SSY2=(SY*SY)/N
      SYY=SY2-SSY2
      B1=SSXY/SXX
      B0=AVE Y-B1*AVE X
      SXY2SX=(SSXY*SSXY)/SXX
      S2Y=(SYY-SXY2SX)/(N-2)
      IF(S2Y.LT.0)  WRITE(6,37)
   37 FORMAT(' CAUTION--NEGATIVE SQRT(S2Y)')
      IF(S2Y.LT.0.0) S2Y=DABS(S2Y)
      SQ=(S2Y-SY*B0-SXY*B1)/(N-2)
      IF(SQ.LT.0)  WRITE(6,38)
   38 FORMAT('CAUTION--SQRT(SQ) IS NEGATIVE')
      IF(SQ.LT.0.0) SQ=DABS(SQ)
      RMS ERR=DSQRT(SQ)
C ESTIMATED VARIANCE OF THE SLOPE
      S2B1=S2Y/SXX
C ESTIMATED VARIANCE OF THE INTERCEPT
      AN=N
      S2B0=S2Y*((1/AN+(AVE X*AVE X))/(SXX))
      XZ=0.0
      VX=0.0
      VY=0.0
      DO 30 I=1,N
      XI=X(I)
      YI=Y(I)
      VX=VX+(XI-AVE X)*(XI-AVE X)
```

```
      VY=VY+(YI-AVE Y)*(YI-AVE Y)
   30 CONTINUE
C CALCULATION OF THE CORRELATION COEFFICIENT
      CC=(XY)/(SQRT(VX*VY))
      DO 40 I=1,N
      XI=X(I)
      YC(I)=AVE Y+B1*(XI-AVE X)
      DEV(I)=Y(I)-YC(I)
   40 CONTINUE
      IF(LPLOTS.GE.0) GO TO 59
      IF(LPLOTS + 2) 45,43,41
C PRINT-OUT FOR LOG-LOG REGRESSION FIT
   41 WRITE(6,42)(X(I), Y(I), YC(I), DEV(I), W(I), I=1,N)
   42 FORMAT('1',9X,'LOG X',17X,'LOG Y',15X,'Y CALC',11X,'DEVIATION' 9X,
     1'ERROR ON LINE '//(' ',5E20.8))
      GO TO 49
C PRINT-OUT FOR LINEAR X, LOGARITHM Y
   43 WRITE(6,44)(X(I), Y(I), YC(I), DEV(I), W(I), I=1,N)
   44 FORMAT('1',9X,'X OBS',17X,'LOG Y',15X,'Y CALC',11X,'DEVIATION',9X,
     1'ERROR ON LINE'//(' ',5E20.8))
      GO TO 49
C PRINT-OUT FOR LOGARITHM X, LINEAR Y
   45 WRITE(6,46)(X(I),Y(I), YC(I), DEV(I), W(I), I=1,N)
   46 FORMAT('1',9X,'LOG x',17X,'Y OBS',15X,'Y CALC',11X,'DEVIATION',9X,
     1'ERROR ON LINE '//(' ',5E20.8))
      GO TO 49
C PRINT-OUT FOR LINEAR X, LINEAR Y
   59 WRITE(6,60)(X(I), Y(I), YC(I), DEC(I), W(I), IDENT(I), I=1,N)
   60 FORMAT('1',9X,'X OBS',17X,'Y OBS',15X,'Y CALC',11X,'DEVIATION',9X,
     1'ERROR ON LINE',9X,'DATE'//(' ',5E20.8,10X,I6))
   49 WRITE(6,50) B1, S2B1, B0, S2BO, RMS ERR
   50 FORMAT(///,'SLOPE=',E15.8,5X,' ESTIMATED VARIANCE OF THE SLOPE='.
     1E15.8 / ' INTERCEPT=',E15.8,5X,' ESTIMATED VARIANCE OF THE INTERCEP
     2T=',E15.8/' RMS ERROR=',E15.8)
      WRITE(6,55) SX2,SX,SXY,N,SY,SY2,AVE X,AVE Y,F
   55 FORMAT(///,'LEAST SQUARES TOTALS  X2 X XY N Y Y2'//.
     1'SUM X2 =',E15.8/' SUM X =',E15.8/' SUM XY =',E15.8/' N =',I4/
     2'SUM Y =',E15.8/' SUM Y2 =',E15.8//'AVE X=',E15.8/' AVE Y =',
     3E15.8//' F VALUE FOR 95% CONFIDENCE INTERVAL, F(2,N-2)=',F5.2)
      WRITE(6,56) CC
   56 FORMAT(./,' CORRELATION COEFFICIENT='F6.3)
   65 IF (LPLOTS.LT.0) INDEX=1
      IF(IPLOTS.GT.0) INDEX=1
      IF (IPLOTS.GT.0) CALL PLOTER (XY,N)
      IF(LPLOTS.LT.0) CALL LGPLOT(XY,N)
      RETURN
      END

      SUBROUTINE LGPLOT (XY,N)
C THIS IS A LOG-LOG LINEAR-LOG PLOTTING SUBROUTINE OF THE BEST FIT
C REGRESSION LINE WITH ASSOCIATED ERROR BARS FOR THE LINE AS A WHOLE.
      IMPLICIT REAL*8 (S)
      INTEGER SKIPMN
      COMMON /PLT PGM/ X,Y,BO,B1,SXX,SSY,AVE X,F, YT,XT,HT,SKIPMN,
     1 LPLOTS, IPLOTS, INDEX
      DIMENSION XY(N,2)
      DIMENSION YT(5), XT(5), HT(5), X(200), Y(200)
      LPLOTS=IABS(LPLOTS)
C XHT SETS LENGTH OF X-AXIS IN CENTIMETERS
      XHT=20.0
C YHT SETS LENGTH OF Y-AXIS IN CENTIMETERS
```

```
      YHT=20.0
      CALL MOVE(YHT,XHT,-1,200)
C CONTROL PARAMETER 'J' DETERMINES TYPE OF X-Y AXES
C FOR LOG-LOG AXES J=0
      IF(LPLOTS.EQ.1) J=0
C FOR LOG Y-AXIS AND LINEAR X-AXIS, J=1
      IF(LPLOTS.EQ.2) J=1
C FOR LOG X-AXIS AND LINEAR Y-AXIS, J=-1
      IF(LPLOTS.EQ.3) J=-1
      CALL LOGPLO(XY,N,1,-1,J,YT,XT,HT,3)
      IF(SKIPMN.GT.0) GO TO 150
C-----SCALES STARTING AND END POINTS FOR LEAST-SQUARES LINE
      IF(LPLOTS-2) 10,11,10
C SCALING FOR LOGARITHM X AXIS
   10 CALL LGSCL(X,Y,N,XHT,XMIN,DX)
      XMIN=ALOG10(XMIN)
      GO TO 12
C SCALING FOR LINEAR X AXIS
   11 CALL SCALE(XY,N,XHT,XMIN,DX)
   12 XMAX=XMIN+(XHT*DX)
      XP=XMIN
      IF(LPLOTS - 2) 13,13,14
C SCALING FOR LOGARITHM Y AXIS
   13 CALL LGSCL(XY(1,2),N,YHT,YMIN,DY)
      YMIN=ALOG10(YMIN)
      GO TO 15
C SCALING FOR LINEAR Y AXIS
   14 CALL SCALE(XY(1,2),N,YHT,YMIN,DY)
   15 YMAX=YMIN+(YHT*DY)
      YP=BO+B1*XP
      IF(YP.GE.YMIN.AND.YP.LE.YMAX) GO TO 115
      IF(YP.LT.YMIN) GO TO 20
      YP=YMAX
      GO TO 21
   20 YP=YMIN
   21 XP=(YP-BO)/B1
  115 XP=(XP-XMIN)/DX
      YP=(YP-YMIN)/DY
      CALL PLOT(XP,YP,3)
      XP=XMAX
      YP=BO+B1*XP
      IF(YP.GE.YMIN.AND.YP.LE.YMAX) GO TO 125
      IF(YP.LT.YMIN) GO TO 30
      YP=YMAX
      GO TO 31
   30 YP=YMIN
   31 XP=(YP-BO)/B1
  125 XP=(XP-XMIN)/DX
      YP=(YP-YMIN)/DY
      CALL PLOT(XP,YP,2)
C NUMBER OF DO STEPS (ISTEPS) DETERMINED BY LENGTH OF X AXIS (XHT IN CM)
C 1  CENTIMETER EQUALS 10 STEPS
      IXHT=10*XHT
      ISTEPS=IXHT+1
C SUBPROGRAM TO PLOT 95% CONFIDENCE INTERVAL OF LINE (+W)
      AN=N
      XQ=-0.1
      IND=3
      DO 130  I=1,ISTEPS
```

```
      XQ=XQ+0.1
  131 XX=XMIN+(XQ*DX)
  131 YY=B0+B1*XX
      Z = (DSQRT((1/AN+((XX-AVE X)**2)/(SXX))))*SSY*(SQRT(2*F))
      YY1=YY+Z
      WQ=(YY1-YMIN)/DY
      IF(WQ.LT.0.0.OR.WQ.GT.YHT)   GO TO 135
      CALL PLOT(XQ,WQ,IND)
      IND=2
      GO TO 130
  135 IND=3
  130 CONTINUE
C SUBPROGRAM TO PLOT 95% CONFIDENCE INTERVAL OF LINE (-W)
      XQ=-0.1
      AN=N
      IND=3
      DO 140 I=1,ISTEPS
      XQ=XQ+0.1
  141 XX=XMIN+(XQ*DX)
  143 YY=B0+B1*XX
      Z =  (DSQRT((1/AN+((XX-AVE X)**2)/(SXX))))*SSY*(SQRT(2*F))
      YY1=YY-Z
      WQ=(YY1-YMIN)/DY
      IF(WQ.LT.0.0.OR.WQ.GT.YHT)   GO TO 145
      CALL PLOT(XQ,WQ,IND)
      IND=2
      GO TO 140
  145 IND=3
  140 CONTINUE
  150 RETURN
      END


      SUBROUTINE PLOTER (XY,N)
C THIS IS A LINEAR PLOTTING SUBROUTINE FOR INCORPORATING THE BEST FIT
C REGRESSION LINE WITH ASSOCIATED ERROR BARS FOR THE LINE AS A WHOLE.
      IMPLICIT REAL*8 (S)
      INTEGER SKIPMN
      COMMON /PLT PGM/ X,Y,B0,B1,SXX,SSY,AVE X,F, YT,XT,HT,SKIPMN,
     1 LPLOTS, IPLOTS, INDEX
      DIMENSION XY(N,2)
      DIMENSION YT(5), XT(5), HT(5), X(200), Y(200)
      DIMENSION XP(2), YP(2)
      EQUIVALENCE (X1,XP(1)),(X2,XP(2)),(Y1,YP(1)),(Y2,YP(2))
C XHT SETS LENGTH OF X-AXIS IN CENTIMETERS
      XHT=24.0
C YHT SETS LENGTH OF Y-AXIS IN CENTIMETERS
      YHT=16.0
      CALL MOVE(YHT,XHT,-1,200)
C BOX GRAPH AND SCALE POINTS TO FIT FIELD. PLACE SYMBOL AT EACH POINT.
      CALL CALPLO(XY,N,1,-1 0,YT,XT,HT,-3)
      IF(SKIPMN.GT.) GO TO 150
C SCALE STARTING AND END POINTS FOR LEAST SQUARES LINE
      CALL SCALE (XY,N, XHT,XMIN,DX)
      CALL SCALE(XY(1,2),N,YHT,YMIN,DY)
      XMAX=XMIN+(XHT*DX)
      YMAX=YMIN+(YHT*DY)
      X1=XMIN
      Y1=B0+B1*XMIN
      IF(Y1.GE.YMIN.AND.Y1.LE.YMAX) GO TO 22
```

```
      IF(Y1.LT.YMIN) GO TO 20
      Y1=YMAX
      GO TO 21
   20 Y1=YMIN
   21 X1=(Y1-BO)/B1
   22 X2=XMAX
      X2=BO+B1*XMAX
      IF(Y2.GE.YMIN.AND.Y2.LE.YMAX) GO TO 23
      IF(Y2.LT.YMIN) GO TO 26
      Y2=YMAX
      GO TO 25
   26 Y2=YMIN
   25 X2=(Y2-BO)/B1
C EQUATION FOR STRAIGHT LINE  Y=B0+B1*X
C DRAW THE LEAST SQUARES STRAIGHT LINE
   23 CALL LINE (XP, YP, 2, 0, 0, XMIN, DX, YMIN, DY)
C NUMBER OF DO STEPS (ISTEPS) DETERMINED BY LENGTH OF X AXIS (XHT IN CM)
C 1 CENTIMETER EQUALS 10 STEPS
      IXHT=10*XHT
      ISTEPS=IXHT + 1
C SUBPROGRAM TO PLOT 95% CONFIDENCE INTERVAL OF LINE (+W)
      XQ=-0.1
      AN=N
      IND=3
      DO 130 I=1,ISTEPS
      XQ=XQ+0.1
      XX=XMIN+XQ*DX
      YQ=BO+B1*XX
      Z = (DSQRT((1/AN+((XX-AVE X)**2)/(SXX))))*SSY*(SQRT(2*F))
      WP=((YQ+Z)-YMIN)/DY
      IF(WP.LT.0.0.OR.WP.GT.YHT)  GO TO 135
      IF(XQ.LT.0.0.OR.XQ.GT.XHT)  GO TO 135
      CALL PLOT (XQ,WP,IND)
      IND=2
      GO TO 130
  135 IND=3
  130 CONTINUE
C SUBPROGRAM TO PLOT 95% CONFIDENCE INTERVAL OF LINE (-W)
      XQ=-0.1
      AN=N
      IND=3
      DO 140 I=1,ISTEPS
      XQ=XQ+0.1
      XX=XMIN+XQ*DX
      YQ=BO+B1*XX
      Z = (DSQRT((1/AN+((XX-AVE X)**2)/(SXX))))*SSY*(SQRT(2*F))
      WP=((YQ-Z)-YMIN)/DY
      IF(WP.LT.0.0.OR.WP.GT.YHT)   GO TO 145
      IF(XO.LT.0.0.OR.XQ.GT.XHT)   GO TO 145
      CALL PLOT(XQ.WP,IND)
      IND=2
      GO TO 140
  145 IND=3
  140 CONTINUE
  150 RETURN
      END
```

REFERENCES.

ALLEN, R.A., SMITH, D.B., OTLET, R.L., and RAWSON, D.S. (1966) Low level tritium measurements in water, Nucl. Inst. Meth., 45, 61-71.

ALVAREZ, L.W. and CORNOG, R. (1939) Helium and hydrogen of mass 3, Phys. Rev., 56, 613.

ALVAREZ, L.W. and CORNOG, R. (1940) Radioactive hydrogen, Phys. Rev., 57, 248.

ANAND, J.S. and LAL, D. (1964) Synthesis of methane from water for tritium measurement, Nature, 201, 775-777.

ATMOSPHERIC RADIOACTIVITY RESEARCH PROJECT (1963) Announced nuclear detonations 1945-1962, Meteorological Research Projects, U.S. Weather Bureau, Washington, D.C., 1963.

BAINBRIDGE, A.E. (1963) Tritium in the north Pacific surface water, J. Geophys. Res., 68, 3785-3789.

BAINBRIDGE, A.E. (1965) Determination of natural tritium, Rev. Sci. Inst., 36, 1779-1782.

BAINBRIDGE, A.E. and O'BRIEN, B.J. (1962) Levels of tritium in a variety of New Zealand waters and some tentative conclusions from these results, in: Tritium in the Physical and Biological Sciences, Symp. Proc., Vienna, 1, 33-39, I.A.E.A., Vienna (STI/PUB/39).

BAINBRIDGE, A.E., SANDOVAL, P. and SUESS, H.E. (1961) Natural tritium measurements by ethane counting, Science, 34, 552-553.

BALLARD, L.F. and ELY, R.L., Jr. (1963) A sensitive tritium monitor, Trans. Amer. Nucl. Soc., 6, 400-401.

BARANOV, G.I. and BOTNIKOV, V.N. (1964) Surface of no motion and water masses in the Weddell Sea, Soviet Antarctic Exped. Inform. Bull., English Translation, 5, 385-388.

BATHEN, K.H. (1972) On seasonal changes in the depth of the mixed layer of the North Pacific Ocean, J. Geophys. Res., 72, 7138-7150.

BAXTER, J.A., FANNING, L.E. and SWARTZ, H.A. (1964) Liquid scintillation solvent systems:water content and related counting efficiencies, Int. J. Appl. Radiat. Isotop., 15, 415-418.

BAXTER, M.S. (1969) Recent fluctuations of atmospheric carbon-14 concentrations, Ph.D. thesis University of Glasgow, 1969.

BECKER, E.W. (1962) Heavy Water Production, Review Series, no. 21, I.A.E.A., Vienna, (STI/PUB/15/21).

BEGEMANN, F. (1963) Earth Science and Meteorites, pp 169-187, North Holland Publishing Co., Amsterdam, 1963.

BEGEMANN, F. and LIBBY, W.F. (1957) Continental water balance, ground water inventory and storage times, surface ocean mixing rates and world wide water circulation patterns from cosmic ray and bomb tritium, Geochim. et Cosmochim., Acta, 12, 277-296.

BEIN, W., HIRSEKORN, H. and MOLLER, L. (1935) Konstantenbestimmungen der Meerwasser und Ergebnisse uber Wasserkorper, Berlin Univ., Inst. Meeresk., Veroff. N.F.A. Geogr., Naturwiss. Reihe, 23.

BIGELEISEN, J. (1962) Correlation of tritium and deuterium isotope effects, in : Tritium in the Physical and Biological Sciences, Symp. Proc., Vienna, 1, 161-168, I.A.E.A., Vienna, (STI/PUB/39).

BISHOP, K.F., DALEFIELD, H.J., EGGLETON, A.E., PEABODY, C.O., and TAYLOR, B.T. (1962) The tritium content of atmospheric methane, in : Tritium in the Physical and Biological Sciences, Symp. Proc., Vienna, 1, 55-67, I.A.E.A., Vienna, (STI/PUB/39).

BJERKNES, V. and SANDSTROM, J.W. (1910) Dynamic Meteorology and Hydrography, Pt.I, Statics. Carnegie Inst. Publ. 88, Washington, D.C., 1910.

BOND, W.D. (1962) Production of Tritium by Contained Nuclear Explosions in Salt : I. Laboratory Studies of Isotopic Exchange of Tritium in the Hydrogen-Water System, U.S.A.E.C. Report ORNL-3334, Oak Ridge National Laboratory.

BOROWITZ, J.L. and GAT, J.R. (1964) Evaluation of elution gas chromatography as a method for the pre-enrichment of tritium for low-level counting, Inst. J. Appl. Radiat. Isotop., 15, 401-406.

BOWDEN, K.F. (1975) Oceanic and estuarine mixing processes, in : Chemical Oceanography, ed. J.P. Riley and G. Skirrow, 2nd edition, VI, Academic Press, New York, 1975.

BOWEN, V.T. and ROETHER, W. (1973) Vertical distribution of Sr-90, Cs-137 and tritium near 45° North in the Atlantic, J. Geophys. Res., 78, 6277-6285.

BOWEN, V.T. and SUGIHARA, T.T. (1960) Strontium-90 in the "mixed layer" of the Atlantic Ocean, Nature, 186, 71-72.

BRENNECKE, W. (1921) Die ozeanographischen Arbeiten der Deutschen Antarktischen Expedition, 1911-1912, Arch. Deutsche Siewarte, 39(1), 1-216.

BROWN, R.M. and GRUMMITT, W.E. (1956) Determination of tritium in natural waters, Canad. J. Chem., 34, 220-226.

BRYDEN, H.L. (1973) New polynomials for thermal expansion, adiabatic temperature gradient and potential temperature of sea water, Deep-Sea Res., 20, 401-408.

BURKE, W.H. and MEINSCHEIN, W.G. (1955) C-14 dating with a methane proportional counter, Rev. Sci. Inst. 26, 1137.

BUTTLAR, H.V. and LIBBY, W.F. (1955) Natural distribution of cosmic-ray produced tritium, part II, J. Inorg. Nucl. Chem., 1, 75-91.

CALDER, R. and LEWIN, G. (1967) Reduction of stainless-steel outgassing in ultra-high vacuum, Br. J. App. Phy. 18, 1459-1472.

CALLAHAN, J.E. (1971) Velocity structure and flux of the Antarctic Circumpolar Current south of Australia, J. Geophys. Res., 76, 5859-5864.

CHAPMAN, S. and DOOTSON, F.W. (1917) Thermal diffusion, Phil. Mag., 33, 248-253.

CHUNG, Y-C. (1971) Pacific deep and bottom water studies based on temperature, radium and excess-radon measurements, Ph.D. Thesis, University of California, San Diego, 1971.

CLOWES, A.J. (1938) Phosphate and Silicate in the Southern Ocean, Discovery Rept., 19, 1-20.

COMMITTEE ON POLAR RESEARCH (1974) Southern Ocean Dynamics. A Strategy for Scientific Exploration 1973-1983. Report of Ad Hoc Working Group on Antarctic Oceanography, Panel on Oceanography, Committee on Polar Research, Nat. Res. Council Nat. Acad. Sci., Washington, D.C., 1974.

CORNOG, R., and LIBBY, W.F. (1941) Production of radioactive hydrogen by neutron bombardment of boron and nitrogen, Phys. Rev., 59, 1046.

CRAIG, H. and GORDON, L.I. (1965) Deuterium and oxygen-18 variations in the ocean and marine atmsophere, in: Proc. Cong. Stable Isotopes in Oceanographic Studies and Paleotemperatures, Spoleto, 1965.

CROMWELL, T., MONTGOMERY, R.B. and STROUP, E.D. (1954) Equatorial undercurrent in the Pacific revealed by new methods, Science, 119, 648-649.

CURRIE, L.A., LIBBY, W.F., and WOLFGANG, R.L. (1956) Tritium production by high-energy protons, Phys. Rev., 101, 1557-1563.

DEACON, G.E.R. (1933) A general account of the hydrology of the South Atlantic Ocean, Discovery Rept., 7, 171-238.

DEACON, G.E.R. (1937) The hydrology of the Southern Ocean, Discovery Rept., 15, 1-24.

DEACON, G.E.R. (1963) The Southern Ocean, ideas and observations on progress in the study of the seas, in: The Sea (vol. 2), ed. M.N. Hill, Interscience Publishers, London, 1963.

DEVINE, M. (1972) Some aspects of the dynamics of the Antarctic Circumpolar Current, J. Geophys. Res., 77, 5987-5992.

DOCKINS, K.O. BAINBRIDGE, A.E., HOUTERMANS, J.C. and SUESS, H.E. (1967) Tritium in the mixed layer of the North Pacific Ocean, in : Radioactive Dating and Methods of Low-Level Counting, International Atomic Energy Agency, Vienna, 1967.

EDMOND, J.M. (1973) The silica budget of the Antarctic Circumpolar Current, Nature, 241, 391-393.

EICHELBERGER, J.F., GROVE, G.R., and JONES, L.V. (1963) Mound Laboratory Progress Report for September 1963, U.S.A.E.C. Report MLM-1176, Mound Laboratory.

ELSEY, R.J. (1975a) Outgassing of vacuum materials -I, Vacuum, 25, 299-306.

ELSEY, R.J. (1975b) Outgassing of vacuum materials -II, Vacuum, 25, 347-361.

ERGIN, M. (1969) Studies of artificial carbon-14 in the carbon cycle, Ph.D. Thesis, University of Glasgow, 1969.

ERICKSSON, E. (1965) An account of the major pulses of tritium and their effects in the atmosphere, Tellus 17, 118-130.

FAIRHALL, A.W., SCHELL, W.R. and TAKASHIMA, Y. (1961) Apparatus for methane synthesis for radiocarbon dating, Rev. Sci. Inst. 32, 323-325.

FALLICK, A.E. (1975) Some applications of stable isotopes of carbon and oxygen in oceanography, Ph.D. Thesis, University of Glasgow, 1975.

FARKAS, A. (1937) On the electrolytic separation of the hydrogen isotopes on a palladium cathode, Trans. Faraday Soc., 33, 552.

FARMER, J.F. (1972) Short-term fluctuation of carbon isotope levels in atmospheric carbon dioxide, Ph.D. Thesis, University of Glasgow, 1972.

FIREMAN, E.L. and SCHWARZER, D. (1954) Measurement of the tritium concentration in natural waters by a diffusion cloud chamber, Phys. Rev., 94, 385-388.

FOFONOFF, N.P. (1956) Some properties of sea water influencing the formation of Antarctic bottom water, Deep-Sea Res., 4, 32-35.

FOSTER, T.D. (1972) An analysis of the cabbeling instability in sea water, J. Phys. Oceanogr., 2, 294-301.

GAT, J.R. (1970) Environmental isotope balance of Lake Tiberias, in : Isotope Hydrology, I.A.E.A., Vienna, 1970.

GILETTI, B.J. and BAZAN, F. (1956) Rates of movement and mixing of water masses in the Atlantic Ocean, Bull. Geol. Soc. Amer., 67, 1698, Abstract.

GILETTI, B.J. and KULP, J.L. (1956) Application of tritium measurements to oceanography and meteorology, Trans. Amer. Geophys. Un., 37, 345, Abstract.

GILL, A.E. (1973) Circulation and bottom water production in the Weddell Sea, Deep-Sea Res., 20, 111-140.

GOLDBERG, E.D., BROECKER, W.S., GROSS, M.G. and TUREKIAN, K.K. (1971) Marine Chemistry, in : R. Gordon Pirie, ed. Oceanography, Contemporary Readings in Ocean Sciences, New York, Oxford University Press, 1971.

GONZALEZ-VIDAL, J. and WADE, W.H. (1960) Survey of tritium-producing nuclear reactions, Phys. Rev., 120, 1354-1359.

GORDON, A.L. (1971) Oceanography of Antarctic Waters, in : Antarctic Oceanology I, ed. J.R. Reid, Antarct. Res. Ser. Am. Geophys. Un., 15, 169-204.

GORDON, A.L. (1972) Introduction : Physical Oceanography of the southeast Indian Ocean, in : Antarctic Oceanology II, ed. D.E. Hayes, Antarct. Res. Ser. Am. Geophys. Un., 19, 3-9.

GORDON, A.L. and TCHERNIA, P. (1972) Waters of the continental margin off Adelie Coast, Antarctica, in : Antarctic Oceanology II, ed. D.E. Hayes, Antarct. Res. Ser. Am. Geophys. Un., 19, 59-70.

GROSSE, A.V., JOHNSTON, W.H., WOLFGANG, R.L. and LIBBY, W.F. (1951) Tritium in nature, Science, 113, 1-2.

GUNTHER, E.R. (1936) A report on oceanographical investigations in the Peru Coastal Current, Discovery Rept., 13, 107-276.

GUTMAN, W. (1961) The continuous detection of low tritium traces in air and other reactor gases, Keintechnouk 3, 552.

HARKNESS, D.D. (1969) Artificial carbon-14, a tracer for carbon in the atmosphere and biosphere, Ph.D. Thesis, University of Glasgow, 1969.

HARTECK, P. (1954) The relative abundance of HT and HTO in the atmosphere, J. Chem. Phys., 22, 1746-1751.

HIDAKA, K. and TSUCHIYA, M. (1953) On the Antarctic Circumpolar Current, J. Mar. Res., 12, 214-222.

HOUTERMANS, J. (1966) Tritium in the surface water of the North Pacific Ocean, Proc. Sixth Int. Conf. on Carbon-14 and Tritium Dating, Washington, 1966.

HOY, J.E. (1968) Tritium enrichment by gas-solid chromatography : techniques for low-level analysis, Science 161, 464-465.

HUFFORD, G.L. and SEABROOKE, J.M. (1970) Water masses of the Weddell Sea, Antarctic J., Jan-Feb. 1970, 13-14.

I.A.E.A. (1969, 1970, 1971, 1973, 1975) Environmental isotope data, Nos. 1,2,3,4 and 5, World Survey of Isotope Concentration in Precipitation, Vienna, International Atomic Energy Agency.

IDYLL, C.P. (1973) The anchovy crisis, Scientific American, 228, 22-29.

INTERNATIONAL COMMISSION ON RADIOLOGICAL UNITS AND MEASUREMENTS (1962) National Bureau of Standards, Handbook 86, Superintendent of Documents, U.S. Government Printing Office, Washington, 1963.

JACOBS, D.G. (1968) Sources of Tritium and its Behaviour upon Release to the Environment, U.S.A.E.C., Division of Technical Information, Oak Ridge National Laboratory, 1968.

JACOBS, S.S., AMOS, A.F. and BRUCHHAUSEN, P.M. (1970) Ross Sea oceanography and Antarctic Bottom Water formation, Deep-Sea Res., 17, 935-962.

JACOBS, S.S., BAUER, E.B., BRUCKHAUSEN, P.M., GORDON, A.L., ROOT, T.F. and ROSSELOT, F.L. (1974) Eltanin Reports. Cruises 47-50, 1971; 52-55, 1972. Lamont-Doherty Geological Observatory of Columbia University, Palisades, New York, 1974.

JONES, A.W., JONES, E. and WILLIAMS, E.M. (1973) Investigation by techniques of electron-stimulated desorption of the merits of glow discharge cleaning of the surfaces of vacuum chambers at the CERN intersecting storage ring, Vacuum, 23, 227-230.

JONES, W.M. (1955) Half-life of tritium, Phys. Rev., 100, 124-125.

KASAHARA, H. (1970) Commercial fisheries, in : Scientific Exploration of the South Pacific, Nat. Acad. Sci., Washington, D.C., W.S. Wooster ed., 1970.

KAUFMAN, S. (1953) The natural distribution of tritium, Ph.D. Thesis, University of Chicago, 1953.

KAUFMAN, S. and LIBBY, W.F. (1954) The natural distribution of tritium, Phys. Rev., 93, 1337-1344.

KILLWORTH,P.D. (1973) A two-dimensional model for the formation of Antarctic Bottom Water, Deep-Sea Res., 20, 941-971.

KIRSHENBAUM, I. (1951) Physical Properties and Analysis of Heavy Water, National Nuclear Energy Series, Division III, Volume 4A, McGraw-Hill Book Company, Inc., New York, 1951.

KNAUSS, J.A. (1966) Further measurements and observations on the Cromwell Current, J. Mar. Res., 24, 204-240.

KNUDSEN, M. (1901) Hydrographical Tables, Copenhagen, 1901.

LAL, D. and ATHAVALE, R.N. (1966) The measurement of tritium activity in natural waters, Part I. Techniques, Proc. Indian Acad. Sci., Sec. A, 63, 166-183.

LAMBERT, R.M. and COMRIE , C.M. (1974) Convenient electrical discharge method for eliminating hydrocarbon contamination from stainless steel UHV systems, J.Vac. Sci. Technol., 11, 530-531.

LANGE, N.A., and FORKER, G.M. (1961) Handbook of Chemistry 10th ed., McGraw-Hill Book Company, Inc., New York, 1961.

LEIPUNSKY, O.I. (1957) At. Energy (USSR), 3, 530.

LE PICHON, X., EITTREM, S.L. and LUDWIG, W.J. (1971) Sediment transport and distribution in the Argentine Basin 1. Antarctic Bottom Current passage through the Falkland Fracture Zone, Phys. Chem. Earth, 8, 1-28.

LEWIN, G. (1965) Fundamentals of Vacuum Science and Technology, McGraw-Hill, New York, 1965.

LI, Y-H. (1967) Equation of state of water and sea-water, J. Geophys. Res., 72, 2665-2678.

LIBBY, W.F. (1946) Atmospheric helium three and radiocarbon from cosmic radiation, Phys. Rev., 69, 671-672.

LINDEMANN, F.A. (1919) Note on the vapour pressure and affinity of isotopes, Phil. Mag., 38, 173-181.

MARTELL, E.A. (1963) On the inventory of artificial tritium and its occurrence in atmospheric methane, J. Geophys. Res., 68, 3759-3769.

METSON, P. (1969) A routine method for the determination of tritium by electrolytic concentration before liquid scintillation counting, Analyst, 94, 1122-1129.

METSON, P. (1969) A routine method for the determination of tritium by electrolytic concentration before liquid scintillation counting, Analyst, 94, 1122-1129.

METSON, P. (1973) The determination of low level tritium, Symp. Det. Radionuc. Environ. Biolog. Materials, 1-7.

MICHEL, R.L. (1974) Uptake of bomb produced tritium by the Pacific Ocean, Ph.D. Thesis, University of California, San Diego, 1974.

MICHEL, R.L. and SUESS, H.E. (1975) Bomb tritium in the Pacific Ocean, J. Geophys. Res., 80, 4139-4152.

MICHEL, R.L. and WILLIAMS, P.M. (1973) Bomb produced tritium in the Antarctic Ocean, Earth Planet. Sci. Letts., 20, 381-384.

MISKELL, J.A. (1964) Characteristics of radioactivity produced by nuclear explosives, in : Engineering with Nuclear Explosives, Proc. Third. Plowshare Symp., Livermore, California, April 21-23, 1964, pp. 153-160, (TID-7695), 1964.

MOELLER, T. (1954) Inorganic Chemistry, John Wiley and Sons, Inc., New York, 1954.

MONTGOMERY, R.B. and STROUP, E.D. (1962) Equatorial Waters and Currents at 150^{o}W in July-August, 1952, Johns Hopkins University Press, Baltimore, Md, 1962.

MONTGOMERY, R.B. and WOOSTER, W.S. (1954) Thermosteric anomaly and the analysis of serial oceanographic data, Deep-Sea Res., 2, 63-70.

MOSBY, H. (1934) The waters of the Atlantic Antarctic Ocean, Sci. Res. Norwegian Antarctic Exped. 1927-1928, 11, 1-131.

MUNNICH, K.O. and ROETHER, W. (1967) Transfer of bomb C-14 and tritium from the atmosphere to the oceans : interal mixing of the ocean on the basis of tritium and C-14 profiles, in : Radioactive Dating and Low-level counting; International Atomic Engery Agency, Vienna, 1967.

MUNK, W.H. (1966) Abyssal recipes, Deep-Sea Res., 13, 707-730.

MUNK, W.H. and PALMEN, E. (1951) Note on the dynamics of the Antarctic Circumpolar Current, Tellus, 3, 53-55.

MUROMTSEV, A.M. (1963) The Principle Hydrological Features of the Pacific Ocean, translated from the Russian by A. Birron and Z.S. Cole, Israel Programme for Scientific Translations, Ltd., Jerusalem.

OESCHGER, H. (1963) Low-level counting methods in : Radioactive Dating, Proc. Symp. Athens, (STI/PUB/68), 1963.

OSTLUND, H.G. (1962) A hydrogen gas counting system for natural tritium measurements, in : Tritium in the Physical and Biological Sciences, Symp. Proc., Vienna, 1, 333-341, IAEA, Vienna (STI/PUB/39).

OSTLUND, H.G., DORSEY, H.G. and ROOTH, C.G. (1974) Geosecs. North Atlantic radiocarbon and tritium results, Earth Planet. Sci. Letts., 23, 69-86.

OSTLUND, H.G. and LUNDGREN, L.B. (1964) Stockholm natural tritium measurements, Tellus, 25, 118-130.

OSTLUND, H.G. and MASON, A.S. (1974) Atmospheric HT and HTO : 1, experimental procedures and tropospheric data, 1968-1972, Tellus, 26, 91-102.

OSTLUND, H.G. and WERNER, E. (1962) The electrolytic enrichment of tritium and deuterium for natural tritium

measurements, in : Tritium in the Physical and Biological Sciences, Symp. Proc., Vienna, 1, 95-105, IAEA, Vienna (STI/PUB/39).

PICKARD, G.L. (1963) Descriptive Physical Oceanography, Pergamon Press, London, 1963.

PITTENDRIGH, L.W.D. and VOUSDEN, J.E. (1954) A differential ionisation chamber method for continuous flow monitoring of tritium in air in the presence of a significant gamma background and with occasional traces of radon in the sampled air, British Report AERE-Hp/R-1585.

PRITCHARD, D.W., REID, R.O., OKUKO, A. and CARTER, H.H. (1971) Physical processes of water movement and mixing in: Radioactivity in the Marine Environment Nat. Acad. Sci., Washington, D.C., 1971.

RANKAMA, K. and SAHAMA, T.G. (1950) Geochemistry, The University of Chicago Press, Chicago, 1950.

REID, J.L. (1959) Evidence of a South Equatorial Countercurrent in the Pacific Ocean, Nature, 184, 209-210.

REID, J.L. (1965) Intermediate waters of the Pacific Ocean, Johns Hopkins University Press, Baltimore, Md., 1965.

REID, J.L. (1973) Transpacific hydrographic sections at Lats. 43°S and 28°S : the SCORPIO Expedition-III. Upper water and a note on southward flow at mid-depth, Deep-Sea Res., 20, 39-49.

REID, J.L. and NOWLIN, W.D. (1971) Transport of water through the Drake Passage, Deep-Sea Res., 18, 51-64.

REID, J.L., STOMMEL, H., STROUP, E.D. and WARREN, B.A. (1968) Detection of a deep boundary current in

the western south Pacific, Nature, 217, 937.

ROBINSON, C.V. (1963) Gas counting of tritium, in : Advances in Tracer Methodology, 1, 178-182, Plenum Press, New York, 1963.

ROETHER, W. (1974) The tritium and C-14 profiles at the GEOSECS I (1969) and GOGO I (1971) North Pacific Stations, Earth Planet. Sci. Letts., 23, 108-115.

ROETHER, W., MUNNICH, K.O. and OSTLUND, H.G. (1970) Tritium profile at the North Pacific (1969) Geosecs intercalibration station, J. Geophys. Res., 75, 7672-7675.

ROOTH, C.G. and OSTLUND, H.G. (1972) Penetration of tritium into the Atlantic thermocline, Deep-Sea Res., 19, 481-492.

ROTSCHI, H. (1970) Variations of equatorial currents, in : Scientific Exploration of the South Pacific, Nat. Acad. Sci., Washington, D.C., W.S. Wooster ed., 75-83, 1970.

RUTHERFORD, L. (1937) The search for the isotopes of hydrogen and helium of mass 3, Nature, 140, 303-305.

SANNES, F. and BANNVILLE, B. (1965) A Portable Tritium-in-Air Monitor, Canadian Report AECL-2283.

SAUZAY, G. and SCHELL, W.R. (1972) Analysis of low level tritium concentrations by electrolytic enrichment and liquid scintillation counting, Int. J. App. Radiat. Isotop, 23, 25-33.

SCHIEN, M., HASKIN, D.M. and GLASSER, R.G., (1956) Heavy unstable particles produced in the high energy pion beam of the Berkeley Bevetron, II Nuovo Cimento, Ser. X, 3, 131-140.

SCHEIN, M., HASKIN, D.M. and LEANOV, D. (1955) Unstable H^4 fragments from the capture of a Σ^- hyperon, Phys. Rev., 100, 1455-1456.

SCHELL, W.R. (1970) An internal gas proportional counter for measuring low level environmental radionuclides, in : Radionuclides in the Environment, ed. R.F. Gould, American Chemical Society, 173-201, 1970.

SCHELL, W.R. and SAUZAY, G. (1973) World distribution of environmental tritium, IAEA-SM-181/34.

SEABROOKE, J.M., HUFFORD, G.L. and ELDER, R.B. (1971) Formation of Antarctic Bottom Water in the Weddell Sea, J. Geophys. Res., 76, 2164-2178.

SHARP, R.A. and ELLIS, J.G. (1965) System design in low background internal gas sample counting of C-14 and tritium, in: Sixth Proc. Radiocarbon and Tritium Dating, 17-28, 1965.

SMITH, D.B. and RAWSON, D.S. (1962) The reconcentration of tritium by distillation, in : Tritium in the Physical and Biological Sciences, Symp. Proc. Vienna, 1, 105-120, IAEA, Vienna (STI/PUB/39).

SOLOMON, H. (1974) Comments on the Antarctic Bottom Water problem and high-latitude thermocline sinking, J. Geophys. Res., 79, 881-884.

STENHOUSE, M.S. (1972) Artificial production of C-14 from nuclear weapon tests and its uptake by man, Ph.D. Thesis, University of Glasgow, 1972.

STOMMEL, H. (1957) A survey of ocean current theory, Deep-Sea Res., 4, 149-184.

STOMMEL, H. (1958) The abyssal circulation, Deep-Sea Res., 5, 80-82.

STOMMEL, H. and ARONS, A.B. (1960) On the abyssal circulation of the world ocean-II. An idealised model of the circulation pattern and amplitude in oceanic basins, Deep-Sea Res., 6, 217-233.

SVERDRUP, H.U. (1933) On vertical circulation in the ocean due to the action of wind with application to conditions within an Antarctic Circumpolar Current, Discovery Rept., 7, 139-170.

SVERDRUP, H.U., JOHNSON, M.W. and FLEMING, R.H. (1942) The Oceans, their Physics, Chemistry and General Biology, Prentice-Hall, Englewood Cliffs, N.J., 1942.

TAMULY, A. (1974) Dispersal of tritium in Southern Ocean Water, Arctic, 27, 27-40.

TAYLOR, C.B. (1966) Tritium in Southern Hemisphere precipitation, 1953-1964, Tellus, 18, 105-130.

TAYLOR, C.B. (1968) A comparison of tritium and strontium -90 fallout in the southern hemisphere, Tellus, 20, 559-576.

THEODORSSEN, P. (1974) Improved tritium counting through high electrolytic enrichment, Int. J. App. Radiat. Isotop., 25, 97-104.

THOMSON, J. and TUREKIAN, K.K. (1976) ^{210}Po and ^{210}Pb distributions in ocean water profiles from the eastern South Pacific, Earth Planet. Sci. Letts., 32, 297-303.

TRIER, R.M., BROECKER, W.S. and FEELY, H.M. (1972) Radium -228 profile at the second Geosecs intercalibration station, 1970, inthe North Atlantic, Earth Planet. Sci. Letts., 16, 141-145.

TSUCHIYA, M. (1968) Upper Waters of the Intertropical Pacific Ocean, Johns Hopkins University Press, Baltimore, Md., 1968.

TSUCHIYA, M. (1970) Equatorial circulation of the South Pacific, in : Scientific Exploration of the South Pacific, Nat. Acad. Sci. Washington, D.C., W.S. Wooster ed., 69-74, 1970.

UREY, H.C. (1933) Separation and properties of isotopes of hydrogen, Science, 78, 566-571.

VERHAGEN, B. Th. and SELLSCHOP, J.P.F. (1963) Enrichment and assay of naturally occurring tritium in : Nat. Conf., Nucl. Energy; Appl. Isotop. Radiat., 109-119, Pelindaba, South Africa, Atomic Energy Board, 1963.

VERHAGEN, B. Th. and SELLSCHOP, J.P.F. (1965) Enrichment of low-level tritium by thermal diffusion for hydrological applications, in : Proc. Third Inst. Conf. Peaceful Uses At. Energy, Geneva, 1964, 12, 398-405, United Nations, New York, 1965.

VERONIS, G. (1969) On theoretical models of the thermocline circulation, Deep-Sea Res., 16 (Supplement), 301-323.

VOLCHOK, H.L., BOWEN, V.T., FOLSOM, T.R., BROECHKER, W.S. SCHUERT, E.A. and BIEN, G.S. (1971) Oceanic distribution of radionuclides from nuclear explosions in : Radioactivity in the Marine Environment, Nat. Acad. Sci., Washington, D.C., 1971.

WANG, D-P. and MILLERO, F.J. (1973) Precise representation of the P-V-T properties of water and seawater determined from sound speeds, J. Geophys. Res. 78, 7122-7128.

WARREN, B.A. (1970) General circulation of the South Pacific, in:Scientific Exploration of the South Pacific, ed. W.S. Wooster, Nat. Acad. Sci., Washington, D.C., 1970.

WARREN, B.A. (1973) Transpacific hydrographic sections at Lats. 43°S and 28°S: the SCORPIO Expedition -II. Deep Water, Deep-Sea Res., 20, 9-38.

WARREN, B.A. and VOSHRIS, A. (1970) Velocity measurements in the deep western boundary current of the South Pacific, Nature, 228, 849-850.

WEAST, R.C. (1968) Handbook of Chemistry and Physics (ed.)., The Chemical Rubber Co., Cleveland, Ohio, 48th ed., 1968.

WEAST, R.C. (1970) Handbook of Chemistry and Physics (ed.)., The Chemical Rubber Co., Cleveland, Ohio, 50th ed., 1970.

WOLFGANG, R.L. (1963) Vapour phase proportional counting, in : Advances in Tracer Methodology, 1, 183-184, Plenum Press, New York, 1963.

WOOSTER, W.S. (1970) Eastern boundary currents in the South Pacific, in : Scientific Exploration of the South Pacific, Nat. Acad. Sci., Washington, D.C., W.S. Wooster, ed., 60-68, 1970.

WOOSTER, W.S. and GILMARTIN, M. (1961) The Peru-Chile Under-Current, J. Mar. Res., 19, 97-122.

WRIGHT, R. (1969) Deep water movement in the Western Atlantic as determined by use of a box model, Deep-Sea Res., 16 (Supplement), 433-446.

WRIGHT, R. (1970) Northward transport of Antarctic Bottom Water in the Western Atlantic Ocean, Deep-Sea Res., 17, 367-371.

WUST, G. (1936) Atlas Schichtung und Zirkulation des Atlantischem Ozeans, Teil A and B : Stratosphere, Wess. Ergebn. dtsch. atlant. Exped. 'Meteor' 1925-1927, 6, (A and B).

WUST, G. (1938) Das Bodenwasser und die Gliederung der Atlantischen Tiefsec, Metecrwerk, Bd. VI, Teil 1.

WUST, G. (1957) Stromgeschwindigkeiten und stommengen in den Tiefen des Atlantischen Ozeans, Wiss. Ergebn, dtsch. atlant. Expend. 'Meteor' 1925- 1927, 6, (2) : 261-420.

WYRTKI, K. (1961) The thermocline circulation in relation to the general circulation in the oceans, Deep-Sea Res., 8, 39-64.

ZUTSHI, P.K. and SAS-HUBIKI, J. (1966) A new cathode treatment for the reproducible electrolytic enrichment of tritium, Int. J. App. Radiat. Isotopes, 17, 670-671.